



HAL
open science

Polymer multilayers : fundamental aspects and application for biomaterials

Lydie Séon

► **To cite this version:**

Lydie Séon. Polymer multilayers : fundamental aspects and application for biomaterials. Other [cond-mat.other]. Université de Strasbourg, 2014. English. NNT : 2014STRAE014 . tel-01599030

HAL Id: tel-01599030

<https://theses.hal.science/tel-01599030>

Submitted on 1 Oct 2017

HAL is a multi-disciplinary open access archive for the deposit and dissemination of scientific research documents, whether they are published or not. The documents may come from teaching and research institutions in France or abroad, or from public or private research centers.

L'archive ouverte pluridisciplinaire **HAL**, est destinée au dépôt et à la diffusion de documents scientifiques de niveau recherche, publiés ou non, émanant des établissements d'enseignement et de recherche français ou étrangers, des laboratoires publics ou privés.



École doctorale physique et chimie-physique - ED 182

THESE

Pour obtenir le grade de

Docteur de l'Université de Strasbourg

Discipline : Chimie-physique

Présentée et soutenue le 30 septembre 2014 par

Lydie Séon

Polymer multilayers: fundamental aspects and application for biomaterials

Membres du jury

<i>Directeurs :</i>	Fouzia BOULMEDAIS	Chargée de recherche, HDR, CNRS, Strasbourg
	Jean-Claude VOEGEL	Directeur de recherche, INSERM, Strasbourg
<i>Rapporteurs :</i>	Bernard MARTEL	Professeur, Université Lille 1, Lille
	Catherine AMIEL	Professeur, Université Paris 12, Paris
<i>Examineurs :</i>	Marie-Hélène METZ-BOUTIGUE	Directeur de recherche, INSERM, Strasbourg
	Alexander ZELIKIN	Professeur, Université d'Aarhus, Danemark

Remerciements

Comme un travail de thèse ne se réalise pas tout seul, je souhaiterais remercier toutes les personnes qui y ont participé et qui m'ont apporté leur aide et leur soutien durant mes trois années de thèse.

Ce travail de thèse a été réalisé dans les laboratoires de l'Institut Charles Sadron, UPR 22-CNRS, au sein de l'équipe Ingénierie Macromoléculaire aux Interfaces ainsi qu'à l'Unité INSERM UMR 1121, Biomatériaux et Bioingénierie, à Strasbourg. Je tiens donc à remercier les directeurs de ces laboratoires : Jean-François Legrand puis Jean-Michel Guenet pour la direction de l'ICS et Jean-Claude Voegel puis Pierre Schaaf pour la direction du laboratoire INSERM. Je remercie également Marie-Hélène Metz-Boutigue pour m'avoir accueillie dans son équipe pour la partie antimicrobienne de mon sujet.

Je tiens à remercier Fouzia Boulmedais et Jean-Claude Voegel, mes directeurs de thèse, pour m'avoir confié ce sujet de thèse multidisciplinaire. Grâce à votre confiance, j'ai pu mener différents projets à bien, rencontrer de nombreuses personnes et apprendre beaucoup aussi bien scientifiquement que humainement. En particulier, je remercie chaleureusement Fouzia pour sa grande disponibilité, pour ses conseils, pour nos nombreux échanges et aussi pour m'avoir donné la possibilité de m'exprimer lors de conférences nationales et internationales. Mon petit MRSA me suit désormais partout où je vais !

Je remercie les membres du jury, Catherine Amiel, Marie-Hélène Metz-Boutigue, Alexander Zelikin et Bernard Martel, pour l'intérêt porté à mon manuscrit ainsi qu'aux riches échanges lors de la soutenance.

Ce travail de thèse a nécessité l'aide de différentes personnes au sein de l'équipe IMI mais aussi au sein de l'ICS et je les en remercie, en particulier Gwenaëlle Cado, Gauthier Rydbeck, César Rios Neyra et Audrey Parat pour m'avoir permis de commencer ma thèse dans de bonnes conditions, Loïc Jierry et Tony Garnier pour leur aide très précieuse en synthèse, André Schroeder pour m'avoir donné accès à l'ITC et m'avoir appris à traiter les données, Thanh Chau Dalencon pour les analyses XPS, l'équipe de Gero Decher qui a toujours été là pour m'ouvrir les portes du labo de QCM et pour prendre le temps de discuter

un moment de LbL ou pas. (Olivier Felix, Michel Tschopp, Rémi Merindol, Paul Rouster, Rebecca Blell, Maria Witt, Alliny Naves...).

Je remercie également toutes les personnes de l'INSERM qui ont participé à ce travail de thèse et qui m'ont permis de mieux comprendre les biologistes! Merci à Armelle Chassepot (culture cellulaire), Rizwan Aslam (tests antimicrobiens), Sophie Hellé (tests de Kirby), Cosette Betscha (HPLC), Céline Marban (tests inflammatoires), Roxane Fabre (microscopie confocale) pour leur formation. Merci à Bernard Senger, Dominique Vautier et Philippe Lavalle pour les conversations enrichissantes. Merci à tous les doctorants et les post-docs qui m'ont de multiples fois aidé : Christophe, Julien, Morgane, Roxane, Engin et Florian. Enfin, un très grand merci à Aurélie Schwarzentrüber qui a été une stagiaire fabuleuse et qui grâce à son efficacité et son indépendance m'a permis de gagner beaucoup de temps à la fin de ma thèse.

Je tiens également à remercier Francis Schneider pour ses informations sur les besoins de l'hôpital concernant les cathéters ce qui m'a permis de m'accrocher à un but concret, Halima Kerdjouj qui a pris plus d'une fois le temps de m'écouter et de répondre à mes questions sur la biologie, Grégory Francius pour ses expériences en AFM force et Jean-Marc Strub pour ses analyses Maldi-Tof.

Pour faire face aux embûches parfois semées sur le chemin de la thèse, j'ai eu la chance d'être entourée au quotidien de doctorants, post-doc et stagiaires qui ont apporté une ambiance joviale et un soutien précieux pendant ces trois ans de thèse. Alex et Johan, quelle joie d'avoir mené cette aventure ensemble du début à la fin ! Clément, Cécile, Elodie, Fabien, Tony, Pauline, Cyril : tout simplement merci pour tous les moments que nous avons partagé ! Merci aussi à l'extension de la Schaaf's team : Eric et Véronique !

Je terminerai en remerciant ma famille pour son appui sans condition et également Andreas qui a été mon soutien de tous les jours pendant ces trois années.

Table of contents

List of abbreviations	iv
Introduction	1
Chapter 1: Bibliographic overview	5
1.1 Coating strategies	7
1.1.1 Langmuir-Blodgett films	7
1.1.2 Self-assembled monolayers	8
1.1.3 Polymer adsorption and grafting	8
1.2 Polyelectrolyte multilayer films	9
1.2.1 Layer-by-layer assembly	9
1.2.2 Deposition methods	10
1.2.3 Growth regimes	12
1.2.4 Tunable properties	14
1.3 Multilayer films based on host-guest interactions	18
1.3.1 From electrostatic to other kinds of interactions	18
1.3.2 Inclusion complexes	19
1.3.3 Polymer multilayers based on host-guest interactions	23
1.4 Multilayer films as antimicrobial coating	25
1.4.1 Medical context: hospital acquired infections	25
1.4.2 Antimicrobial peptides	27
1.4.3 Polyelectrolyte multilayers as antimicrobial surfaces	31
Chapter 1 references	63
Chapter 2: Materials and methods	81
2.1 Materials	83
2.1.1 Polyelectrolytes	83
2.1.2 Neutral polymers	86
2.1.3 Host and guest molecules	87
2.1.4 Antimicrobial peptides	87
2.1.5 Bis-maleimide linkers	88
2.2 Physico-chemical characterizations	90

2.2.1 Quartz crystal microbalance	90
2.2.2 Surface plasmon resonance	93
2.2.3 Atomic force microscopy	94
2.2.4 Confocal laser scanning microscopy	97
2.2.5 Isothermal titration calorimetry	99
2.2.6 High-performance liquid chromatography	101
2.3 Biological characterizations	103
2.3.1 Buildup in cell culture plates	103
2.3.2 Cytocompatibility tests	103
2.3.3 Antibacterial and antifungal tests	104
2.3.4 Hemolysis assays	106
2.3.5 Inflammatory assays	106
Chapter 2 references	109
Chapter 3: Influence of the interaction strength between supramolecular complexes on the topography of neutral polymer multilayers	111
3.1 Introduction	113
3.2 Association constant of the β-CD/guest complexes	114
3.3 Neutral polymer multilayer buildup based on β-CD/guest interactions	117
3.4 Influence of the host-guest affinity on neutral polymer multilayer buildup	124
3.5 Conclusion	130
Chapter 3 references	131
Chapter 4: Antibacterial and antifungal self-defensive polysaccharides multilayer films	135
4.1 Introduction	137
4.2 Physical-chemical characterization of CHI/HA-CTL-C films	138
4.3 Antibacterial and antifungal assays of CHI/HA-CTL-C films	142
4.4 Mechanism of pathogen growth inhibition of CHI/HA-CTL-C films	144
4.5 Biocompatibility tests of CHI/HA-CTL-C films	146
4.6 Conclusion	148
Chapter 4 references	150

Chapter 5: CTL-C based dimers and dendrimers: syntheses and biological tests in solution **153**

5.1 Introduction	155
5.2 Syntheses of CTL-C based dimers and dendrimer	155
5.2.1 Choice of the linkers	156
5.2.2 Syntheses of CTL-C dimers and dendrimer monitored by HPLC.....	157
5.3 Determination of the minimal inhibitory concentration	161
5.3.1 CTL-C dimers and dendrimer G1	162
5.3.2 “D”-CTL-C.....	163
5.4 Evaluation of the toxicity	164
5.5 Evaluation of the inflammatory response	165
5.6 Conclusion	167
Chapter 5 references	168

Chapter 6: Toward the design of a robust antimicrobial coating for medical catheter **169**

6.1 Introduction	171
6.2 Chemical crosslinking of PEM films and mechanical characterization	172
6.3 PU surface modification and covalent grafting of a PEM film	177
6.3.1 Development of flat PU surfaces	178
6.3.2 Functionalization of PU surfaces	181
6.3.3 Buildup up of CHI-SH/HA-P-CTL-C films on PU surfaces	183
6.4 Buildup of antimicrobial step-by-step crosslinked PEM films on PU surfaces	184
6.5 Conclusion	185
Chapter 6 references	187

Conclusion and outlooks **189**

Annexe A: Syntheses of PAH-CD, PHPMA-CD and PHPMA-X (X = Ad, Fc and Py) **194**

Annexe B: Syntheses of modified HA and CHI **203**

List of abbreviations

A

Ad	Adamantane
Ad-COOH	Adamantane-1-carboxylic acid
AFM	Atomic force microscopy
ALG	Alginate
AMP	Antimicrobial peptide

B

BSA	Bovine serum albumin
-----	----------------------

C

<i>C. albicans</i>	<i>Candida albicans</i>
CD	Cyclodextrin
β -CD	β -cyclodextrin
CFU	Colony forming unit
CgA	Chromogranin A
CHI	Chitosan
CSLM	Confocal laser scanning microscopy
CTL	Cateslytin
CTL-C	Cateslytin with a cysteine residue at the C-terminal end
CX	Chlorhexidine

D

DMEM	Dulbecco's Modified Eagle Medium
------	----------------------------------

E

<i>E. coli</i>	<i>Escherichia coli</i>
EDTA	Ethylenediaminetetraacetic acid

F

Fc	Ferrocene
Fc(MeOH) ₂	1'-ferrocenedimethanol
FITC	Fluorescein isothiocyanate

H

HA	Hyaluronic acid
HEP	Heparin
HEPES	4-(2-hydroxyethyl)-1-piperazineethanesulfonic acid
HGF	Human gingival fibroblast
HPLC	High performance liquid chromatography

I

ITC	Isothermal titration calorimetry
-----	----------------------------------

L	
LbL	Layer-by-layer
M	
<i>M. luteus</i>	<i>Micrococcus luteus</i>
Mal	Maleimide
MALDI-TOF	Matrix-Assisted Laser Desorption/Ionisation-Time Of Flight
MB	Methylene blue
MHB	Mueller Hinton Broth
MIC	Minimal inhibitory concentration
MRSA	Methicillin-resistant <i>Staphylococcus aureus</i>
N	
NMR	Nuclear magnetic resonance
NP	Nanoparticle
O	
OD	Optical density
P	
P	Pyridyl disulfide
PAA	Poly(acrylic acid)
PAAm	Polyacrylamide
PAH	Poly(allylamine hydrochloride)
PBS	Phosphate buffered saline
PDA	Polydopamine
PDADMAC	Poly(diallyldimethylammonium chloride)
PDMS	Polydimethylsiloxane
PEG	Poly(ethylene glycol)
PEI	Polyethylenimine
PEM	Polyelectrolyte multilayer
PFA	Paraformaldehyde
PGA	Poly(L-glutamic acid)
PHPMA	Poly(N-hydroxypropylmethacrylamide)
PLL	Poly(L-lysine)
PMAA	Poly(methacrylic acid)
PSS	Poly(styrene sulfonate)
PU	Polyurethane
PVAm	Polyvinylamine
Py	Pyrene
Q	
QAC	Quaternary ammonium compounds
QCM	Quartz crystal microbalance
QCM-D	Quartz crystal microbalance with dissipation monitoring

S

<i>S. aureus</i>	<i>Staphylococcus aureus</i>
<i>S. epidermis</i>	<i>Staphylococcus epidermis</i>
SAM	Self-assembled monolayer
SH	Thiol
SPR	Surface plasmon resonance
SWNT	Single-wall carbon nanotube

T

THF	Tetrahydrofuran
TRIS	2-amino-2-hydroxymethyl-propane-1,3-diol

X

XPS	X-ray photoelectron spectroscopy
-----	----------------------------------

Introduction

The surface of a material is the privileged location where the interactions between the material and its environment take place. In the field of biomaterials, the challenge is to control these interactions to enhance their biocompatibility. This can be achieved by tailoring the surface properties of the biomaterial, especially through the application of a coating.

A very versatile and convenient coating technique is the layer-by-layer (LbL) assembly of polyelectrolytes, which consists in the alternated deposition of polyanions and polycations. The cohesion of the polyelectrolyte multilayer (PEM) films is ensured by electrostatic interactions. However, it was extended to other driving forces such as hydrogen bonding or metal-ion coordination. Only few studies described the use of host-guest interactions to build multilayer films and none of them focused on the topography of the formed films.

The advantage of the LbL technique mainly comes from the fact that any substrate, whatever its nature or geometry, can be coated and also from the width of possibilities for further functionalization. Since more than 10 years, INSERM UMR 1121 and ICS focused on the development and the application of PEM films in the biomedical field. Several biomolecules have been embedded in PEM films such as proteins, enzymes, peptides and hydrophobic drugs to give different properties to the biomaterial, among them catalytic activities, anti-inflammatory properties and antimicrobial properties.

The prevention of pathogen colonization of implantable medical devices constitutes a major medical and financial issue. Indeed, the formation of microbial biofilms at the surface of biomaterials leads if untreated to chronic microbial infection, inflammation, tissue necrosis and eventually to death. Microbial biofilms are extremely difficult to remove because of their high resistance to antibiotic treatment. The only way to treat them is to remove the device from the patient. The key to stop infections lies in killing bacteria that come near the device before they form a biofilm. PEM films were developed for the functionalization of implants in order to inhibit the adhesion and the proliferation of microbes such as bacteria, fungi and yeasts. Three main kinds of PEM coatings have been developed to reduce microbial colonization of biomaterial surfaces: adhesion-resistant coatings (based on pegylated polyelectrolytes or stiff PEM films), contact-killing coatings (based on chitosan, quaternary ammonium polymers or carbon nanotubes) and antimicrobial agents leaching coatings (based on metal/metal ions, oxygen reactive species, antibiotics or natural antimicrobial peptides).

However, none of the developed PEM films exhibited both antibacterial and antifungal properties. So, it would be interesting to develop PEM films that can be multi-defensive, i.e. active against bacteria, fungi and yeasts.

My thesis work deals with the physical chemical study of polymer multilayer films based on supramolecular interactions and with antimicrobial peptides based molecules and multilayer films. In the first part of the manuscript, we were interested in the buildup of neutral polymer multilayer films based on host-guest interactions and in particular on the influence of the strength of the inclusion complex on their topography. In the second part, in collaboration with Pr. Francis Schneider (Centre Hospitalier Universitaire d'Haute-pierre, Strasbourg) and Dr. Marie-Hélène Metz-Boutigue (INSERM U1121), cateslytin, a natural antimicrobial peptide derived from the natural processing of chromogranin A, was immobilized in polysaccharide multilayer films to develop self-defensive and multi-defensive coatings against bacteria and yeasts. Antimicrobial and anti-inflammatory properties of cateslytin functionalized dimers and dendrimers were also studied in order to improve the bioactivity of the original peptide. Finally, the functionalization of polyurethane, a polymer used for catheters, was achieved by polydopamine chemistry and the step-by-step cross-linking of polysaccharide films embedding cateslytin.

The manuscript of the thesis is divided in six chapters. In chapter 1, different surface coating methods allowing the functionalization of materials are described and more details concerning the layer-by-layer deposition technique are given. In particular, studies on multilayer films based on host-guest interactions are reported. Then, after a brief description of natural antimicrobial peptides and their properties, a complete state of the art of antimicrobial polyelectrolyte multilayer films is given. Chapter 2 presents the materials and methods (physico-chemical and biological) used during this thesis.

In chapter 3, we investigated the buildup and the topography of neutral polymer multilayer films. The step-by-step deposition of poly(N-hydroxypropylmethacrylamide) bearing β -cyclodextrin hosts and different hydrophobic guests (adamantane, ferrocene, pyrene) induces the formation of a continuous or a droplet-like film depending on the strength of the inclusion complex. This strength can be modulated either by changing the hydrophobic guest involved in the buildup or by the type and the concentration of the salt present during the film buildup. This study is a first attempt to rationalize the evolution of the coating structure as a function of the strength of the interactions between the polymers constituting the multilayer film.

Chapter 4 describes the development of a new self-defensive antibacterial and antifungal coating based on a polysaccharide multilayer film with embedded antimicrobial peptides. Cateslytin including a cysteine residue at the C-terminal position was grafted on hyaluronic acid and assembled with chitosan to form a PEM film. The optimal number of layers required for a complete inhibition of *Micrococcus luteus*, *Staphylococcus aureus* and *Candida albicans* was determined. The antimicrobial mechanism was also studied thanks to confocal microscopy.

In chapter 5, cateslytin functionalized dimers and dendrimers were synthesized to improve the bioactivity of the original peptide. Their antibacterial and antifungal properties, their toxicity and for some, their inflammatory properties were assessed and compared to cateslytin.

Chapter 6 reports the development of a robust self-defensive antimicrobial coating for medical catheter using the polydopamine chemistry and the step-by-step cross-linking of polysaccharide multilayer films. While keeping the antimicrobial properties of the PEM film, an increase of its mechanical properties as well as its covalent attachment onto a catheter was pursued.

Finally, a general conclusion is drawn and some outlooks, in particular for the development of antimicrobial coatings for biomaterial application, are given.

Chapter 1:
Bibliographic overview

Chapter 1:

Bibliographic overview

Summary

1.1 Coating strategies	7
1.1.1 Langmuir-Blodgett films	7
1.1.2 Self-assembled monolayers	8
1.1.3 Polymer adsorption and grafting	8
1.2 Polyelectrolyte multilayer films	9
1.2.1 Layer-by-layer assembly	9
1.2.2 Deposition methods	10
1.2.3 Growth regimes	12
1.2.4 Tunable properties	14
1.3 Multilayer films based on host-guest interactions	18
1.3.1 From electrostatic to other kinds of interactions	18
1.3.2 Inclusion complexes	19
1.3.3 Polymer multilayers based on host-guest interactions	23
1.4 Multilayer films as antimicrobial coating	25
1.4.1 Medical context: hospital acquired infections	25
1.4.2 Antimicrobial peptides	27
Cateslytin	31
1.4.3 Polyelectrolyte multilayers as antimicrobial surfaces	31
Chapter 1 references	63

This chapter briefly describes the different surface coating methods allowing the functionalization of materials. Among them, the layer-by-layer technique will be further discussed. First based on electrostatic interactions, this technique has been extended to other types of interactions such as the host-guest interactions for example. The interest of layer-by-layer films in the biomaterials field will also be presented. We will in particular focus on the development of antimicrobial coatings since their development was one of the goals of my PhD.

1.1 Coating strategies

Control of the interactions between material surfaces and their environment can be achieved by tailoring their surface properties, especially through the application of coatings. Different techniques of surface functionalization forming a thin film on a surface have been developed usually depending on the nature of both the material and the deposited molecules or macromolecules.

1.1.1 Langmuir-Blodgett films

One of the first surface functionalization technique was proposed by Langmuir and Blodgett in the 1930s [1]. The Langmuir-Blodgett technique allows the deposition of one or several monolayers of amphiphilic molecules on a solid surface with high control of the spatial arrangement. A layer of amphiphilic molecules is first formed at a liquid-air interface and then transferred to a substrate (Figure 1.1). This process can be repeated several times which allows obtaining several monolayers. However, this technique is restricted to amphiphilic molecules and to planar surfaces. Furthermore, due to the weakness of the interactions involved, the obtained coatings have only a limited stability. Nowadays, the Langmuir-Blodgett technique is mainly used in the study of lipid bilayers mimicking cell membranes.

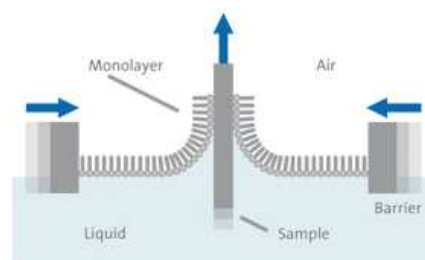


Figure 1.1: Schematic illustration of Langmuir-Blodgett deposition of amphiphilic molecules by withdrawing of a hydrophilic substrate across the liquid-air interface keeping the surface pressure constant. [2]

1.1.2 Self-assembled monolayers

An alternative technique to obtain organic thin films on the surface of a material is the self-assembled monolayer (SAM) technique. SAMs are ordered molecular assemblies spontaneously formed by the adsorption of surfactants on a solid surface [3] (Figure 1.2). For example, thiols and disulfides functionalized organic molecules can form highly ordered SAMs on gold surfaces. This technique provides very dense, stable and homogeneous films. Functionalities can be brought to the surface by using functional alkanethiols bearing for example carboxylic acid, alcohol or amine groups as tail groups [4]. The SAMs technique is restricted to surfaces that have appropriate interactions with thiols, thus essentially noble metal surfaces and silanes.

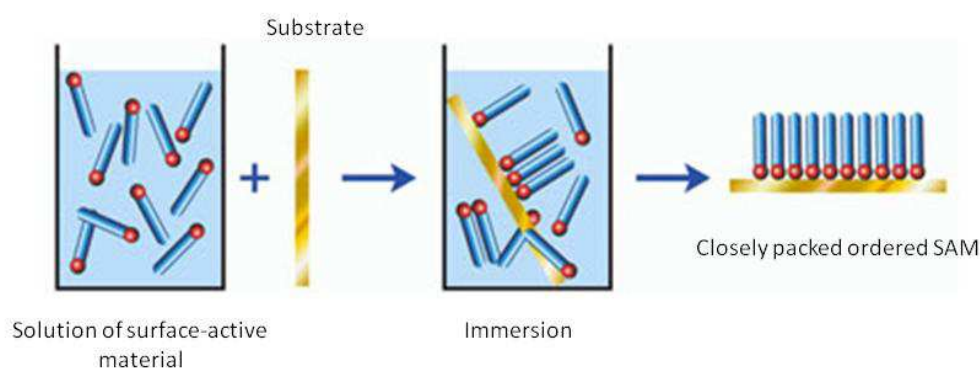


Figure 1.2: Schematic illustration of SAM deposition. The thiol head groups bind to the metal substrate; the alkane chains form a well-organized interface and act as spacers. The tail groups are located at the interface with the medium and define the surface properties. [5]

1.1.3 Polymer adsorption and grafting

Polymers can be brought to the surface by simple adsorption from solution, by spin casting or by solvent evaporation. Adhesion is in this case mainly obtained by the sum of van der Waals attractions between the individual polymer segments and the surface. For example, poly(ethylene oxide)/poly(propylene oxide)/poly(ethylene oxide) (PEO/PPO/PEO) triblock copolymers were used to anchor PEO chains on hydrophobic surfaces. While PPO segments interact with the hydrophobic surface, PEO chains are extended in the bulk solution [6].

Covalent grafting allows to anchor the polymers more firmly on the surface, either by introduction of reactive groups at chain ends and/or side chains on polymers that can be grafted to the surface (“grafting to”) or by using surface-initiated polymerization (“grafting from”) [7]. As example of a “grafting to” approach, Mansky et al. synthesized by living radical polymerization a series of hydroxyl-terminated random copolymers of styrene and

methyl methacrylate at different ratios. The copolymers reacted then with silanol groups on a silicon wafer surface to form tethered random polymer brushes [8].

1.2 Polyelectrolyte multilayer films

The layer-by-layer (LbL) method was developed by Prof Gero Decher at the beginning of the 1990s [9]. It consists in the alternated deposition of polyanions and polycations through electrostatic interactions. The LbL technique presents a lot of advantages among them the possibility of being used on all kinds of surfaces. Also, it does not require the use of any organic solvent.

1.2.1 Layer-by-layer assembly

Polyelectrolyte multilayer (PEM) films are obtained by the layer-by-layer deposition method through the alternated deposition of negatively charged polymer chains (polyanions) and positively charged polymer chains (polycations) on a substrate (Figure 1.3). The substrate, usually negatively charged, is brought into contact with a polycation solution allowing the adsorption of positively charged chains on the surface through electrostatic interactions. A rinsing step is usually employed after each polyelectrolyte deposition to eliminate weakly adhering polymer chains. The surface becomes positively charged (charge overcompensation) and a layer of polyanions can thus be adsorbed by the same process. Again charge overcompensation takes place and at the end of the polyanion deposition the surface is negatively charged allowing the deposition process to be continued again with a polycation. This process can be repeated until the desired film thickness is obtained.

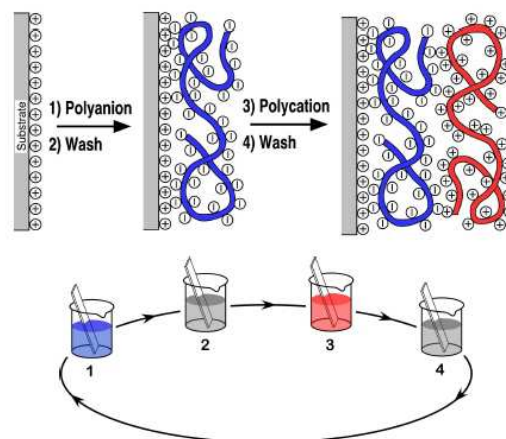


Figure 1.3: Schematic representation of a polyelectrolyte multilayer film buildup by successive adsorptions of polycation and polyanion followed by rinsing steps using the dipping method. [9]

1.2.2 Deposition methods

Different processes have been developed for the buildup of PEM films: the dip-coating, the spin-coating and the spray-coating method.

Dip-coating method

The dip-coating method (Figure 1.4a) has been introduced in the 1990s by Decher et al. to form for example poly(allylamine hydrochloride)/poly(styrene sulfonate) (PAH/PSS) films [10]. The substrate was alternately dipped in polycation and polyanion solutions, each dipping being followed by a rinsing step. This simple technique can be used on various substrates, whatever their shape. The time needed for the adsorption of the polyelectrolytes on the substrate ranges typically from 5 to 20 minutes. Dip-coating is thus a slow deposition method. However, one of the advantages of this method is the low consumption of products since the same polyelectrolyte solution can be used for several deposition steps. The thickness and the roughness of the obtained films depend mainly on the immersion time, the film growth regime, the ionic strength, the pH and the temperature (see 1.2.3 and 1.2.4).

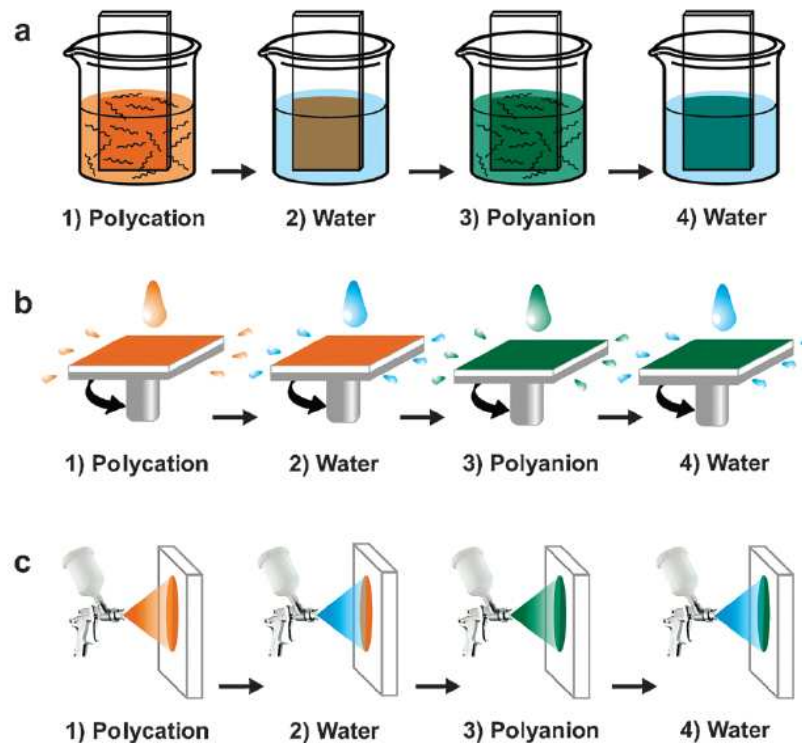


Figure 1.4: Schematic representation of the processes used to build PEM films: (a) dipping LbL assembly, (b) spin-assisted LbL assembly and (c) spray-assisted LbL assembly. The growth of the films is based on the repetition of the cycle (steps 1 to 4). [11]

Spin-coating method

Used over several decades for the application of thin organic films on planar surfaces, the spin-coating method has been used in the 2000s to decrease the buildup time of PEM films [12]. In this process, the polyelectrolyte solution is first deposited on the substrate which is then accelerated rapidly to the desired rotation speed. Due to the action of the centrifugal force, the liquid solution flows radially and its excess is ejected off the substrate. This allows a uniform covering of the substrate by a polyelectrolyte monolayer (Figure 1.4b). No rinsing step is required in this technique so the oppositely charged polyelectrolyte solution can be immediately deposited to form the second layer. The deposition time of a monolayer is about 1 minute; spin-coating is thus a very fast deposition method. The thickness and the roughness of the PEM films depend mainly on the rotation speed and the viscosity of the polyelectrolyte solutions. For example, a low rotation speed or a high concentration of polyelectrolytes in solution leads to thicker films [12]. A planar surface and a reasonable size of the substrate are required to use the spin-coating process.

Spray-coating method

The spray-coating method has been reported for the first time in the literature by Schlenoff et al. who sprayed alternately PSS and poly(diallyldimethylammonium chloride) (PDADMAC) solutions on a vertical substrate, allowing the drainage of the excess solution [13] (Figure 1.4c). Each deposition step was followed by a rinsing step which was performed by spraying pure water. Highly uniform films were obtained. The major advantages of the spray-coating method compared to the dip-coating one are that spraying is fast and allows the coating of large surface areas. However, the spray-coating method consumes a high amount of polyelectrolytes solution. Most of the sprayed solution is indeed lost by drainage and not reusable afterwards. Spraying time, spraying distance, pH, ionic strength and concentrations of the polyelectrolyte solutions have an influence on the thickness and the roughness of the films. Izquierdo et al. showed that the rinsing step can be omitted without impairing the film buildup [14]. This led Porcel et al. to propose, in 2005, to spray simultaneously the polyanion and the polycation solutions on a substrate held vertically [15]. This process, now denoted as the Simultaneous Spray Coating of Interacting Species (SSCIS), leads to organic films whose thickness increases linearly with the spraying time. The method was recently shown to be quite more general, applying (i) to almost any kind of polycation/polyanion systems, (ii) to polyelectrolyte/small multi-charged molecule systems, (iii) to polyelectrolyte/nanoparticles

systems and even (iv) to the simultaneous spraying of two inorganic solutions [16]. This simultaneous spraying method allows reducing the buildup time of polyelectrolyte films since the spraying time can be divided by two but the films are generally rougher and no longer structured [17].

1.2.3 Growth regimes

Two types of growth regimes are observed for PEM films, generally named linear and exponential growth, which are represented figure 1.5.

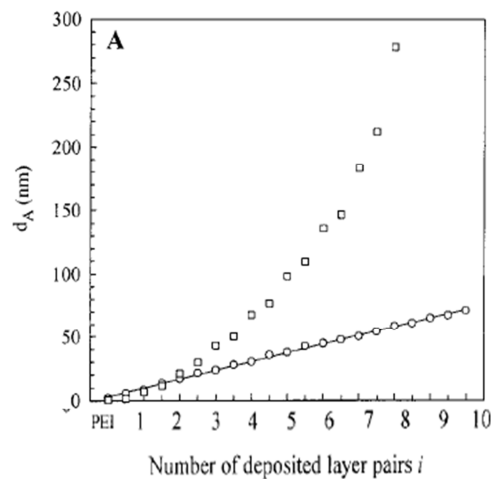


Figure 1.5: Evolution of the thickness of a (○) PEI-(PSS/PAH)_i system and a (□) PEI-(PGA/PLL)_i system depending on the number of deposited bilayers i . The first system is linear whereas the second one is exponential. [18] (PGA: poly(glutamic acid); PLL: poly-L-(lysine))

Linear growth

In the case of linearly growing films, the thickness or the mass increment of the adsorbed pair of layers (one layer of polyanion and one layer of polycation, also called bilayer) is constant whatever the number of adsorption cycles. The polyelectrolytes from the solution interact only with the top outer layer of the film forming stratified PEM films as it was shown by neutron reflectometry measurements [19]. PAH/PSS film is one of the most prominent example of linearly growing films [9, 19].

Exponential growth

Until 1999, it was assumed that the thickness of PEM films always increased linearly or super-linearly with the number of deposition steps. The super-linearly growth, which is a slightly faster growth than the linear one, was attributed to an increase of the film roughness

along the whole buildup process [20, 21]. In 1999, Hubbell and coworkers found that the LbL deposition of poly(L-lysine) (PLL) and alginate (ALG) led to the formation of gel-like films where the thickness is exponentially increasing with the number of deposition steps instead of the usually observed linear thickness increase [22]. Shortly later, Picart and coworkers [23-25] found that it was not an isolated example: exponentially growing films constitute a new class of polyelectrolyte multilayers. Exponentially growing films are characterized by an exponential thickness and mass increase with the number of adsorption cycles. The exponential growth can be explained by the diffusion of at least one of the polyelectrolytes into the entire film during each deposition step. When the film is brought into contact with the polyelectrolyte of opposite charge, the polyelectrolyte that has already diffused into the film diffuses again partly out. Once it reaches the film-solution interface, it is complexed by the oppositely charged polyelectrolyte from the solution. These complexes remain bound to the film and form an additional layer on the top of the film. The mass and the thickness of this layer being proportional to the amount of polyelectrolytes that diffused in and out of the film, the film growth becomes exponential. The obtained films are highly hydrated and thus resemble to hydrogels. Most polypeptides and polysaccharides films have an exponential growth. That is for example the case of the poly(L-lysine)/hyaluronic acid (PLL/HA) [26] or PLL/poly(L-glutamic acid) (PLL/PGA) systems [27].

Some exponentially growing films enter into a linear growth phase after a certain number of deposition steps. This has been first reported by Hübsch et al. [28] for the buildup of a $(\text{PGA}_{0.5}\text{-PSS}_{0.5}/\text{PAH})_n$ multilayer film (Figure 1.6) where the growth goes from exponential to linear after deposition of 26 layers.

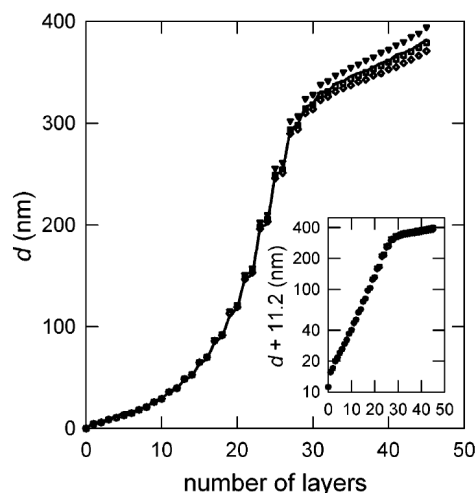


Figure 1.6: Thickness of a $(\text{PGA}_{0.5}\text{-PSS}_{0.5}/\text{PAH})_n$ multilayer film. There is an exponential growth until the 26th layer and then a linear regime. [28]

Such a transition was also described later in the case of PLL/HA [29] and seems to be valid for all exponentially growing PEMs. The reason for the exponential to linear transition is still not fully understood. It could be related to the fact that, when the polyelectrolytes diffuse out of the film, only the first chains reaching the film-solution interface can form polycation/polyanion complexes that remain bound to the film. The interactions between the surface and the complexes are not sufficient anymore to be maintained on the surface and they diffuse in the solution.

The growth regime of a PEM film was related to the interaction strength between the two polyelectrolytes. Linearly growing films, like PAH/PSS, are based on polyelectrolyte pairs that have a negative complexation enthalpy and hence an enthalpic contribution to the free energy of complexation. In this case the buildup process is both enthalpically and entropically driven. On the other hand exponentially growing films, like PLL/PGA, are based on polyelectrolytes that have a positive complexation enthalpy and so the complexation is entirely entropically driven [30].

Moreover, depending on the buildup parameters, some PEM films based on the same two polyelectrolytes can be exponential or linear. The influence of the main parameters on the PEM buildup is described in the next paragraph.

1.2.4 Tunable properties

Many parameters have an influence on the buildup of PEM films, especially on their growth mode, thickness, roughness and density.

Ionic strength

The ionic strength of the polyelectrolyte solutions used during the buildup of the PEM films has a strong influence on their thickness and on their growth mode. An increase of salt concentration usually leads to thicker films [31-33]. For example, PAH/PSS multilayer films were reported to possess an average bilayer thickness increasing from 10.9 to 22.6 Å for NaCl concentrations increasing from 0 to 2.0 mol.L⁻¹ [32]. At low ionic strength, the polyelectrolytes adopt a “flat” or rigid-rod like conformation since the charges on the polyelectrolyte repel each other, whereas they adopt a “loopy” one at high ionic strength

(Figure 1.7). A higher thickness of PEM films is thus obtained at high ionic strengths due to the adsorption of polyelectrolytes in “loopy” conformation [32].

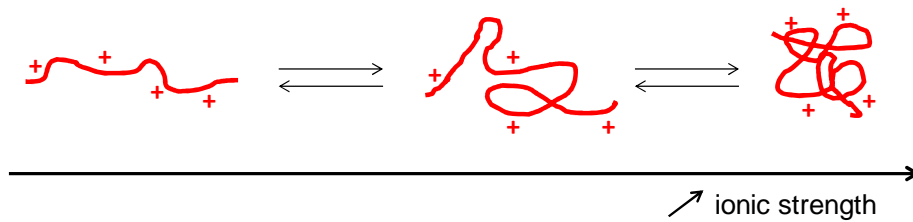


Figure 1.7: Evolution of a polycation chain conformation with the ionic strength.

Richert et al. [34] showed the influence of the ionic strength on the growth regime of a chitosan/hyaluronic acid (CHI/HA) PEM film. When the polyelectrolytes are dissolved in 10^{-4} M NaCl, the CHI/HA film possesses a linear growth but tends to an exponential growth when built in the presence of 0.5 M NaCl (Figure 1.8).

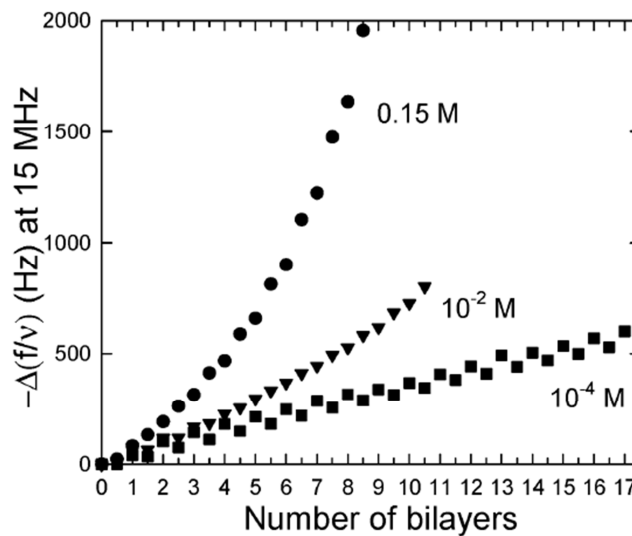


Figure 1.8: Effect of the ionic strength on the buildup of a (CHI/HA) multilayer film followed by quartz crystal microbalance. The system goes from linear to exponential with a NaCl concentration increase. [34]

Nature of the counterions

The nature of the counterions has also a major influence on the PEM buildup. Salomäki et al. showed for example that the thickness of a PDADMAC/PSS multilayer film is depending on the anion present in solution, keeping sodium as cation [35]. Ions can be ranked by their degree of hydration, especially anions because they usually have a higher effect on water than cations. The smaller the hydration sphere of the anion is, the higher is the interaction between the anions and the positive charges of the polyelectrolytes. In the case of

weakly hydrated ions, the anions interact more strongly with the positive charges of the polycations which leads to a reduction of the polyanion/polycation interactions resulting in an increase of the film thickness as well as its roughness. This effect is similar to the one obtained by increasing the ionic strength. Thus, the use of kosmotropic anions, i.e. highly hydrated anions, leads to thinner films, whereas the use of chaotropic ones, i.e. weakly hydrated anions, allows the buildup of thicker films and eventually even exponentially growing ones [35] (Figure 1.9). A comparable study was performed on a PAH/PSS film. This PEM film was reported to be two times thicker for chaotropic counterions than for kosmotropic ones, but linear growth was kept in both cases [36].

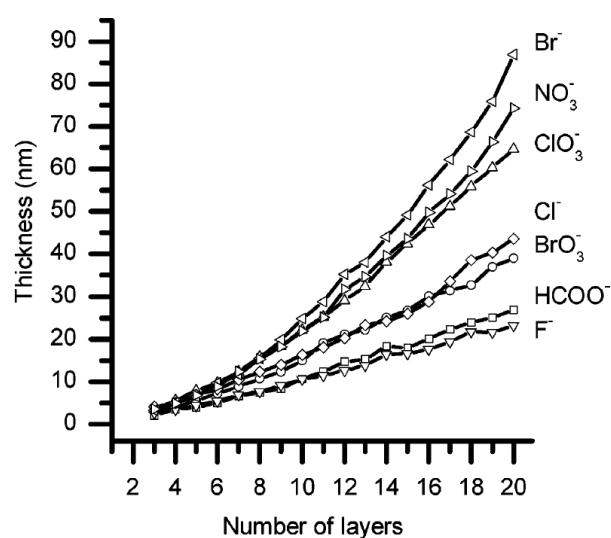


Figure 1.9: Effect of the counterion on the buildup of a (PDADMAC/PSS) multilayer film in a 0.1 M sodium salt solution of the corresponding anion. The system goes from linear to exponential when using anions going from kosmotropes to chaotropes. [35]

Temperature

The influence of the temperature on the buildup of PEMs has been mainly studied on linearly growing films. Salomäki et al. [37] showed that a PDADMAC/PSS multilayer film grows linearly at 15°C and 25°C whereas the buildup becomes exponential for higher temperatures, 45°C and 55°C (Figure 1.10). This growth mode change is due to a faster diffusion of the polyelectrolytes at higher temperatures. Relying on a model, Salomäki et al. proposed that every LbL buildup is inherently exponential and turns linear when the diffusion rate is not fast enough to transport the polyelectrolyte within the entire thickness of the formed layer.

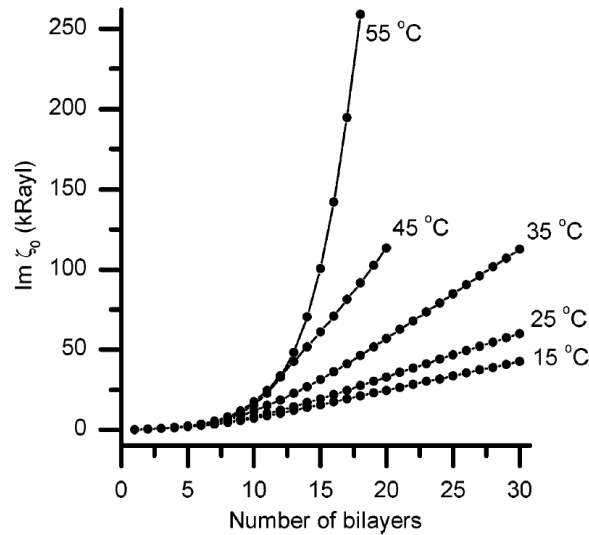


Figure 1.10: Effect of the temperature on the buildup of a (PDADMAC/PSS) multilayer film in a 0.1 M NaBr solution followed by the acoustic impedance evolution of a gold-covered quartz substrate. The system goes from linear to exponential with a temperature increase. [37]

Other parameters can influence the PEM buildup such as the pH in the case of weak polyelectrolytes [38, 39], the molecular weight of the polyelectrolytes [40, 41] or their concentrations [42].

The influence of pH has been studied for PEM films involving weak polyelectrolytes because their ionization degree depends on pH. A variation in pH induces a change on the number of charges on the polyelectrolytes which leads therefore to a change of the polymer chain conformation in solution. For example, when the polymer chains are highly ionized, they adopt a “flat” conformation leading to thin films. This effect is similar to the one described previously for the ionic strength. Rubner and coworkers showed that a variation of pH has a large effect on a PAH/Poly(acrylic acid) (PAA) system. By varying the pH between 2.5 and 8.5, they could modulate the thickness of the adsorbed PAA layer over the range of 5 to 80 Å. It was also reported that the control of the ionization degree by pH allowed the control of the bulk and surface composition of the PEM film [39].

The molecular weight of the polyelectrolytes plays a role in the diffusion process. Kujawa et al. showed that the thickness of an exponentially growing CHI/HA film depends on the molecular weight of both polyelectrolytes: the diffusing one (CHI) and the non-diffusing one (HA) [41]. Short polymer chains can diffuse easily in contrary to long polymer chains, which diffusion can be blocked

1.3 Multilayer films based on host-guest interactions

The cohesion of PEM films is primarily based on electrostatic interactions but it was extended over the years to other driving forces such as hydrogen bonding [43, 44], metal-ion coordination [45] or host-guest interactions. After a brief description of hydrogen bonding and metal-ion coordination based PEM, a closer interest will be taken on host-guest interactions especially the one involving β -cyclodextrin.

1.3.1 From electrostatic to other kinds of interactions

The buildup of PEM films based on other driving forces than the electrostatic interactions allowed a new control of the cohesion of the assemblies. Some elements will be given in this paragraph about hydrogen bonding and metal-ion coordination.

Hydrogen-bonding based PEM

The hydrogen bond [46], whose energy is between 5 and 30 $\text{kJ}\cdot\text{mol}^{-1}$, is stronger than a van der Waals interaction but weaker than an ionic bond. Rubner's team proposed in 1997 to use this type of interaction to build multilayer films [44]. Films made of polyaniline and a hydrogen-bonding polymer such as poly(ethylene oxide), poly(acrylamide) or poly(vinyl alcohol) could be assembled in a layer-by-layer manner. PAA/poly(4-vinylpyridine) (PVP) films were also assembled at low pH, PAA being fully protonated [47]. By modifying the pH, it was possible to break the hydrogen bonds leading to the film dissolution above pH 6.9 [48]. This can be explained by an increasing ionization of PAA carboxylic acid groups when the pH is increased. This induces an electrostatic repulsion between the layers. Hydrogen-bonding films or capsules with tunable dissolution have been extensively studied for biomedical application [49].

Metal-ion coordination based PEM

In 1998, Xiong et al. introduced the coordination chemistry in the LbL assembly field by building up poly(copper styrene 4-sulfonate)/PVP films. By infrared spectroscopy, they showed that the buildup is possible thanks to the formation of a complex involving copper ions, pyridine groups of PVP and sulfonate groups of poly(copper styrene 4-sulfonate). Using a bifunctional polyelectrolyte (BiPE) bearing bipyridine metal ion receptors and positively charged ammonium groups, Krass et al. [45] built a multilayer film with either electrostatic

cohesion when BiPE was assembled with a negatively charged polymer such as PSS or by metal coordination cohesion with BiPE only (Figure 1.11). In the first case, the layers can reversibly accept and release transition metal ions. In the second case, the layers are disassembled with a complexing agent such as EDTA.

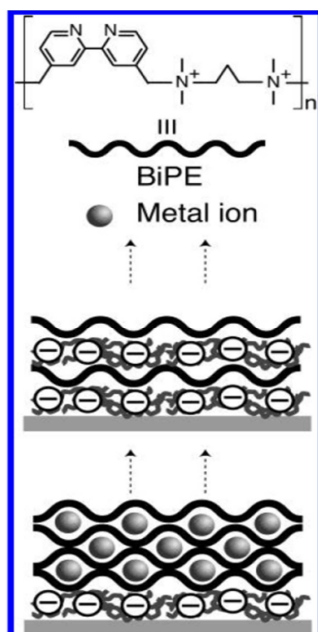


Figure 1.11: Structure of the bifunctional polyelectrolyte (BiPE) bearing bipyridine metal ion receptors and positively charged ammonium groups. BiPE can be assembled through electrostatic interactions with negatively charged polymers such as PSS (top) or it can be assembled through metal ion coordination (bottom) [45].

1.3.2 Inclusion complexes

The “host-guest interaction” expression is used to designate an inclusion complex between a molecule, i.e. the guest, that is trapped within the cavity of a broader one, i.e. the host. Guest molecules can be encapsulated by more than one host or a host can interact with multiple guests. Figure 1.12 represents a 1:1 inclusion complex between a cyclodextrin (CD) and a guest compound.

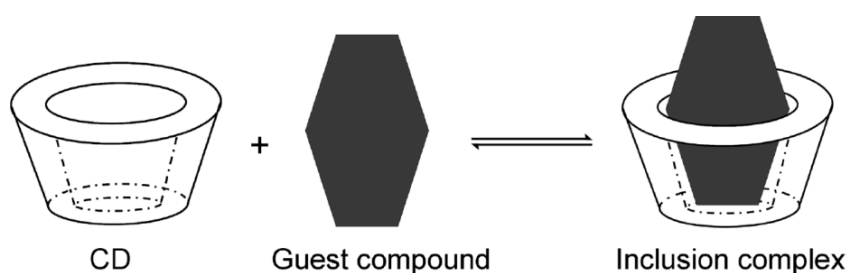


Figure 1.12: Representation of inclusion complex formation (1:1) between a CD and a guest molecule. [50]

A common host molecule: β -cyclodextrin

In the pharmaceutical and biomedical field, cyclodextrins (CD) [50] are the most common used host molecules, especially β -cyclodextrin. CDs are cyclic oligosaccharides composed of D-glucose subunits that are joined by α -1,4 glucosidic linkages. These natural molecules, obtained by enzymatic degradation of starch, possess a truncated cone structure. The CD's hydroxyl groups are located at the outer surface of the molecule which makes CD water-soluble and let a hydrophobic cavity within it (Figure 1.13).

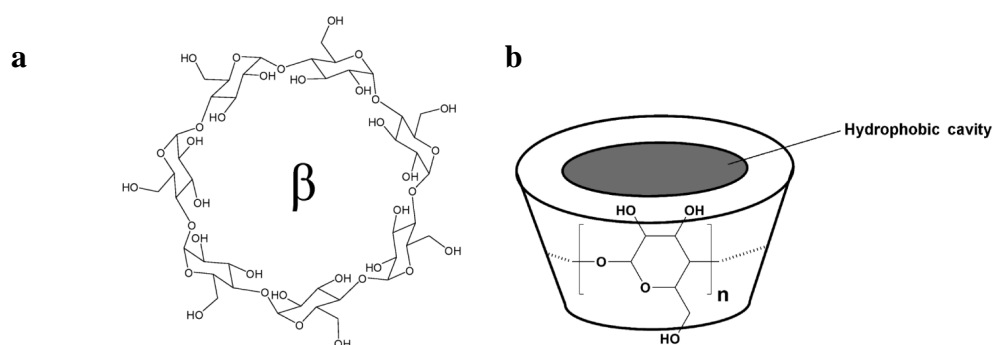


Figure 1.13: (a) Chemical structure of β -cyclodextrin and (b) its schematic 3D representation.[50]

Because of this hydrophobic interior cavity, CD has the ability to form inclusion complexes with various non-polar molecules. The main driving forces of the inclusion complexes are hydrophobic and van der Waals interactions. An important factor for the formation of an inclusion complex is the size of the guest. If the guest is too small, the distance between the guest and the interior of the CD is too high and the intermolecular forces will not exist. If the guest is too large, complex formation cannot happen due to steric hindrance. Among the numerous guest molecules, adamantane (Ad) and ferrocene (Fc) are the ones that have the highest binding affinity with β -CD. Ad is a cycloalkane that consists of three rings fused to each other in a chair conformation (Figure 1.14a). Fc is an organometallic compound that is composed of two planar cyclopentadienyl rings bound to a central iron atom from opposite side like a sandwich (Figure 1.14b).



Figure 1.14: Guest molecules of β -cyclodextrin: (a) adamantane and (b) ferrocene.

Association constant

The stability of a host-guest complex is described by its association constant K . In the case of a 1:1 inclusion complex with CD, K is defined as following for a guest G :

$$G + CD \rightleftharpoons (G - CD) \quad K = \frac{[G-CD]}{[G][CD]} \quad (1.1)$$

Where $[G]$ is the concentration in guest molecule; $[CD]$ is the concentration in cyclodextrin molecules and $[G - CD]$ the concentration in host-guest complexes. The association constant provides a qualitative measurement of the binding affinity. The higher K is, the higher is the binding affinity. For inclusion complexes between CD and a guest molecule, association constants are typically in the range of 10^3 - 10^5 M^{-1} [51]. For example, at 25°C , $\log K = 4.26$ for β -CD/ferrocene carboxylate in pure water at pH 8.5 [52] and $\log K = 3.33$ for β -CD/ferrocene carboxylate in 50 mM phosphate buffer at pH 8.6 with 0.1 M NaCl [53]. Thermodynamic parameters of the complexation of cyclodextrins with hydrophobic guests, including association constants, have been mainly determined with microcalorimetry techniques, especially isothermal titration calorimetry since it is the most sensitive method available at the moment. But a wide variety of other experimental methods are found in the literature: electronic absorption, circular dichroism, fluorescence, nuclear magnetic resonance, electron spin resonance spectroscopy, gas- and liquid-phase chromatography, capillary electrophoresis, pH potentiometry, the use of ion selective electrodes, kinetic experiments and solubility determination [53]. Whereas calorimetric methods allow the direct and simultaneous determination of the association constant and the reaction enthalpy, other methods have to be used carefully since they allow access to the thermodynamic parameters from the van't Hoff equation based on some assumptions which can impair the accuracy of the results.

Influence of the environment on the association constant

Since the pioneering experiments of Hofmeister about specific ion effects [54], numerous studies about salts affecting inclusion complexes equilibrium involving β -CD have been reported in the literature [55-57]. Depending on the type of salt present in solution, the binding affinity is stronger or weaker. Some key elements to understand the role of the salts on the inclusion complex will be presented.

One first has to remind that all molecules in an aqueous solution are surrounded by surface-hydrating water molecules. Thus, the specific association of host and guest in solution

is regulated by their desolvation. Thermodynamic studies have shown that β -CD/Ad complexation in aqueous solution involves the release of water from the interacting surfaces (Figure 1.15). It was estimated by Harries et al. that 15 to 25 water molecules are released during the formation of this complex [51].

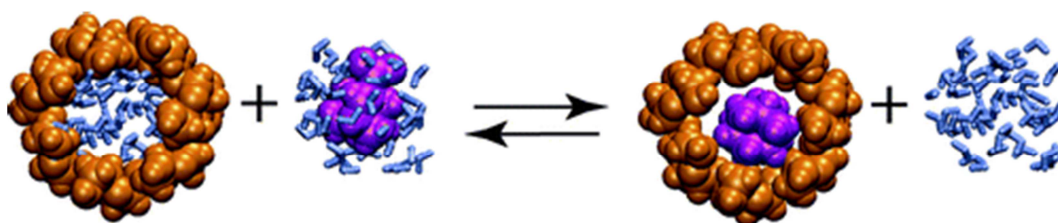


Figure 1.15: Schematic of the complexation reaction between adamantane carboxylate and β -CD. The scheme shows that the release of surface-hydrating water molecules from both interacting molecules is required in order to make it possible for the adamantane carboxylate to fit in the β -CD cavity. [51]

The Hofmeister series constitutes a classification of ions depending on their ability to stabilize the structure of proteins. Except some relative positions in the series, they are basically ranked by their degree of hydration (Figure 1.16). The weakly hydrated anions (exhibiting weaker interactions with water) are called chaotropes whereas the strongly hydrated ones (exhibiting strong interactions with water molecules) are called cosmotropes.

Strongly hydrated anions

Weakly hydrated anions



Figure 1.16: Hofmeister series: ranking of anions by their hydration degree. The hydration degree is decreasing from the left to the right of the scheme.

Several studies pointed out that the stability and the association constant of β -CD/Ad [58], γ -CD/Ad [59], β -CD/nabumetone [60], β -CD/1-butanol [61], β -CD/phenylbenzothiazole derivatives [62], CD/nitroxide radical probe [63] complexes can be modulated by co-solutes such as salts. Chaotropic anions have the tendency to destabilize host-guest complex formation in contrary to cosmotropic anions that promote it. From the literature, it is known that chaotropic anions, like ClO_4^- [64-66] and SCN^- [65, 67], can both form 1:1 complexes with β -CD with a stability constant $\log K = 1.42$ [65] and 0.99 [65], respectively. In contrast, cosmotropic ones, like SO_4^{2-} and F^- anions, do not form 1:1 inclusion complexes with β -CD, since their stability constant are negative [64, 66]. It has been proposed that the inside of β -CD cavity is composed of positively polarized carbon atoms leading to the inclusion of

hydrophobic anionic guest [68]. In the case of ClO_4^- and SCN^- anions, hydrophobic interactions are presumed to contribute to their inclusion within the β -CD cavity. Since SO_4^{2-} and F^- anions are strongly hydrated, they do not bind to β -CD. The decrease of affinity constant when a chaotropic anion is involved can be explained by the competition with the guest for the binding site. The increase of the association constant when a kosmotropic anion is involved is correlated with the water molecules released from both the β -CD cavity and the guest upon the formation of the complex. The presence of a kosmotropic anion such as SO_4^{2-} or F^- disturbs indeed the internal structure of water around the β -CD and its guest, rendering the releasing step of water easier and thus displacing the equilibrium toward the complex formation. Both phenomena are exacerbated when the salt concentration is higher.

1.3.3 Polymer multilayers based on host-guest interactions

β -CD is readily available and is also an effective host for a large range of hydrophobic guests including drug molecules. So, β -CD was often embedded in multilayer films based on polyelectrolyte/ β -CD [69], polyelectrolyte/ β -CD-modified polyelectrolyte [70], polyelectrolyte/poly(CD) [71] or even more recently poly(CD)/poly(CD) systems [72].

But only few examples of multilayer films based on host-guest interactions between β -CD and a guest molecule are reported in the literature. In 2002, Suzuki et al. reported the first assembly based on host-guest interactions [73]. They showed that electrostatic repulsions between PAH chains can be overcome through interactions between ferrocene moieties grafted on the PAH chains and a β -CD homobifunctionalized molecule. Three deposition steps of PAH-Fc alternating with the β -CD homobifunctionalized molecule were successfully performed on a gold substrate (Figure 1.17).

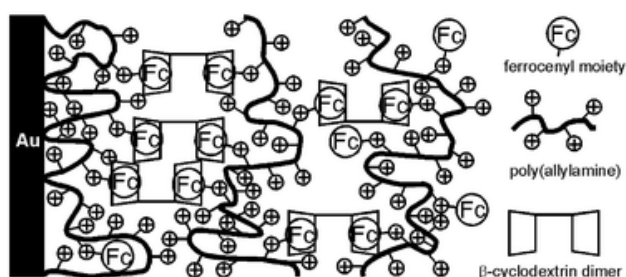


Figure 1.17: Assembly of positively charged-ferrocene-modified poly(allylamine) multilayer on a gold surface with the assistance of a β -CD dimer. [73]

Huskens and coworkers developed then a layer-by-layer assembly of adamantane-functionalized dendrimers and β -CD-functionalized gold nanoparticles on a β -CD SAM, obtaining well-defined thin multilayer films (Figure 1.18) [74]. Using nano-imprint lithography or transfer printing, they created 3D supramolecular assemblies with controlled size and geometry.

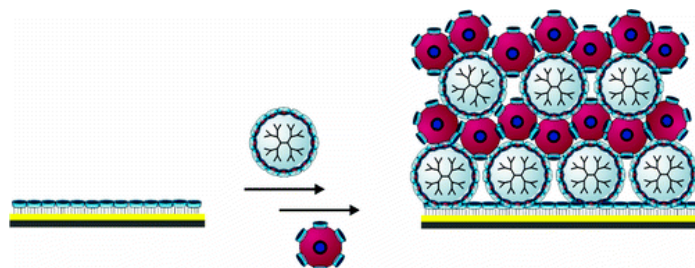


Figure 1.18: Assembly of adamantane-functionalized dendrimers and β -CD-modified gold nanoparticles. [74]

Later, in 2006, van der Heyden et al. reported the first assembly only based on host- and guest-modified polymers [75]. They showed that chitosan chains onto which were grafted respectively β -CD and Ad moieties can be alternately deposited on a gold surface covered with Ad-functionalized SAMs. PEM films constituted of only 2 to 4 layers were built depending on the density of Ad moieties exhibited by the surface (Figure 1.19). By using Fc- and β -CD-modified poly(allylamine), Wang et al. succeeded in depositing at least 8 bilayers on CaCO_3 particles [76]. The alternated incubation of the substrate in PAH-CD aqueous and PAH-Fc methanol solution allowed decreasing both the charge repulsion and the polymer dissolution during the film formation.

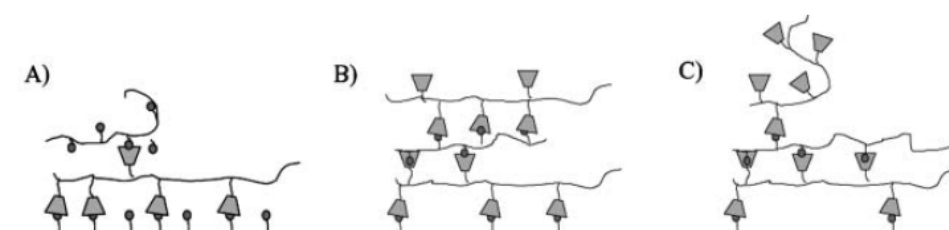


Figure 1.19: Schematic representation of the influence of the SAMs adamanty densities on the self-assembly buildup: (A) high, (B) medium and (C) low adamanty ratio exhibited by the SAM. [75]

Since the use of polyelectrolytes limits the number of effective deposition cycles, Dubacheva et al. developed a new approach by using neutral polymers. They succeeded in an unlimited host-guest multilayer film buildup in aqueous solution by using alternately neutral poly(N-hydroxypropylmethacrylamide) chains bearing respectively β -CD and Fc moieties.

Yet, none of these studies focused on the topography of the formed film and this will be one of the goals of my PhD.

1.4 Multilayer films as antimicrobial coating

PEM films have been developed for a large range of applications in fields as different as photodiodes [77, 78], optical devices [79], filtration membranes [80, 81], fuel cell membranes [82], biologically active membranes [83], drug release [84, 85] or biologically active coatings [86-88]. Here, we are interested in their use as antimicrobial coatings since it is in the context of my thesis. After a short presentation of the hospital acquired infections, a description of the antimicrobial peptides will be given. Finally, the different studies about PEM films used as antibacterial and antifungal coatings will be reported.

1.4.1 Medical context: hospital acquired infections

Implantable medical devices are widely used in surgery not only to replace altered or lost tissues but also in critical care for fluid or gas administration using catheters or tracheal tubes, respectively. These devices constitute an open gate for pathogen invasion [89]. Prevention of pathogen colonization of medical implants constitutes a major medical and financial issue since nosocomial infections represent one of the most serious complications after surgery or critical care. Indeed each year in Europe, 5% of patients admitted to hospitals suffer from hospital-acquired infections leading to a mortality of 10% [90]. The most encountered pathogens in nosocomial infections are *Staphylococcus aureus* (*S. aureus*) and *Candida albicans* (*C. albicans*). *S. aureus* [91] is a gram-positive bacterium and is one of the most virulent bacteria leading to high rates of device-related systemic infections and mortality. *C. albicans* is the most common human yeast pathogen and possesses the ability of forming biofilms that are sources of local and systemic infections. Biofilms are communities of pathogens embedded in a polysaccharide matrix adhering to a surface. These communities can form within a few hours [92]. First, free-floating bacteria encounter a submerged surface (such as a catheter), attach to it within a few minutes and start then to produce extracellular polymeric substances which allow the development of a complex three-dimensional structure: the biofilm (Figure 1.20).



Figure 1.20: The biofilm life cycle: (1) attachment of free-floating microorganisms to a surface and production of extracellular polymer substances (EPS) that lead to irreversible attachment, (2) maturation of the biofilm and (3) detachment of clumps or individual cells and propagation of the biofilm. [93]

Reaching a critical size, the biofilm can propagate through detachment of individual cells or groups of cells that attach to another surface. Bacteria are 10 to 1000 times more resistant to antibiotic under a biofilm form than under a planktonic one. Biofilms are responsible for 2/3 of hospital-acquired infections developed in the blood. In particular, *C. albicans* biofilms allow the formation of *S. aureus* microcolonies on their surface and by symbiotic interactions even enhance *S. aureus* resistance to antibiotics increasing the frequency or the severity of diseases [94].

The capacity of bacteria to more or less strongly adhere on a surface and to build a biofilm is depending on the kind of bacteria. Bacteria can be classified by their shape. For example, *Staphylococcus epidermis* (*S. epidermis*) is a spherical cocci and *Escherichia coli* (*E. coli*) is a cylindrical bacilli. But they are also commonly classified as Gram positive or Gram negative (Figure 1.21). Gram positive bacteria such as *S. epidermis* exhibit an outermost multilayered peptidoglycan cell wall, embedded with teichoic acid polymers at the top of the inner cell membrane that can include ion channels and protein receptors. In contrast, Gram negative bacteria such as *E. coli* exhibit a single peptidoglycan layer between a lipopolysaccharide-rich outer layer and phospholipid-rich inner layer [95].

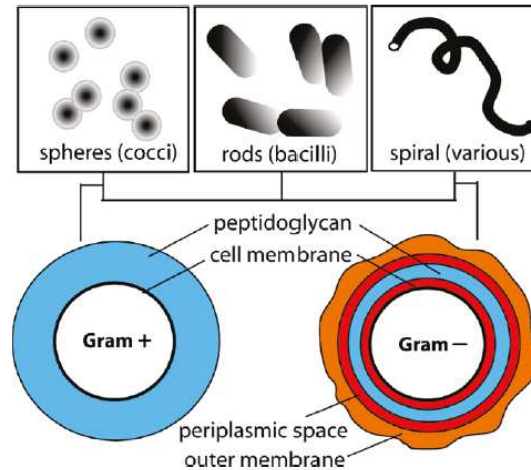


Figure 1.21: Classification of bacteria by shape and then by their outermost cell envelope composition [95].

Prevention of pathogen colonization of implantable medical devices constitutes a major medical and financial issue. For these reasons, there is a growing interest in the biomaterial field to provide new coatings and materials to prevent bacterial adhesion and biofilm formation.

1.4.2 Antimicrobial peptides

Antimicrobial peptides (AMPs) [96-99] are endogenous polypeptides that are part of the innate immune system of multicellular organisms including animals, plants, bacteria, fungi, viruses and humans. More than 800 different AMPs have been isolated in the last decades. Used in the macromolecular range, they are known to display a broad spectrum of antimicrobial activities against various microorganisms such as viruses, fungi, bacteria and parasites.

Classification of AMPs

AMPs form a chemically and structurally heterogeneous family, which renders it hard to define them, but most of them still share some common features. They generally are constituted of less than 50 amino acids and possess a cationic amphiphilic character. They have indeed the ability to adopt an amphipathic shape in which clusters of hydrophobic and hydrophilic amino acids segregate. Several classifications of AMPs exist in the literature but they are often classified into five categories based on their amino acid composition and structure: anionic, linear amphipathic α -helical, cationic peptides enriched in specific amino

acids, peptide fragments and peptides with cysteines that form intramolecular bonding (see Table 1.1).

Table 1.1: Classification of antimicrobial peptides by their amino acid composition and structure. Inspired from Brogden et al. [100].

Class	Characteristics	Examples
Anionic peptides	Contain glutamic or aspartic acids	Maximin H5 from amphibians [101], dermcidin from humans [102]
Linear cationic α -helical peptides	Lack in cystein	Cecropin P1 from nematodes [103], magainin 2 from amphibians [104]
Cationic peptides enriched for specific amino acids	Rich in proline, arginine, phenylalanine, glycine, tryptophan	Abaecin from bees [105], indolicidin from bovines [106]
Peptide fragments	Cationic, β -turn	Lactoferrin from lactoferrin [107], cathelicidins from mammals [108]
Charged peptides with cysteine	Contain 1 to 3 disulfide bonds	Defensins A from insects [109], protegrin from porcines [110]

The first group is composed of anionic peptides. These peptides are rich in aspartic acid or glutamic acid, which provide negative charges. The second group contains linear cationic α -helical peptides that are disordered in solution but that adopt an α -helical secondary structure once in contact with membranes. The third group is composed of linear peptides enriched in specific amino acids such as proline, tryptophan, glycine, histidine and arginine. AMPs of this group lack of cysteine residue, making them very flexible and fluid in solution. The fourth group is formed by charged peptides that are fragments of large proteins. The fifth group is composed of AMPs rich in cysteine residues. They are usually cyclic peptides with β -sheets that are stabilized by disulfide bonds.

Mechanism of action

Despite their vast diversity, most AMPs act by disrupting the integrity of the microbial cell membrane. Diamond et al. [98] proposed a mechanism of action in three steps: attraction, attachment and insertion of the peptides in the membrane. Attraction is presumed to occur via electrostatic interactions between the cationic peptides and the negatively charged moieties on the microbial cell membrane. Beside electrostatic interactions, hydrophobic and polar residues

play a crucial role in the attachment step. AMPs can indeed adopt a secondary structure, which is energetically favorable, once close to phospholipids membranes. The last step is the insertion of the peptides in the membrane. Several models of penetration have been found that depend on the class of the AMPs and also on the microorganisms [100, 111]. The three main models are the carpet model, the barrel-stave and the toroidal pore model (Figure 1.22). In the case of the carpet model, there is an accumulation of AMPs on the bilayer surface until a saturation point is reached where the membrane disintegrates and forms micelles. In the case of the barrel-stave model, AMPs form a bundle in the membrane with a pore in the center. The hydrophobic regions of the AMPs interact with the phospholipids of the membrane while the hydrophilic ones are oriented inward into the water-filled pore. The toroidal pore model is rather similar to the barrel-stave model. They differ by the fact that the AMPs are always associated with the lipid head groups even when perpendicularly inserted into the lipid bilayers.

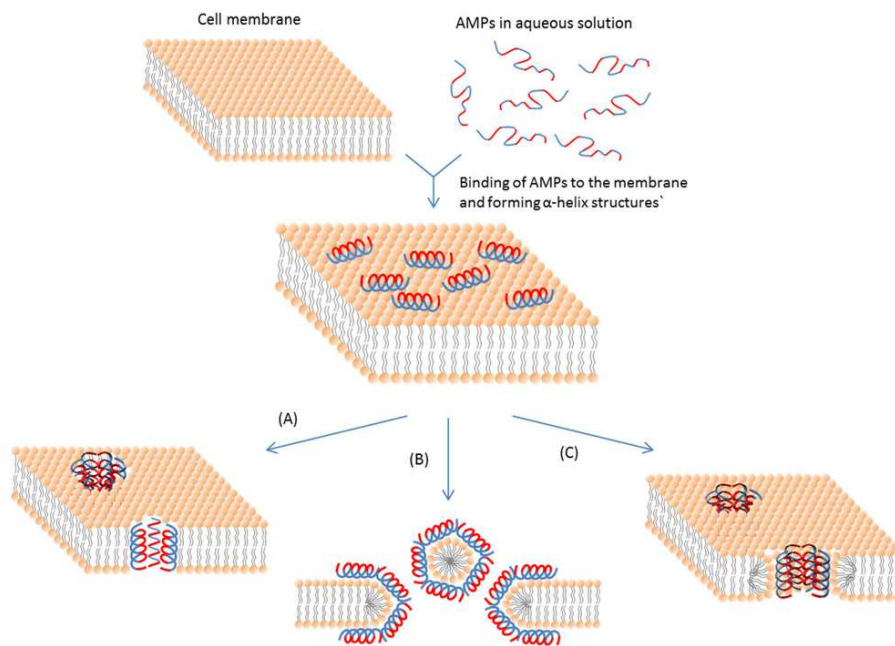


Figure 1.22: Schematic representation of some action mechanisms of AMPs disrupting the microbial cell membrane. (A) Barrel-stave model: AMPs insert themselves into the membrane perpendicularly. (B) Carpet model: Small areas of the membrane are coated with AMPs with hydrophobic sides facing inward leaving pores behind in the membrane. (C) Toroidal pore model: This model resembles the barrel-stave model but in this case AMPs are always in contact with phospholipid head groups of the membrane. The blue color represents the hydrophobic parts of AMPs whereas the red color represents their hydrophilic part.[111]

Besides the membrane disruption, AMPs have other ways to kill a pathogen. Once they have penetrated inside the cell, AMPs act on intracellular targets of cytoplasmic

components crucial to proper cellular physiology. They can for example inhibit protein or cell-wall synthesis and also interact with DNA or RNA [98].

Chromogranin A and its derived antimicrobial peptides

Chromogranin A (CgA) is a protein composed of 439 amino acid residues for humans and 431 for bovines and belongs to the granin family. This protein is located in secretory vesicles of endocrine, immune and neuron cells [112]. Chromofungin, vasostatin, catestatin and its active form cateslytin are four antimicrobial peptides derived from CgA (Figure 1.23) [113, 114]. We took an interest in particular for cateslytin, corresponding to CgA₃₄₄₋₃₅₈, that is a positively charged (5+) arginine-rich AMP and that possesses antimicrobial activities against both bacteria and yeasts. In the intragranular matrix, CgA fragments result from the processing of CgA by numerous enzymes such as prohormone convertases (PC1 and 2), aminopeptidases and carboxypeptidases. In the extracellular medium, larger forms may be processed by kallikrein located at the plasmic membrane level and by circulatory proteolytic enzymes such as plasmin and thrombin [115]. In addition, some virulent bacteria produce proteolytic enzymes, for example Glu-C protease for *S. aureus*, and might continue the natural processing of CgA to generate the chromofungin and catestatin fragments during infections [115, 116].

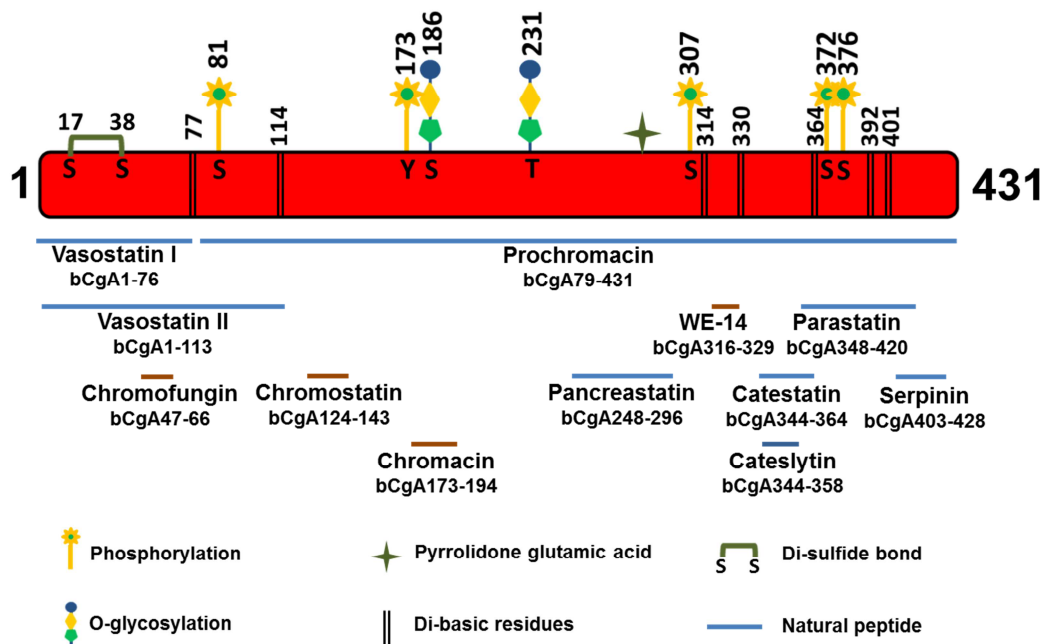


Figure 1.23: Localization on the sequence of bovine chromogranin A of derived peptides. [117]

Cateslytin

As antimicrobial peptide of interest for my thesis, the antimicrobial mechanism of action of cateslytin will be briefly described here. It was demonstrated that cateslytin interacts with fungal membrane by adopting an aggregated antiparallel beta-sheet structure at the negatively charged surface of the bacterial membranes [118] and generates pores of 1 nm diameter [119] that destabilize then the membranes leading to the bacteria death. The five arginine residues that CTL possesses are essential for the binding to the negatively charged lipids of the bacterial membrane.

1.4.3 Polyelectrolyte multilayers as antimicrobial surfaces

Prevention of microbial adhesion and proliferation on implant surfaces is a topic of major medical and financial importance. Three main kinds of coatings have been developed to reduce microbial colonization of material surfaces: adhesion-resistant, contact-killing and antimicrobial agent leaching coatings (Figure 1.24). PEM films were developed for the functionalization of implants in order to inhibit the adhesion and the proliferation of microbes such as bacteria, fungi and yeasts. After a brief description of the methods used to evaluate anti-adhesive and antimicrobial properties of PEM films, the state of the art will be described in details for PEM films.

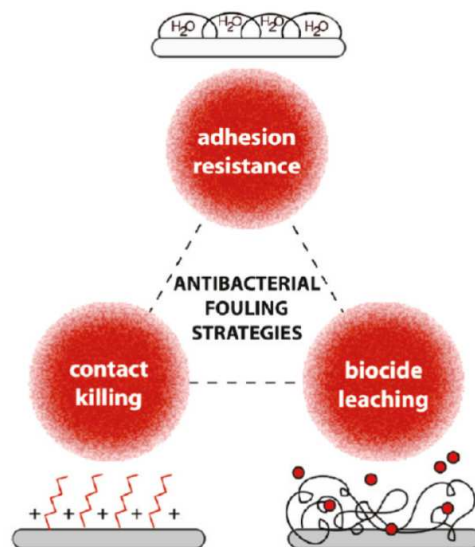


Figure 1.24: Three main strategies for antimicrobial surface design. [95]

Methods used to characterize adhesion-resistant and antimicrobial PEM films

Adhesion-resistant PEM films are coatings that inhibit or limit microbial adhesion on their surfaces. To evaluate microbial adhesion, PEM films were submitted to typical microbial adhesion assays. No agreement on a unique method exists in the literature but similar microbial adhesion assays are reported. After overnight culture at a defined temperature, generally 37°C, pathogens are harvested in mid-exponential growth phase, diluted in the suitable culture media at 10^6 - 10^7 cells.mL⁻¹ and plated on the substrate. After 30 min to 2 h of contact, the substrate is rinsed with a buffer solution. Adhered pathogens are visualized and counted using an optical, a scanning electron or a fluorescent microscope when pathogens are fluorescently tagged. After an incubation of the rinsed substrate on an agar plate in the culture media, the growth of the adhered bacteria can be evaluated by counting the colonies formed (Figure 1.25a and b).

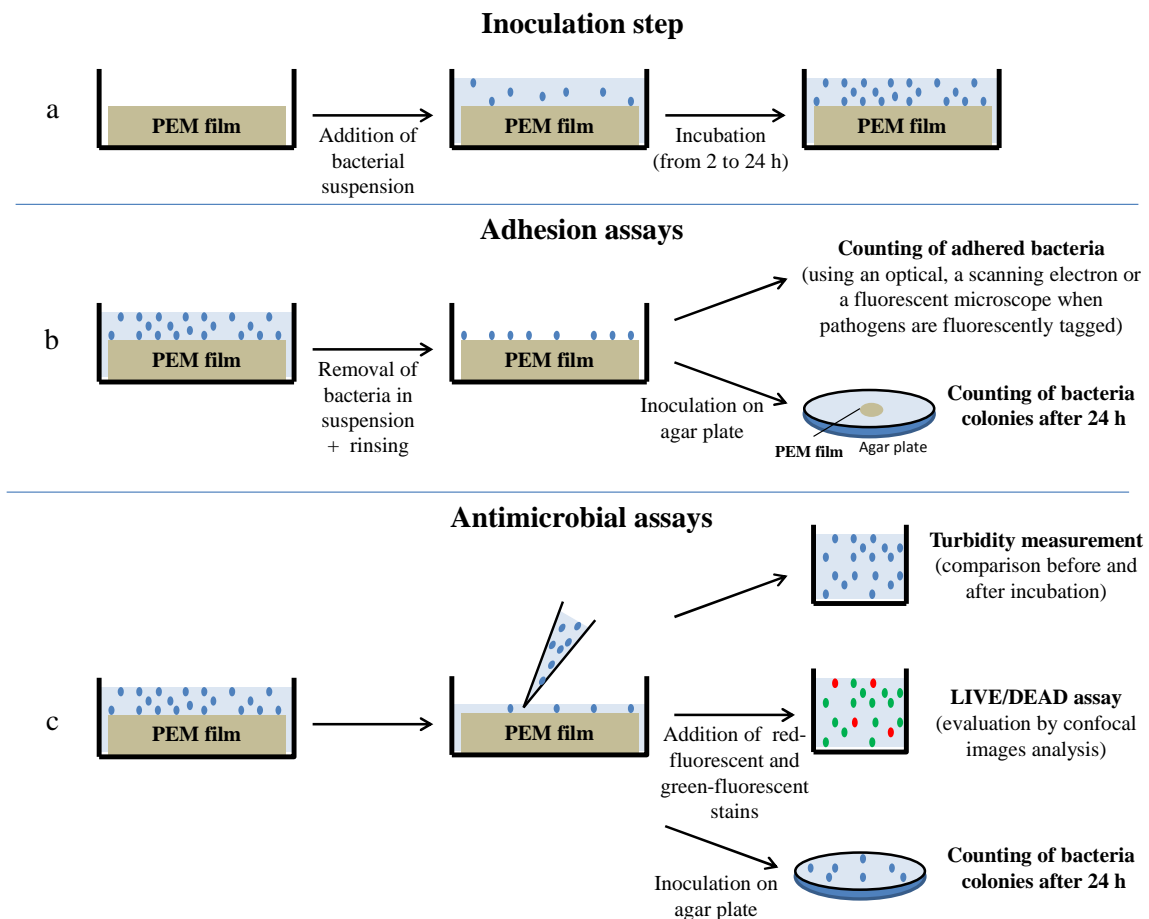


Figure 1.25: Schematic representation of adhesion and antimicrobial assays performed on PEM films: first an inoculation step is performed followed by an adhesion or an antimicrobial assay. (a) Inoculation step: contact between the PEM film and the microbes for a certain time. (b) Adhesion assays: after removal of the bacterial suspension, the remaining bacteria on the surface of the PEM film are counted or an agar plate assay is performed to see if adhered bacteria are forming new colonies. (c) Antimicrobial assays: the number of bacteria in the suspension is evaluated by turbidity measurement, by LIVE/DEAD assay or by agar plate assay.

Contact-killing PEM films inhibit bacterial adhesion by disrupting the bacterial membranes leading to their death. Several tests are reported in the literature to determine the antimicrobial properties of such films. One approach is to determine the bacterial growth in contact with the coating by turbidity measurements using a spectrophotometer at a wavelength of 600-650 nm. A bacterial suspension with a known turbidity is put in contact with the tested coating. After 24 h of incubation at 37°C, the turbidity of the suspension is measured and compared to the value of the suspension in the absence of any biocidal agent. A decrease in turbidity is directly linked to a microbial growth inhibition [120]. A second approach for evaluating antibacterial activity is to incubate the coating with 10^6 - 10^7 bacteria cells.mL⁻¹ suspension at 37°C for 24 h on a shaker table and to determine the number of surviving bacteria in the culture medium. To achieve that, two methods can be used: the spread plate method which consists in inoculating the supernatant on agar plates and in counting the colonies after 24 h of incubation [121, 122] or the LIVE/DEAD assay. The LIVE/DEAD assay is based on the use of mixtures of two nucleic acid stains, a green-fluorescent (emission wavelength at 500 nm) and a red-fluorescent (emission wavelength at 635 nm). These stains differ in their ability to penetrate healthy bacterial cells. The red-fluorescent stain generally labels all bacteria present, those with intact membranes and those with damaged membranes. In contrast, the green-fluorescent stain penetrates only bacteria with damaged membranes, causing a reduction in the red fluorescence stain when both dyes are present. Thus, bacteria with intact cell membranes appear fluorescent in red, whereas bacteria with damaged membranes are fluorescent in green [123, 124]. The number of dead and live bacteria is determined through image analysis using a confocal laser scanning microscope (Figure 1.25a and c).

Release-killing PEM films possess antimicrobial agents that leach in the environment. The Kirby disk diffusion (Figure 1.26) method allows evaluating the antimicrobial properties of biocide leaching coatings. This method is based on the diffusion of an antimicrobial agent from a disk into a solid culture medium seeded with bacteria. The coated substrate is placed on the top of an agar plate, where bacteria have initially been spread on, and incubated at 37°C for 24 h. A gradient of the antimicrobial agent is obtained by diffusion from the coating into the seeded culture media. The zone of inhibition becomes visible when the antimicrobial agent concentration becomes too diluted. An inhibition diameter proportional to the bacterial susceptibility of the antimicrobial agent present in the coating is determined [125].

Antimicrobial assays such as the ones reported in Figure 1.25c were also conducted on release-killing PEMs.

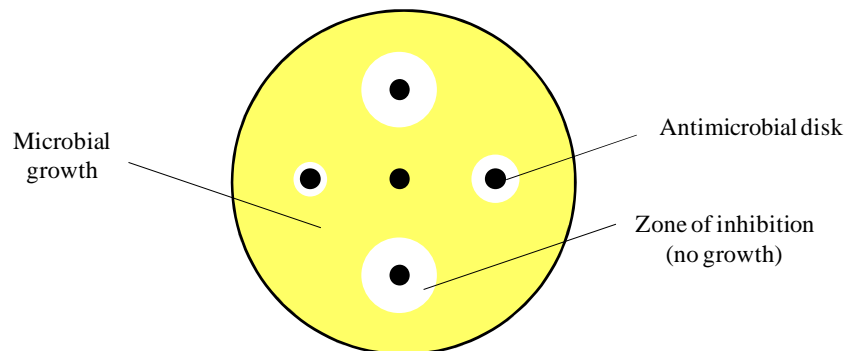


Figure 1.26: Example of a Kirby disk diffusion assay. A bacterial culture is first deposited on a nutrient agar plate, then the antimicrobial disks to be tested are placed on the surface and the zones of inhibition can be measured after 24 hours of incubation.

All these methods can be adapted to antifungal tests simply by using an adapted culture medium and conditions for fungi [126].

Adhesion-resistant PEMs

Adhesion-resistant PEMs were obtained by two main strategies: (1) inhibiting the close approach or the contact of the bacteria with the surfaces by building hydrophilic polymers based PEM films and (2) modulating the stiffness of the PEM films so that the bacteria do not adhere once entering in contact with them (Figure 1.27).

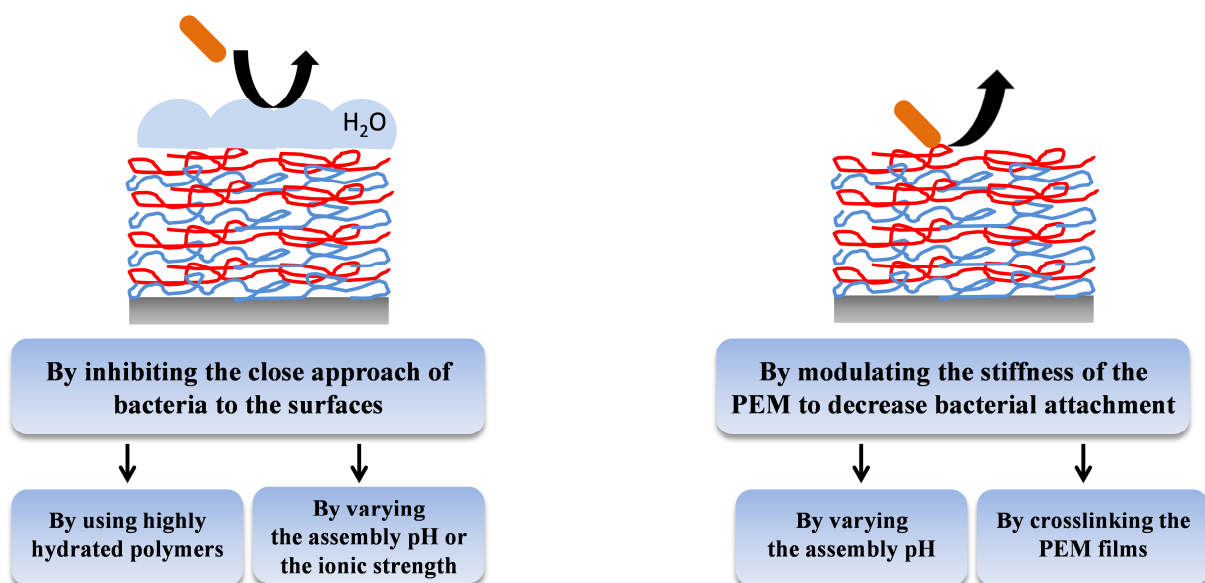


Figure 1.27: Scheme of the different strategies that have been used to build adhesion-resistant PEMs.

Hydrophilic polymers based PEMs

To develop bacterial adhesion-resistant surfaces, one of the strategies consists in the use of hydrophilic polymers that can inhibit contact or close approach of bacteria with the surfaces due to their strong affinity with water molecules. Adsorbed or grafted on a surface, poly(ethylene glycol) (PEG) molecules form a highly hydrated polymer layer reducing protein adsorption [111, 127, 128], platelet adhesion [129] and bacterial adhesion [130]. The first study reporting the insertion of PEG in a multilayer film in order to enhance its anti-adhesive properties towards bacteria was done by Boulmedais et al. in 2004 [131]. A PEG functionalized poly(L-glutamic acid), PGA-g-PEG (Figure 1.28a), was synthesized and combined with poly(L-lysine) (PLL) to build PEM films. In comparison with the uncoated glass substrate, the adhesion of *E. coli* was reduced by 72% on PEM films ended by one PLL/PGA-g-PEG bilayer and by 92% on films ended by three PLL/PGA-g-PEG bilayers (Figure 1.28b).

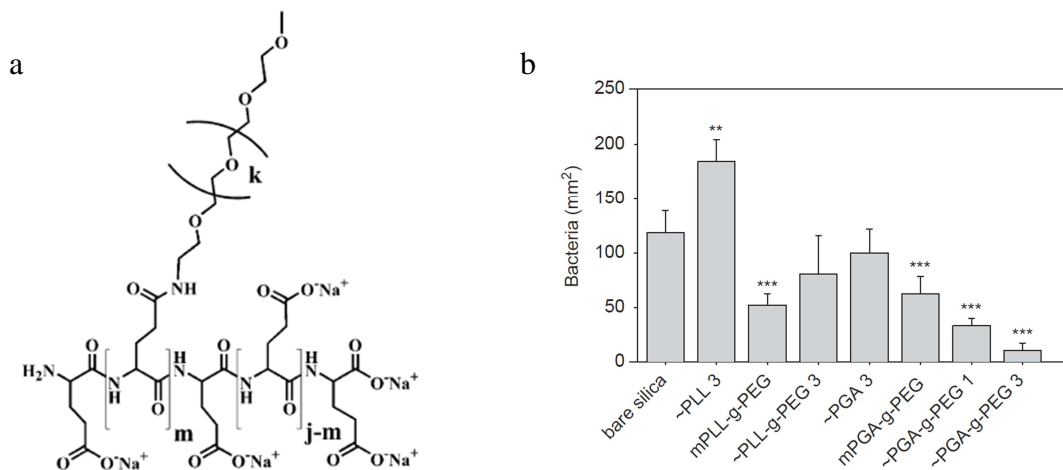


Figure 1.28: (a) Chemical structure of PGA-g-PEG where $k \sim 45$, $j \sim 330$ and $m \sim 60$. (b) Bacterial adhesion per mm^2 on bare silica, mPLL-g-PEG = PLL-g-PEG monolayer, mPGA-g-PEG = (PLL/PGA-g-PEG)₁ and multilayer films ~PLL 3 = Pre-(PLL/PGA)₂, ~PLL-g-PEG 3 = Pre-PLL-(PGA/PLL-g-PEG)₃, ~PGA 3 = Pre-(PLL/PGA)₃, ~PGA-g-PEG 1 = Pre-(PLL/PGA-g-PEG)₁ and ~PGA-g-PEG 3 = Pre(PLL/PGA-g-PEG)₃ with Pre PEI-(PEI-(PLL/PGA)₂-PGA precursor film. [131]

Later to minimize non-specific adhesion in poly(dimethylsiloxane) (PDMS) based microfluidic devices, a similar approach was used against a yeast, *Saccharomyces cerevisiae*. A pegylated PAA (PAA-g-PEG) was adsorbed as terminal layer on a PAA/PAH or a PAA/PDADMAC PEM film [132, 133]. Compared to a bare PDMS substrate, a reduction of yeast cell adhesion of at least two orders of magnitude was found for the most efficient coating, i.e. a PAA-g-PEG ended PAA/PDADMAC film. It has to be noted that hydrated PAA/PAH and PAA/PDADMAC films already possess some anti-adhesive properties when

deposited on PDMS substrates [132, 133] or polysulfone microfiltration membranes [134]. This is attributed to their highly swollen and hydrated structure. Using a zwitterionic group present at the surface of cell membranes, Reisch et al. investigated the anti-adhesive properties of PEM films ended by PAA modified by triethylene glycol bearing phosphorylcholine moieties (PAA-(EO)₃PC). The adhesion of *C. albicans*, a yeast, was completely inhibited when only one layer of PAA-(EO)₃PC was deposited [135].

Highly hydrated polysaccharides can also be used to build anti-adhesive PEM films. Heparin (HEP) [136], a strong polysaccharide and HA [137], a weak polysaccharide, are known to prevent the adhesion of bacteria due to their hydrophilicity. Chitosan (CHI) is a weak cationic polysaccharide known for its intrinsic antibacterial property [138]. The assembly pH plays a crucial role in the anti-adhesive properties of CHI/HEP films [139, 140]. By varying the assembly pH from 2.9 to 6, the ionization degree of CHI is varied. At high pH values, CHI chains, with low charge density, adopt loopy structures and tend to adsorb as thick layers. At low pH values, CHI chains adopt flatter structures and the adsorbed layer is thinner. The surface composition of PEM films could thus be tuned by the assembly pH. The most hydrophilic PEM film, rich in HEP, entailed the better anti-adhesive properties whereas the most CHI rich surfaces had the most efficient antimicrobial properties against *E. coli* [139]. The effect of the ionic strength on the anti-adhesive properties of CHI/HA films was studied by Richter et al [34]. Compared to a bare glass substrate, CHI/HA films assembled at 0.15 M NaCl led to a decrease of about 80% in *E. coli* adhesion whereas only 40% of decrease was found when assembled at 10⁻² M NaCl. The higher adhesion of bacteria on the latest could be explained by the fact that thin films with high rigidity were obtained at 10⁻² M NaCl. The chemical crosslinking of CHI/HA films allowed retaining the anti-adhesive properties even after 21 days of immersion in PBS [141].

Influence of PEMs stiffness

The first study reporting the influence of the elastic moduli of PEM films on bacterial adhesion was performed by Lichter et al. in 2008 [142]. The effective stiffness of PAH/PAA films was varied over several orders of magnitude (elastic modulus ranging from 1 to 100 MPa) by tuning the assembly pH. Bacterial attachment of *Staphylococcus epidermis* (Gram positive bacteria) and *E. coli* (Gram negative bacteria) increased with the stiffness of the PAH/PAA films independently of other surface characteristics such as surface roughness, surface interaction energy or surface charge density. More recently and for lower elastic

moduli, further investigations on this matter were conducted by Saha et al. [143]. Photocrosslinkable PEM films with different mechanical properties (elastic modulus ranging from 30 to 150 kPa) were prepared from PLL and HA modified by photoreactive vinylbenzyl groups (HAVB) under UV light illumination (Figure 1.29c). PLL/HAVB films were put in contact during 1 h with Gram positive and Gram negative bacteria strains. After a gentle rinsing, the growth of bacteria was followed for 8 h of incubation at 37°C with their specific media. While the growth of Gram positive *Lactococcus lactis* was independent of the rigidity of PLL/HAVB PEM films, the growth of Gram negative *E. coli* was slowed down on stiffer films compared to softer ones. When incubated onto photo-patterned PLL/HAVB films having a rigidity micropattern, a larger amount of *E. coli* was observed on softer background and on the border between softer and stiffer regions (Figure 1.29a and Figure 1.29b). In the same range of variation of the elastic moduli, an opposite effect was found for mammalian cells [144]. Stiff PLL/HAVB PEM films can thus promote the growth of mammalian cells while limiting the bacterial colonization.

To conclude, the film stiffness seems to play a crucial role in the adhesion of bacteria cells. Depending on the range of the elastic modulus, an increase of PEM films stiffness can favor or limit bacterial adhesion.

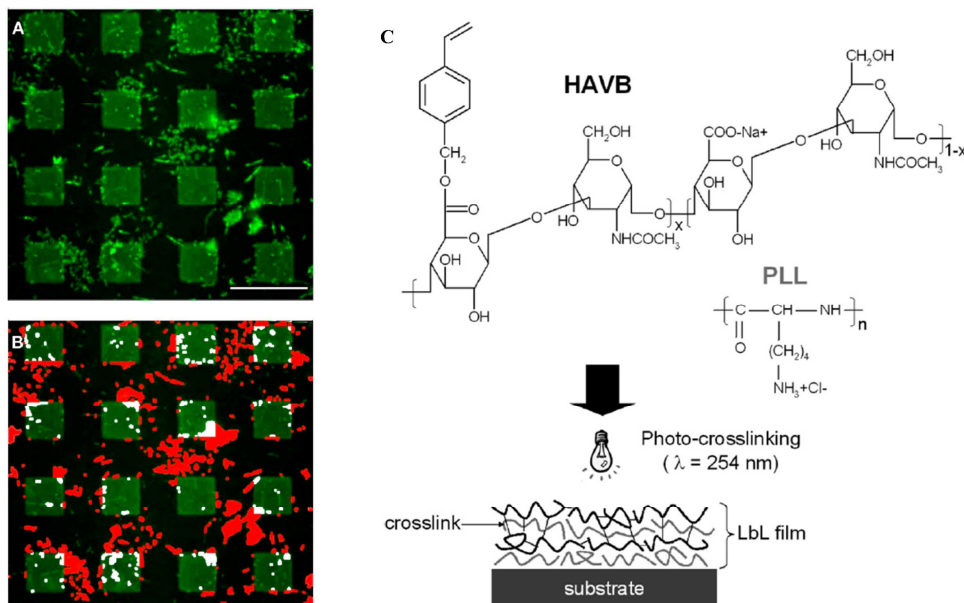


Figure 1.29: (A) Microscopy epifluorescence image showing *E. coli* M6155 after 4.5 h of growth on photopatterned films; the lighter $20 \times 20 \mu\text{m}^2$ features correspond to stiffer photo-crosslinked regions while the dark background corresponds to a non-crosslinked film. The fluorescent contrast observed between the features and the background results from the presence of a photomask incorporated into the transparent fused silica substrate used to prepare the film. The scale bar represents $40 \mu\text{m}$. (B) Analysis of the same image to discriminate the bacteria colonies adhered on the photo-crosslinked regions (white patches) and the non-crosslinked background (red patches). For this specific image, the relative surface occupied by the bacteria is 8 and 12% over photo-crosslinked and non-crosslinked regions. (C) Preparation of photo-crosslinked (PLL/HAVB) LbL films. [143]

Contact-killing PEMs

Most bacterial cell membranes are negatively charged, hence most antimicrobial polymers are positively charged. Cationic contact-killing PEM films could be developed using positively charged polyelectrolytes. Due to cationic charges available on their surface, they inhibit bacterial adhesion and proliferation by disrupting their membranes leading to death. Only few contact-killing PEMs were obtained by immobilizing antimicrobial agents within them that do not act by cationic contact-killing. (Figure 1.30)

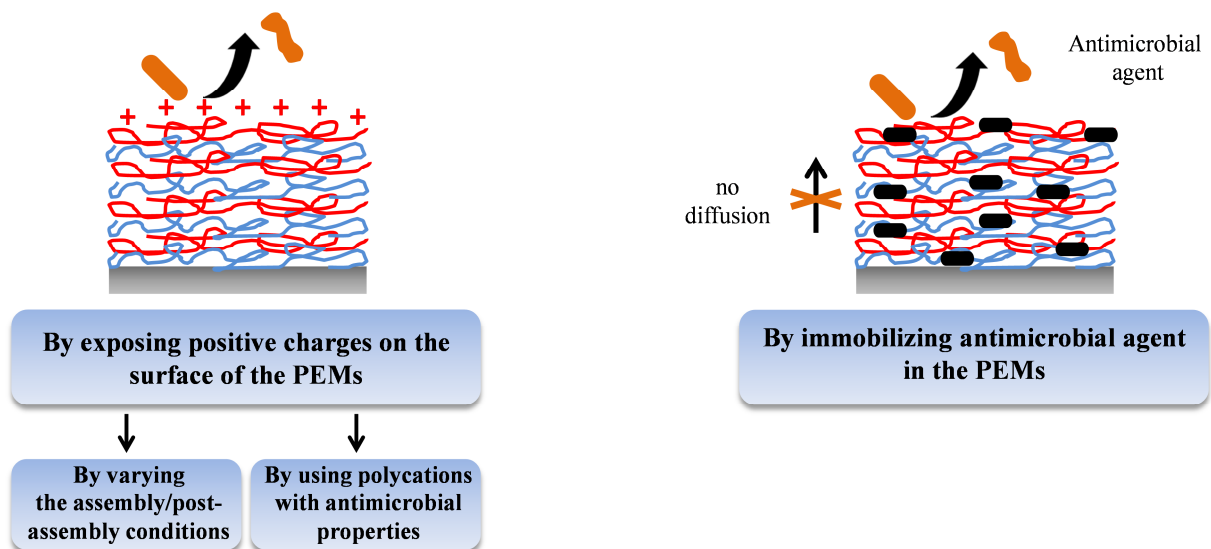


Figure 1.30: Scheme of the different strategies that have been used to build contact-killing PEMs.

Influence of the assembly and post-assembly conditions of PEMs

The assembly and post-assembly pH of PEM films such as PAH/PSS and PAH/PAA were modified in order to expose enough mobile cationic charges and to obtain antimicrobial activity against *S. epidermis* and *E. coli* [145]. At high pH, near or above their pKa, PAH chains are incorporated with many uncharged amine groups into PEM films, revealing no contact-killing ability. By lowering the pH, these uncharged amines are protonated creating sufficient positive charges to induce cell death (Figure 1.31).

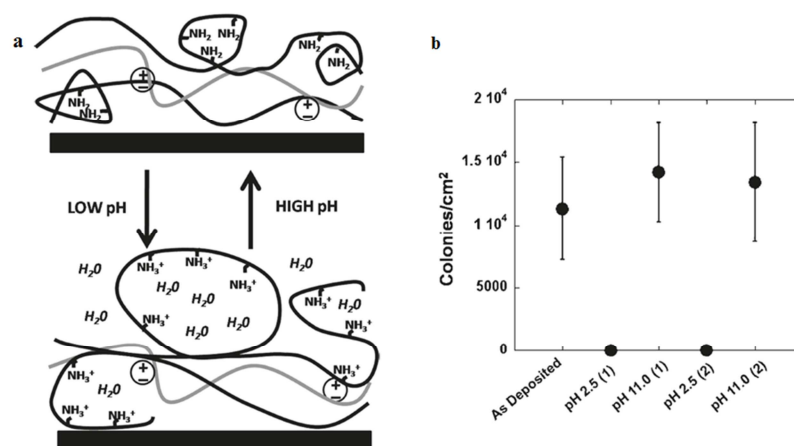


Figure 1.31: (a) Schematic representation of acid-activated opening of hydrophobic clusters in PSS/PAH 9.3/9.3 PEMs. The hydrophobic clusters can be reformed with subsequent treatment at high pH. (b) Airborne antibacterial tests with *S. epidermis* (non-biofilm forming strain) with films that have been cyclically pH treated to form swollen or unswollen structures. Note that each point represents a different set of samples cycled a different number of times (given by the number in parentheses). For example, pH 2.5 (2) was treated at pH 2.5, then pH 11.0 and then again pH 2.5 before the bacteria assay. [145]

Phenolic compounds are known to cause bacterial cell death through disintegration of the cell membrane. They interact with the surface of the cell through van der Waals interactions of the phenyl ring and the hydrophobic tails of the lipids. Pinto et al. reported the use of poly(4-vinylphenol) (PVPh) assembled with PAH or PDADMAC at pH ranging from 10.5 to 12.5 [146]. Both systems led to a high *S. epidermis* growth inhibition, which was of about 60% at pH 10.5. Only a small antibacterial activity was found against *E. coli*. The increase in antimicrobial efficacy at the lower assembly pH was likely due to the protonation of the phenol moiety that increased the mode of action of the multilayer.

Chitosan based PEMs

Most of the other approaches involved the use of polyelectrolytes that possess intrinsic antimicrobial properties. Associated with other polysaccharides such as pectin [126], lentinans [122], carrageenans [123], alginate [125, 147] or poly(amino acids) [147], CHI (Figure 1.32) based PEM films inhibited bacterial and fungal growth when a sufficient number of layers was reached. PEMs ended by a CHI layer were reported to possess slightly better antibacterial properties which is explained by a higher amount of amino groups available on the surface [123, 125]. In the case of the poly(lentinan sulfate)/CHI system, poly(lentinan sulfate) ended PEM films exhibited better antimicrobial properties than CHI ended ones, showing clearly the inherent antibacterial activities of poly(lentinan sulfate) itself. The antibacterial properties of CHI/ALG [148] or CHI/pectin [149] films deposited on

nanofibrous mats were slightly improved by binding a layered silicate, organic rectorite, with one of the polyelectrolytes during the assembly [150].

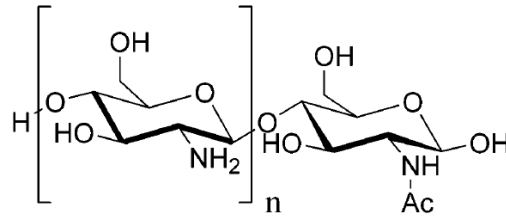


Figure 1.32: Chemical structure of chitosan [138].

To further improve the antibacterial properties of CHI based PEM films, CHI was assembled with antibacterial proteins like phosvitin [151] and lysozyme [152]. Phosvitin (PV), a polyanionic phosphoglycoprotein present in egg yolk, is one of the strongest metal (iron, calcium, etc.) chelating agents. Its antimicrobial property is based on its iron binding ability to disrupt bacteria cell membranes [153]. Lysozyme is a protein which can damage bacterial cell walls by acting on their peptidoglycans [154].

In order to further enhance the properties of antibacterial coatings in particular in the first 24 h decisive period, a strategy was developed by Wang et al. where an adhesion-resistant PEM film, a thermally crosslinked polyvinylpyrrolidone (PVP)/PAA film, was built on top of a contact-killing CHI/HEP film (Figure 1.33a) [155]. Incubated in phosphate buffer at pH 7.4 and at 37°C, the continuous removal of the top PVP/PAA film inhibited *S. aureus* adhesion. After degradation of the outmost surface, the underlying CHI/HEP film was exposed to the external environment and showed contact-killing properties. Figure 1.33b shows indeed that a (HEP/CHI)₁₀ film greatly inhibited *S. aureus* adhesion after 5 min, 4 h and 24 h compared to a bare silicon surface. It also shows that a (HEP/CHI)₁₀-(PVP/PAA)₁₀, which was crosslinked at 110°C for 16 h, exhibited enhanced anti-adhesiveness of bacteria. However, when the (HEP/CHI)₁₀-(PVP/PAA)₁₀ was crosslinked at 170°C for 4 h, it became non degradable and lots of bacteria adhered on the surface already after 5 min.

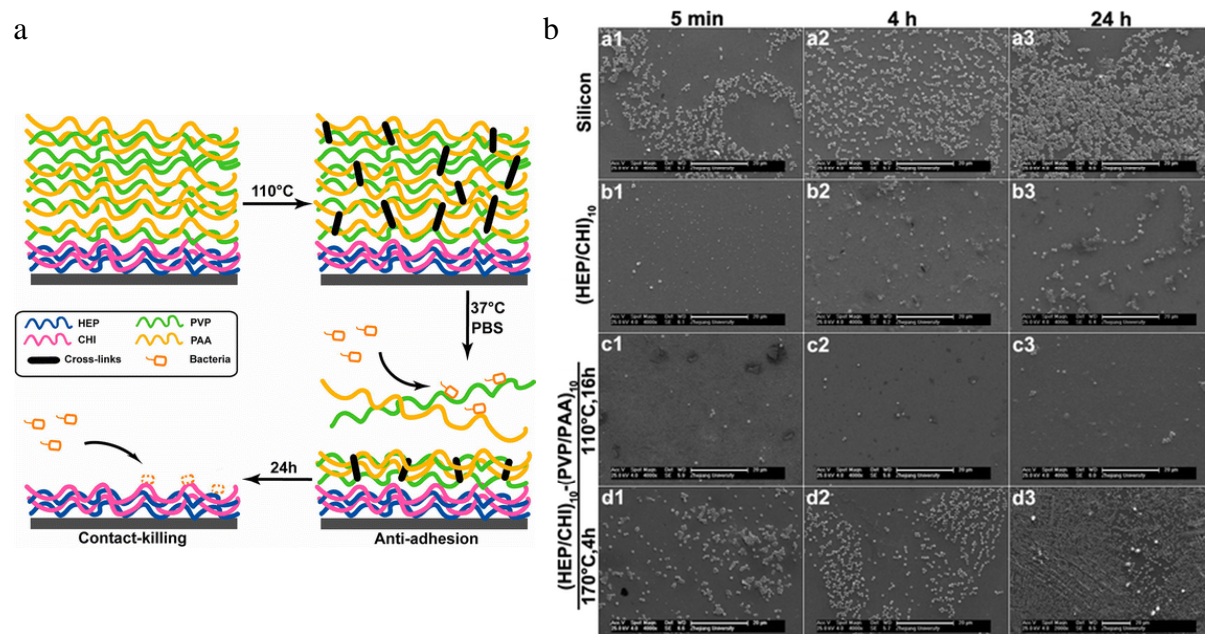


Figure 1.33: (a) Schematic representation of construction, crosslinking, degradation, and antibacterial properties of the $(\text{HEP}/\text{CHI})_{10}$ – $(\text{PVP}/\text{PAA})_{10}$ multilayer film. (b) SEM images of water-borne assays of *S. aureus* adhesion on silicon wafer (a1–a3), the $(\text{HEP}/\text{CHI})_{10}$ multilayer film (b1–b3), and the $(\text{HEP}/\text{CHI})_{10}$ – $(\text{PVP}/\text{PAA})_{10}$ multilayer films cross-linked at 110 °C for 16 h (c1–c3) or at 170 °C for 4 h (d1–d3). Samples were measured after bacterial contacting for 5 min, 4 h, and 24 h. Scale bars are 20 μm . [155]

To improve the antibacterial activity of CHI, quaternized derivatives of CHI (QCHI) were synthesized [156] and incorporated into PEM films [157, 158]. The degree of substitution of QCHI (Figure 1.34c) was demonstrated to be a crucial parameter to inhibit bacterial growth. The higher degree of substitution led to the lowest survival of *E. coli* bacteria (Figure 1.34d). Contact-killing QCHI/HA microcapsules, based on QCHI with the highest degree of substitution, presented thus the most efficient effect on killing *E. coli* [157]. QCHI ended capsules appeared to be more effective at killing bacteria than HA ended ones as it is visible in Figure 1.34a and 1.34b, knowing that a red labelling corresponds to living cells. Bacteria appeared to be stuck on microcapsules probably due to attractive electrostatic interactions between the positively charged capsules and the negatively charged bacteria (Figure 1.34b).

CHI derivatives were associated with HEP to obtain both anti-adhesive and antibacterial PEM films [159]. The first reported PEM films that are both antibacterial and antifungal were obtained using carboxymethyl CHI and pectin crosslinked by glutaraldehyde [126]. Coated on a polypropylene film, these films were used for tomato packaging and kept it almost intact with no apparent rotting infection for 13 days.

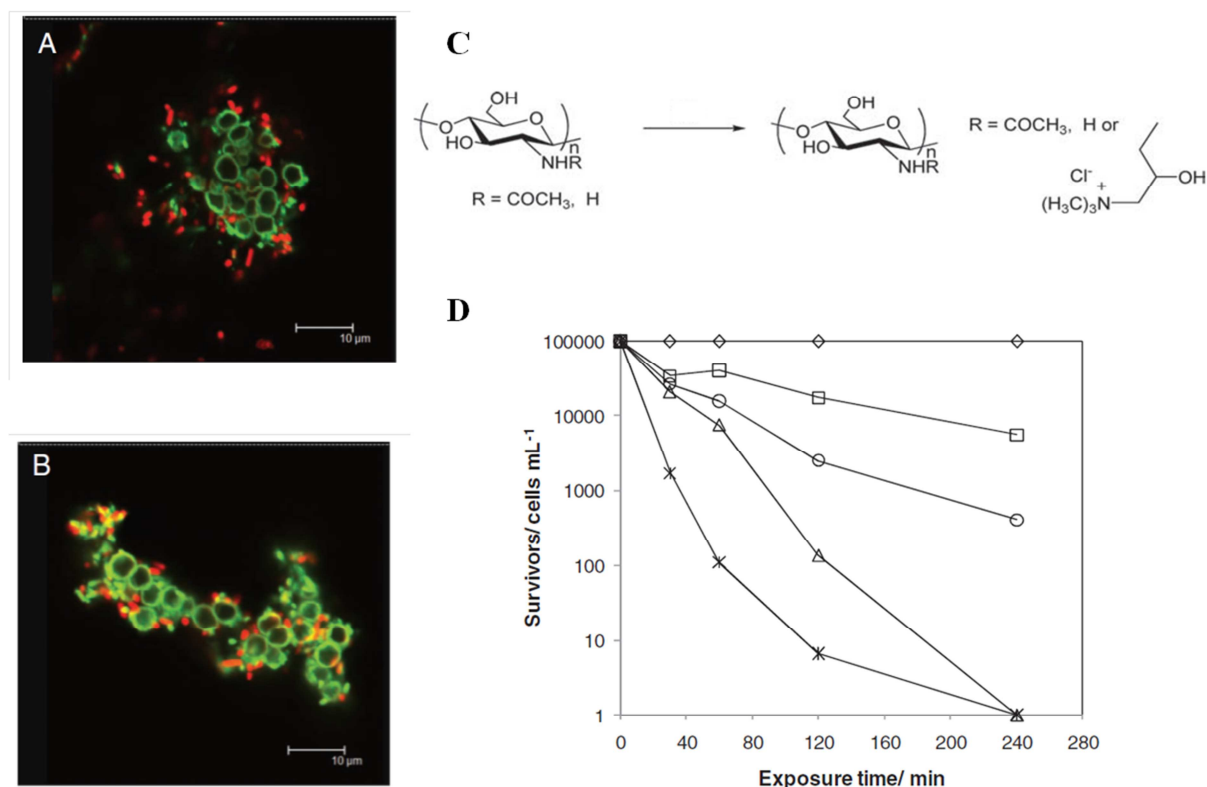


Figure 1.34: (A) and (B): confocal microscopy images obtained by the overlay of the green and the red channels. (A) (HA/QCHI)_{4,5} capsules ending with HA and (B) (HA/QCHI)₅ capsules ending with QCHI after 20 h of incubation with *E. coli* bacteria (capsules/bacterial cells ratio ~ 1). Some diffusion of the green dye within the microcapsules wall was observed. Most bacteria co-incubated with HA-ending capsules were alive (red fluorescence). In contrast, most bacteria associated with QCHI-ending capsules appeared green, which indicates they have been killed. The intense and dense green spots at the capsules wall, which is particularly observed in (B) is attributed to the presence of dead bacteria and bacterial debris. Bacteria appeared to be stuck on the QCHI-ending capsules, which reflects the preferential interactions of these capsules with the bacteria. (C) Quaternization reaction of chitosan. (D) Antibacterial activity against *E. coli* of QCHI derivatives with different degrees of substitution: (□) 0.31, (○) 0.39, (△) 0.55, (X) 0.66, (◇) control PBS. [157]

Quarternary ammonium polymers based PEMs

Quaternary ammonium compounds (QAC), that possess the advantage of being permanently charged independently of the solution pH, are known to possess antimicrobial properties. Polymeric quaternary ammonium salts have thus been incorporated into PEM films [160-162]. The association of N,N-dodecyl,methyl-polyethylenimine (DMLPEI) and PAA leads to the growth inhibition of both Gram positive and Gram negative bacteria as well as of an influenza A/WSN (H1N1) virus when built in optimal conditions [161]. After Rubner and coworkers [145], Wong et al. demonstrated the importance of the pH assembly using PAA, a weak polyacid. Thicker and more brush-like PAA layers were obtained at low pH that left more available positive charges on the surface for interaction with the bacterial cell

membrane. At higher pH, flat layers of PAA underwent greater electrostatic interactions with DMLPEI. By varying the length of the polycation alkyl chains, they also proved, along with a high charge density, the importance of the hydrophobicity of the polycation for its antibacterial activity. In 2012, Yang et al. used click chemistry to assemble via the layer-by-layer technique a QAC-containing polymer and a PEG copolymer [162]. Thanks to the respective antibacterial and anti-adherent properties of these two polymers, the final coating exhibited a good resistance to bacterial adhesion and a high efficiency against marine *Pseudomonas sp.* NCIMB 2021. Moreover, the antibacterial activity of the coating was maintained after exposition to filtered natural seawater at 30°C for 30 days.

Polyguanidines associated with a temperature-responsive copolymer [163] or polyvinylamines (PVAm) associated with PAA [121] were deposited on cellulosic fibers reducing bacterial growth by 99.9% already with one layer deposited and after 1 h of contact. Polyguanidines/HEP PEM films built on polyacrylonitrile nanofibrous membranes showed antibacterial properties after 1 h of contact. Ended by polyguanidines, PEM films appeared to be more efficient at killing bacteria. The outer layer of the nanofibrous membrane plays a dominant role on the antibacterial activity [164]. Westman et al. brought some hydrophobic modifications on PVAm which led to an increase of the antibacterial efficiency of this polyelectrolyte in solution [165]. However, the same effect was not found when the modified PVAm was immobilized into multilayers [166]. Unmodified PVAm/PAA exhibited better antibacterial properties than hydrophobically modified PVAm/PAA, showing that the antibacterial properties of such films seem to only come from the cationic charges of PVAm. Using a quarternized poly(pyridinium)/carboxymethyl-cellulose (QPVP/CMC) system, Amim et al. showed the importance of the hydrophobicity of the substrate on the chain conformation of the first layer affecting the antibacterial activity of the resulting PEM [120]. In the case of a hydrophilic surface (Si/SiO₂ wafer), QPVP chains are thicker (more expanded) due to a better hydration, while for a hydrophobic surface (polystyrene films), the chains seem to be less hydrated and tend to be in a more compact conformation. The biocidal activities of QPVP ended PEM films built on PS films were generally weaker than those observed for the ones deposited on Si/SiO₂ wafers, indicating less exposure of pyridinium groups to the aqueous dispersion.

N-halamines are contact biocides that contain oxidative halogen which can be directly transferred to the microbial cell membrane and inactivate a microorganism in a very short time without the release of free halogen into the systems [167]. Cerkez et al. synthesized

anionic and cationic *N*-halamine precursor polyelectrolytes and coated them onto cotton via the layer-by-layer method [168]. Once chlorinated, these coatings exhibited biocidal properties against *S. aureus* and *E. coli* after only 15 min of contact time.

Carbon based PEM films

Single-wall carbon nanotubes (SWNTs) were proven to exhibit antimicrobial activity by direct contact causing severe bacterial membrane damage [169]. Van Tassel's group dispersed SWNTs in an aqueous solution by using different amphiphiles and incorporated them into PLL/PGA films [170]. Compared to pure PLL/PGA films, the antibacterial activity of carbon based PEMs was enhanced against *E. coli* and *S. epidermis* up to 90% of inhibition after 24 h of incubation. They also demonstrated the importance of tube bundling effects [171]. Films containing isolated SWNTs inactivated 90% of *E. coli* after 24 h, whereas films containing bundled nanotubes reached this level in only 1 hour (Figure 1.35e). This suggests a fast-acting mechanism possibly related to enhanced SWNT content and/or bacterial contact due to the engulfing of bacteria in SWNT bundles (Figure 1.35a-d). In the case of PEM films based on lysozyme capped SWNTs and DNA capped SWNTs, the antimicrobial activity of the coating was specifically due to the lysozyme enzyme reaction and not to the presence of SWNTs [172].

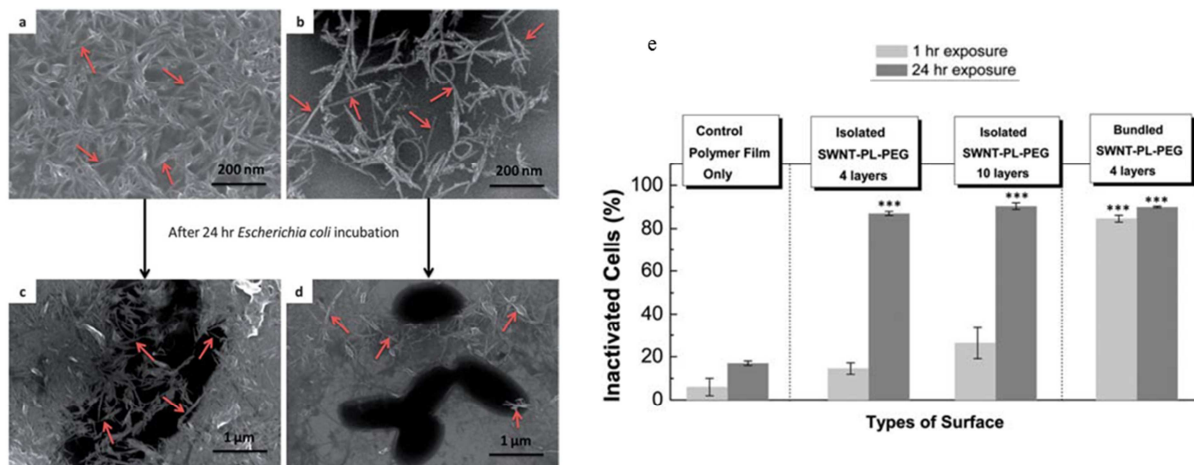


Figure 1.35: Scanning electron microscopy images of (a) (PLL/SWNT-PL-PEG_{bundled}/PGA)₄, (b) (PLL/SWNT-PL-PEG_{isolated}/PGA)₄, (c) sample (a) following 24 h *E. coli* incubation, and (d) sample (b) following 24 h *E. coli* incubation. Red arrows identify some of the SWNT present. *E. coli* are clearly visible as intact, black objects in (c) and (d). Bacteria appear to be engulfed by the bundled (c) but not isolated (d) SWNT-PL-PEG. (e) Inactivation of *E. coli* at 1 and 24 h on various substrates, as determined by LIVE/DEAD assay. [171]

Enzymatic based PEM films

To develop an anti-infective surface, a strategy that involves incorporation of a biofilm-dispersing enzyme within PEM coated hydrogels was proposed by Sukhishvili [173]. A biofilm-degrading glycoside hydrolase dispersin B (DspB), which cleaves polysaccharides contained in the biofilm matrix, was immobilized in PAH/Poly(methacrylic acid) (PMAA) crosslinked PEM films. DspB-containing PEMs showed 98% inhibition in biofilm growth and a good biocompatibility towards osteoblasts.

Release-killing PEMs

Whereas contact-killing PEM films have an action restricted to their surface, release-killing PEM films possess antimicrobial agents that leach in their environment. Figure 1.36 shows the two main strategies that have been used to develop contact-killing PEM films: (1) by direct diffusion of antimicrobial agents outside the PEM films and (2) by degradation of the PEM films and thus liberation of the antimicrobial agents. In this part, all the reported contact-killing PEMs will be described first depending on the antimicrobial agent involved and then by the strategies used to release it.

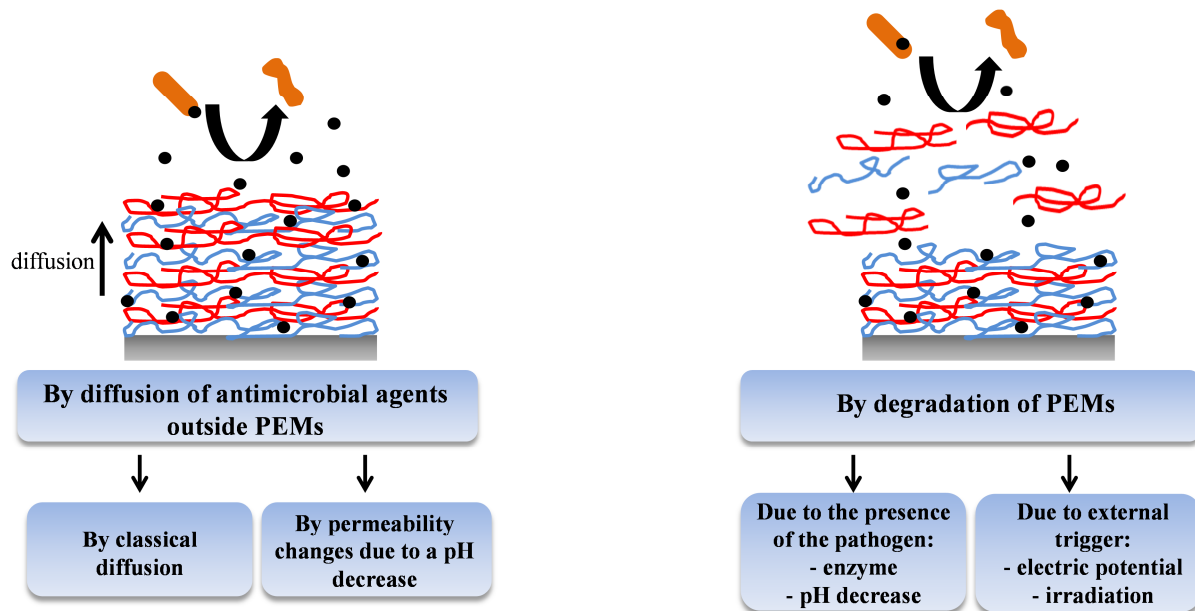


Figure 1.36: Scheme of the different strategies that have been used to build release-killing PEMs.

Metal and metal ion based PEM films

The most common antimicrobial agents embedded in PEM films are silver and silver ions (Ag^+). The bactericidal properties of silver have been known for centuries. Non-toxic to human cells, silver and silver ions can act against a broad spectrum of bacterial and fungal strains [174]. The ability of metallic silver to be dissociated in silver ions is the main reason for its antibacterial property [175, 176]. Ag^+ ions bind to the microbial cell membrane, diffuse into the cell and coagulate with bacterial proteins or enzymes, thus inactivating membrane-related enzymes and preventing DNA replication.

Two main strategies have been developed to incorporate silver nanoparticles into PEM films: direct incorporation of silver nanoparticles and *in situ* reduction of Ag^+ ions contained in PEM films to form silver metal (Figure 1.37). In the first strategy, silver nanoparticles capped by a polyanion were directly incorporated as one of the charged species in the buildup (Figure 1.37a) [177-181]. For example, PMAA coated silver nanoparticles could be assembled with PDADMAC on fibers to obtain 80% of *S. aureus* growth inhibition for 20 bilayers deposited on silk fibers [177]. To enhance PEMs mechanical properties for implant device functionalization, Prof Nicholas Kotov developed an hybrid PEM film composed of montmorillonite clay nanosheets, PDADMAC and uncoated silver nanoparticles [182]. Recently, Rahaman et al. added polymer brushes on top of a PEI coated silver nanoparticles/PAA film in order to both decrease *E. coli* adhesion and proliferation [179]. 95% of bacteria attached to the surface were killed within 1 hour of contact.

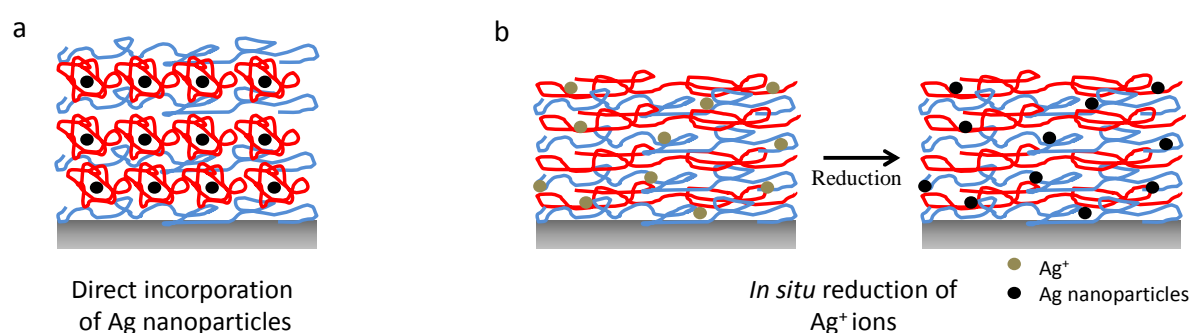


Figure 1.37: Two main strategies developed to incorporate silver nanoparticles into PEM films: (a) direct incorporation of Ag nanoparticles and (b) *in situ* reduction of Ag^+ ions contained in PEM films.

To incorporate silver nanoparticles in PEM films, a second strategy in two steps was used: (i) the buildup of films containing Ag^+ ions and (ii) the reduction of Ag^+ ions to silver metal (Figure 1.37b). Two methods can be used to obtain Ag^+ ions containing PEM films:

loading of Ag^+ in pre-assembled PEM films or incorporation by direct deposition during PEM buildup. Pre-assembled PEM films [183-191] or microcapsules [185, 192, 193], containing free carboxylic acid or sulfonate groups, are immersed into an Ag^+ ions solution leading to Ag^+ ion trapping by exchange with acid protons. The amount of trapped ions can be modulated by tuning the concentration of free carboxylic acid groups available in the PEM films depending on the assembly pH [187]. A similar work has been done by varying the ionic strength instead of the assembly pH allowing to obtain sandwiched films with AgNPs (Figure 1.38) [188]. This method possesses the advantage that it can be used with different polyelectrolyte types, not only weak ones.

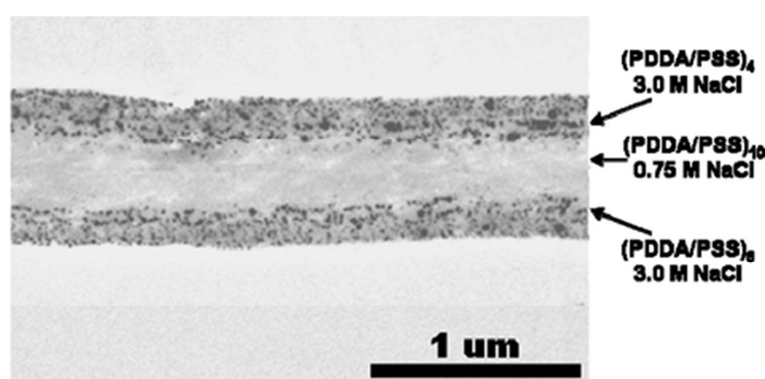


Figure 1.38: Cross-sectional TEM image of a $(\text{PDDA/PSS})_6/\text{Ag}(0)/(\text{PDDA/PSS})_{10}/(\text{PDDA/PSS})_4/\text{Ag}(0)$ sandwiched film. The blocks containing silver and the spacer block were assembled at 3.0 and 0.75 M NaCl concentration, respectively. [188]

Silver ions within the films are then reduced *in situ* to silver nanoparticles (AgNPs) by chemical reducing agents such as NaBH_4 [183, 184, 194-196] or UV-radiation [177, 186]. In addition to form AgNPs, this procedure regenerates the carboxylic groups of the polyanions within the PEMs allowing additional loading of Ag^+ into the PEMs [184, 185]. The use of non-physiological solutions, such as reducing agents, is not suitable to build PEMs directly on biological tissues, including wound-beds. To address this limitation, Abbott and co-workers proposed the pre-fabrication of PEMs loaded with AgNPs on elastomeric stamps and the mechanical transfer (Figure 1.39b) of AgNPs loaded PEMs onto the surfaces of biological tissues [184] and dressing (Biobrane) [184, 197]. The mechanical transfer onto soft materials is greatly facilitated by the incorporation of polymeric microspheres (1–2 μm in diameter) into PEMs. The antibacterial activity of Ag coated Biobrane was tested with *S. aureus in vitro* and *in vivo*. After 72 hours, wounds treated with Ag coated Biobrane showed significantly (P

< 0.001) less colony-forming units than wounds treated with unmodified Biobrane (more than 4 log₁₀ difference) [184, 197].

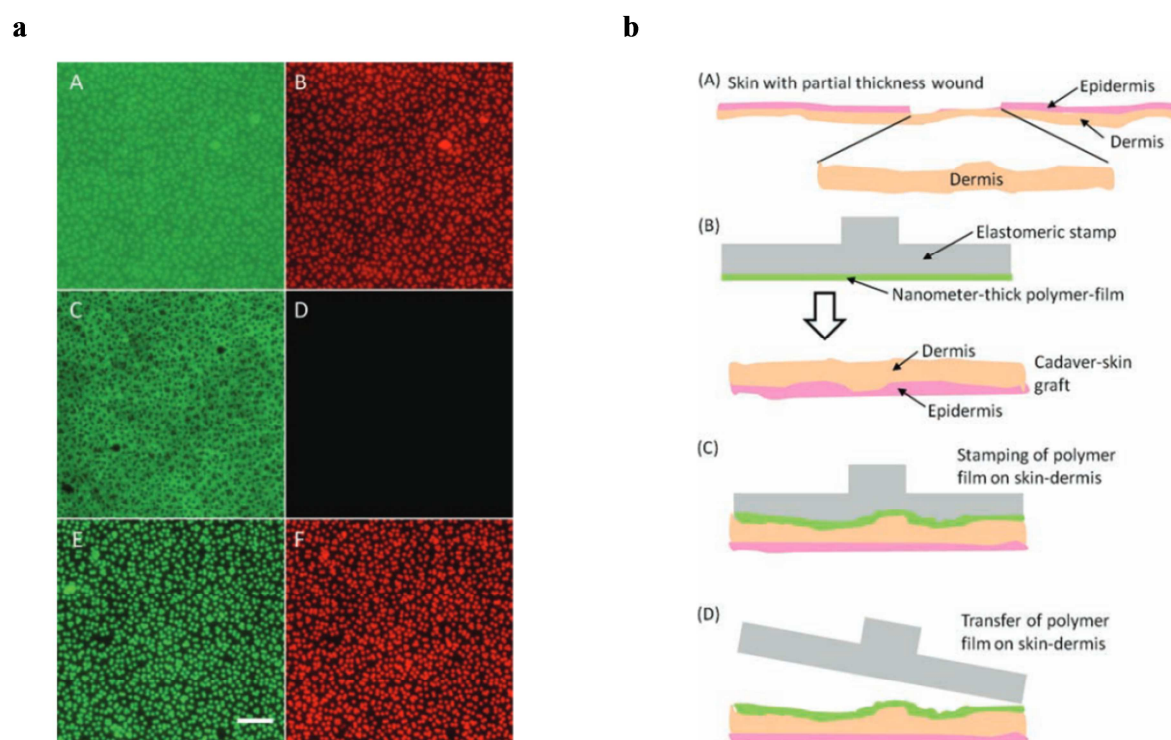


Figure 1.39: (a) Fluorescence microscopy images showing that microspheres integrated into PEMs facilitate the transfer of the PEMs above and below the microspheres onto silicone sheets ($E' \sim 450$ kPa). The images show fluorescence from PAH (green) and PS microspheres (red) on: A,B) PDMS stamp before printing; C,D) PDMS stamp after stamping and E,F) silicone sheets after printing. Scale bar = 10 μ m. (b): A) Schematic illustration of a partial thickness skin wound that exposes the dermis. B-D) Schematic illustration of the mechanical transfer of nanometer-thick polymer-films, pre-fabricated on PDMS stamps, onto the dermis of human-cadaver skin-graft. [184]

To avoid the addition of any reducing agent for the silver ion reducing step, the latent reactivity of catechol functional groups within the PEM was exploited [198, 199]. AgNPs were thus immobilized on a titanium alloy surface by simple immersion of CHI/dopamine modified alginate PEM films in AgNO₃ solution [199]. Self-polymerization of dopamine groups are reported to be able to spontaneously reduce noble metal ions to metal nanoparticles, requiring no aid of reducing agent, surfactant, or energy-consuming steps [200-202]. Still in the idea to maximize the antibacterial properties of the coatings, PEM films were designed to possess also some contact-killing abilities by immobilization of quaternary ammonium silanes on a silver containing PAH/PAA film [203].

Silver ions can also be incorporated in PEM films by alternate deposition of silver ions/polyelectrolyte complexes and oppositely charged polyelectrolytes [194, 196, 204-208].

As for the previous strategy, silver ions within the films are then reduced *in situ* to AgNPs by chemical reducing agents [194, 196], heating or UV-irradiation. The advantage of this strategy is a higher control of the amount of metal ions incorporated in the film, which in turn allows control over AgNPs size by changing the concentration of metal ions present during the PEM buildup [194, 196, 204-208]. Using SiO₂ NPs in suspension with a bisamine silver nitrate solution ([Ag(NH₃)₂]NO₃) and a PAH solution, AgNPs synthesis occurred *in situ* during the LbL assembly where the amino groups of PAH acted as reducing agents [205]. PAH/SiO₂ films were previously reported as antibacterial coatings, probably due to a combination between their hydrophilic properties and their nanotexturized rough surfaces [209]. Adding contact-killing properties to these kind of PEMs was done by using a quaternized poly(ethylene imine) (PEI) as polycation [196] or using a CHI/HEP film which is already known for decreasing bacterial adhesion [204]. To increase the long-term antibacterial performance, Yin and coworkers deposited silanes on a PEI-Ag⁺/PAA film creating a superhydrophobic surface that enhanced the stability of the coating, prevented the bacterial adhesion and prolonged the release of silver [195, 210].

Another approach to include silver in a PEM was by embedding liposomes filled with AgNO₃ (Figure 1.40a). Malcher et al. showed that no silver ions were leaked from the AgNO₃-liposome aggregates embedded in a PLL/HA film at room temperature whereas it was the case when the temperature is increased at 37°C (Figure 1.40b). After 30 min of incubation, 11% of the silver ions encapsulated in the coating were released and 100% within 15 hours. So, by raising the temperature above the transition temperature of the vesicles (~34°C), silver ions release effectively killed *E. coli* populations [211].

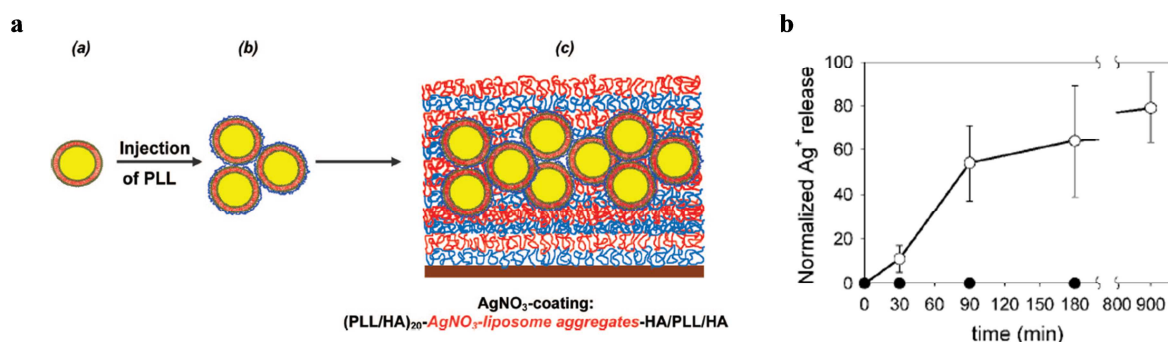


Figure 1.40: (a): (a→b) Liposomes complexation with PLL resulted in the formation of AgNO₃-liposome aggregates, (b→c) Deposition of AgNO₃-liposome aggregates on (PLL/HA)₂₀ film followed by additional coating with HA/PLL/HA layers. (b) Release of silver ions from AgNO₃ coating versus time at (●) room temperature and (○) 37°C. [211]

Copper was also trapped into multilayers and the release of Cu^{2+} was followed under different stimuli: pH, salt and surfactants [212]. Although copper is known to have lower antibacterial activity than silver, its ability to bind closer to CHI and alginate (ALG) led to copper containing CHI/ALG films that inhibit efficiently bacterial proliferation [213].

Oxygen reactive species / radicals releasing PEM films

Compounds forming oxygen reactive species were incorporated into PEM films to develop antibacterial surfaces. Polyoxometalates, nanoclusters of transition metals, embedded in a CHI based PEM film have been used to kill bacteria by oxidation of their cell membrane [214]. Titanium (TiO_2), known to form biocidal radicals upon UV-irradiation, was also used in combination with silver nanoparticles. Yuan et al. built silver loaded CHI- TiO_2 /HEP films to obtain a coating with both contact-active properties due to titania and release-active properties due to silver nanoparticles [215]. Corbitt et al. built photoactive conjugated polyelectrolytes capsules that can entrap and kill bacteria under exposure to white light (Figure 1.41) [124]. Illumination of the capsules leads to produce oxygen singlet at the polymer/bacteria interface and this oxygen singlet or some subsequently produced reactive oxygen intermediates interact with the bacteria resulting in bacterial killing and eventual degradation. Figure 1.41c shows that the live-to-dead ratio decreases from 7 to 0.33 when hollow capsules with trapped *P aeruginosa* after 15 min of irradiation with a fiber-optic lamp.

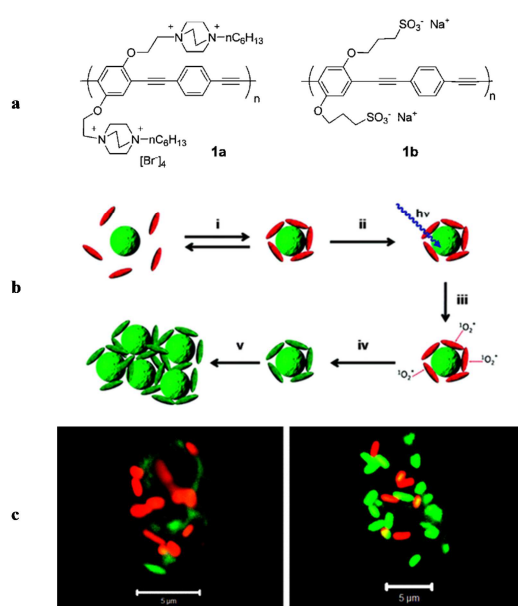


Figure 1.41: (a) Chemical structures of the two charged poly(phenylene ethynylene)-type conjugated polyelectrolytes. (b) Mechanism of biocidal action of photoactive conjugated polyelectrolytes (CPE) capsules. (c) Composite confocal microscope images of the hollow CPE capsules with trapped *P. aeruginosa* (a) before and (b) after 15 min of irradiation with the fiber-optic lamp. Approximate live-to-dead ratios are (a) 7.0 and (b) 0.33. [124]

Gabriel et al. reported a photoactive surface coating consisting of crosslinked hyaluronic acid and poly-L-lysine modified with a photoactive molecule triggered upon irradiation with near infrared (NIR) light [216]. The strength of such a coating is that it can be triggered even inside a body since NIR light can penetrate tissue which is not the case for UV light that is used to trigger titanium oxide for example.

Antimicrobial organic molecule based PEM films

Beside metal ions, antimicrobial organic small molecules have also been incorporated into PEMs to be further released. Antiseptics and antibiotics (Figure 1.42) belong to this category. They both prevent the growth and the development of microorganisms but have significant differences. Applied externally to tissues or skin, antiseptics prevent bacteria, fungi, yeasts and other microorganisms from colonizing a wound. They only weaken and slow down the growth of microorganisms, which helps to prevent bacteria from causing further infection. Used to kill only bacteria, antibiotics act by inhibiting the cell wall, nucleic acid and protein syntheses. They are used to deal with systemic infections, post-operative infections and during surgical procedures. Unlike most antiseptics, bacteria may become resistant to antibiotics after prolonged use.

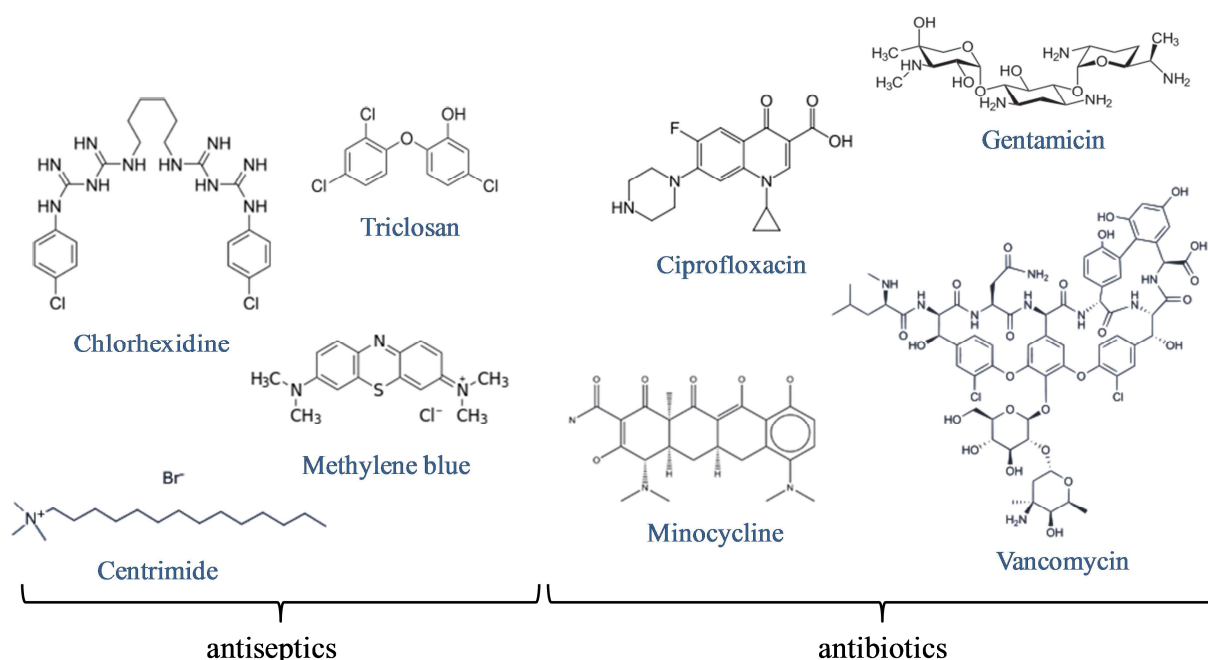


Figure 1.42: Chemical structure of different antiseptics and antibiotics that have been embedded into PEMs.

The insertion of antimicrobial organic molecules into PEMs has been widely studied and different strategies have been developed. The chemical structure of the different antiseptics and antibiotics that have been embedded into PEMs are listed Figure 1.42. Positively or negatively charged molecules can bind to polyelectrolyte chains. Thus, the first strategy consists in a simple immersion of pre-assembled PEM films into an antibiotic or an antiseptic solution [217-219]. The second strategy is based on the direct deposition of the molecules either by association with one of the polyelectrolytes [208, 220, 221] or as one of the component [222-229]. The loading and release of antibiotics was shown to be tunable by the number of deposited layers, the assembly pH, the incubation time and also the use of heat-treatment after film buildup [217]. A variety of PEM films has been studied to control drug release [230] by diffusion through the film [208, 228, 229], by hydrolytic degradation of one of the polyelectrolytes [222-224, 227, 231, 232], by pH changes [233] [226, 234] or by external triggers such as electric potential [235], laser light [236, 237] or ultrasound [236, 237]. These four control release methods will be described in details below.

Release by diffusion out of PEM films

Among the antiseptics used in clinical practice, chlorhexidine (Figure 1.42) exerts its antimicrobial activity through its positive charge at physiological pH. It destabilizes bacterial cell walls and alters bacterial osmotic equilibrium leading in the precipitation of cytoplasmic contents and triggering microbial cell death. Chlorhexidine (CX) was successfully incorporated into PEMs built directly on suture materials [228, 229] or stamped on wound dressing [228, 229]. Stamped CX/PAA PEM films on Biobrane led to a localized non-toxic release of CX allowing the decrease of *S. aureus* colonization and promoting normal wound healing in mice (Figure 1.43) [229]. Cetrimide (Figure 1.42), an organic quaternary ammonium antiseptic molecule, was also embedded alone in a PEI/PAA PEM film or in combination with silver nitrate [208].

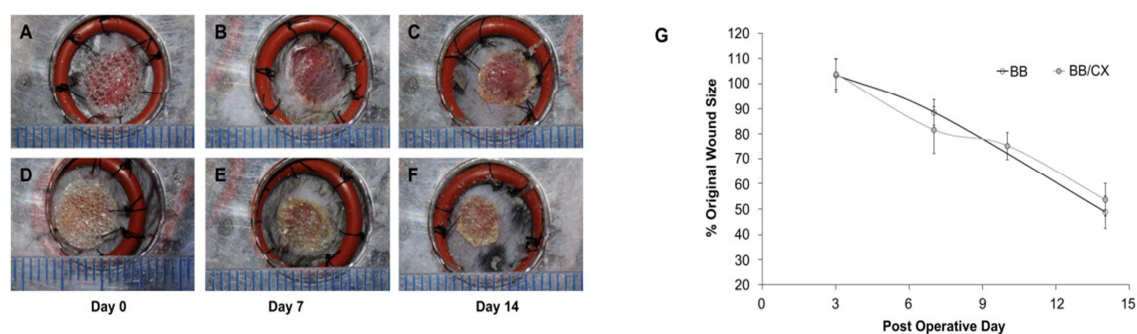


Figure 1.43: Biobrane functionalized with CX/PEMs promoted normal healing in 'full-thickness' splinted dermal wounds (6 mm diameter) in normal wild-type mice. Digital images showing simple, gross observation of wound healing on post-operative days 0, 7 and 14, respectively, in groups treated with: (A, B, C) Biobrane, or (D, E, F) Biobrane functionalized with PEMs of $(\text{PAH/PAA})_{10.5}(\text{PS-microspheres})(\text{CX/PAA})_{80}$. (G) Percentage of original wound size on post-operative days 3, 7, 10 and 14 in groups treated with either Biobrane functionalized with CX/PEMs, or unmodified Biobrane. Each data point presents mean \pm SEM of relative wound size ($n \geq 5$ mice). Results show that CX/PEMs do not impair the adherence of the dressing to the wounds (as seen from gross images), nor the rate of wound closure. [229]

Methylene blue (Figure 1.42), a cationic dye known for its antimicrobial activities, has been inserted into PEMs as a model bioactive compound [217, 238] but only Martel's group used its antimicrobial properties [71]. Using the ability of methylene blue (MB) to form stable inclusion complexes with β -cyclodextrin (β -CD), MB loaded CHI/poly(β -CD) PEM films were built and showed a sustained antibacterial activity against *S. epidermis* over 72 h of contact. Triclosan (Figure 1.42) has a broad antibacterial spectrum and is also an antifungal agent that is found in numerous consumer products such as soaps or detergents and is used for healthcare in surgical scrubs and personnel hand washes. Due to its hydrophobic nature, it is difficult to incorporate triclosan directly into LbL-assembled films. By using linear-dendritic block copolymer micelles, triclosan could be released over a period of several weeks and the drug still remained efficient to inhibit *S. aureus* growth [239]. Recently, triclosan was encapsulated into cetyltrimethylammonium bromide (CTAB) surfactant micelles that were then inserted by diffusion into a preformed PEI/PAA PEM film [240]. The triclosan-loaded PEI/PAA films could inhibit the growth of both Gram-negative and Gram-positive bacteria by the sustained release of triclosan molecules for over 20 days. CTAB was also used as cationic species and assembled with PAA to form a PEM with antibacterial properties [241].

Hydrolytically degradable PEM films

Hammond and co-workers developed PEM films based on a hydrolytically degradable poly(β -amino ester) and different polyanions that efficiently release gentamicin (Figure 1.42)

against *S. aureus* proliferation *in vitro* and *in vivo* [223]. Later, vancomycin (Figure 1.42), a glycopeptide antibiotic, was incorporated in PEMs based on hydrolytically degradable cationic poly (β -amino esters) and anionic polysaccharides using both the dip and the spray methods. Secondary interactions between the film components provided control over drug densities and release profiles. Release time from sprayed films was greatly accelerated compared to release from dipped films (Figure 1.44). By combining the dipping and spraying assembly with dextran sulfate and alginate, a composite architecture was built that had a rapid initial drug release followed by a linear release above the antibiotic minimum inhibitory concentration [224]. To increase the releasing period of antibiotics embedded in hydrolytically degraded PEM films, a laponite clay interlayer barrier was introduced to physically block antibiotic diffusion. Using this strategy with two drugs embedded in the same PEM film, Min et al. obtained a rapid release of gentamicin for the first few days before reaching a sustained release for weeks [227].

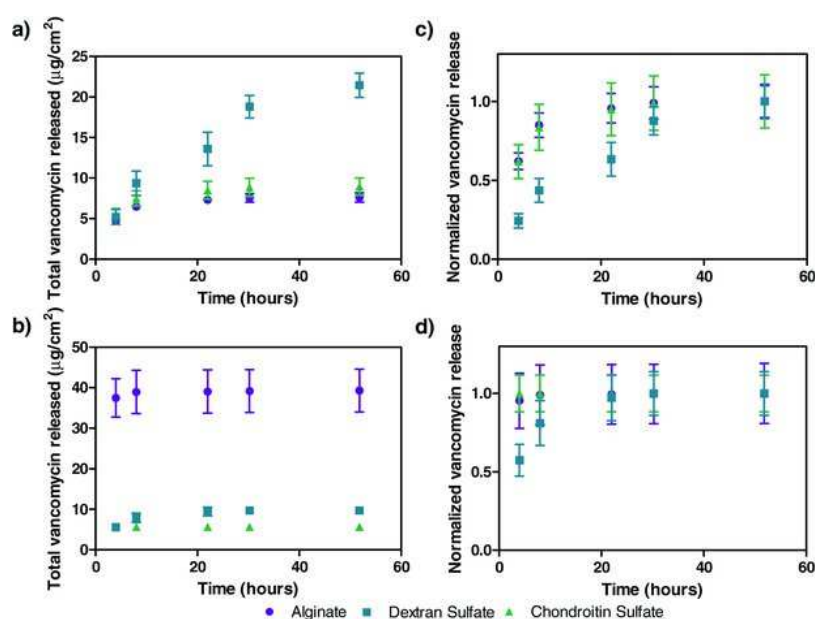


Figure 1.44: Vancomycin release from $(\text{poly } 2/\text{polyanion}/\text{vancomycin}/\text{polyanion})_{60}$ films with alginate, dextran sulfate and chondroitin sulfate as polyanion. a) Total vancomycin release over time from dipped films. b) Total vancomycin release over time from sprayed films. c) Normalized vancomycin release over time from dipped films. d) Normalized vancomycin release over time from sprayed films. [224]

Non-charged antibiotics have been incorporated into PEM films using the ability of cyclodextrin (CD) to host neutral or hydrophobic molecules by making inclusion compounds in aqueous environments. A poly(carboxymethyl- β -cyclodextrin) (polyCD) complexed with a small molecule alternated with a poly(β -amino ester) allowed obtaining surface-eroding films

(Figure 1.45a) with a release kinetics independent of the therapeutic agent incorporated but regulated through the choice of the degradable polycations (Figure 1.45b) [232]. This approach was applied on LbL delivery thin films that simultaneously released the broad spectrum charged antibiotic vancomycin and an anti-inflammatory drug [231].

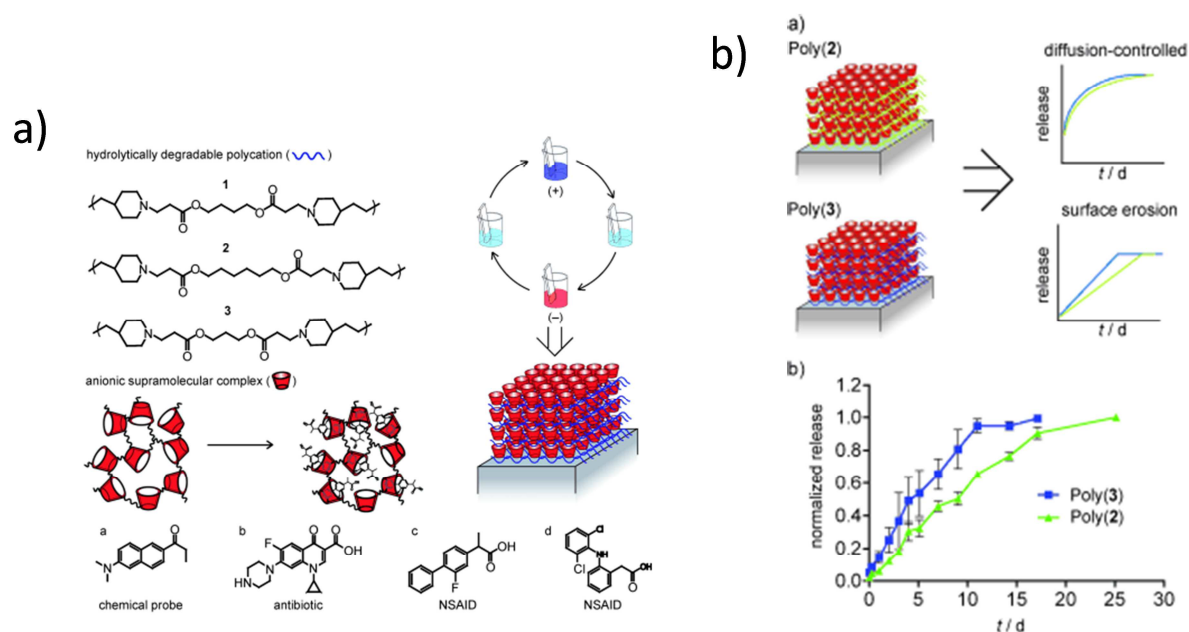


Figure 1.45: (a) Methodology for LbL films. Left: film components. Three poly(β -amino esters) were investigated as degradable polycations. Poly(carboxymethyl- β -cyclodextrin) was used as the anionic supramolecular complex. Right: electrostatic assembly. Light blue: water. (+) indicates addition of polycation. (-) indicates addition of anionic supramolecular complex. Bottom shows molecules used in experimentation. NSAID = nonsteroidal anti-inflammatory drug. (b) a) Two possible release profiles for poly(2) and poly(3). b) Release from poly(2)/polyCD-flurbiprofen₂₀ and poly(3)/polyCD-flurbiprofen₂₀ films at 37 °C in PBS. [232]

pH-triggered release

Antibiotic release from PEMs can also be triggered by pH changes. Depending on the system, the increase or decrease of pH induces the diffusion of the drug by degradation [239, 242], by permeability changes of the PEM films [234] or by binding affinity decrease [226]. Block copolymer micelles, containing triclosan, were assembled through H-bonds with PAA at acidic pH [239, 242]. Triclosan was further released at physiological pH. Hollow capsules composed of two weak polyelectrolytes PAH and PMA prepared by LbL assembly showed excellent loading capacity for ciprofloxacin (Figure 1.42). The pH-induced permeability of microcapsules allowed the loading of ciprofloxacin at low pH and its subsequent release at neutral pH. The release of ciprofloxacin from microcapsules showed significant antibacterial activity against bacterial pathogen *E. coli* for 7 h [234]. While most of the coatings can

release antibiotics for a period of some hours to a few days, Zhong and coworkers reached a sustained release over 35 days of minocycline (Figure 1.42), an antibiotic and anti-inflammatory drug [226]. Based on binding-mediated interactions between calcium and minocycline, the antibiotic was incorporated and released from a dextran/gelatin PEM. Due to the fact that the binding affinity decreases with the pH, minocycline release only lasted 13 days at pH 6.0, with a high initial burst release, whereas a 35 days sustained release and a small burst release was found at physiological pH (Figure 1.46). Since tissue injuries, inflammations and infections commonly lead to a reduced extracellular pH, a pH-triggered release of antibiotics at the implant-tissue interface is very pertinent.

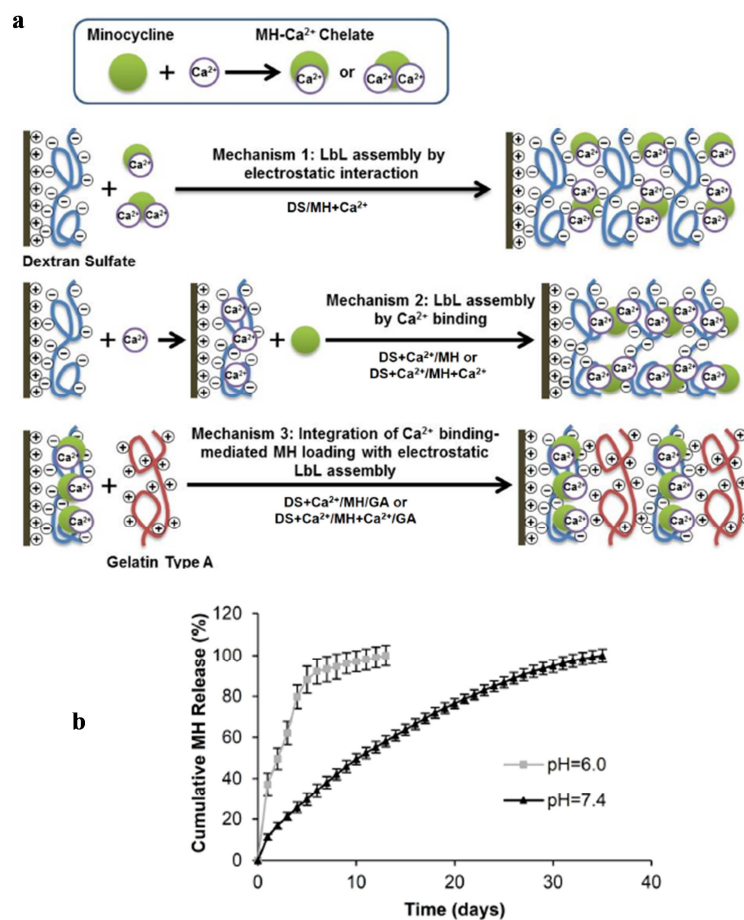


Figure 1.46: (a) Schematic illustration of the mechanism of MH incorporation and LbL assembly. (b) Effect of pH on MH release from $(DS+Ca^{2+}/MH+Ca^{2+}/GA+Ca^{2+})_8$ LbL films. [226]

External triggered release

Recently, few studies emerged that use external trigger for the release of antibiotics. Gentamicin (Figure 1.42) was incorporated in a CHI/Prussian Blue PEM film deposited on an electrode to obtain an electrically triggered release by application of a small (<1.0 V) electric potential. When oxidized, the Prussian Blue nanoparticles shift from negatively charged to

neutral, inducing the dissolution of the film. Drug release kinetics ranging from triggered burst release to on/off, or pulsatile release were achieved by applying different electric potential profiles. The *in vitro* efficacy of the released drug was confirmed against *S. aureus* bacteria [235].

Combining antibiotics and silver nanoparticles antimicrobial properties, Raishur and co-workers showed that the release of the antimicrobial agents can be triggered by laser light or ultrasound due to the rupture of the PEM film (Figure 1.47) [236, 237].

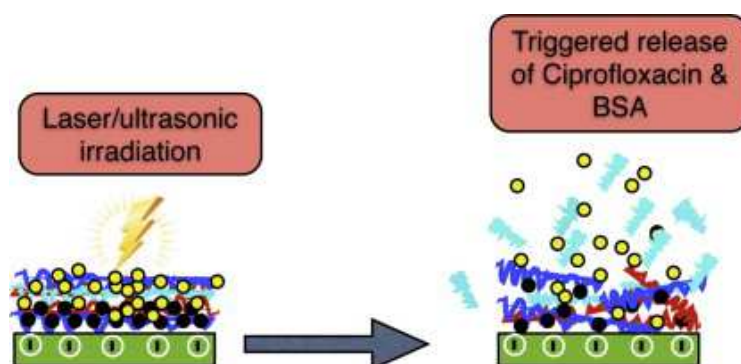


Figure 1.47: Laser/ultrasound-induced release of ciprofloxacin and BSA. [236]

While the quantity of antibiotics embedded in the multilayers is usually estimated after release in the medium, by UV absorption measurement for example, new methods such as 7.87 eV Laser Desorption Postionization MS imaging [219] or in situ-ATR-FTIR analysis [220] were developed to quantify it within the multilayers.

Antimicrobial peptide based PEM films

The last family of antimicrobial agents that have been included into release-killing PEMs are antimicrobial peptides (AMPs) [243-249]. AMPs, polypeptides secreted by numerous living organisms against pathogens, gained an increased attention due to their broad spectrum of antimicrobial activity and their low cytotoxicity. They predominantly act by disruption of the membrane integrity of pathogen agents and thus are unlikely to initiate the development of pathogen resistance. Different strategies were applied to incorporate AMPs in PEM films: by electrostatic adsorption or by loading when they are cationic [243, 245, 247, 250, 251], by association with one of the polyelectrolytes when they are poorly water soluble [246] or by grafting them on one of the polyelectrolyte components [248, 252].

Constituted of 36 to 46 amino acids and positively charged, defensin was the first AMP embedded in a PEM film based on PLL and PGA [243]. The antibacterial activity was

obtained only with functionalized PLL ended PEM films. The adhesion of bacteria on the PEM surface was needed for the peptide to be sufficiently in contact with the pathogens, showing thus a contact-killing mechanism. Another positively charged AMP, Ponicin G1, was successfully incorporated into a hydrolytically degradable PEM, based on poly(β -amino ester), to obtain a release killing mechanism [245]. The degradation of the film, thus the release profile, depended on the polyanion itself. Obtained from a pre-assembled PEM film, Pavlukhina et al. developed an ultrathin poly(methacrylic acid) (PMAA) hydrogel able to incorporate and release polycationic charged antimicrobial agents [247]. After the buildup of poly(*N*-vinyl pyrrolidone) (PVPON)/PMAA hydrogen bonded PEM films, PMAA was crosslinked with the use of a cross-linker, ethylenediamine (EDA), before the removal of PVPON (Figure 1.48a). The ultrathin PMAA hydrogel can thus retain cationic antimicrobial agents by an electrostatic mechanism. Associated with growth of *S. epidermidis*, pH variations were used as an internal trigger to release an antibiotic, gentamicin and an AMP, peptide L5. In response to pH variation, EDA-cross-linked hydrogel swelled while releasing its load (Figure 1.48b). The antibacterial activity, mainly obtained at the surface of the hydrogel, was demonstrated for 4 h of incubation with the gram-positive bacterium *S. epidermidis*.

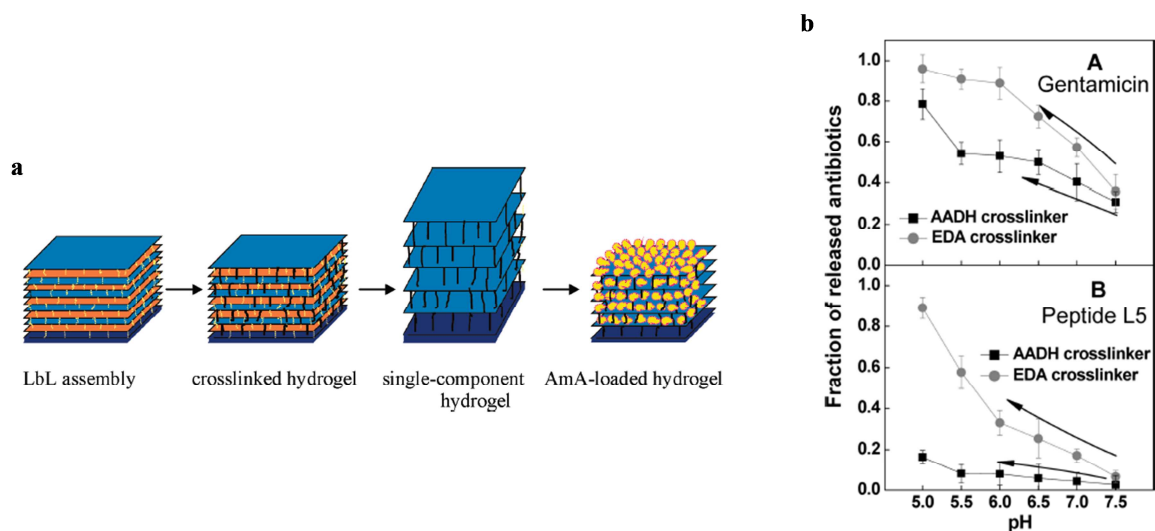


Figure 1.48: (a) Procedure for preparation of functional antibacterial films. (b) Effect of pH on retention of peptide L5 from EDA- and AADH-stabilized (PMAA)₁₀ hydrogels. The fraction released was determined as the ratio of ellipsometric thickness of peptide-loading after pH-triggered release into 0.01 M phosphate buffer containing 0.2 M NaCl thickness to the thickness of antibiotics loaded into (PMAA)₁₀ films at pH 7.5. All error bars represent the average standard deviation obtained from three separate experiments. [247]

Antifungal AMP-loaded PEM films were developed [250] [251] and tested *in vivo* [250]. Embedded in PLL/PGA PEM films, a small polycationic AMP, chromofungin, was able to interact with the surface of the membrane of the fungi reducing the growth of *C. albicans* by 64% and fully inhibiting the growth of *Neurospora crassa*. Tested *in vivo* on rat with an oral candidosis, the chromofungin-loaded PEMs postponed the fungal infection [250]. Using the same PEM system, Karlsson et al. incorporated cationic amphiphilic oligomers of β -substituted amino acids (β -peptides) designed to mimic AMPs that exhibited toxicity toward *C. albicans*. β -peptides were released without physical PEM film erosion and occurred gradually over a period of 17 days as opposed to a burst release during the first few hours.

Using amphiphilic polysaccharides, poor water soluble AMP, gramicidin A, was incorporated in PEM films [246]. The antibacterial activity of the functionalized PEM films resulted from a double mechanism: contact-killing and release of the peptide into the solution surrounding the film.

To functionalize stainless steel that is widely used in medicine, Detrembleur and coworkers developed antimicrobial PEM films based on a water soluble poly(methacrylamide) bearing oxidized 3,4-dihydroxyphenylalanine groups (Pox(mDOPA)), PAH and an AMP, nisin [252]. Thanks to DOPA moieties, cross-linked PEM films, where nisin was covalently attached, were obtained at room temperature and without the use of any toxic reagent (Figure 1.49a). Tested against *Bacillus subtilis*, the coating showed a sustainable antibacterial activity even after immersion for one night in tap water or after several mechanical cleaning with a wet sponge (Figure 1.49b).

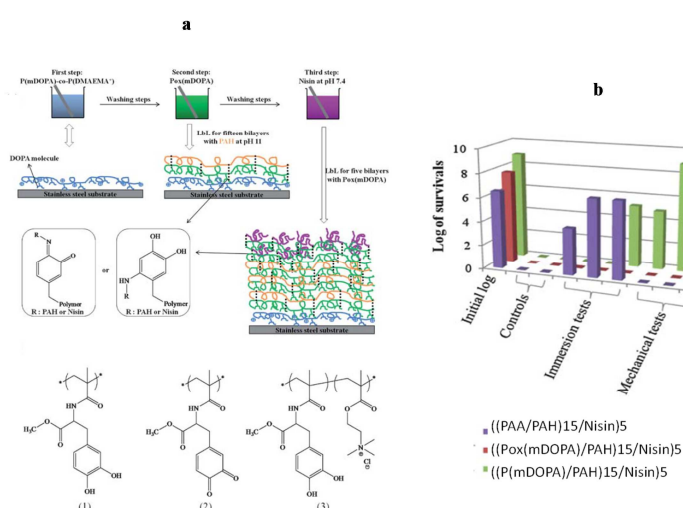


Figure 1.49: (a) LbL process for imparting long-lasting antibacterial properties to stainless steel and chemical structures of (1) P(mDOPA), (2) Pox(mDOPA) and (3) P(mDOPA)-co-P(DMAEMA⁺). (b) Antibacterial assessments against *B. subtilis* using the JIS Z method; all durability experiments were done in triplicate; purple colour corresponds to an initial bacteria log of 6.2, red colour to 7.7 and the green one to 8.9 (controls = antimicrobial coating on stainless steel before mechanical and immersion tests). [252]

Discussion on the evolution of PEM films as antimicrobial surfaces

The first antimicrobial PEM films have been reported in the early 2000s, which was only ten years after the introduction of PEMs by Decher [10]. Since then, the different teams involved in this field aimed at improving the coating properties in order to render them usable for specific applications. Thanks to the versatile LbL method, numerous surfaces and commercially used objects could be coated showing all potential applications (Table 1.2).

Table 1.2: Summary of the different surfaces that have been coated by PEM films and their applications.

Coated surfaces	Application	References
Polymers		
Polypropylene films	Packaging	[126]
Polyethylene terephthalate films	Water purification, textile	[139], [160], [71]
Polystyrene films	Flacons, laboratory plates	[159]
Polyurethane	Medical devices (catheters)	[122]
Poly(L-lactic acid) membranes	Tissue engineering	[180]
SBS membranes	Wound dressings	[147]
Polydimethylsiloxane	Microfluidic devices, stamp for tissue transfer	[132], [184], [229]
Metals		
Titanium	Orthopedic implants	[141], [199], [223]
Stainless steel	Marine coatings, orthopedic implants	[133], [162], [196]
Copper	Marine coatings	[210]
Magnetic microspheres	Delivering to specific locations	[185]
Fibers mat		
Polyacrylonitrile fibers	Filtration, wound dressing, vascular graft	[164]
Nylon fibers	Textile	[177]
Silk fibers	Textile	[177]
Wood fibers	Filter paper	[178]
Cellulosic fibers	Wound dressings, tissue engineering	[152] [165], [163]
Medical materials		
Porous gelatin sponge	Adsorption of blood during invasive surgeries	[225]
Cortical bone		[140]
Biobrane	Biological dressing	[197], [190]
Suture materials		[228], [231]
Bandages		[231]
Orthopedic implants		[218], [253]
Microfiltration membranes	Drinking water treatment, wastewater reuse	[134]
Intraocular lenses		[221], [231]
Reverse osmosis polyamide membranes	Production of fresh water from saline water or wastewater	[179]

Except for the first antimicrobial PEM films and some rare exceptions, a systematic evaluation of the biocompatibility of the antimicrobial PEM coatings was performed *in vitro* and even sometimes *in vivo* [197, 223, 229, 250]. Interestingly for tissue engineering, it was

shown that the stiffness of the coating has an opposite effect on bacteria and cells, i.e. stiffer films promote cell adhesion while they limit bacterial proliferation [143].

Each strategy for forming an antimicrobial PEM film, i.e. adhesion-resistant, contact-killing and release-killing, was extensively studied. In particular, new polymers were synthesized to bring better contact-killing properties [157, 158] and new antimicrobial agents such as antimicrobial peptides, which do not induce an increase of pathogen resistance, were incorporated into release-killing PEM films. Each of the strategies possesses advantages but also drawbacks which are mostly listed in Table 1.3.

Table 1.3: Main advantages and drawbacks of the PEM films built following an adhesion-resistant, a contact-killing or a release-killing strategy.

	Advantages	Drawbacks
Adhesion-resistant	Prevent from the first step of biofilm formation that is crucial	Do not kill the bacteria
Contact-killing	Constant efficiency with time	Action restricted to the surface
Release-killing	Extensive action	Consumption of all the antimicrobial agents after a certain time Possible toxicity Possible induction of bacterial resistance

So, to further increase the antimicrobial abilities of the coatings, two strategies out of the three main ones were combined, allowing a limitation of the drawbacks. PEM films exhibiting both adhesion-resistant and contact-killing [155, 162] or both contact-killing and release-killing properties [179, 196, 203, 204, 215] were developed. Release-killing coatings based on the embedding of two different antimicrobial agents were also prepared [208, 215, 227]. Beside antimicrobial properties, new functionalities could be added. For example, a coating having both anti-inflammatory and antibacterial properties was prepared [231].

Work was also performed to increase the durability of the coatings. A first aspect was to improve the mechanical properties. This was done by chemical crosslinking of the films [185, 252] or by the introduction of PS microspheres [184]. A second aspect was to obtain long-term release periods, especially by slowing down the diffusion of antimicrobial agents outside the film. For example, a coating with a clay interlayer barrier could release antibiotics for weeks [227].

An important evolution in PEM coatings was to obtain a triggered release. Internal trigger such as temperature [211] and pH [226, 233, 247] or external trigger such as white light [124], laser light [236], near infrared light [216] or ultrasound [237] were successfully used. However, the problem for the internal trigger is that the release can be immediate after the pH or the temperature change and thus the antimicrobial agent can be exhausted before the bacteria is even present. Concerning the external trigger, besides the need of specific equipment, it is not possible to know when the bacteria are present and thus when it is necessary to activate the trigger.

So, one step further was to obtain a release that is only triggered by the presence of the pathogen. This was first introduced by Sukhishvili using pH changes due to bacteria proliferation [247].

This suggests that future antimicrobial PEM films could consist in coatings presenting several functionalities and also in smart coatings that can become active only in the presence of bacteria.

Chapter 1 references

1. Blodgett, K.B., Monomolecular Films of Fatty Acids on Glass, *Journal of the American Chemical Society*, **1934**, 56, 495.
2. <http://www.ksvnama.com/>.
3. Ulman, A., Formation and structure of self-assembled monolayers, *Chemical Reviews*, **1996**, 96 (4), 1533-1554.
4. Keselowsky, B.G., et al., Surface chemistry modulates fibronectin conformation and directs integrin binding and specificity to control cell adhesion, *Journal of Biomedical Materials Research Part A*, **2003**, 66A (2), 247-259.
5. www.ias.tuwien.ac.at.
6. Amiji, M., et al., Prevention of protein adsorption and platelet-adhesion on surfaces by PEO/PPO/PEO triblock copolymers *Biomaterials*, **1992**, 13 (10), 682-692.
7. Zhao, B., et al., Polymer brushes: surface-immobilized macromolecules, *Progress in Polymer Science*, **2000**, 25 (5), 677-710.
8. Mansky, P., et al., Controlling polymer-surface interactions with random copolymer brushes, *Science*, **1997**, 275 (5305), 1458-1460.
9. Decher, G., Fuzzy Nanoassemblies: Toward Layered Polymeric Multicomposites, *Science*, **1997**, 277 (5330), 1232-1237.
10. Decher, G., et al., Buildup of ultrathin multilayer films by a self-assembly process: III. Consecutively alternating adsorption of anionic and cationic polyelectrolytes on charged surfaces, *Thin Solid Films*, **1992**, 210 (1-2), 831-835.
11. Li, Y., et al., Layer-by-layer assembly for rapid fabrication of thick polymeric films, *Chemical Society Reviews*, **2012**, 41 (18), 5998-6009.
12. Lee, S.S., et al., Layer-by-layer deposited multilayer assemblies of ionene-type polyelectrolytes based on the spin-coating method, *Macromolecules*, **2001**, 34 (16), 5358-5360.
13. Schlenoff, J.B., et al., Sprayed polyelectrolyte multilayers, *Langmuir*, **2000**, 16 (26), 9968-9969.
14. Izquierdo, A., et al., Dipping versus spraying: Exploring the deposition conditions for speeding up layer-by-layer assembly, *Langmuir*, **2005**, 21 (16), 7558-7567.
15. Porcel, C.H., et al., Ultrathin coatings and (poly(glutamic acid)/polyallylamine) films deposited by continuous and simultaneous spraying, *Langmuir*, **2005**, 21 (2), 800-802.
16. Lefort, M., et al., Spray-On Organic/Inorganic Films: A General Method for the Formation of Functional Nano- to Microscale Coatings, *Angewandte Chemie-International Edition*, **2010**, 49 (52), 10110-10113.

17. Cado, G., et al., Polysaccharide Films Built by Simultaneous or Alternate Spray: A Rapid Way to Engineer Biomaterial Surfaces, *Langmuir*, **2012**, 28 (22), 8470-8478.
18. Lavallo, P., et al., Comparison of the structure of polyelectrolyte multilayer films exhibiting a linear and an exponential growth regime: An in situ atomic force microscopy study, *Macromolecules*, **2002**, 35 (11), 4458-4465.
19. Felix, O., et al., Are sprayed LbL-films stratified? A first assessment of the nanostructure of spray-assembled multilayers by neutron reflectometry, *Comptes Rendus Chimie*, **2009**, 12 (1-2), 225-234.
20. Ruths, J., et al., Polyelectrolytes I: Polyanion/polycation multilayers at the air/monolayer/water interface as elements for quantitative polymer adsorption studies and preparation of hetero-superlattices on solid surfaces, *Langmuir*, **2000**, 16 (23), 8871-8878.
21. McAloney, R.A., et al., Atomic force microscopy studies of salt effects on polyelectrolyte multilayer film morphology, *Langmuir*, **2001**, 17 (21), 6655-6663.
22. Elbert, D.L., et al., Thin polymer layers formed by polyelectrolyte multilayer techniques on biological surfaces, *Langmuir*, **1999**, 15 (16), 5355-5362.
23. Picart, C., et al., Buildup mechanism for poly(L-lysine)/hyaluronic acid films onto a solid surface, *Langmuir*, **2001**, 17 (23), 7414-7424.
24. Picart, C., et al., Molecular basis for the explanation of the exponential growth of polyelectrolyte multilayers, *Proceedings of the National Academy of Sciences of the United States of America*, **2002**, 99 (20), 12531-12535.
25. Lavallo, P., et al., Modeling the buildup of polyelectrolyte multilayer films having exponential growth, *Journal of Physical Chemistry B*, **2004**, 108 (2), 635-648.
26. Picart, C., et al., Buildup Mechanism for Poly (L -lysine)/ Hyaluronic Acid Films onto a Solid Surface, *Langmuir*, **2001** (17), 7414-7424.
27. Boulmedais, F., et al., Buildup of exponentially growing multilayer polypeptide films with internal secondary structure, *Langmuir*, **2003**, 19 (2), 440-445.
28. Hubsch, E., et al., Controlling the growth regime of polyelectrolyte multilayer films: Changing from exponential to linear growth by adjusting the composition of polyelectrolyte mixtures, *Langmuir*, **2004**, 20 (5), 1980-1985.
29. Porcel, C., et al., From exponential to linear growth in polyelectrolyte multilayers, *Langmuir*, **2006**, 22 (9), 4376-83.
30. Laugel, N., et al., Relationship between the growth regime of polyelectrolyte multilayers and the polyanion/polycation complexation enthalpy, *The journal of physical chemistry. B*, **2006**, 110 (39), 19443-9.
31. Lvov, Y., et al., Assembly, structural characterization, and thermal-behavior of layer-by-layer deposited ultrathin films of poly(vinyl sulfate) and poly(allylamine) *Langmuir*, **1993**, 9 (2), 481-486.

32. Decher, G., Scmitt, J., Fine-tuning of the film thickness of ultrathin multilayer films composed of consecutively alternating layers of anionic and cationic polyelectrolytes, *Progress in Colloid & Polymer Science*, **1992**, 89, 160-164.
33. Ladam, G., et al., In situ determination of the structural properties of initially deposited polyelectrolyte multilayers, *Langmuir*, **2000**, 16 (3), 1249-1255.
34. Richert, L., et al., Layer by layer buildup of polysaccharide films: Physical chemistry and cellular adhesion aspects, *Langmuir*, **2004**, 20 (2), 448-458.
35. Salomaki, M., et al., The Hofmeister anion effect and the growth of polyelectrolyte multilayers, *Langmuir*, **2004**, 20 (9), 3679-3683.
36. El Haitami, A.E., et al., Effect of the Supporting Electrolyte Anion on the Thickness of PSS/PAH Multilayer Films and on Their Permeability to an Electroactive Probe, *Langmuir*, **2009**, 25 (4), 2282-2289.
37. Salomäki, M., et al., Effect of temperature on the buildup of polyelectrolyte multilayers, *Langmuir* **2005**, 21 (24), 11232-40.
38. Yoo, D., et al., Controlling bilayer composition and surface wettability of sequentially adsorbed multilayers of weak polyelectrolytes, *Macromolecules*, **1998**, 31 (13), 4309-4318.
39. Shiratori, S.S., et al., pH-dependent thickness behavior of sequentially adsorbed layers of weak polyelectrolytes, *Macromolecules*, **2000**, 33 (11), 4213-4219.
40. Porcel, C., et al., Influence of the polyelectrolyte molecular weight on exponentially growing multilayer films in the linear regime, *Langmuir*, **2007**, 23 (4), 1898-1904.
41. Kujawa, P., et al., Effect of molecular weight on the exponential growth and morphology of hyaluronan/chitosan multilayers: A surface plasmon resonance spectroscopy and atomic force microscopy investigation, *Journal of the American Chemical Society*, **2005**, 127 (25), 9224-9234.
42. Dubas, S.T., et al., Factors controlling the growth of polyelectrolyte multilayers, *Macromolecules*, **1999**, 32 (24), 8153-8160.
43. Zhang, Y., et al., Novel alternating polymer adsorption/surface activation self-assembled film based on hydrogen bond, *Thin Solid Films*, **2003**, 437, 280-284.
44. Stockton, W.B., et al., Molecular-level processing of conjugated polymers .4. Layer-by-layer manipulation of polyaniline via hydrogen-bonding interactions, *Macromolecules*, **1997**, 30 (9), 2717-2725.
45. Krass, H., et al., Layer-by-Layer Self-assembly of a Polyelectrolyte Bearing Metal Ion Coordination and Electrostatic Functionality, *Chemistry of Materials*, **2003**, 15 (1), 196-203.
46. Arunan, E., et al., Definition of the hydrogen bond (IUPAC Recommendations 2011), *Pure and Applied Chemistry*, **2011**, 83 (8), 1637-1641.

47. Wang, L.Y., et al., A new approach for the fabrication of an alternating multilayer film of poly(4-vinylpyridine) and poly(acrylic acid) based on hydrogen bonding, *Macromolecular Rapid Communications*, **1997**, 18 (6), 509-514.
48. Sukhishvili, S.A., et al., Layered, erasable polymer multilayers formed by hydrogen-bonded sequential self-assembly, *Macromolecules*, **2002**, 35 (1), 301-310.
49. Quinn, J.F., et al., Next generation, sequentially assembled ultrathin films: beyond electrostatics, *Chemical Society Reviews*, **2007**, 36 (5), 707-718.
50. van de Manakker, F., et al., Cyclodextrin-Based Polymeric Materials: Synthesis, Properties, and Pharmaceutical/Biomedical Applications, *Biomacromolecules*, **2009**, 10 (12), 3157-3175.
51. Harries, D., et al., Solutes Probe Hydration in Specific Association of Cyclodextrin and Adamantane, *Journal of the American Chemical Society*, **2005**, 127, 2184-2190.
52. Eftink, M.R., et al., Cyclodextrin inclusion complexes - studies of the variation in the size of alicyclic guests *Journal of the American Chemical Society*, **1989**, 111 (17), 6765-6772.
53. Rekharsky, M.V., et al., Complexation Thermodynamics of Cyclodextrins, *Chemical reviews*, **1998**, 98 (5), 1875-1918.
54. Kunz, W., et al., 'Zur Lehre von der Wirkung der Salze' (about the science of the effect of salts): Franz Hofmeister's historical papers, *Current Opinion in Colloid & Interface Science*, **2004**, 9 (1-2), 19-37.
55. Lo Nostro, P., et al., Hofmeister effects in supramolecular and biological systems, *Biophysical Chemistry*, **2006**, 124 (3), 208-213.
56. Rohrbach, R.P., et al., An Equilibrium and Kinetic Investigation of Salt-Cycloamylase Complexes, *Journal of Physical Chemistry*, **1977**, 81 (10), 944-948.
57. Buvari, A., et al., Complex Formation of Inorganic Salts with beta-cyclodextrin, *Journal of Inclusion Phenomena*, **1989**, 7 (3), 379-389.
58. Harries, D., et al., Solutes probe hydration in specific association of cyclodextrin and adamantane, *Journal of the American Chemical Society*, **2005**, 127 (7), 2184-2190.
59. Gurnev, P.A., et al., The Dynamic Side of the Hofmeister Effect: A Single-Molecule Nanopore Study of Specific Complex Formation, *Chemphyschem*, **2009**, 10 (9-10), 1445-1449.
60. Goyenechea, N., et al., Inclusion complexes of nabumetone with beta-cyclodextrins: thermodynamics and molecular modelling studies. Influence of sodium perchlorate, *Luminescence*, **2001**, 16 (2), 117-127.
61. Fini, P., et al., The effects of increasing NaCl concentration on the stability of inclusion complexes in aqueous solution, *Journal of Thermal Analysis and Calorimetry*, **2003**, 73 (2), 653-659.

62. Dey, J., et al., Effect of sodium perchlorate on the binding of 2-(4'-aminophenyl)- and 2-(4'-(N,N'-dimethylamino)phenyl)benzothiazole with beta-cyclodextrin in aqueous solution, *Journal of Physical Chemistry A*, **1998**, 102 (1), 301-305.
63. Kotake, Y., et al., Effect of Ph and Salt Concentration on Bimodal Inclusion of a Nitroxide by Cyclodextrins, *Journal of the American Chemical Society*, **1989**, 111 (19), 7319-7323.
64. Yi, Z.P., et al., Investigation of buffer-cyclodextrin systems, *Physical Chemistry Chemical Physics*, **1999**, 1 (3), 441-444.
65. Rohrbach, R.P., et al., An Equilibrium and Kinetic Investigation of Salt-Cycloamylose Complexes, *J. Phys. Chem.*, **1977**, 81 (10), 944-948.
66. Chamberlain, R.V., et al., Electrostatically-induced inclusion of anions in cyclodextrin monolayers on electrodes, *Langmuir*, **2000**, 16 (3), 1388-1396.
67. Sasaki, M., et al., Kinetic-Study on Inclusion Compound Formation Reaction of Beta-Cyclodextrin Polymer with Scn- Using the Electric-Field Pulse Technique, *Journal of Physical Chemistry*, **1983**, 87 (1), 5-6.
68. Kano, K., et al., Tetraarylporphyrins as probes for studying mechanism of inclusion-complex formation of cyclodextrins. Effect of microscopic environment on inclusion of ionic guests, *Chemistry Letters*, **1996** (11), 925-926.
69. Sato, K., et al., Preparation of polyelectrolyte-layered assemblies containing cyclodextrin and their binding properties, *Langmuir*, **2003**, 19 (18), 7406-7412.
70. Daubine, F., et al., Nanostructured polyelectrolyte multilayer drug delivery systems for bone metastasis prevention, *Biomaterials*, **2009**, 30 (31), 6367-6373.
71. Martin, A., et al., Build-up of an antimicrobial multilayer coating on a textile support based on a methylene blue-poly(cyclodextrin) complex, *Biomedical Materials*, **2013**, 8 (6), 14.
72. El Fagui, A., et al., Layer- by- Layer Coated PLA Nanoparticles with Oppositely Charged similar to- Cyclodextrin Polymer for Controlled Delivery of Lipophilic Molecules, *Macromolecular Chemistry and Physics*, **2014**, 215 (6), 555-565.
73. Suzuki, I., et al., Construction of positively-charged layered assemblies assisted by cyclodextrin complexation, *Chemical communications* **2002** (2), 164-5.
74. Crespo-Biel, O., et al., Supramolecular layer-by-layer assembly: Alternating adsorptions of guest- and host-functionalized molecules and particles using multivalent supramolecular interactions, *Journal of the American Chemical Society*, **2005**, 127 (20), 7594-7600.
75. Van der Heyden, A., et al., Multilayer films based on host-guest interactions between biocompatible polymers, *Chemical communications* **2006** (30), 3220-2.

76. Wang, Z.P., et al., Stepwise assembly of the same polyelectrolytes using host-guest interaction to obtain microcapsules with multiresponsive properties, *Chemistry of Materials*, **2008**, 20 (13), 4194-4199.
77. Fou, A.C., et al., Fabrication and properties of light-emitting diodes based on self-assembled multilayers of poly(phenylene vinylene), *Journal of Applied Physics*, **1996**, 79 (10), 7501-7509.
78. Eckle, M., et al., Tuning the performance of layer-by-layer assembled organic light emitting diodes by controlling the position of isolating clay barrier sheets, *Nano Letters*, **2001**, 1 (1), 45-49.
79. Hiller, J., et al., Reversibly erasable nanoporous anti-reflection coatings from polyelectrolyte multilayers, *Nature Materials*, **2002**, 1 (1), 59-63.
80. Liu, X.Y., et al., Size-selective transport of uncharged solutes through multilayer polyelectrolyte membranes, *Chemistry of Materials*, **2004**, 16 (2), 351-357.
81. Stanton, B.W., et al., Ultrathin, multilayered polyelectrolyte films as nanofiltration membranes, *Langmuir*, **2003**, 19 (17), 7038-7042.
82. Farhat, T.R., et al., Designing a new generation of proton-exchange membranes using layer-by-layer deposition of polyelectrolytes, *Advanced Functional Materials*, **2005**, 15 (6), 945-954.
83. Onda, M., et al., Sequential reaction and product separation on molecular films of glucoamylase and glucose oxidase assembled on an ultrafilter, *Journal of Fermentation and Bioengineering*, **1996**, 82 (5), 502-506.
84. Izumrudov, V.A., et al., Multilayers of a globular protein and a weak polyacid: Role of polyacid ionization in growth and decomposition in salt solutions, *Biomacromolecules*, **2005**, 6 (3), 1782-1788.
85. Vazquez, E., et al., Construction of hydrolytically-degradable thin films via layer-by-layer deposition of degradable polyelectrolytes, *Journal of the American Chemical Society*, **2002**, 124 (47), 13992-13993.
86. Chluba, J., et al., Peptide hormone covalently bound to polyelectrolytes and embedded into multilayer architectures conserving full biological activity, *Biomacromolecules*, **2001**, 2 (3), 800-805.
87. Jessel, N., et al., Bioactive coatings based on a polyelectrolyte multilayer architecture functionalized by embedded proteins, *Advanced Materials*, **2003**, 15 (9), 692-695.
88. Thierry, B., et al., Delivery platform for hydrophobic drugs: Prodrug approach combined with self-assembled multilayers, *Journal of the American Chemical Society*, **2005**, 127 (6), 1626-1627.
89. von Eiff, C., et al., Infections associated with medical devices - Pathogenesis, management and prophylaxis, *Drugs*, **2005**, 65 (2), 179-214.

90. Guggenbichler, J.P., et al., Incidence and clinical implication of nosocomial infections associated with implantable biomaterials - catheters, ventilator-associated pneumonia, urinary tract infections, *GMS Krankenhaushygiene interdisziplinär*, **2011**, 6 (1), Doc18.
91. Lowy, F.D., Medical progress - Staphylococcus aureus infections, *New England Journal of Medicine*, **1998**, 339 (8), 520-532.
92. Donlan, R.M., et al., Biofilms : Survival Mechanisms of Clinically Relevant Microorganisms *Biofilms : Survival Mechanisms of Clinically Relevant Microorganisms*, **2002**, 15 (2).
93. Cunningham B., L.J.E.a.R.R.J., *Biofilms: the hypertextbook*, **2011**.
94. Harriott, M.M., et al., Candida albicans and Staphylococcus aureus Form Polymicrobial Biofilms: Effects on Antimicrobial Resistance, *Antimicrobial Agents and Chemotherapy*, **2009**, 53 (9), 3914-3922.
95. Lichter, J.A., et al., Design of Antibacterial Surfaces and Interfaces: Polyelectrolyte Multilayers as a Multifunctional Platform, *Macromolecules*, **2009**, 42 (22), 8573-8586.
96. Costa, F., et al., Covalent immobilization of antimicrobial peptides (AMPs) onto biomaterial surfaces, *Acta biomaterialia*, **2011**, 7 (4), 1431-40.
97. Peters, B.M., et al., Antimicrobial Peptides: Primeval Molecules or Future Drugs?, *Plos Pathogens*, **2010**, 6 (10), 4.
98. Diamond, G., et al., The Roles of Antimicrobial Peptides in Innate Host Defense, *Current Pharmaceutical Design*, **2009**, 15 (21), 2377-2392.
99. Seo, M.D., et al., Antimicrobial Peptides for Therapeutic Applications: A Review, *Molecules*, **2012**, 17 (10), 12276-12286.
100. Brogden, K.A., Antimicrobial peptides: Pore formers or metabolic inhibitors in bacteria?, *Nature Reviews Microbiology*, **2005**, 3 (3), 238-250.
101. Lai, R., et al., An anionic antimicrobial peptide from toad Bombina maxima, *Biochemical and Biophysical Research Communications*, **2002**, 295 (4), 796-799.
102. Schitteck, B., et al., Dermcidin: a novel human antibiotic peptide secreted by sweat glands, *Nature Immunology*, **2001**, 2 (12), 1133-1137.
103. Gazit, E., et al., Interaction of the mammalian antibacterial peptide cecropin P1 with phospholipid-vesicles *Biochemistry*, **1995**, 34 (36), 11479-11488.
104. Yang, L., et al., Neutron off-plane scattering of aligned membranes. I. Method of measurement, *Biophysical Journal*, **1998**, 75 (2), 641-645.
105. Saltykova, E.S., et al., Interracial differences in expression of genes of antibacterial peptides, abaecin, hymenoptaecin, and defensin, in bees Apis mellifera mellifera and

- Apis mellifera caucasica*, *Journal of Evolutionary Biochemistry and Physiology*, **2005**, 41 (5), 506-510.
106. Subbalakshmi, C., et al., Mechanism of antimicrobial action of indolicidin, *Fems Microbiology Letters*, **1998**, 160 (1), 91-96.
107. Ward, P.P., et al., Lactoferrin and host defense, *Biochemistry and Cell Biology-Biochimie Et Biologie Cellulaire*, **2002**, 80 (1), 95-102.
108. Ramanathan, B., et al., Cathelicidins: microbicidal activity, mechanisms of action, and roles in innate immunity, *Microbes and Infection*, **2002**, 4 (3), 361-372.
109. Cociancich, S., et al., Insect defensin, an inducible antibacterial peptide, forms voltage-dependent channels in micrococcus luteus *Journal of Biological Chemistry*, **1993**, 268 (26), 19239-19245.
110. Yamaguchi, S., et al., Solid-state NMR investigations of peptide-lipid interaction and orientation of a ss-sheet antimicrobial peptide, protegrin, *Biochemistry*, **2002**, 41 (31), 9852-9862.
111. Bahar, A.A., et al., Antimicrobial peptides, *Pharmaceuticals* **2013**, 6 (12), 1543-75.
112. Helle, K.B., The granin family of uniquely acidic proteins of the diffuse neuroendocrine system: comparative and functional aspects, *Biological Reviews*, **2004**, 79 (4), 769-794.
113. Briolat, J., et al., New antimicrobial activity for the catecholamine release-inhibitory peptide from chromogranin A, *Cellular and molecular life sciences : CMLS*, **2005**, 62 (3), 377-85.
114. Lugardon, K., et al., Antibacterial and antifungal activities of vasostatin-1, the N-terminal fragment of chromogranin A, *Journal of Biological Chemistry*, **2000**, 275 (15), 10745-10753.
115. Metz-Boutigue, M.H., et al., Intracellular and extracellular processing of chromogranin A - determination of cleavage sites *European Journal of Biochemistry*, **1993**, 217 (1), 247-257.
116. Radek, K., et al., Antimicrobial peptides: natural effectors of the innate immune system, *Seminars in Immunopathology*, **2007**, 29 (1), 27-43.
117. Aslam, R., *Chromogranin A derived antimicrobial peptides and Staphylococcus aureus: from host pathogen interaction analysis to development of antimicrobial polymer coating*. 2013.
118. Jean-François, F., et al., Aggregation of cateslytin beta-sheets on negatively charged lipids promotes rigid membrane domains. A new mode of action for antimicrobial peptides?, *Biochemistry*, **2008**, 47 (24), 6394-402.
119. Jean-François, F., et al., Pore formation induced by an antimicrobial peptide: electrostatic effects, *Biophysical journal*, **2008**, 95 (12), 5748-56.

120. Amim, J., et al., Structural aspects of polyanion and hydrophobically modified polycation multilayers on hydrophilic or hydrophobic surfaces, *Soft Matter*, **2012**, 8 (24), 6462-6470.
121. Illergard, J., et al., Biointeractive antibacterial fibres using polyelectrolyte multilayer modification, *Cellulose*, **2012**, 19 (5), 1731-1741.
122. Wang, Y.F., et al., Surface properties of polyurethanes modified by bioactive polysaccharide-based polyelectrolyte multilayers, *Colloids and Surfaces B-Biointerfaces*, **2012**, 100, 77-83.
123. Bratskaya, S., et al., Adhesion and viability of two enterococcal strains on covalently grafted chitosan and chitosan/kappa-carrageenan multilayers, *Biomacromolecules*, **2007**, 8 (9), 2960-2968.
124. Corbitt, T.S., et al., Conjugated Polyelectrolyte Capsules: Light-Activated Antimicrobial Micro "Roach Motels", *Acs Applied Materials & Interfaces*, **2009**, 1 (1), 48-52.
125. Gomes, A.P., et al., Layer-by-layer deposition of antimicrobial polymers on cellulosic fibers: a new strategy to develop bioactive textiles, *Polymers for Advanced Technologies*, **2013**, 24 (11), 1005-1010.
126. Elsabee, M.Z., et al., Surface modification of polypropylene films by chitosan and chitosan/pectin multilayer, *Carbohydrate Polymers*, **2008**, 71 (2), 187-195.
127. Elbert, D.L., et al., Self-assembly and steric stabilization at heterogeneous, biological surfaces using adsorbing block copolymers, *Chemistry & Biology*, **1998**, 5 (3), 177-183.
128. Kenausis, G.L., et al., Poly(L-lysine)-g-poly(ethylene glycol) layers on metal oxide surfaces: Attachment mechanism and effects of polymer architecture on resistance to protein adsorption, *Journal of Physical Chemistry B*, **2000**, 104 (14), 3298-3309.
129. Cheng Y., K.E.T., Neoh K.G., Wang P., Tan K.L., Surface modification of polyaniline film grafting of poly(ethylene glycol) for reduction in protein adsorption and platelet adhesion, *Synth. Met.*, **2000**, 110, 47-55.
130. Park, K.D., et al., Bacterial adhesion on PEG modified polyurethane surfaces, *Biomaterials*, **1998**, 19 (7-9), 851-859.
131. Boulmedais, F., et al., Polyelectrolyte multilayer films with pegylated polypeptides as a new type of anti-microbial protection for biomaterials, *Biomaterials*, **2004**, 25 (11), 2003-2011.
132. Schmolke, H., et al., Polyelectrolyte multilayer surface functionalization of poly(dimethylsiloxane) (PDMS) for reduction of yeast cell adhesion in microfluidic devices, *Biomicrofluidics*, **2010**, 4 (4), 12.
133. Schmolke, H., et al., Poly(acrylic acid)-graft-poly(ethylene glycol) preparation and adsorption on polyelectrolyte multilayers (PEMs) for custom-made antiadhesive

- surfaces, *Physica Status Solidi a-Applications and Materials Science*, **2011**, 208 (6), 1290-1300.
134. Tang, L., et al., Bacterial anti-adhesive properties of polysulfone membranes modified with polyelectrolyte multilayers, *Journal of Membrane Science*, **2013**, 446, 201-211.
135. Reisch, A., et al., Anti-fouling phosphorylcholine bearing polyelectrolyte multilayers: Cell adhesion resistance at rest and under stretching, *Soft Matter*, **2010**, 6 (7), 1503-1512.
136. Riedl, C.R., et al., Heparin coating reduces encrustation of ureteral stents: a preliminary report, *International Journal of Antimicrobial Agents*, **2002**, 19 (6), 507-510.
137. Cassinelli, C., et al., Evaluation of interfacial properties of hyaluronan coated poly(methylmethacrylate) intraocular lenses, *Journal of Biomaterials Science-Polymer Edition*, **2000**, 11 (9), 961-977.
138. Rabea, E.I., et al., Chitosan as antimicrobial agent: Applications and mode of action, *Biomacromolecules*, **2003**, 4 (6), 1457-1465.
139. Fu, J.H., et al., Construction of anti-adhesive and antibacterial multilayer films via layer-by-layer assembly of heparin and chitosan, *Biomaterials*, **2005**, 26 (33), 6684-6692.
140. Almodovar, J., et al., Chitosan-heparin polyelectrolyte multilayers on cortical bone: Periosteum-mimetic, cytophilic, antibacterial coatings, *Biotechnology and Bioengineering*, **2013**, 110 (2), 609-618.
141. Chua, P.H., et al., Structural stability and bioapplicability assessment of hyaluronic acid-chitosan polyelectrolyte multilayers on titanium substrates, *Journal of Biomedical Materials Research Part A*, **2008**, 87A (4), 1061-1074.
142. Lichter, J.A., et al., Substrata mechanical stiffness can regulate adhesion of viable bacteria, *Biomacromolecules*, **2008**, 9 (6), 1571-1578.
143. Saha, N., et al., Influence of Polyelectrolyte Film Stiffness on Bacterial Growth, *Biomacromolecules*, **2013**, 14 (2), 520-528.
144. Vazquez, C.P., et al., Variation of Polyelectrolyte Film Stiffness by Photo-Cross-Linking: A New Way To Control Cell Adhesion, *Langmuir*, **2009**, 25 (6), 3556-3563.
145. Lichter, J.A., et al., Polyelectrolyte Multilayers with Intrinsic Antimicrobial Functionality: The Importance of Mobile Polycations, *Langmuir*, **2009**, 25 (13), 7686-7694.
146. Pinto, M.S., et al., The use of the pseudo-polyelectrolyte, poly(4-vinylphenol), in multilayered films as an antimicrobial surface coating, *Colloids and Surfaces a-Physicochemical and Engineering Aspects*, **2011**, 377 (1-3), 182-186.

147. Yang, J.M., et al., Chitosan/polyanion surface modification of styrene-butadiene-styrene block copolymer membrane for wound dressing, *Materials Science & Engineering C-Materials for Biological Applications*, **2014**, 34, 140-148.
148. Deng, H.B., et al., Enhanced bacterial inhibition activity of layer-by-layer structured polysaccharide film-coated cellulose nanofibrous mats via addition of layered silicate, *Carbohydrate Polymers*, **2011**, 83 (1), 239-245.
149. Xin, S.J., et al., Cytotoxicity and antibacterial ability of scaffolds immobilized by polysaccharide/layered silicate composites, *Carbohydrate Polymers*, **2013**, 92 (2), 1880-1886.
150. Wang, X.Y., et al., Preparation, characterization and antimicrobial activity of chitosan/layered silicate nanocomposites, *Polymer*, **2006**, 47 (19), 6738-6744.
151. Zhou, B., et al., Chitosan/phosvitin antibacterial films fabricated via layer-by-layer deposition, *International Journal of Biological Macromolecules*, **2014**, 64, 402-408.
152. Huang, W.J., et al., Antibacterial multilayer films fabricated by LBL immobilizing lysozyme and HTCC on nanofibrous mats, *International Journal of Biological Macromolecules*, **2013**, 53, 26-31.
153. Khan, M.A.S., et al., Bactericidal action of egg yolk phosvitin against Escherichia coli under thermal stress, *Journal of Agricultural and Food Chemistry*, **2000**, 48 (5), 1503-1506.
154. Lian, Z.X., et al., Preparation and characterization of immobilized lysozyme and evaluation of its application in edible coatings, *Process Biochemistry*, **2012**, 47 (2), 201-208.
155. Wang, B.L., et al., Construction of Degradable Multilayer Films for Enhanced Antibacterial Properties, *Acs Applied Materials & Interfaces*, **2013**, 5 (10), 4136-4143.
156. van der Merwe, S.M., et al., Trimethylated chitosan as polymeric absorption enhancer for improved peroral delivery of peptide drugs, *European Journal of Pharmaceutics and Biopharmaceutics*, **2004**, 58 (2), 225-235.
157. Cui, D., et al., Contact-Killing Polyelectrolyte Microcapsules Based on Chitosan Derivatives, *Advanced Functional Materials*, **2010**, 20 (19), 3303-3312.
158. Graisuwan, W., et al., Multilayer film assembled from charged derivatives of chitosan: Physical characteristics and biological responses, *Journal of Colloid and Interface Science*, **2012**, 376, 177-188.
159. Follmann, H.D.M., et al., Antiadhesive and Antibacterial Multilayer Films via Layer-by-Layer Assembly of TMC/Heparin Complexes, *Biomacromolecules*, **2012**, 13 (11), 3711-3722.
160. Tripathi, B.P., et al., Functional polyelectrolyte multilayer membranes for water purification applications, *Journal of Hazardous Materials*, **2013**, 252, 401-412.

161. Wong, S.Y., et al., Bactericidal and virucidal ultrathin films assembled layer by layer from polycationic N-alkylated polyethylenimines and polyanions, *Biomaterials*, **2010**, 31 (14), 4079-4087.
162. Yang, W.J., et al., Layer-by-Layer Click Deposition of Functional Polymer Coatings for Combating Marine Biofouling, *Biomacromolecules*, **2012**, 13 (9), 2769-2780.
163. Pan, Y.F., et al., Antimicrobial and Thermal-Responsive Layer-by-Layer Assembly Based on Ionic-Modified Guanidine Polymer and PVA, *Polymer Bulletin*, **2008**, 61 (5), 541-551.
164. Mei, Y., et al., A simple approach to constructing antibacterial and anti-biofouling nanofibrous membranes, *Biofouling*, **2014**, 30 (3), 313-322.
165. Westman, E.H., et al., Antimicrobial activity of polyelectrolyte multilayer-treated cellulose films, *Holzforchung*, **2009**, 63 (1), 33-39.
166. Illergard, J., et al., Bacterial-growth inhibiting properties of multilayers formed with modified polyvinylamine, *Colloids and Surfaces B-Biointerfaces*, **2011**, 88 (1), 115-120.
167. Barnes, K., et al., Synthesis and antimicrobial applications of 5,5'-ethylenebis 5-methyl-3-(3-triethoxysilylpropyl)hydantoin, *Biomaterials*, **2006**, 27 (27), 4825-4830.
168. Cerkez, I., et al., N-Halamine Biocidal Coatings via a Layer-by-Layer Assembly Technique, *Langmuir*, **2011**, 27 (7), 4091-4097.
169. Kang, S., et al., Single-walled carbon nanotubes exhibit strong antimicrobial activity, *Langmuir*, **2007**, 23 (17), 8670-8673.
170. Aslan, S., et al., Carbon nanotube-based antimicrobial biomaterials formed via layer-by-layer assembly with polypeptides, *Journal of Colloid and Interface Science*, **2012**, 388, 268-273.
171. Aslan, S., et al., Carbon nanotube bundling: influence on layer-by-layer assembly and antimicrobial activity, *Soft Matter*, **2013**, 9 (7), 2136-2144.
172. Nepal, D., et al., Strong antimicrobial coatings: Single-walled carbon nanotubes armored with biopolymers, *Nano Letters*, **2008**, 8 (7), 1896-1901.
173. Pavlukhina, S.V., et al., Noneluting Enzymatic Antibiofilm Coatings, *Acs Applied Materials & Interfaces*, **2012**, 4 (9), 4708-4716.
174. *Biofunctional Textiles and the Skin*, ed. P.E. U.-C. Hipler. Vol. 33. Karger.
175. Kumar, R., et al., Silver ion release from antimicrobial polyamide/silver composites, *Biomaterials*, **2005**, 26 (14), 2081-2088.
176. Kumar, R., et al., Polyamide/silver antimicrobials: Effect of filler types on the silver ion release, *Journal of Biomedical Materials Research Part B-Applied Biomaterials*, **2005**, 75B (2), 311-319.

177. Dubas, S.T., et al., Layer-by-layer deposition of antimicrobial silver nanoparticles on textile fibers, *Colloids and Surfaces a-Physicochemical and Engineering Aspects*, **2006**, 289 (1-3), 105-109.
178. Imani, R., et al., Production of antibacterial filter paper from wood cellulose *Bioresources*, **2011**, 6 (1), 891-900.
179. Rahaman, M.S., et al., Control of biofouling on reverse osmosis polyamide membranes modified with biocidal nanoparticles and antifouling polymer brushes, *Journal of Materials Chemistry B*, **2014**, 2 (12), 1724-1732.
180. Yu, D.G., et al., Surface modification of poly(L-lactic acid) membrane via layer-by-layer assembly of silver nanoparticle-embedded polyelectrolyte multilayer, *Bioconjugate Chemistry*, **2007**, 18 (5), 1521-1529.
181. Wang, B.L., et al., Fast and long-acting antibacterial properties of chitosan-Ag/polyvinylpyrrolidone nanocomposite films, *Carbohydrate Polymers*, **2012**, 90 (1), 8-15.
182. Podsiadlo, P., et al., Layer-by-layer assembly of nacre-like nanostructured composites with antimicrobial properties, *Langmuir*, **2005**, 21 (25), 11915-11921.
183. Agarwal, A., et al., Surfaces modified with nanometer-thick silver-impregnated polymeric films that kill bacteria but support growth of mammalian cells, *Biomaterials*, **2010**, 31 (4), 680-690.
184. Agarwal, A., et al., Polymeric Multilayers that Contain Silver Nanoparticles can be Stamped onto Biological Tissues to Provide Antibacterial Activity, *Advanced Functional Materials*, **2011**, 21 (10), 1863-1873.
185. Lee, D., et al., Antibacterial properties of Ag nanoparticle loaded multilayers and formation of magnetically directed antibacterial microparticles, *Langmuir*, **2005**, 21 (21), 9651-9659.
186. Cui, X.Q., et al., In situ fabrication of silver nanoarrays in hyaluronan/PDDA layer-by-layer assembled structure, *Journal of Colloid and Interface Science*, **2008**, 327 (2), 459-465.
187. Wang, T.C., et al., Polyelectrolyte multilayer nanoreactors for preparing silver nanoparticle composites: Controlling metal concentration and nanoparticle size, *Langmuir*, **2002**, 18 (8), 3370-3375.
188. Zan, X.J., et al., Incorporation of Nanoparticles into Polyelectrolyte Multilayers via Counterion Exchange and in situ Reduction, *Langmuir*, **2009**, 25 (20), 12355-12360.
189. Zan, X.J., et al., Counterions in polyelectrolyte multilayers: A vehicle for introducing functionalities, *Thin Solid Films*, **2009**, 518 (1), 116-119.
190. Guthrie, K.M., et al., Integration of Silver Nanoparticle-impregnated Polyelectrolyte Multilayers Into Murine-Splinted Cutaneous Wound Beds, *Journal of Burn Care & Research*, **2013**, 34 (6), E359-E367.

191. Zan, X.J., et al., Polyelectrolyte multilayer films containing silver as antibacterial coatings, *Thin Solid Films*, **2010**, 518 (19), 5478-5482.
192. Choi, W.S., et al., Synthesis of two types of nanoparticles in polyelectrolyte capsule nanoreactors and their dual functionality, *Journal of the American Chemical Society*, **2005**, 127 (46), 16136-16142.
193. Lee, D., et al., Formation of nanoparticle-loaded microcapsules based on hydrogen-bonded multilayers, *Chemistry of Materials*, **2005**, 17 (5), 1099-1105.
194. Dai, J.H., et al., Catalytic nanoparticles formed by reduction of metal ions in multilayered polyelectrolyte films, *Nano Letters*, **2002**, 2 (5), 497-501.
195. Yin, B., et al., Prolonging the Duration of Preventing Bacterial Adhesion of Nanosilver-Containing Polymer Films through Hydrophobicity, *Langmuir*, **2012**, 28 (49), 17019-17025.
196. Shi, Z., et al., In vitro antibacterial and cytotoxicity assay of multilayered polyelectrolyte-functionalized stainless steel, *Journal of Biomedical Materials Research Part A*, **2006**, 76A (4), 826-834.
197. Guthrie, K.M., et al., Antibacterial Efficacy of Silver-Impregnated Polyelectrolyte Multilayers Immobilized on a Biological Dressing in a Murine Wound Infection Model, *Annals of Surgery*, **2012**, 256 (2), 371-377.
198. Lee, H., et al., Substrate-independent layer-by-layer assembly by using mussel-adhesive-inspired polymers, *Advanced Materials*, **2008**, 20 (9), 1619-+.
199. Zhang, X.M., et al., Cytotoxicity and antibacterial property of titanium alloy coated with silver nanoparticle-containing polyelectrolyte multilayer, *Materials Science & Engineering C-Materials for Biological Applications*, **2013**, 33 (5), 2816-2820.
200. Celen, B., et al., Green catalysts based on bio-inspired polymer coatings and electroless plating of silver nanoparticles, *Journal of Molecular Catalysis a-Chemical*, **2011**, 350 (1-2), 97-102.
201. Sureshkumar, M., et al., Magnetic antimicrobial nanocomposite based on bacterial cellulose and silver nanoparticles, *Journal of Materials Chemistry*, **2010**, 20 (33), 6948-6955.
202. Wang, W.C., et al., Dopamine-Induced Surface Functionalization for the Preparation of Al-Ag Bimetallic Microspheres, *Journal of the Electrochemical Society*, **2011**, 158 (4), D228-D233.
203. Li, Z., et al., Two-level antibacterial coating with both release-killing and contact-killing capabilities, *Langmuir*, **2006**, 22 (24), 9820-9823.
204. Fu, J.H., et al., Construction of antibacterial multilayer films containing nanosilver via layer-by-layer assembly of heparin and chitosan-silver ions complex, *Journal of Biomedical Materials Research Part A*, **2006**, 79A (3), 665-674.

205. Urrutia, A., et al., Single-stage in situ synthesis of silver nanoparticles in antibacterial self-assembled overlays, *Colloid and Polymer Science*, **2012**, 290 (9), 785-792.
206. Charlot, A., et al., All-in-one strategy for the fabrication of antimicrobial biomimetic films on stainless steel, *Journal of Materials Chemistry*, **2009**, 19 (24), 4117-4125.
207. Gao, S.Y., et al., Preparation and characterization of polyoxometalate-Ag nanoparticles composite multilayer films, *Thin Solid Films*, **2011**, 519 (7), 2317-2322.
208. Grunlan, J.C., et al., Antimicrobial behavior of polyelectrolyte multilayer films containing cetrinide and silver, *Biomacromolecules*, **2005**, 6 (2), 1149-1153.
209. Urrutia, A., et al., An antibacterial surface coating composed of PAH/SiO₂ nanostructured films by layer by layer, *Physica Status Solidi C: Current Topics in Solid State Physics, Vol 7, No 11-12*, **2010**, 7 (11-12), 2774-2777.
210. Liu, T., et al., Complementary Effects of Nanosilver and Superhydrophobic Coatings on the Prevention of Marine Bacterial Adhesion, *Acs Applied Materials & Interfaces*, **2012**, 4 (9), 4683-4690.
211. Malcher, M., et al., Embedded Silver Ions-Containing Liposomes in Polyelectrolyte Multilayers : Cargos Films for Antibacterial Agents, *Society*, **2008** (4), 10209-10215.
212. Huang, X.Y., et al., Formation and Tunable Disassembly of Polyelectrolyte-Cu²⁺ Layer-by-Layer Complex Film, *Langmuir*, **2013**, 29 (42), 12959-12968.
213. de Paiva, R.G., et al., Multilayer biopolymer membranes containing copper for antibacterial applications, *Journal of Applied Polymer Science*, **2012**, 126, E17-E24.
214. Feng, Y.H., et al., Fabrication and characterization of multilayer films based on Keggin-type polyoxometalate and chitosan, *Materials Letters*, **2006**, 60 (13-14), 1588-1593.
215. Yuan, W.Y., et al., A facile method to construct hybrid multilayered films as a strong and multifunctional antibacterial coating, *Journal of Biomedical Materials Research Part B-Applied Biomaterials*, **2008**, 85B (2), 556-563.
216. Gabriel, D., et al., A photo-triggered layered surface coating producing reactive oxygen species, *Biomaterials*, **2013**, 34 (38), 9763-9769.
217. Jiang, B.B., et al., Tunable drug loading and release from polypeptide multilayer nanofilms, *International Journal of Nanomedicine*, **2009**, 4 (1), 37-53.
218. Li, H.S., et al., Cefazolin Embedded Biodegradable Polypeptide Nanofilms Promising for Infection Prevention: A Preliminary Study on Cell Responses, *Journal of Orthopaedic Research*, **2010**, 28 (8), 992-999.
219. Blaze, M.M.T., et al., Quantification of Antibiotic in Biofilm-Inhibiting Multilayers by 7.87 eV Laser Desorption Postionization MS Imaging, *Analytical Chemistry*, **2012**, 84 (21), 9410-9415.

220. Torger, B., et al., In situ-ATR-FTIR analysis on the uptake and release of streptomycin from polyelectrolyte complex layers, *Spectrochimica Acta Part a-Molecular and Biomolecular Spectroscopy*, **2013**, 104, 546-553.
221. Manju, S., et al., Layer-by-Layer modification of Poly (methyl methacrylate) intra ocular lens: Drug delivery applications, *Pharmaceutical Development and Technology*, **2010**, 15 (4), 379-385.
222. Chuang, H.F., et al., Polyelectrolyte multilayers for tunable release of antibiotics, *Biomacromolecules*, **2008**, 9 (6), 1660-1668.
223. Moskowitz, J.S., et al., The effectiveness of the controlled release of gentamicin from polyelectrolyte multilayers in the treatment of Staphylococcus aureus infection in a rabbit bone model, *Biomaterials*, **2010**, 31 (23), 6019-6030.
224. Shukla, A., et al., Tunable Vancomycin Releasing Surfaces for Biomedical Applications, *Small*, **2010**, 6 (21), 2392-2404.
225. Shukla, A., et al., Release of vancomycin from multilayer coated absorbent gelatin sponges, *Journal of Controlled Release*, **2012**, 157 (1), 64-71.
226. Zhang, Z.L., et al., Calcium Binding-Mediated Sustained Release of Minocycline from Hydrophilic Multilayer Coatings Targeting Infection and Inflammation, *Plos One*, **2014**, 9 (1), 8.
227. Min, J., et al., Tunable staged release of therapeutics from layer-by-layer coatings with clay interlayer barrier, *Biomaterials*, **2014**, 35 (8), 2507-2517.
228. Harnet, J.C., et al., Antibacterial protection of suture material by chlorhexidine-functionalized polyelectrolyte multilayer films, *Journal of Materials Science-Materials in Medicine*, **2009**, 20 (1), 185-193.
229. Agarwal, A., et al., Polymeric multilayers that localize the release of chlorhexidine from biologic wound dressings, *Biomaterials*, **2012**, 33 (28), 6783-6792.
230. Zelikin, A.N., Drug Releasing Polymer Thin Films: New Era of Surface-Mediated Drug Delivery, *Acs Nano*, **2010**, 4 (5), 2494-2509.
231. Shukla, A., et al., Design of multi-drug release coatings targeting infection and inflammation, *Journal of Controlled Release*, **2011**, 155 (2), 159-166.
232. Smith, R.C., et al., Layer-by-Layer Platform Technology for Small-Molecule Delivery, *Angewandte Chemie-International Edition*, **2009**, 48 (47), 8974-8977.
233. Minati, L., et al., Sustained in vitro release and cell uptake of doxorubicin adsorbed onto gold nanoparticles and covered by a polyelectrolyte complex layer, *International Journal of Pharmaceutics*, **2012**, 438 (1-2), 45-52.
234. Anandhakumar, S., et al., Polyelectrolyte microcapsules for sustained delivery of water-soluble drugs, *Materials Science & Engineering C-Materials for Biological Applications*, **2011**, 31 (2), 342-349.

235. Schmidt, D.J., et al., Electrically Triggered Release of a Small Molecule Drug from a Polyelectrolyte Multilayer Coating, *Chemistry of Materials*, **2010**, 22 (23), 6416-6425.
236. Anandhakumar, S., et al., Polyelectrolyte/silver nanocomposite multilayer films as multifunctional thin film platforms for remote activated protein and drug delivery, *Acta Biomaterialia*, **2013**, 9 (11), 8864-8874.
237. Sripriya, J., et al., Laser receptive polyelectrolyte thin films doped with biosynthesized silver nanoparticles for antibacterial coatings and drug delivery applications, *International Journal of Pharmaceutics*, **2013**, 457 (1), 206-213.
238. Pinheiro, A.C., et al., K-carrageenan/chitosan nanolayered coating for controlled release of a model bioactive compound, *Innovative Food Science & Emerging Technologies*, **2012**, 16, 227-232.
239. Nguyen, P.M., et al., Extended release antibacterial layer-by-layer films incorporating linear-dendritic block copolymer micelles, *Chemistry of Materials*, **2007**, 19 (23), 5524-5530.
240. Wang, X., et al., Optically Transparent Antibacterial Films Capable of Healing Multiple Scratches, *Advanced Functional Materials*, **2014**, 24 (3), 403-411.
241. Dvoracek, C.M., et al., Antimicrobial Behavior of Polyelectrolyte-Surfactant Thin Film Assemblies, *Langmuir*, **2009**, 25 (17), 10322-10328.
242. Kim, B.S., et al., Hydrogen-bonding layer-by-layer assembled biodegradable polymeric micelles as drug delivery vehicles from surfaces, *Acs Nano*, **2008**, 2 (2), 386-392.
243. Etienne, O., et al., Multilayer polyelectrolyte films functionalized by insertion of defensin: A new approach to protection of implants from bacterial colonization, *Antimicrobial Agents and Chemotherapy*, **2004**, 48 (10), 3662-3669.
244. Shukla, A., et al., *Antimicrobial Peptide Delivery from Degradable Polymer Thin Films*. 2009 35th Annual Northeast Bioengineering Conference. 2009, New York: Ieee. 26-27.
245. Shukla, A., et al., Controlling the release of peptide antimicrobial agents from surfaces, *Biomaterials*, **2010**, 31 (8), 2348-2357.
246. Guyomard, A., et al., Incorporation of a Hydrophobic Antibacterial Peptide into Amphiphilic Polyelectrolyte Multilayers: A Bioinspired Approach to Prepare Biocidal Thin Coatings, *Advanced Functional Materials*, **2008**, 18 (5), 758-765.
247. Pavluchhina, S., et al., Polymer Multilayers with pH-Triggered Release of Antibacterial Agents, *Biomacromolecules*, **2010**, 11 (12), 3448-3456.
248. Cado, A.S., Self-defensive biomaterial coating against bacteria and yeasts : polysaccharide multilayer film with embedded antimicrobial peptide, *advanced functional materials*, **2013**, 23 (28), 4801-4809.

249. Vreuls, C., et al., Biomolecules in multilayer film for antimicrobial and easy-cleaning stainless steel surface applications, *Biofouling*, **2010**, 26 (6), 645-656.
250. Etienne, O., et al., Antifungal coating by biofunctionalized polyelectrolyte multilayered films, *Biomaterials*, **2005**, 26 (33), 6704-12.
251. Karlsson, A.J., et al., Polyelectrolyte Multilayers Fabricated from Antifungal beta-Peptides: Design of Surfaces that Exhibit Antifungal Activity Against *Candida albicans*, *Biomacromolecules*, **2010**, 11 (9), 2321-2328.
252. Faure, E., et al., Sustainable and bio-inspired chemistry for robust antibacterial activity of stainless steel, *Journal of Materials Chemistry*, **2011**, 21 (22), 7901-7904.
253. Li, B.Y., et al., Multilayer polypeptide nanoscale coatings incorporating IL-12 for the prevention of biomedical device-associated infections, *Biomaterials*, **2009**, 30 (13), 2552-2558.

Chapter 2:

Materials and methods

Chapter 2:

Materials and methods

Summary

2.1 Materials	83
2.1.1 Polyelectrolytes	83
2.1.2 Neutral polymers	86
2.1.3 Host and guest molecules	87
2.1.4 Antimicrobial peptides	87
2.1.5 Bis-maleimide linkers	88
2.2 Physico-chemical characterizations	90
2.2.1 Quartz crystal microbalance	90
2.2.2 Surface plasmon resonance	93
2.2.3 Atomic force microscopy	94
2.2.4 Confocal laser scanning microscopy	97
2.2.5 Isothermal titration calorimetry	99
2.2.6 High-performance liquid chromatography	101
2.3 Biological characterizations	103
2.3.1 Buildup in cell culture plates	103
2.3.2 Cytocompatibility tests	103
2.3.3 Antibacterial and antifungal tests	104
2.3.4 Hemolysis assays	106
2.3.5 Inflammatory assays	106
Chapter 2 references	109

This second chapter describes the materials and methods used for this thesis work. All polymers and molecules are listed. The various physico-chemical characterizations either on surfaces or on molecules in solution and the biological characterizations performed are reported.

2.1 Materials

Commercial polymers, synthesized polymers, host/guest molecules and antimicrobial peptides solutions were all prepared using Milli-Q ultrapure water (Milli-Q Plus system, Millipore, Billerica, MA) that has a resistivity of 18.2 M Ω .cm. All commercial chemical compounds were used without further purification.

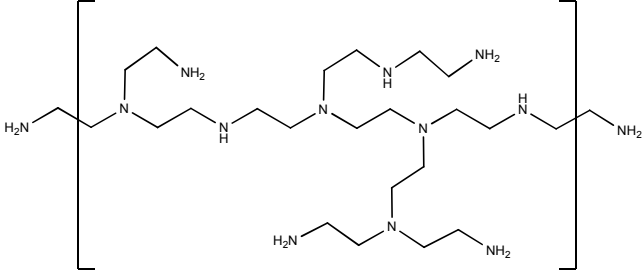
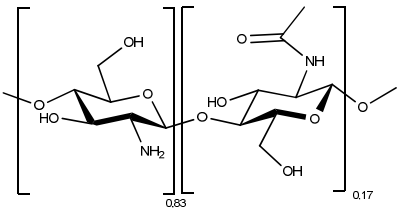
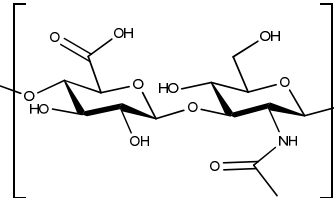
2.1.1 Polyelectrolytes

Commercial polyelectrolytes

The commercial polyelectrolytes used for the buildup of the antimicrobial multilayer films are listed in Table 2.1. The branched poly(ethylene imine) (PEI) is a polycation used as a first anchoring layer for the buildup of a polyelectrolyte multilayer film. Chitosan (CHI), a polycation, and hyaluronic acid (HA), a polyanion, are both polysaccharides. Due to their opposite charged chains, they can be alternately deposited to form a polyelectrolyte multilayer thanks to electrostatic interactions.

The polyelectrolytes were dissolved in a 150 mM NaCl solution prepared with Milli-Q water. PEI was dissolved at a concentration of 0.5 mg.mL⁻¹ and the pH of the solution was adjusted to 7.4 by addition of a 0.1 M NaOH solution. CHI and HA were dissolved at 0.3 mg.mL⁻¹. The pH of the HA solution was adjusted to 4 by addition of a 0.1 M HCl solution. CHI was first dissolved in a 150 mM NaCl solution at pH 2 before adjusting the pH to 4 by addition of a 0.1 NaOH solution.

Table 2.1: Polyanions and polycations used for the buildup of antimicrobial PEM films.

Polyelectrolyte	Structure	Mw (g.mol ⁻¹)	Supplier
Branched poly(ethylene imine) PEI		60 000	Sigma-Aldrich
Chitosan CHI		260 000	Novamatrix
Hyaluronic acid HA		420 000	Lifecore Biomedical

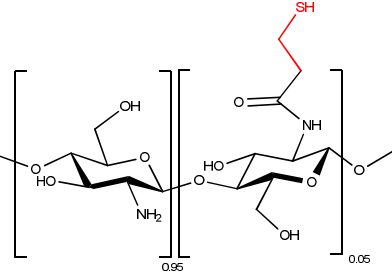
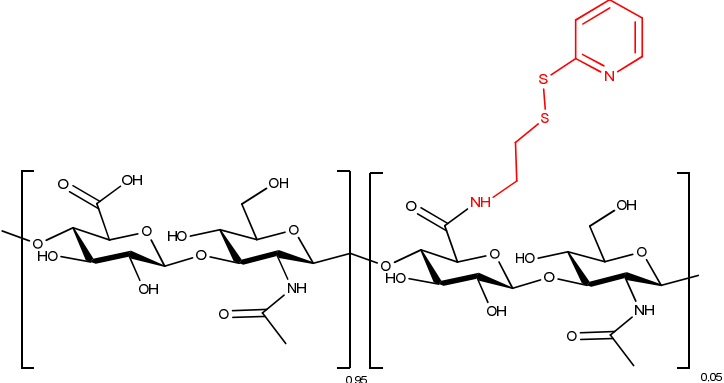
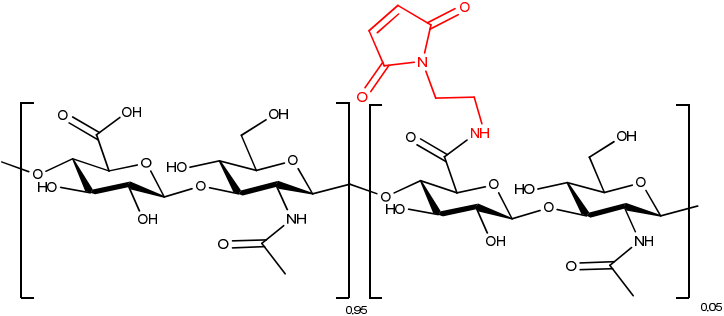
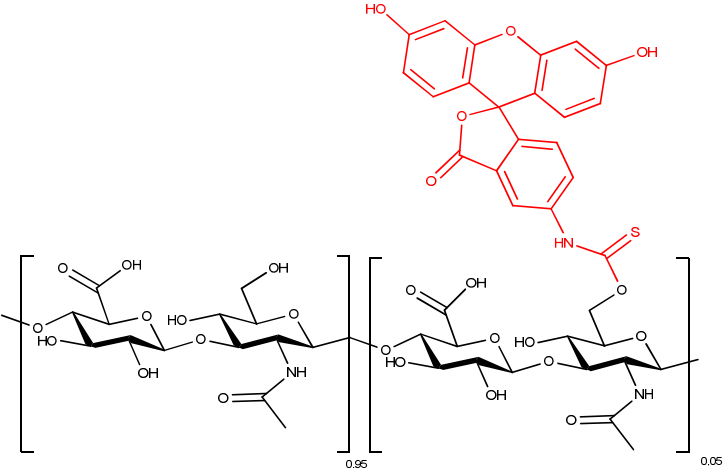
Modified polyelectrolytes

Commercial chitosan and hyaluronic acid have been chemically modified by crosslinkable functions and antimicrobial peptides (Annexe B).

In order to increase the mechanical properties of the multilayer films, evaluated by the Young's modulus, an approach where the polyelectrolytes are crosslinked step-by-step has been chosen. This approach is based on the rapid chemical reaction between pyridyl disulfide (P) groups and thiol (SH) groups. Chitosan was therefore chemically modified by thiol groups with a rate of 5% and is noted CHI-SH, whereas hyaluronic acid was modified by pyridyl disulfide with also a rate of 5% and is noted HA-P (Table 2.2).

An antimicrobial peptide consisting in a cysteine modified cateslytin and noted CTL-C was grafted on a HA previously grafted with maleimide moieties (HA-Mal) via its cysteine group. The resulting polyelectrolyte grafted with about 5% of peptides is noted HA-CTL-C.

Table 2.2: Modified polyanions and polycations used for the buildup of antimicrobial PEM films.

Modified polyelectrolyte abbreviation	Structure
Thiol functionalized chitosan CHI-SH	
Pyridyl disulfide functionalized hyaluronic acid HA-P	
Maleimide functionalized hyaluronic acid HA-Mal	
Fluorescein isothiocyanate functionalized hyaluronic acid HA^{FITC}	

In order to visualize the multilayer films by confocal microscopy, HA and HA-CTL-C were functionalized by a fluorescein isothiocyanate (FITC) probe and are respectively noted HA^{FITC} (Table 2.2) and HA^{FITC}-CTL-C.

All these modified polyelectrolytes have been prepared in solution similarly as described in paragraph 2.1.1 but with some exceptions. HA-CTL-C and HA^{FITC}-CTL-C solutions were prepared at 0.2 mg.mL⁻¹ and 0.1 mg.mL⁻¹, respectively. HA-Mal and HA-P solutions were prepared at 0.2 mg.mL⁻¹ and pH 5.5.

2.1.2 Neutral polymers

For the buildup of neutral polymer multilayer films based on host-guest interactions, the anchoring layer consists in a polycation bearing host moieties to allow the film buildup. Poly(allylamine hydrochloride) has been modified by β -cyclodextrin (β -CD) moieties at 8% in grafting rate and is named PAH-CD. After its synthesis, neutral polymer poly(N-hydroxypropylmethacrylamide) (PHPMA) was modified at 5% by guest moieties (G = Ad, Fc or Py) or β -CD host moieties as described in Annexe A. The PHPMA derivatives were named PHPMA-G (*i.e.* PHPMA-Fc, PHPMA-Py or PHPMA-Ad) and PHPMA-CD, respectively. These functionalized neutral polymers are represented in Figure 2.1. All these PHPMA polymers were prepared by chemical modification of a PHPMA precursor having the following molecular features: $M_n = 34040 \text{ g.mol}^{-1}$ and $M_w = 92640 \text{ g.mol}^{-1}$.

PAH-CD, PHPMA-CD, PHPMA-Py, PHPMA-Fc and PHPMA-Ad solutions were prepared at a concentration of 0.1 mg.mL⁻¹ in Milli-Q water containing 10 mM Hepes, a sodium salt at a fixed ionic strength ranging from 0 to 3 M and adjusted at pH 7.4. Sodium chloride (NaCl), sodium sulfate (Na₂SO₄), sodium perchlorate (NaClO₄), sodium thiocyanate (NaSCN) were purchased from Sigma-Aldrich (Saint-Quentin Fallavier, France). Sodium fluoride (NaF) was purchased from Merck (Darmstadt, Germany). All salts were used as received.

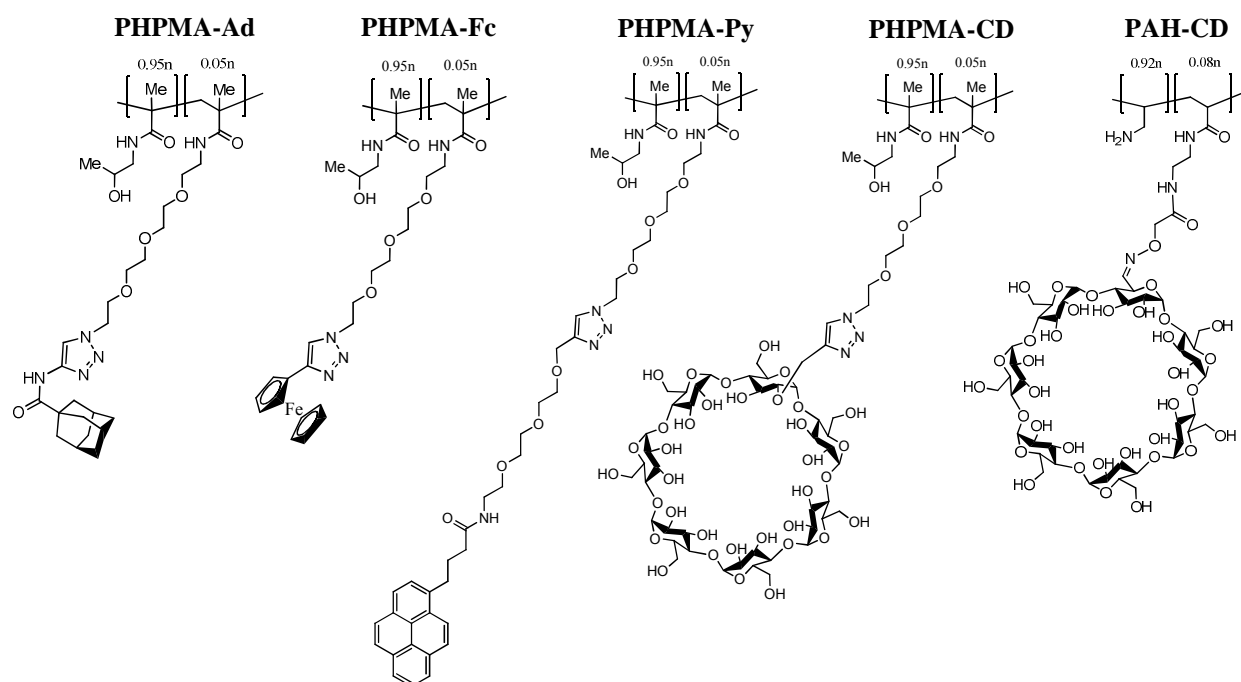


Figure 2.1: Chemical structures of PHPMA-Ad, PHPMA-Fc, PHPMA-Py, PHPMA-CD and PAH-CD.

2.1.3 Host and guest molecules

1,1'-ferrocenedimethanol ($\text{Fc}(\text{MeOH})_2$) and β -cyclodextrin were purchased from Sigma-Aldrich (Saint-Quentin Fallavier, France). Adamantane-1-carboxylic acid (Ad-COOH) was purchased from Alfa Aesar (Karlsruhe, Germany). All products were used without further purification.

2.1.4 Antimicrobial peptides

Cateslytin (CTL) is the antimicrobial peptide at the center of this work. It possesses a sequence of 15 amino acids: RSMRLSRFARGYGFR. In order to be able to graft it, a cysteine group (C) possessing a thiol group has been added at the C-terminal end of the peptide. This modified peptide is noted CTL-C and is represented Figure 2.2. The synthesis of CTL-C was performed by ProteoGenix (Schiltigheim, France).

The synthesis of a CTL-C peptide in D-configuration was also performed by ProteoGenix.

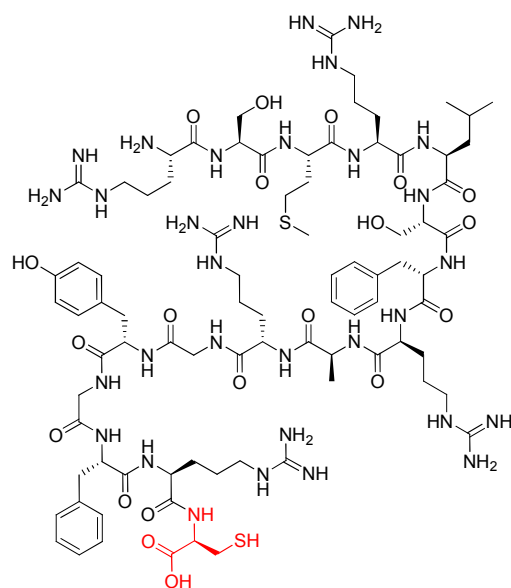


Figure 2.2: Formula of the antimicrobial peptide CTL-C. The sequence is: RSMRLSRFARGYGFRG. It is a cateslytin peptide modified by a cysteine group (in red) at its C-terminal end.

2.1.5 Bis-maleimide linkers

Four different linkers, noted linker D1, linker D4, linker D6 and linker G1 were synthesized. The synthesis of the linker D1 was done by Tony Garnier according to Kim et al. [1]. The linker D4, the linker D6 and the linker G1 have also been synthesized by Tony Garnier. The first step was to obtain linkers ended by amine groups. For the linker G1, it was done according to Amaral et al. [2]. The following procedure was then applied on the linkers ended by amine groups to obtain linkers ended by maleimide groups. 3-(Maleimido)propionic acid-N-hydroxysuccinimide ester (Mal-OSu, CAS: 55750-62-4) (1.0 eq.) was added in one portion to a solution of free di- or triamine (0.55 or 0.35 eq. respectively) in anhydrous CH_2Cl_2 (50 mM) and the resulting solution was stirred at room temperature overnight. Then, the reaction mixture was quenched with saturated aqueous NaHCO_3 (10 mL) and extracted with CH_2Cl_2 (3×20 mL). The combined organic layers were dried using MgSO_4 , filtered and concentrated under reduce pressure to obtain the desired linker which was used without further purification.

One of the linker was commercially available: linker D15 (alpha,omega-Bis-maleinimido poly(ethylene glycol), PEG = 2000 Da, Irisbiotech).

The names of the linkers used for the dimer synthesis were attributed depending on the length between the two nitrogen atoms of the maleimide groups. The shorter linker possessed

9 covalent bonds between the two nitrogen atoms and was named D1. The linker D4 is four times longer than D1, the linker D6 is 6 times longer than D1 and so on. This nomenclature is not exact but facilitates the notation of the dimers and also allows being able to directly compare the lengths of the dimers. Linker G1 was used to synthesize a CTL-C based dendrimer. All linkers are reported Table 2.3.

Table 2.3: Names and chemical structure of the linkers used for the synthesis of CTL-C based dimers and dendrimer.

Name	Chemical structure
Linker D1	
Linker D4	
Linker D6	
Linker D15	
Linker G1	

2.2 Physico-chemical characterizations

2.2.1 Quartz crystal microbalance

Quartz crystal microbalance with dissipation monitoring (QCM-D) is an acoustic technique used to follow processes at surfaces, especially the adsorption *in situ* of molecules or macromolecules on a substrate. In our case, QCM-D was used to follow the buildup of both charged polyelectrolytes and neutral polymer based multilayer films. This technique allows the measurement of mass deposition with a sensitivity out of the order of 1 ng.cm^{-2} .

Principle of the QCM-D

The principle of quartz crystal microbalance (QCM) has fundamentally and experimentally been developed by G. Sauerbrey in the 1950s [3]. The technique relies on the piezoelectric properties of quartz. Quartz is a material that deforms when an electrical potential difference is applied to it, and inversely when quartz is subjected to a mechanical stress a polarization appears at its terminals. The substrates used for QCM are quartz crystals coated on both sides with gold layers that serve as electrodes. One of the electrodes can be covered by a conductive or an insulating coating (ITO, silicon...). The application of an electrical potential between the two electrodes induces a shear movement of the quartz crystal. By fixing the lower side of the crystal on a stationary support, the upper side undergoes a horizontal translational movement resulting in mechanical oscillations at its fundamental frequency and its harmonics. The system behaves as a harmonic oscillator that can be characterized by its resonance frequency f_r :

$$f_r = \frac{1}{2\pi} \sqrt{\frac{k}{M}} \quad (2.1)$$

Where M is the oscillator mass and k the spring constant.

When a mass m is deposited on the surface of the crystal ($m \ll M$), the total mass of the resonator changes and a new resonance frequency f is associated:

$$f = \frac{1}{2\pi} \sqrt{\frac{k}{M + m}} \approx f_r \left(1 - \frac{m}{2M}\right) \quad (2.2)$$

The resonance frequency shift Δf induced by the mass deposition m on the crystal can be written as following:

$$\Delta f = f - f_r = -\frac{m f_r}{2M} = -\frac{m}{C} \quad (2.3)$$

C , called the Sauerbrey constant, is a constant that depends only on the thickness and on the inherent properties of the quartz crystal. C is defined as:

$$C = \frac{2M}{f_r} \quad (2.4)$$

By measuring the resonance frequency shift of the system during an experiment, QCM gives access to the deposited mass per surface unit on the crystal over time. It is also possible to determine the frequencies of all odd harmonics of the fundamental resonance frequency and to follow their shifts during an experiment. The Sauerbrey equation can be written as following:

$$m = -C \frac{\Delta f_v}{v} \quad (2.5)$$

Where v is the overtone number.

The Sauerbrey equation is valid only for the ideal case of a rigid and uniform adsorbed film and in absence of friction and viscoelastic effects. It can be applied as a good first approximation in liquid conditions when all the harmonic signals are superimposed. The use of highly hydrated polymers leads sometimes to assemblies that behave as viscous liquids or gels. In this case, the Sauerbrey equation is not valid. The model of Voigt-Voinova [4], that takes the viscoelastic properties of the deposited material into account, can be applied.

To determine the viscoelastic properties of the deposited material on the crystal, an extension of the technique is used: the QCM-D, where D stands for dissipation. QCM-D allows the measurement of the dissipation factor D , defined as the proportion of energy lost at each crystal oscillation versus the energy stocked in the oscillator. D is experimentally determined by exciting the quartz crystal at its fundamental frequency and measuring the relaxation time of the system as the resonator energy is dissipated in the crystal, in the deposited material and in the liquid in contact with the crystal (Figure 2.3). This relaxation time is inversely proportional to the damping constant of the system and allows the determination of the dissipation factor D . The dissipation measured by the QCM-D gives access to informations on the viscoelastic properties of the deposited material.

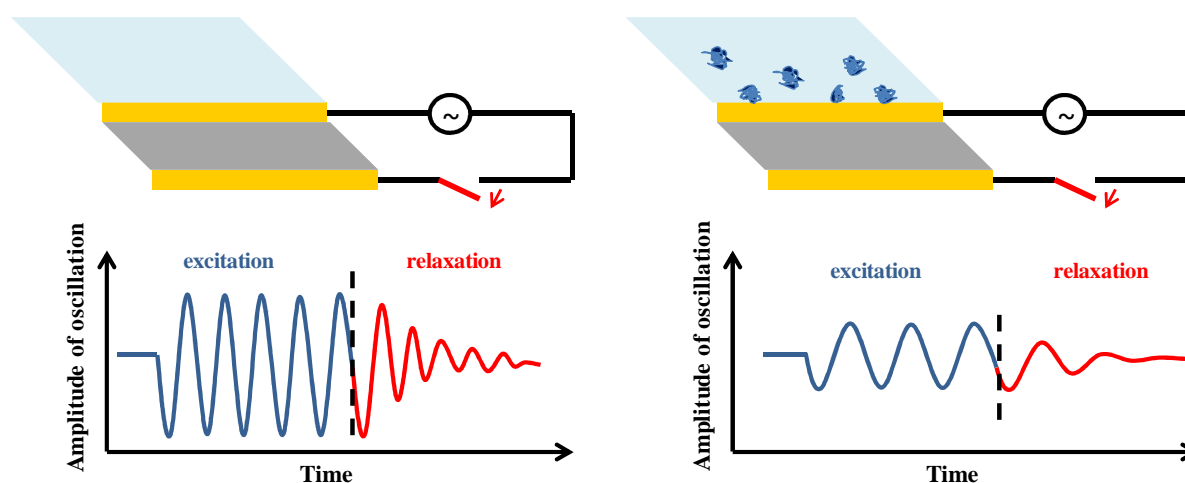


Figure 2.3: Schematic view of the frequency and dissipation change upon adsorption of molecules on the surface of a quartz crystal. The gold coated crystal and its driving circuit is represented above, the corresponding signal below. The blue part of the curve corresponds to the signal during excitation whereas the red part corresponds to the signal after stopping the excitation potential.

Experimental setup

All experiments were performed using a quartz crystal microbalance with dissipation monitoring Q-Sense E4 (Q-Sense, Göteborg, Sweden). The apparatus is equipped with four thermostated measurement cells (volume of about 100 μL) allowing the “in” and “out” fluxes of the solutions above the crystal surface. The temperature was fixed to 22°C. Quartz crystals (1.4 cm diameter / 0.3 mm thickness) are made of silicon and have a fundamental resonance frequency of 5 MHz. The surface coating, which is 100 nm thick, is gold. The response is followed over time at the fundamental resonance frequency ($\nu = 1$) and at its three first odd overtones: 15, 25 and 35 MHz, which corresponds to $\nu = 3, 5$ and 7.

Prior to each experiment the crystal was cleaned by an UV-Ozone exposure for 10-15 minutes. It was then left to stabilize in the buffer solution for around 30 minutes. The multilayer films were built *in situ* by layer-by-layer deposition on the crystal surface. 600 μL of the corresponding solutions were injected with an automatic pump into the measurement cell, in order to completely replace the previous solution, and then let in contact with the surface for 5 minutes. After each polymer deposition, the cell was rinsed with the buffer solution during 5 minutes. The injection and rinsing steps were applied until a number n of bilayers were deposited. At the end of the experiment, the crystal is cleaned *in situ* with a 2% Hellmanex solution for 10 min, then with a 0.1 M HCl solution for 10 min and finally with a 0.1 M NaOH solution for 10 min. It is rinsed with water and dried under compressed air.

When the sample has to be kept for AFM imaging, the crystal is removed from the measurement cell and kept in a buffer solution at 4°C.

2.2.2 Surface plasmon resonance

Surface plasmon resonance (SPR) as quartz crystal microbalance is an *in situ* method that can monitor the buildup of a polymer film on a solid surface.

Principle of SPR

When a beam of light passes from a material of refractive index n_1 into a material with a lower refractive index n_2 some light is reflected from the interface. When the angle of incidence of the light on the interface θ is greater than $\theta_{\text{TIR}} = \arcsin(n_2/n_1)$, the light is completely reflected.

In the case of a SPR instrument (Figure 2.4), the refractive medium is a BK7-glass prism. Because the bottom surface of the prism is coated with a thin film of a noble metal (gold), this reflection is not total; some of the light is “lost” into the metallic film. There exists then a second angle, $\theta_{\text{SPR}} > \theta_{\text{TIR}}$, at which the intensity of the reflected light goes through a minimum. In addition, an evanescent electrical field travels for a short distance into the medium from the metallic film. The probing distance reaches generally a few hundreds of nanometers depending on the refractive index of the probed medium and θ_{SPR} is sensitive to the optical characteristics of the deposited film. The reflection curves, i.e. the variation of the intensity of the reflected light with θ , corresponding to depositions on the substrate is then analyzed and the mass of film per unit area can be obtained.

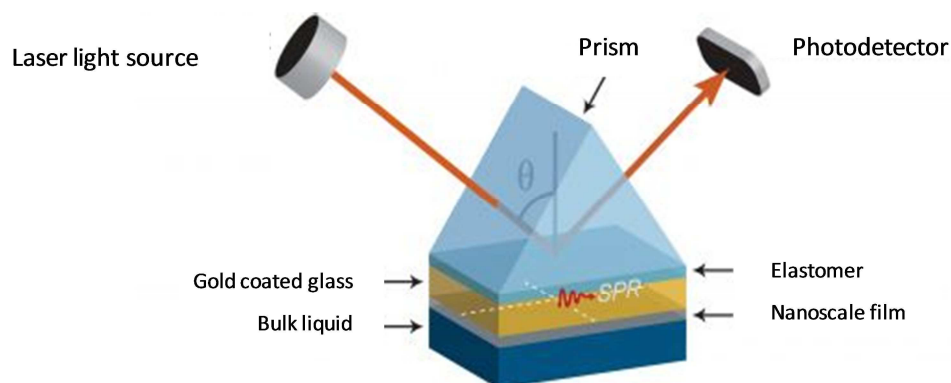


Figure 2.4: Schematic representation of surface plasmon resonance (SPR), from Bionavis.

Experimental setup

The SPR instrument used was a SPR NaviTM 200 from Bionavis (Finland). The reflection curves corresponding to the successive polymer deposition steps have been analyzed with a home-made software based on Maxwell's equations. The parameters involved are the refractive indices of the prism, the chromium and gold layers, the polymer film (n_{film}) and the buffer solution (n_{sol}), as well as the thickness of the chromium and gold layers and of the film (d_{film}). From n_{film} , n_{sol} and d_{film} , we derive the mass of film per unit area:

$$m = \frac{(n_{film} - n_{sol})d_{film}}{\frac{dn}{dc}} \quad (2.6)$$

where dn/dc is the change in refractive index with concentration and is equal to $0.197 \text{ cm}^3 \cdot \text{g}^{-1}$ for polyelectrolytes.

The SPR experiment was performed under a continuous flow rate of $100 \mu\text{L} \cdot \text{min}^{-1}$ of 150 mM NaCl solution adjusted at pH 4. The time of deposition and of rinsing of polyelectrolytes was fixed at 5 min.

2.2.3 Atomic force microscopy

Atomic force microscopy (AFM) is a scanning probe microscopy technique that allows getting access to the topography of a sample surface with sub-nanometer vertical resolution. [5]

Principle of AFM

The principle of AFM relies on the detection of interatomic forces (electrostatic forces, Van der Waals forces, ionic repulsion forces...) that exist between a tip attached to the end of a lever arm (cantilever), which has a fixed spring constant, and the sample surface. AFM enables the detection of forces in the piconewton range which allows imaging the topography of a sample with a high resolution.

The cantilever deflection is followed by positioning a laser beam on its back. This beam is reflected on a system composed of photodiodes that monitor the cantilever position changes (Figure 2.5). A piezoelectric ceramic allows the movement of the sample in the three directions (x , y and z). 3D-images of the sample surface are thus obtained.

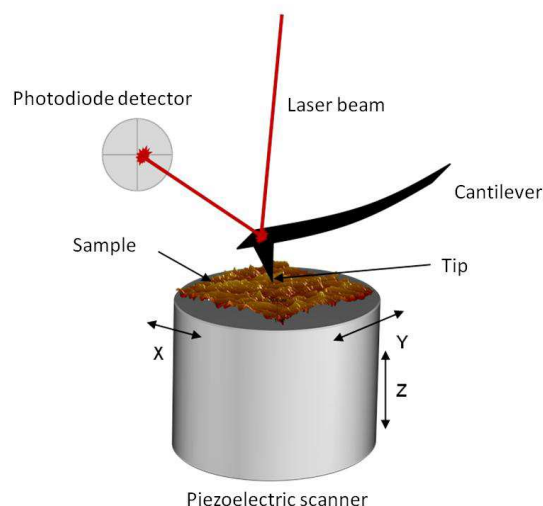


Figure 2.5: Schematic representation of atomic force microscopy (AFM). The sample is fixed on a piezoelectric scanner. The cantilever tip is approached on the surface. Interactions between the tip and the sample surface occur and lead to the deflection of the cantilever. A laser beam is sent on the back of the cantilever and then is reflected on the photodiodes which allows following the cantilever deflection. [6]

There are two main modes for AFM imaging: contact mode and tapping mode. In contact mode (Figure 2.6a), the tip is in contact with the sample and is “dragged” across its surface. In tapping mode (Figure 2.6b), the tip oscillates at its resonance frequency close to the sample surface without making contact. The interaction between the tip and the surface, mainly due to Van der Waals forces, can be attractive or repulsive which modifies then the oscillation frequency of the cantilever. Since the oscillation frequency is maintained constant, the cantilever has to move away from the sample surface through a control loop.

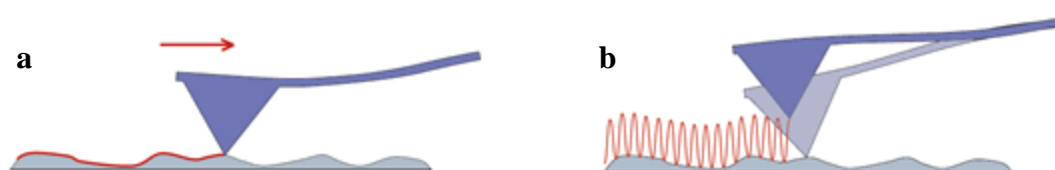


Figure 2.6: Schematic representations of the two main modes for AFM imaging: (a) contact mode and (b) tapping mode. [7]

Experimental setup

Using a Veeco Multimode Nanoscope IV microscope from Digital Instruments (Santa Barbara, USA), AFM imaging were performed on multilayer films directly built on silicon wafers, QCM quartz crystal and glass sides. The samples were imaged in contact mode under liquid (Milli-Q water) and dry conditions. The images were carried out with silicon nitride cantilevers possessing a spring constant of 0.03 N.m^{-1} (MSCT-AUWH model, Veeco, CA).

Deflection and height mode images were scanned simultaneously at a fixed scan rate (2 Hz) with a resolution of 512×512 pixels.

AFM was used to characterize the topography of the films. In order to determine their thickness, profilometric section analysis of scratched films was performed. Scratches were achieved with a plastic cone tip. The mean thickness of a scratched film was determined by measuring the thickness at least on three different areas. The film roughness was evaluated by calculating the RMS roughness (Root Mean Squared roughness) on $15 \times 15 \mu\text{m}^2$ images. Data evaluations were performed with the NanoScope software version 5.31r1 (Digital Instruments, Veeco).

Force-distance curves by AFM

AFM force-distance curves have been performed by Dr. Gregory Francius (LCPME, Nancy) for the determination of the elasticity of PEM films. AFM images and force-distance curves were recorded using a MFP3D-BIO instrument (Asylum Research Technology, Atomic Force F&E GmbH, Mannheim, Germany). Silicon nitride cantilevers of conical shape were purchased from Bruker (MLCT-AUNM, Bruker-Nano AXS, Palaiseau, France), and their spring constants were determined using the thermal calibration method [8], providing k values of 15 pN/nm. Topographic images were performed with contact mode in aqueous medium (NaCl 0.15 M at pH 7.4). The applied force was minimized at values lower than 250 pN to avoid mechanical damages of the polyelectrolytes films.

Mechanical properties were measured by recording a grid of 32-by-32 force curves obtained upon approach of the tip to the film, using a maximum applied force of about 4 nN in order to avoid a too important indentation depth. The elastic modulus was calculated according to Sneddon model applied to the approach force curves [9]:

$$F = \frac{2E \tan(\alpha)}{\pi(1-\nu^2)} \delta^2 \quad (2.7)$$

where F is the loading force, δ the indentation depth, E the Young's modulus, ν the Poisson coefficient, and α the semi-top angle of the tip.

Equation 2.7 refers to cases where compression and deformation of a soft planar interface is occasioned by a tip of conical geometry. Elastic moduli were determined for a piezodriven speed of 1,000 nm/s (0.5 Hz), which ensures full relaxation of the biopolymer film upon successive measurements. This also fully justifies the use of the static physical model of

Sneddon as adopted in our analysis. In addition, the model is valid for elastic surfaces on the premise that tip-surface adhesion is absent or insignificant. The mathematical analysis was performed on 1024 measured force-distance curves with an automatic Matlab algorithm described elsewhere [10] using $\alpha = 17.5^\circ$, as inferred from tip geometry, and $\nu = 1/2$.

2.2.4 Confocal laser scanning microscopy

Confocal Laser Scanning Microscopy (CLSM) is an improved optical microscopy technique based on fluorescence that allows imaging fluorescently labeled films.

Basics of fluorescence

When subjected to light excitation at a certain wavelength, a fluorescent molecule is brought into an orbital of an excited electronic state (S_1). At room temperature, part of the adsorbed energy is lost by molecular vibrations (non-radiative transition). The molecule is then in a less high energy state. One way to return to the ground state (S_0) is by the emission of a photon, called fluorescence (Figure 2.7). A smaller amount of energy is emitted than the one initially absorbed. The emitted wavelength is thus shifted to higher values and the intensity is lower.

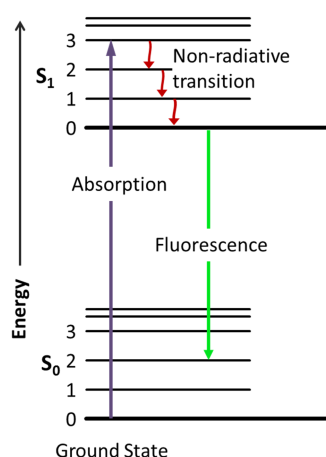


Figure 2.7: Jablonski diagram. By adsorption of a photon, a fluorescent molecule is excited from its ground state S_0 to an excited state with a higher energy S_1 . Due to molecular vibrations (non-radiative transition in the diagram), a loss of energy occurs. Then the molecule can return to its ground state by emission of a photon. [11]

Principle of CLSM

In standard fluorescence microscopy, the sample is illuminated with light filtered with an excitation filter. This light is reflected with a dichromatic mirror towards the sample. The emitted fluorescence is radiated in all directions and partly passes through the microscope

objective. It passes then through the dichromatic mirror and is filtered by an emission filter. The signal is recorded by a camera. The main drawback of this method is the complete illumination of the sample that leads to a high amount of out-of-focus light. In order to obtain a higher resolution, confocal microscopy uses point illumination at a precise point of the sample (focal point) and a spatial pinhole to eliminate light that comes from planes other than the focal planes. The excitation of the sample is thus performed by a laser with a defined wavelength and a pinhole is placed between the dichromatic mirror and the emission filter. The emitted light is typically detected pixel by pixel using a photomultiplier. The sample is scanned line by line and a two-dimensional image can be reconstructed. Confocal microscopy also allows building a three-dimensional image of a sample from a stack of individual XY slices (Figure 2.8).

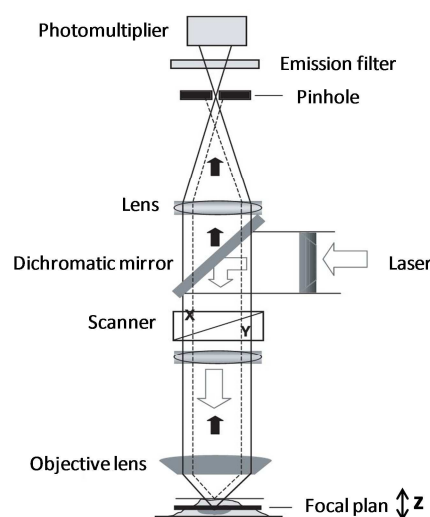


Figure 2.8: Schematic representation of a confocal laser scanning microscopy setup and light pathways. A laser beam is condensed by a dichromatic mirror and an objective lens on a focal point on the sample. The fluorescence is then collected by a photomultiplier. In order to eliminate the out-of-focus fluorescence (dotted line), a pinhole is placed at the image plan of the objective. [12]

Experimental setup

All experiments were performed with a LSM 510 META confocal microscope (Zeiss, Le Pecq, France) mounted on a AxioVert 100M microscope with HeNe (543 nm) and Ar (459, 488, and 514 nm) lasers. It is equipped with an oil immersion lens with a magnification of 40. Fluorescein isothiocyanate (FITC) is detected, after excitation by the Ar laser at 488 nm, through a filter whose bandwidth is between 505 and 530 nm (green). Image analysis was performed using ImageJ software.

Fluorescently labeled PEM films (HA^{FITC}/CHI or HA^{FITC}-CTL-C/CHI) underwent a fixing and anti-fading treatment before imaging in order to reduce light-induced fading of the

fluorophore. For that, the coatings were washed with fresh culture medium and treated for 30 minutes with 4% paraformaldehyde in phosphate buffer saline (PBS) at pH 7.3. After several rinsing with PBS, slides were then covered with Mowiol 4-88 (Sigma-Aldrich).

2.2.5 Isothermal titration calorimetry

Isothermal titration calorimetry (ITC) is a technique used to determine the variation of thermodynamic quantities (stoichiometry, affinity constant and enthalpie) when mixing two solutions. ITC is often used to characterize complexation reactions between macromolecules and small molecules (ligands) or between ligands and receptors.

Principle of ITC

Isothermal titration calorimetry is based on the measurement of the required heating power to maintain at constant temperature a volume of A in which small volumes of B are periodically injected.

The calorimeter, shown in Figure 2.9, possesses a reference cell and a sample cell in an adiabatic jacket. These two cells are maintained at a fixed temperature during an experiment. A small volume of B is injected with a microsyringe in the sample cell containing A. The system measures then the temperature shift ΔT , due to the interaction between A and B, between the reference cell and the sample cell. A Peltier element allows heating or cooling down the sample cell in order to maintain ΔT as close as possible to 0. ITC system monitors therefore the heating power necessary to maintain the thermal equilibrium over time.

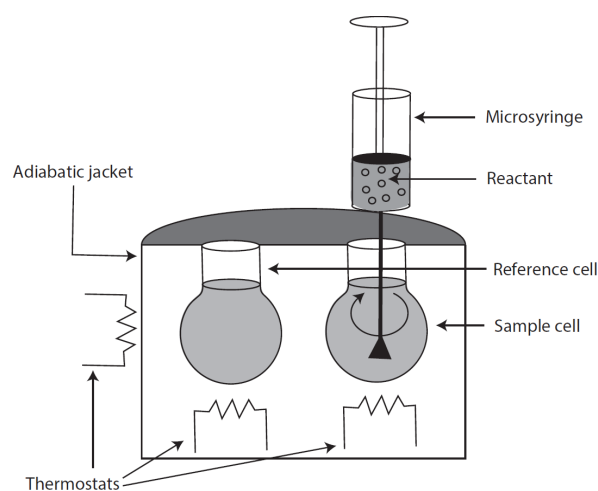


Figure 2.9: Schematic illustration of an isothermal titration calorimeter. Two identical cells are surrounded by an adiabatic jacket and kept at the same temperature with a constant power input. Upon addition of titrant, reaction between molecules occurs, causing a temperature change of the sample cell. Power consumption has to be regulated to maintain isothermic conditions and is recording versus time. [13]

Experimental setup

The “heat of reaction” between β -CD and Fc(MeOH)₂ (respectively Ad-COOH) was measured by means of an isothermal titration microcalorimeter (Nano Isothermal Titration Calorimeter, TA Instruments, New Castle, USA). This microcalorimeter is fitted with two thermostated cells with a volume of 1 mL: one reference cell containing MilliQ water and a sample cell containing Fc(MeOH)₂ (or Ad-COOH) solution to be titrated. All solutions were degassed 30 min under vacuum before use. The titration cell was regulated at 25°C. A typical experiment consisted in 20 sequential 12.29 μ L injections of β -CD solution (8.8 mM) into the ITC cell containing Fc(MeOH)₂ (or Ad-COOH) solution (1.2 mM). The concentrations were chosen high enough regarding the sensitivity range of the apparatus and in order that the “mixing molar ratio” between β -CD and the hydrophobic molecules is 2 at the end of the injections. The injections were realized by an automated microsyringue (250 μ L) ended by a propeller which allowed to stir the solution at 250 rpm. Two consecutive injections were separated by a resting period of 400 s to allow the microcalorimeter trace to come back to a baseline corresponding to the absence of any heat flow between the sample cell, in which host-guest interactions took place, and the reference cell, filled with MilliQ water. For each sodium salt and each salt concentration, the dilution heats were determined by injecting β -CD, Fc(MeOH)₂ and Ad-COOH solutions into Hepes buffer solution. The peak integration was performed with Origin 7.5. The first injection was not taken into account in the data analysis. The measured heat data were processed using a home-made data analysis program assuming a binding model of 1-site in order to obtain the association constant of the complex. Two fitting parameters are used in this model: the binding constant K and the heat of binding ΔH . They were adjusted in the equation (2.7) so that the fitting curve is as close as possible to the experimental data. At each injection k , $\frac{dQ_{AB}}{dB_T}(k) = \frac{Q_{AB(k)} - Q_{AB(k-1)}}{B_{T(k)} - B_{T(k-1)}}$ can be calculated.

$$(A + B \leftrightarrow AB) \quad / \quad \frac{dQ_{AB}}{dB_T} = \frac{\Delta H}{2} \left(1 + \frac{1 - \frac{[B_T]}{[A_T]} - \frac{1}{K[A_T]}}{\sqrt{\left(1 + \frac{[B_T]}{[A_T]} + \frac{1}{K[A_T]}\right)^2 - 4 \frac{[B_T]}{[A_T]}}} \right) \quad (2.7)$$

Where Q_{AB} is the heat of the reaction leading to the AB complex formation and $[A_T]$ and $[B_T]$ are respectively the total concentration of A and B ($[A_T] = [A] + [AB]$ and $[B_T] = [B] + [AB]$).

The reproducibility of these microcalorimetry experiments was of the order of 10%.

2.2.6 High-performance liquid chromatography

High-performance liquid chromatography (HPLC) is an analytical method. It allows the identification, the separation and the dosage of molecules in a mixture depending on their hydrophilicity. In this work, HPLC has been used to follow the kinetic of the syntheses of peptide dimers and dendrimers, and also to purify them.

Principle of HPLC

HPLC principle consists in the migration of molecules, which need to be separated, on a stationary phase, the chromatographic column, with a liquid mobile phase. A simplified configuration of an HPLC is represented Figure 2.10. Note that the waste container can be replaced by a collector one when the product injected on HPLC needs to be collected, in the case of purification for example.

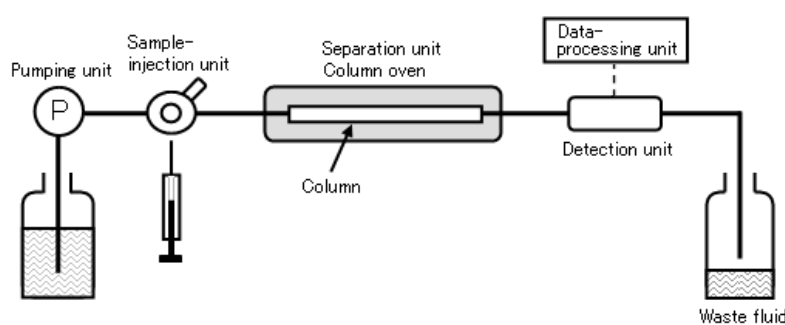


Figure 2.10: Simplified configuration of an HPLC system. [14]

The sample mixture to be separated is initially injected into the stream of the mobile phase that runs through the column. The components of the sample move through the column at different velocities depending on their interaction with the column (Figure 2.11) which is the result of their chemical nature, the nature of the column and also the composition of the mobile phase. The components emerge thus from the column one after another and are separated. The time at which a component emerges from the column is called retention time. This time is characteristic for a molecule for a given set of parameters (nature and size of the column, mobile phase...). At the exit of the column, a detector continuously measures the absorbance of the liquid at a defined wavelength chosen depending on the target molecule. This allows following the exit of different molecules from the column. A plot, called chromatogram, draws the absorbance change of the liquid at the exit of the column over time. Each peak corresponds ideally to the exit of a unique molecular species. The amplitude of the

peaks or the area under the peaks allows the measurement of the concentration of each compound from the mixture.

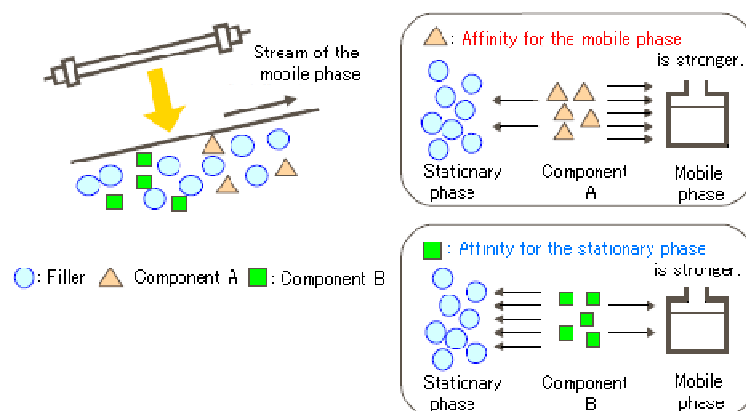


Figure 2.11: Schematic illustration of a separation inside of a HPLC column. Components are separated depending on their affinity with the stationary phase. [14]

Experimental setup

For our experiments a reversed-phase chromatography was used. This means that the stationary phase is apolar whereas the mobile phase is polar. The molecules that are rather not polar have a longer retention time and the polar molecules are faster eluted. The chromatography column used (the stationary phase) is an Uptisphere Strategy 100A 3 μ m RP model (Interchim). For the mobile phase, a solvent gradient going from a polar solvent A (H₂O 99.9% + TFA 0.1%) to a rather apolar solvent B (MeCN 70% + H₂O 29.91% + TFA 0.09%) is used. The method is given in Table 2.4 below. The solvent flow is fixed at 1 mL.min⁻¹ and the absorbance is measured at 214 nm.

Table 2.4: Method used for following the kinetics of peptide dimers and dendrimers synthesis.

t (min)	Solvent A	Solvent B
	H ₂ O 99.9% TFA 0.1%	MeCN 70% H ₂ O 29.91% TFA 0.09%
0	100%	0%
10	100%	0%
40	0%	100%
45	0%	100%
55	100%	0%

2.3 Biological characterizations

2.3.1 Buildup in cell culture plates

To be able to achieve biological characterizations, glass sides of 14 mm diameter were used as surfaces for the multilayer film depositions. The buildup of multilayer films on these glass sides was performed manually.

Glass sides were put into a 24-well cell culture plate. The anchoring layer was deposited by adding 500 μL of PEI solution per well with a micropipette maintained in contact for 10 minutes. The solution was then removed with a pipette and replaced by 500 μL of a buffer solution for 5 min as a rinsing step. Then 300 μL , which is the minimum volume to cover a glass side in a well, of polyanion or polycation solution were alternately put in contact with the glass side and let in contact for 5 min. A rinsing step was always achieved between two consecutive polyelectrolyte depositions. After their buildup, multilayer films were kept overnight in the buffer solution of the buildup at 4°C.

2.3.2 Cytocompatibility tests

The biocompatibility of antimicrobial films has been tested by evaluating the viability and the proliferation of human gingival fibroblasts (HGFs). This study was done by Gwenaëlle Cado. HGFs were extracted from human gingival connective tissue of healthy patients from the faculty of dental surgery of Strasbourg after informed consent. Cells were grown in the culture medium DMEM (Dublecco's Modified Eagle's Medium, Gibco) containing 1 $\text{g}\cdot\text{L}^{-1}$ of glucose and supplemented with 10% fetal bovin serum and 100 $\mu\text{g}\cdot\text{mL}^{-1}$ penicillin-streptomycin. They were cultured at 37°C under a 5% CO_2 atmosphere. HGFs were used between the 6th and the 9th passage. Before cell seeding, glass coverslips ($\text{Ø} = 14 \text{ mm}$) coated with different architectures were irradiated by UV for 15 min. Then HGFs were seeded at 3×10^4 cells per cm^2 and cultivated at 37°C under 5% CO_2 humidified atmosphere for different culture times (Day 1, Day 2 and Day 7).

Cell viability

Cell viability was assessed by AlamarBlueTM assay [15] (Biosource International). This assay is based on the reduction of resazurin, a non fluorescent blue dye, to resorufin, a pink and fluorescent dye by the living cells. Resazurin is first put in contact with the cells.

Then it diffuses inside the cells. It is reduced by mitochondrial enzymes, which induces a change of color that can be measured by spectrophotometry (Thermo Scientific Multiskan EX). This change of color occurs only if the cells are alive and so its intensity is proportional to the cell activity. Viability was assessed after 1, 2 and 7 days.

Cell visualization: immunolabeling

Actin filament staining with tetramethylrhodamine B isothiocyanate coupled phalloidin® (Sigma-Aldrich) and DAPI (Invitrogen) nuclei counterstaining were performed as follows: cells were fixed with 3.7% paraformaldehyde for 10 min at 4°C, permeabilized in 0.25% Triton X-100 in PBS for 10 min, and blocked in 1% BSA-PBS for 30 min. Thereafter, cells were incubated for 30 min at room temperature with 5×10^{-5} mg.mL⁻¹mL phalloidin® followed by nuclear counterstaining with DAPI (50 ng.mL⁻¹) incubated for 2 min at room temperature. Washed slides were mounted on blades with DAKO fluorescent mounting medium and fluorescence distribution was examined by means of an inverse fluorescence microscope (Axiovert, Zeiss).

2.3.3 Antibacterial and antifungal tests

Antibacterial activities of CTL, CTL-C, “D”-CTL-C, HA-CTL-C, dimers and dendrimers of CTL-C as well as peptide functionalized multilayer films were assessed by using a microdilution assay on two bacterial strains: *Micrococcus luteus* (A270) and *Staphylococcus aureus* (ATCC25923). The antifungal activity was tested against one yeast strain: *Candida albicans*.

Microbial preculture

Preparing a microbial culture consists in multiplying microbial organisms by letting them reproduce in predetermined culture.

Bacteria were precultured aerobically in a Mueller-Hinton Broth (MHB) growth medium (Merck, Darmstadt, Germany) under stirring for 18 h at 37°C in an incubator (Tritamax 1000, Heidolph, Germany). *Candida albicans* preculture was carried out on a Sabouraud Broth (SB) medium (BioMérieux S.A., Marcy l’Etoile, France) under stirring for 24 h at 30°C in an incubator.

Antimicrobial activity assay

The antimicrobial activity was tested using a bacterial suspension with an optical density at a 620 nm wavelength (OD_{620}) of 0.001 prepared from the microbial preculture. This corresponds to about $5 \cdot 10^8$ cells per milliliter.

For CTL, CTL-C, HA-CTL-C, dimers and dendrimers of CTL-C, the antimicrobial tests were performed in solution. Aqueous solutions of these compounds were prepared in bacterial or yeast medium at different concentrations by dilution of a stock solution. 10 μ L of these solutions were incubated in 96-well microplates (Falcon, Becton Dickinson, USA) with 90 μ L of bacteria or yeast with final concentrations ranging from 1 to 100 μ M of peptide. After 24 h of incubation, at 37°C under gentle stirring for the bacterial strains and at 30°C without stirring for the yeast strain, the OD_{620} of the 96-well plate was measured by a microplate reader (Multiscan EX, Shanghai, China). The minimal inhibitory concentration (MIC) of a peptide is defined as the lowest peptide concentration that inhibits the bacterial growth after 24 h incubation at 37°C.

To test the antibacterial and antifungal properties of the multilayer films, 400 μ L of the bacterial suspension with OD_{620} equals to 0.001 were placed in a 24-well plate containing the multilayer films. For each tested film, 100 μ L of the supernatant was taken to measure its OD_{620} by a microplate reader.

Several controls were used: a fresh medium without inoculation of pathogens was used to ensure sterility, a mixture of tetracycline (10 μ g.mL⁻¹) and cefotaxime (0.1 μ g.mL⁻¹) for antibacterial assay and voriconazole (1 μ g.mL⁻¹) for antifungal assay were used as positive control (90 μ L of culture and 10 μ L of antibiotics or antifungal) and a fresh inoculated culture medium without any addition was taken as negative control. Each assay was performed in triplicate and the experiments were repeated at least three times.

The normalized growth of pathogens (in %) was estimated by comparing the OD_{620} values in the presence of the multilayer films to the positive and the negative controls. The OD_{620} value of control cultures growing in the absence of films and antibiotics was taken as 100% growth (negative control) and the OD_{620} value of cultures growing in the presence of antibiotics (tetracycline and cefotaxime) was taken as 0% growth (positive control). Using the following equation, the normalized pathogen growth can be evaluated:

$$\text{normalized pathogen growth} = 100 \times \frac{OD_{620, \text{sample}} - OD_{620, \text{positive control}}}{OD_{620, \text{negative control}} - OD_{620, \text{positive control}}}$$

2.3.4 Hemolysis assays

Hemolysis assays were performed in order to evaluate the ability of the peptides to cause the lysis of red blood cells, also called erythrocytes, and thus to assess their toxicity to mammalian cells. This was done by Aurélie Schwartzentruber.

Principle of the test

If a peptide is toxic to red blood cells, it provokes a hemolysis, i.e. the breakdown of red blood cells. During the hemolysis, hemoglobin, which is the protein that gives the red color to the red blood cells, is released and this release can thus directly be followed by spectroscopy measurement.

Protocol

1 mg of fresh rat's blood (obtained from Unité INSERM 1119 Biopathologie de la Myéline, Neuroprotection et Stratégies thérapeutiques) was incubated with 10 mg of sodium citrate in order to avoid blood clotting. The blood was kept on ice until its use. It was then washed twice with PBS (phosphate buffered saline) at 12 000 rpm for 10 min. The erythrocyte pellet was then resuspended in 5 mL PBS. 45 μ L of this suspension was incubated with 5 μ L of the peptide solution at different concentrations at 37°C under agitation for 40 min. The suspension was then diluted in 1 mL water and the OD of the solution was measured at 420 nm. Two controls were performed as well. The negative control consists in a suspension of erythrocytes where 5 μ L of water have been added instead of the peptides, which corresponds to 0% of lysis. The positive control consists in a suspension of erythrocytes where 5 μ L of a 2% SDS (sodium dodecyl sulfate) solution has been incubated with the cells, which corresponds to a complete lysis (100%). The percentage of erythrocytes lysis could be evaluated and compared with these two controls.

2.3.5 Inflammatory assays

Inflammatory assays were performed in order to evaluate the inflammatory properties of some antimicrobial peptides. There are many ways to assess the inflammatory properties of molecules. One of them is to quantify the activity of NF- κ B, a transcription factor responsible for the expression of numerous pro-inflammatory cytokines [16]. This was done by Aurélie Schwartzentruber.

Principle of the inflammatory test

A plasmid expressing the luciferase reporter gene under the control of the NF- κ B promoter is transfected into THP-1, a monocytic cell line, by using Lipofectamine LTX (Invitrogen). Those cationic lipids can form vesicles that can easily cross the plasma membrane. Thanks to electrostatic interactions, those cationic lipids can form aggregates with the negatively charged DNA. Once in the cytoplasm of the cell, the liposomes dissociate and free the DNA (Figure 2.12).

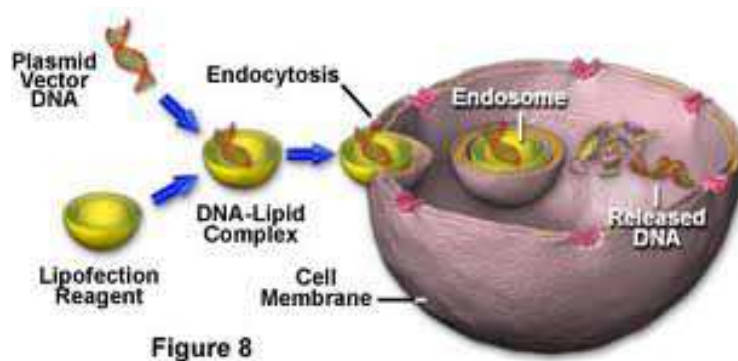


Figure 2.12: Lipid-mediated transfection in mammalian cells.

When NF- κ B is activated, the gene encoding the luciferase is expressed and the luciferase enzyme is produced. In the presence of its substrate, luciferase emits light that can be quantified by luminescence measurement (Figure 2.13). The level of luciferase activity directly reflects the level of NF- κ B activity.

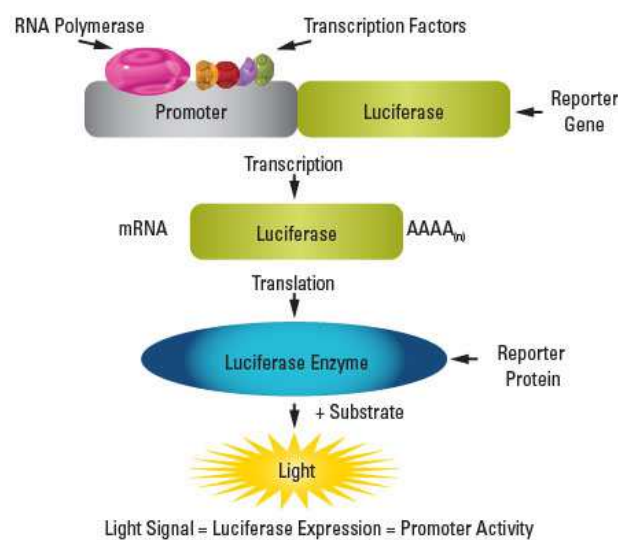


Figure 2.13: Schematic of the luciferase reporter assay [17].

Protocol

For the inflammatory assays, the protocol used is based on a transfecting kit (Transfecting Plasmid DNA into THP-1 cells using LipofectamineTM LTX reagent, Invitrogen by Life Technologies) and a luciferase reporter assay kit (Dual-Luciferase[®] Reporter Assay, Invitrogen).

The first step consists in the lipid-mediated transfection of plasmid DNA into THP-1 cells. 9.5 µg of DNA and 38 µL of LipofectamineTM LTX were incubated in Opti-MEM I[®] reduced Serum Medium up to 2 mL for 25 minutes at room temperature. 100 µL of this solution was deposited into $2 \cdot 10^5$ cells of THP-1 cultured in RPMI medium supplemented with 10% fetal calf serum. Cells were then incubated for 6 h at 37°C under a atmosphere of 5% CO₂.

Cells were then treated with the dimer D1 and CTL-C so that their final concentration in solution was 20 µM and incubated at 37°C for another 6h or 24h. Each condition was done in duplicate.

After incubation, cells were lysed. Protein lysates were prepared and the luciferase assay was performed according to the manufacturer's instructions. Briefly, 75 µL of a reagent from the luciferase reporter assay kit containing the luciferase substrate were incubated with 90 µL of protein extract and luciferase activity was measured using a spetrofluorimeter (Xenius XC, SAFAS, Monaco). Luciferase activities were normalized according to the protein contents of the samples. Protein contents were determined using a Bradford protein assay, which is a colorimetric protein assay based on the absorbance shift of a dye (Coomassie Brilliant Blue G-250) that is red under acidic condition and changes to a bluer color when bind to the protein being assayed through the amine groups. The number of protein can be determined by spectrophotometry measurement at 280 nm after coloration.

Chapter 2 references

1. Kim, Y.H., et al., Effects of excluded volume upon protein stability in covalently cross-linked proteins with variable linker lengths, *Biochemistry*, **2008**, 47 (33), 8804-8814.
2. Amaral, S.P., et al., Efficient Multigram Synthesis of the Repeating Unit of Gallic Acid-Triethylene Glycol Dendrimers, *Organic Letters*, **2011**, 13 (17), 4522-4525.
3. Sauerbrey, G., Verwendung von Schwingquartzen zur Waegung duenner Schichten und zur Mikrowaegung, *Z. Phys*, **1959**, 155, 206-222.
4. Voinova, M.V., et al., Viscoelastic acoustic response of layered polymer films at fluid-solid interfaces: Continuum mechanics approach, *Physica Scripta*, **1999**, 59 (5), 391-396.
5. The NanoWizard AFM Handbook, **2005**.
6. <http://www.biophyresearch.com>.
7. <http://www.jpk.com/imaging-mode-practicalities.434.en.html>.
8. Lévy R., M.M., Measuring the spring constant of atomic force microscope cantilevers: thermal fluctuations and other methods, *Nanotechnology*, **2002**, 13, 33-37.
9. Sneddon, I.N., The relation between load and penetration in the axisymmetric boussinesq problem for a punch of arbitrary profile, *International Journal of Engineering Science*, **1965**, 3, 47-57.
10. P.Polyakov, Automated Force Volume Image Processing for Biological Samples, *PLoS One*, **2011**, 6, 18887.
11. commons.wikimedia.org/wiki/File:Jablonski_Diagram_of_Fluorescence_Only.png.
12. Morot-Gaudry, J.-F., *La génomique en biologie végétale*. 2006.
13. Billot, V., *Deux approches de l'interaction entre membranes et supramolécules : effets de polymères et de cyclodextrines*. 2005, PhD Thesis, Université Louis Pasteur Strasbourg 1.
14. http://www.hitachi-hitec.com/global/science/lc/lc_basic_1.html.
15. O'Brien, J., et al., Investigation of the Alamar Blue (resazurin) fluorescent dye for the assessment of mammalian cell cytotoxicity, *European Journal of Biochemistry*, **2000**, 267 (17), 5421-5426.
16. Natoli, G., et al., The genomic landscapes of inflammation, *Genes & Development*, **2011**, 25 (2), 101-106.
17. <http://www.piercenet.com/method/luciferase-reporters>.

Chapter 3:

Influence of the interaction strength between supramolecular complexes on the topography of neutral polymer multilayers

Chapter 3:

Influence of the interaction strength between supramolecular complexes on the topography of neutral polymer multilayers

Summary

3.1 Introduction	113
3.2 Association constant of the β-CD/guest complexes	114
3.3 Neutral polymer multilayer buildup based on β-CD/guest interactions	117
3.4 Influence of the host-guest affinity on neutral polymer multilayer buildup	124
3.5 Conclusion.....	130
Chapter 3 references	131

3.1 Introduction

Step-by-step film buildup processes constitute a very general way to functionalize surfaces [1, 2]. Multilayer films are obtained by alternated adsorption of two types of interacting species on inorganic [3-5] or organic [6, 7] substrates. Deposition of polymer layers through electrostatic interactions [8-10] is the most prominent example of this type of coatings. Such multilayer films have become extremely popular because it is often believed that step-by-step deposition of polymers leads to a thin coating covering the whole substrate with a nicely stratified structure. Such stratification has been proven for several polyelectrolyte systems rendering them very appealing for multi-functionalization [1, 11-13]. Yet, whole coverage of the substrate is not systematically obtained. Grain- or island-like topographies are often encountered during the multilayer buildup. In 2001, Picart et al. showed that the step-by-step deposition of hyaluronic acid (HA) and poly(L-lysine) (PLL) leads to the formation of islands on silica surfaces during the initial deposition steps [14, 15]. As the number of deposition steps increases these islands merge and form a gel-like film whose thickness increases exponentially with the number of deposition steps. Similarly poly(vinyl sulfate)/PAH gives rise to a grainy structure during the initial deposition steps [4]. Other systems of polymers lead to the formation of islands or grains beyond the early deposition steps. Cini et al. found that poly(sodium phosphate)/PAH leads to an island-like deposit on silicon wafers up to at least 150 deposition steps [16]. Despite its crucial importance for the entire subsequent multilayer film, only few studies tried to explain the topography observed (grain- or island-like, droplets, gel-like, etc.) during the initial deposition steps. A recent study by Guillaume-Gentil et al. has focused on this aspect comparing a weakly interacting polyelectrolyte couple (HA/PLL) and a strongly interacting polyelectrolyte couple (PSS/PAH). After a given number of deposition steps, a HA/PLL multilayer can be either a continuous film or an assembly of droplets, depending on the nature of the substrate [17]. In the case of the PSS/PAH system, a continuous film is obtained independently on the type of the substrate. Comparing their results to recent simulations, Guillaume-Gentil et al. proposed an explanation based on the dielectric constant of the substrate which directly affects the strength of the interactions between the polyelectrolytes and the substrate. According to these simulations, the strength of the monomer-monomer interactions strongly influences the topography of the polyelectrolyte multilayer films [18-20]. Complexation processes between polycations and polyanions can induce a dewetting of the polyelectrolytes

from the substrate. For weakly interacting monomers, this dewetting induced the formation of small complexes on the surface leading to droplet or island morphologies.

Multilayer films based on polymers interacting through supramolecular interactions such as hydrogen bonding [21-23], ligand-receptor [24] or host-guest interactions [25-28] are also reported. The multilayer films based on polymers interacting through host-guest interactions are however not numerous (see bibliographic overview part 1.3.3) and none of the studies focused on the topography of the formed films. The only way that has been reported until now to obtain an unlimited growth of the multilayer films is by using neutral polymers but no investigation on the structures has been conducted. We proposed thus to study the influence of the host-guest interaction strength on the topography of neutral poly(*N*-hydroxypropylamide) (PHPMA) multilayer films formed in a step-by-step manner. The association constant of β -CD/Ad, β -CD/Fc and β -CD/Py complexes is known to be decreasing in this order [29]. The host-guest interaction strength was thus first modulated by involving the different guests in the construction, i.e building PHPMA-CD/PHPMA-Py, PHPMA-CD/PHPMA-Fc and PHPMA-CD/PHPMA-Ad films. The β -CD/Fc complex association constant can be tuned by the presence of different types and concentrations of salts (see bibliographic overview part 1.3.3). The influence of the inclusion complex strength was in a second time studied by building up PHPMA-CD/PHPMA-Fc films in the presence of different sodium salts at different ionic strengths.

3.2 Association constant of the β -CD/guest complexes

Before the study of the buildup of PHPMA-CD and PHPMA-G multilayer films with different guests, we first determined the association constant of the β -CD/G complexes in solution. It is well known that the stability constants of β -CD/Ad, β -CD/Fc and β -CD/Py complexes are decreasing in this order. Ad-COOH and Fc(MeOH)₂ were used for isothermal titration microcalorimetry (ITC) experiments. ITC allows getting access to the association constants (*K*) of β -CD/Fc(MeOH)₂ and β -CD/Ad-COOH, that can be compared to that of the literature [29]. In 10 mM HEPES buffer solutions at pH 7.4 and 25°C (without additional salt), the constants were estimated at $\log K = 4.27 \pm 0.02$ for β -CD/Ad-COOH and $\log K = 3.23 \pm 0.04$ for β -CD/Fc(MeOH)₂. These values are in good agreement with the values found in the literature for the similar systems: $\log K = 4.26$ for β -CD/Ad-COOH in pure water at pH

8.5 and 25°C [30] and $\log K = 3.33$ for β -CD/ferrocene carboxylate in 50 mM phosphate buffer at pH = 8.6 with 0.1 M NaCl at 25°C [29]. Due to the poor water solubility of Py, the stability constant of β -CD/Py complex was not determined in our conditions. This constant is estimated in the literature at 2.69 in water at 25°C [31].

To confirm the ability of salt to tune the strength of the host/guest interaction, we determined the association constant of the β -CD/Fc(MeOH)₂ complex in different types of salts varying the ionic strength. We used four different sodium salts: Na₂SO₄, NaF, NaClO₄ and NaSCN. The results are gathered in Figure 3.1, where the $\log K$ is presented as a function of the ionic strength.

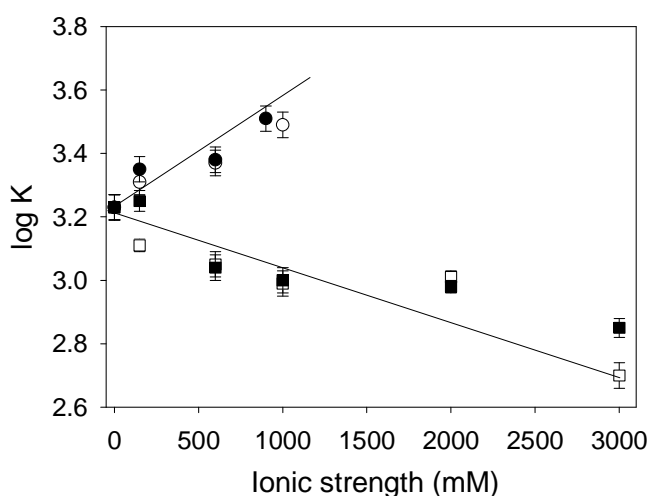


Figure 3.1: Association constant ($\log K$) of β -CD/Fc(MeOH)₂, measured by ITC, as a function of the ionic strength for (●) NaF, (○) Na₂SO₄, (■) NaSCN and (□) NaClO₄. ITC experiments were performed in 10 mM HEPES buffer at pH 7.4 and 25°C. The data represents the mean and the standard deviation of at least two independent experiments. The lines are there to help guide the eye.

The ionic strength was increased up to 3 M for NaSCN and NaClO₄ but limited to 900 mM for NaF and 1 M for Na₂SO₄ due to the limited solubility of the respective salts (Table 3.1) or of β -CD in the salt.

Table 3.1: Solubility of the salts used in water at 20°C from Handbook of Chemistry and Physics, 94th edition.

	Solubility at 20°C	
	g/100 mL	mol.L ⁻¹
NaF	4.06	0.97
Na ₂ SO ₄	19.5	6.30
Na ₂ ClO ₄	201	17.15
NaSCN	125	15.40

We observed two different trends according to the salt present in solution. On the one hand, by increasing the ionic strength of NaClO₄ and NaSCN concentration from 0 up to 3 M, the association constant of the β-CD/Fc(MeOH)₂ complex decreases from 3.23 down to 2.85 and 2.70, respectively. The influence of the perchlorate (ClO₄⁻) and the thiocyanate (SCN⁻) anions on the stability constant of β-CD/Fc(MeOH)₂ measured in solution can be rationalized as follows: both ClO₄⁻ [32-34] and SCN⁻ [33, 35] anions form 1:1 complexes with β-CD (with an association constant of log *K* = 1.42 [33] and 0.99 [33], respectively) and compete with the formation of the β-CD/Fc(MeOH)₂ complex. Indeed, it has been proposed that the inside of the CD cavity is composed of positively polarized carbon atoms leading to the inclusion of hydrophobic anionic guests [36] such as the ClO₄⁻ and SCN⁻ anions. A similar decrease of the association constant of β-CD/nabumetone [37], β-CD/phenylbenzothiazole derivatives [38] and β-CD/3-hydroxy-2-naphthoic acid [32] complexes has been reported in the presence of ClO₄⁻ anions. On the other hand, the increase of the Na₂SO₄ and NaF ionic strength up to respectively 1 M and 0.9 M induces an increase of log *K* of the β-CD/Fc(MeOH)₂ complex value up to about 3.5 (Figure 3.1). Similarly, Harries and co-workers obtained a linear increase of the β-CD/Ad association constant when increasing the K₂SO₄ and KF concentration [39]. Sulfate (SO₄²⁻) and fluoride (F⁻), strongly hydrated anions, do not bind to β-CD [32, 34]. The increase of the association constant is correlated with the water molecules released from both the β-CD cavity and Fc(MeOH)₂ upon the formation of the complex. The presence of SO₄²⁻ and F⁻ disturbs the internal structure of water around the β-CD and its guest, rendering the releasing step of water easier and thus displacing the equilibrium toward the complex formation [40].

By changing the nature and the concentration of the anion in solution, the association constant between β-CD and Fc(MeOH)₂ can be modulated. After checking this effect in the bulk, we investigated the influence of the interaction strength on the buildup of neutral polymer multilayers based on cyclodextrin/guest interactions.

3.3 Neutral polymer multilayer buildup based on β -CD/guest interactions

Multilayer assemblies were prepared by alternated depositions of PHPMA-G (i.e. PHPMA-Ad, PHPMA-Fc or PHPMA-Py) and PHPMA-CD. The PHPMA backbone being a neutral polymer, the cohesion of the resulting assemblies is only due to the supramolecular host-guest interactions that occur between cyclodextrins and adamantane, ferrocene or pyrene moieties. Functionalized PHPMA polymers were prepared in two steps: the synthesis of PHPMA-N₃ ($M_w=34\,040\text{ g}\cdot\text{mol}^{-1}$, $M_n=92\,640\text{ g}\cdot\text{mol}^{-1}$, PDI=2.72) with a grafting ratio of 5% and its functionalization by the guest through click-chemistry. Using the same batch of PHPMA-N₃ allows us to obtain functionalized PHPMA with different guests and β -CD having roughly the same length of polymer chains and the same grafting ratio (5%). The chemical structure of all polymers can be found in Figure 3.2.

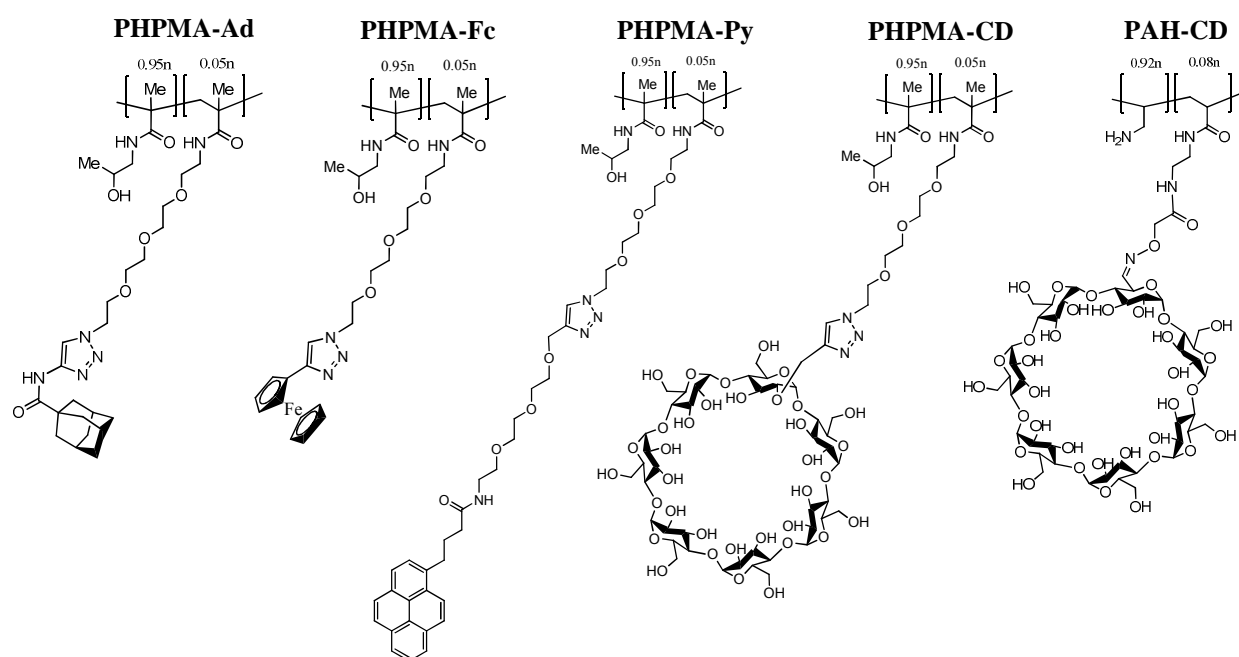


Figure 3.2: Chemical structures of PHPMA-Ad, PHPMA-Fc, PHPMA-Py, PHPMA-CD and PAH-CD.

The buildup of the multilayer films was followed by QCM-D. An anchoring layer of polycationic PAH-CD was first adsorbed. A strong and almost linear evolution of the normalized frequency shift ($-\Delta f_v/v$), measured at 15 MHz, is observed for both PHPMA-CD/PHPMA-Ad and PHPMA-CD/PHPMA-Fc systems reaching roughly 750 and 600 Hz at the end of the sixth bilayer, respectively (Figure 3.3a). In contrast, the PHPMA-CD/PHPMA-

Py buildup is limited to one bilayer (40 Hz). The association constant between β -CD and pyrene ring ($\log K = 2.69$ in water at 25°C [31]) is probably too weak.

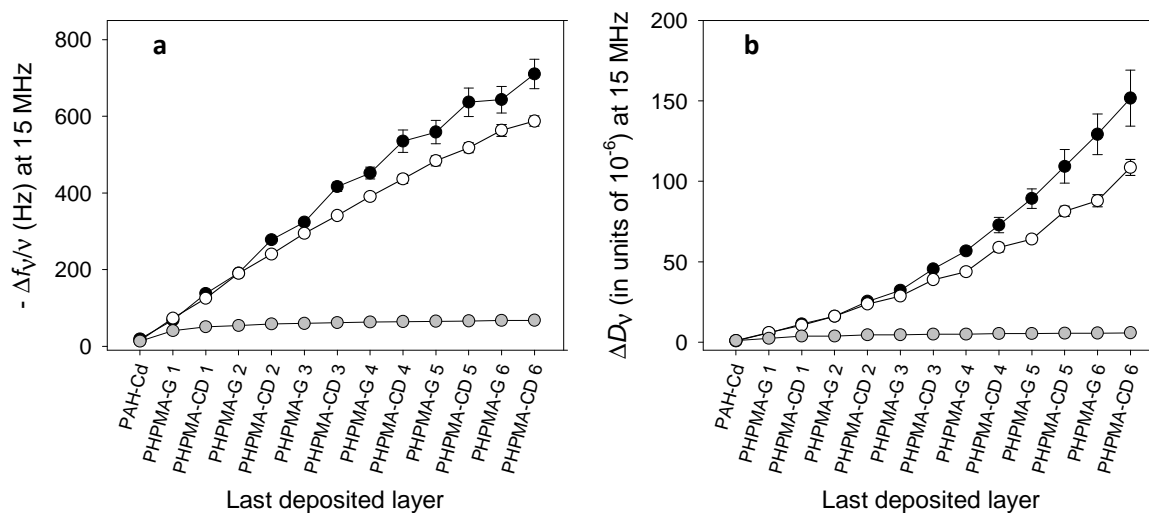


Figure 3.3: Typical evolution of the normalized frequency shift $-\Delta f_v/v$ (a) and of the energy dissipation ΔD_v (b), measured at 15 MHz ($\nu = 3$) by QCM-D, as a function of the last deposited layer for (●) PHPMA-CD/PHPMA-Ad, (○) PHPMA-CD/PHPMA-Fc and (●) PHPMA-CD/PHPMA-Py. Polymer solutions were prepared at $0.1 \text{ mg}\cdot\text{mL}^{-1}$ in 10 mM HEPES - 150 mM NaCl buffer at pH 7.4. The data represents the mean and the standard deviation of three independent experiments. The values of the standard deviation are smaller or similar size compared to the reported symbol.

After 6 bilayers, the dissipation values reach 150×10^{-6} and 110×10^{-6} of PHPMA-CD/PHPMA-Ad and PHPMA-CD/PHPMA-Fc, respectively. These values are relatively large suggesting that the assemblies are highly hydrated as was shown in our former study. Indeed, PHPMA-CD/PHPMA-Fc films were found to have 95% content in water [28]. To show that the buildup is obtained only due to host-guest interactions, we performed two sets of control experiments: one where only PHPMA-CD was used and the second one where at least one of the host or guest functionalized PHPMA was replaced by PHPMA- N_3 . We thus followed by QCM the buildup of the following systems: PHPMA-CD/PHPMA-CD, PHPMA-CD/PHPMA- N_3 , PHPMA- N_3 /PHPMA-Fc and PHPMA- N_3 /PHPMA- N_3 (Figure 3.4). We can notice that no buildup of films is obtained in all this cases. The host/guest couple is thus necessary showing that PHPMA-CD/PHPMA-Fc and PHPMA-CD/PHPMA-Ad buildups are only obtained due to the host/guest interactions.

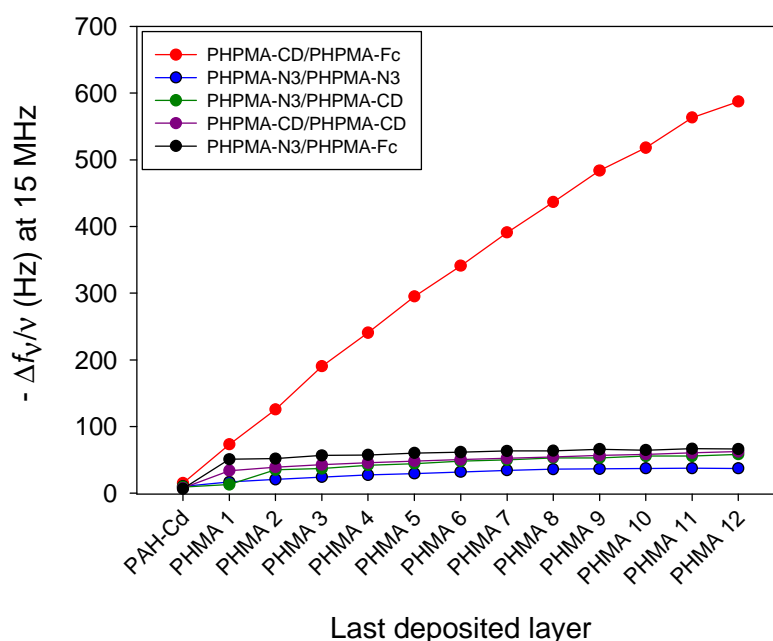


Figure 3.4: Typical evolution of the normalized frequency shift $-\Delta f_v/v$, measured at 15 MHz ($\nu = 3$) by QCM-D, as a function of the last deposited layer for PHPMA-CD/PHPMA- N_3 , PHPMA- N_3 /PHPMA-Fc, PHPMA- N_3 /PHPMA- N_3 and PHPMA-CD/PHPMA-CD. Polymer solutions were prepared at $0.1 \text{ mg}\cdot\text{mL}^{-1}$ in 10 mM HEPES - 150 mM NaCl buffer at pH 7.4.

In order to determine the topography of PAH-CD-(PHPMA-G/PHPMA-CD) $_n$ based films (with G = Ad, Fc and Py), AFM images were performed in contact mode and in liquid state at different numbers of bilayers ranging from 5 up to 22 bilayers. The films were scratched to determine their thicknesses by a profilometric section (Figure 3.5). The film thickness, i.e. the z distance between the bare substrate and the surface of the film, is considered as the minimal film thickness covering all the substrate. Although similar QCM-D signal evolutions were observed along the buildup of PHPMA-CD/PHPMA-Ad and PHPMA-CD/PHPMA-Fc films, the topography evolutions are not similar. On the one hand, the PHPMA-CD/PHPMA-Ad system leads to extremely rough films mainly constituted of droplets that grow in number and in size with the number of deposition steps (Figure 3.5, first row).

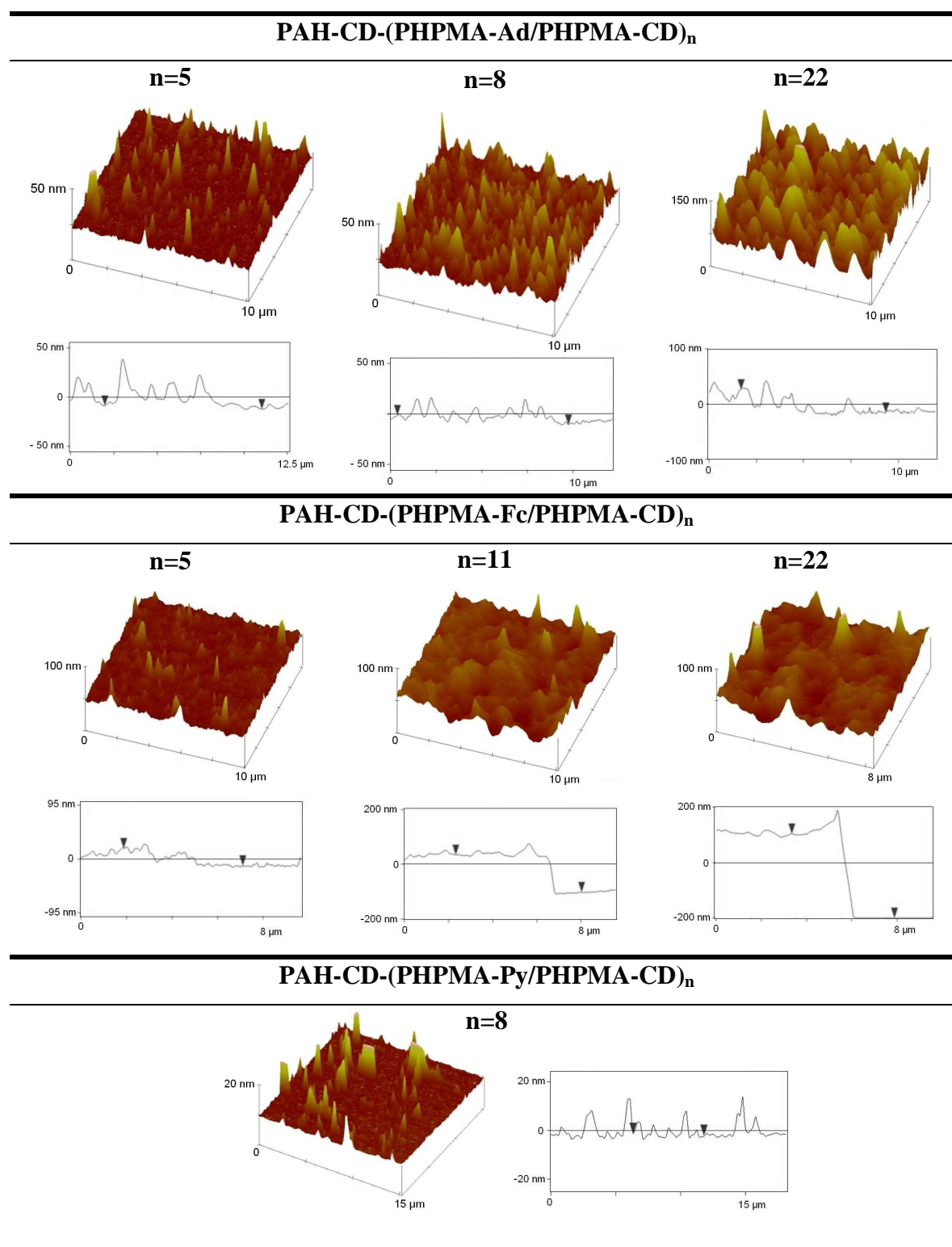


Figure 3.5: Morphologies and profilometric sections, obtained by AFM in contact mode in liquid state, of PAH-CD-(PHPMA-Ad/PHPMA-CD)_n, of PAH-CD-(PHPMA-Fc/PHPMA-CD)_n at different numbers of deposited bilayers (n) and of PAH-CD-(PHPMA-Py/PHPMA-CD)₈. Profilometric sections are obtained on scratched films. Polymer solutions were prepared at 0.1 mg·mL⁻¹ in 10 mM HEPES - 150 mM NaCl buffer at pH 7.4.

On the other hand, the PHPMA-CD/PHPMA-Fc system forms fairly flat and smooth films whose thickness increases with the number of deposition steps (Figure 3.5, second row). Concerning the PHPMA-CD/PHPMA-Py system, only few and isolated aggregates are visible on the substrate showing almost no adsorbed polymer (Figure 3.5, third row). After 22 deposited bilayers, PHPMA-CD/PHPMA-Fc films reach a thickness of about 300 nm with a roughness of 21 nm when a PHPMA-CD/PHPMA-Ad film has a thickness of 20 nm with the largest extension of its islands of about 50 nm (Figure 3.5 and Table 3.2). The roughness of PHPMA-CD/PHPMA-Ad films is similar or higher than the thickness (Table 3.2) as it is shown in the profilometric section (Figure 3.5, first row).

Table 3.2: Evolution of the thicknesses and the roughnesses of PHPMA-CD/PHPMA-Ad and PHPMA-CD/PHPMA-Fc based films (AFM data extracted from Figure 3.5) allowing the denomination of the topography of the films.

	n	d_{AFM} (nm)	RMS roughness (nm)	Film topography
PAH-CD-(PHPMA-Ad/PHPMA-CD)_n	5	11	6	rough continuous
	8	13	11	droplet-like
	22	20	26	
	n	d_{AFM} (nm)	RMS roughness (nm)	
PAH-CD-(PHPMA-Fc/PHPMA-CD)_n	5	31	6	smooth
	11	136	13	continuous
	22	337	21	

All the results reported above were obtained with a polymer concentration of 0.10 mg.mL⁻¹. To favor the buildup of the films, we investigated the effect of the polymer concentration. Two polymer concentrations were further used: 0.05 and 0.50 mg.mL⁻¹. Figure 3.6 shows the topography and the profilometric section of the PAH-CD-(PHPMA-Fc/PHPMA-CD)_n and PAH-CD-(PHPMA-Ad/PHPMA-CD)_n films built at polymer concentrations of 0.05 and 0.10 mg.mL⁻¹ up to $n = 22$ bilayers and built at the polymer concentration of 0.50 mg.mL⁻¹ up to $n=11$ bilayers. The topography of these films does not depend on the concentration of the polymer solutions used during the buildup process (Figure 3.6). However, higher polymer concentrations result in larger islands in the case of PHPMA-CD/PHPMA-Ad and thicker films in the case of PHPMA-CD/PHPMA-Fc (Table 3.3). Based

on these results, three types of film topography can be defined: smooth continuous films when the film roughness is below 20% of the film thickness, rough continuous films when the film roughness is above 20% of the film thickness and island-like films when the film thickness is below the film roughness. PHPMA-Ad, PHPMA-Fc and PHPMA-Py have the same length of polymer chains and the same grafting ratio in hydrophobic groups along the polymer backbone (5%). The differences in film topography and buildup can only be attributed to the host-guest interaction strength between Ad, Fc or Py groups and β -CD. The association constant of Ad and β -CD being one of the highest reported in the literature, we will qualify the strength of the interaction between PHPMA-Ad and PHPMA-CD as “strong”. According to the AFM images whatever the polymer concentration, strong interactions between neutral polymers through host-guest association lead to a rough continuous film or an island-like film, whereas, regardless of the number of bilayers or of the concentration of the polymers used, intermediate strength interactions (involving Fc groups) lead to a smooth continuous film. Too weak interactions (involving Py derivatives) allow no longer film construction but rather the formation of isolated aggregates.

Table 3.3: Evolution of the thicknesses and the roughnesses of PHPMA-CD/PHPMA-Ad and PHPMA-CD/PHPMA-Fc films (AFM data from Figure 3.6)

	[Polymer] (mg.mL ⁻¹)	<i>n</i>	<i>d</i> _{AFM} (nm)	RMS (nm)	Film topography
PAH-CD/(PHPMA-Ad/PHPMA-CD) _n	0.05	22	13	7	rough continuous film
	0.1	22	20	26	droplet-like film
	0.5	11	27	46	
	[Polymer] (mg.mL ⁻¹)	<i>n</i>	<i>d</i> _{AFM} (nm)	RMS (nm)	Film topography
PAH-CD/(PHPMA-Fc/PHPMA-CD) _n	0.05	22	95	22	smooth continuous film
	0.1	22	337	21	
	0.5	11	736	17	

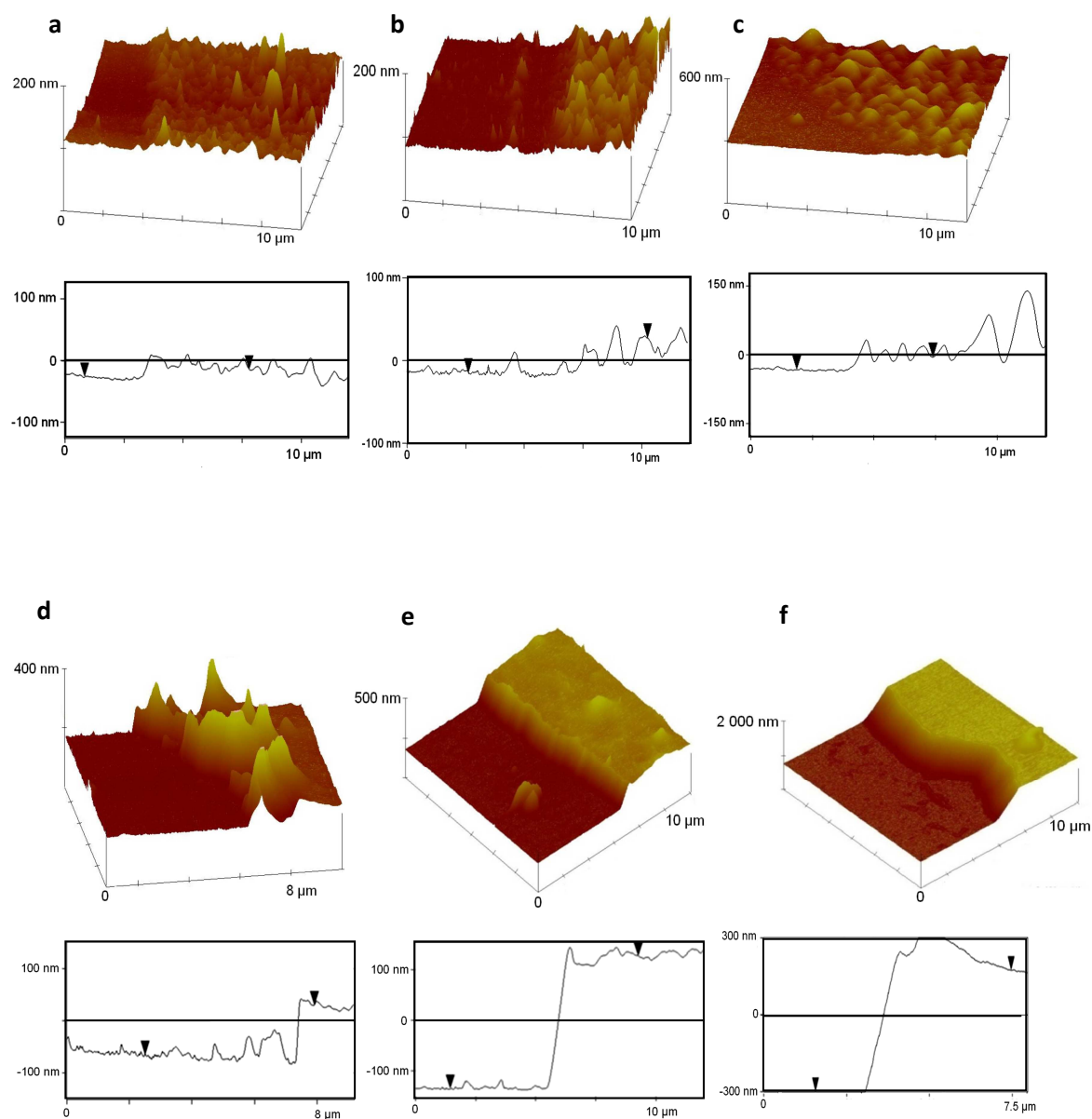


Figure 3.6: 3D images and profilometric sections, obtained by AFM in contact mode in liquid environment, of scratched PAH-CD-(PHPMA-Ad/PHPMA-CD)_n films with polymer solutions prepared at (a) 0.05 mg.mL⁻¹ with $n = 22$, (b) 0.1 mg.mL⁻¹ with $n = 22$, and (c) 0.5 mg.mL⁻¹ with $n = 11$; and of PAH-CD-(PHPMA-Fc/PHPMA-CD)_n films with polymer solutions prepared at (d) 0.05 mg.mL⁻¹ with $n = 22$, (e) 0.1 mg.mL⁻¹ with $n = 22$ and (f) 0.5 mg.mL⁻¹ with $n = 11$. All polymer solutions were prepared in 10 mM HEPES - 150 mM NaCl buffer at pH 7.4.

3.4 Influence of the host-guest affinity on neutral polymer multilayer buildup

First, using ITC, we showed that the interaction of β -CD with $\text{Fc}(\text{MeOH})_2$ can be modulated by changing the nature and the concentration of anions. Then, we observed that PHPMA-CD/PHPMA-Ad multilayers are droplet-like whereas PHPMA-CD/PHPMA-Fc ones are rather smooth. Based on this observation, our idea was to modulate the affinity of the β -CD interaction with Fc by varying the nature of the sodium salt anions and their concentration in the PHPMA solutions used to build PAH-CD-(PHPMA-Fc/PHPMA-CD)_n films. The polymer concentration was fixed at $0.1 \text{ mg}\cdot\text{mL}^{-1}$. First, the film buildup was performed in 10 mM HEPES buffer at pH 7.4 and at an ionic strength of 150 mM using different sodium salts, namely NaF, Na₂SO₄, NaSCN and NaClO₄ (Figure 3.7). It appears that the normalized frequency shifts measured by QCM-D corresponding to F⁻ and SO₄²⁻ are significantly higher than those corresponding to films constructed in the presence of SCN⁻ and ClO₄⁻ as the anions of the supporting electrolyte. Without added salt, the buildup of the film is close to the one obtained in the presence of F⁻ and SO₄²⁻. The QCM measurements confirm that the buildup of PHPMA-CD/PHPMA-Fc films can be modulated by the choice of the supporting electrolyte anion.

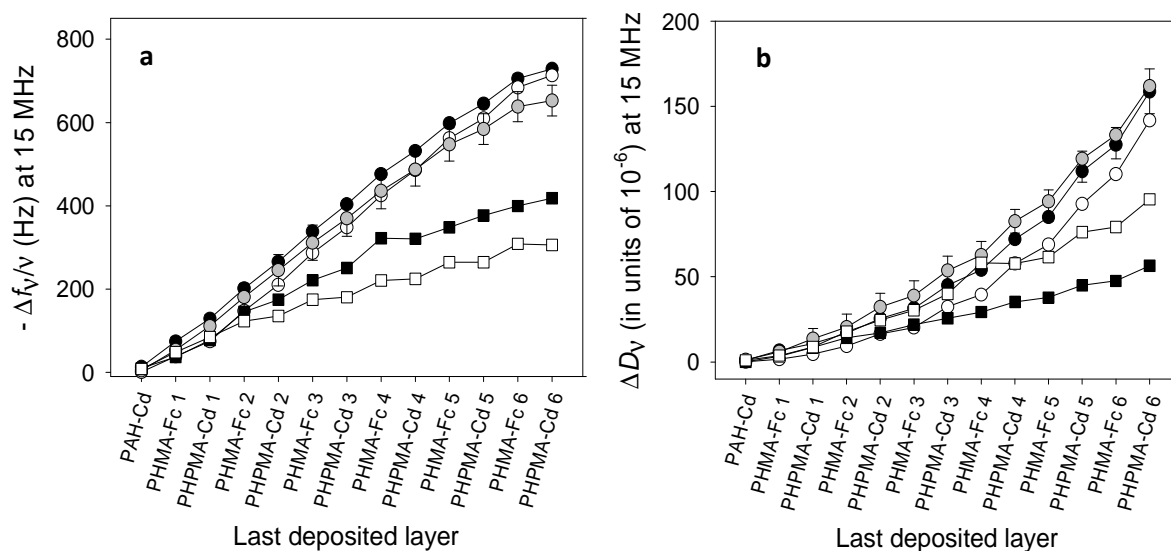


Figure 3.7: Evolution of (a) the normalized frequency shift $-\Delta f_v/\nu$ and (b) the dissipation factor ΔD_v , measured at 15 MHz ($\nu = 3$) by QCM, as a function of the sequence of adsorbed polymer layers during the buildup of PAH-CD-(PHPMA-Fc/PHPMA-CD)₇ in 10 mM HEPES at pH 7.4 without added salt (●) and with (●) NaF, (○) Na₂SO₄, (■) NaSCN and (□) NaClO₄ at the ionic strength of 150 mM.

Furthermore, the topography and the thickness of PAH-CD-(PHPMA-Fc/PHPMA-CD)₇ films were determined by AFM when built in the different types of salts at different ionic strengths. In the absence of salt, the buildup process leads to a smooth continuous film with a thickness of 116 nm and a roughness of 9 nm (Figure 3.8).

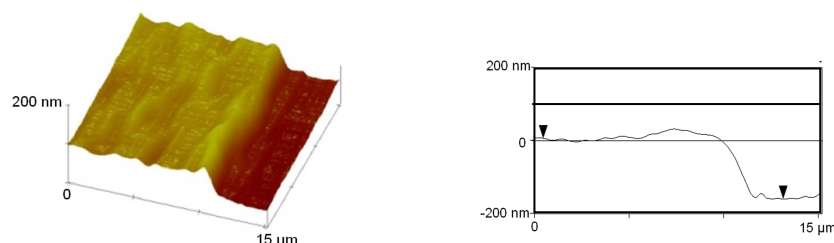


Figure 3.8: 3D AFM image and profilometric section, obtained by AFM in contact mode in liquid environment, of a scratched PAH-CD-(PHPMA-Fc/PHPMA-CD)₇ film built in 10 mM HEPES buffer solution at pH 7.4 without added salt. The polymer solution was prepared at 0.1 mg.mL⁻¹.

By increasing the concentration of Na₂SO₄ (or NaF), corresponding to an increase of the β-CD/Fc interaction strength (Figure 3.1), smooth and continuous films are formed until 800 mM (Figure 3.9 and Figure 3.10). A decrease of the film thickness is observed keeping almost the same roughness (Table 3.4). By increasing the concentration of NaSCN (or NaClO₄), corresponding to a decrease of the β-CD/Fc interaction strength (Figure 1), the film buildup becomes less and less effective leading to a smaller film thickness (Figure 3.9 and Figure 3.10) and higher the roughness (Table 3.4). The film topography is changing from a smooth continuous film towards a droplet-like film.

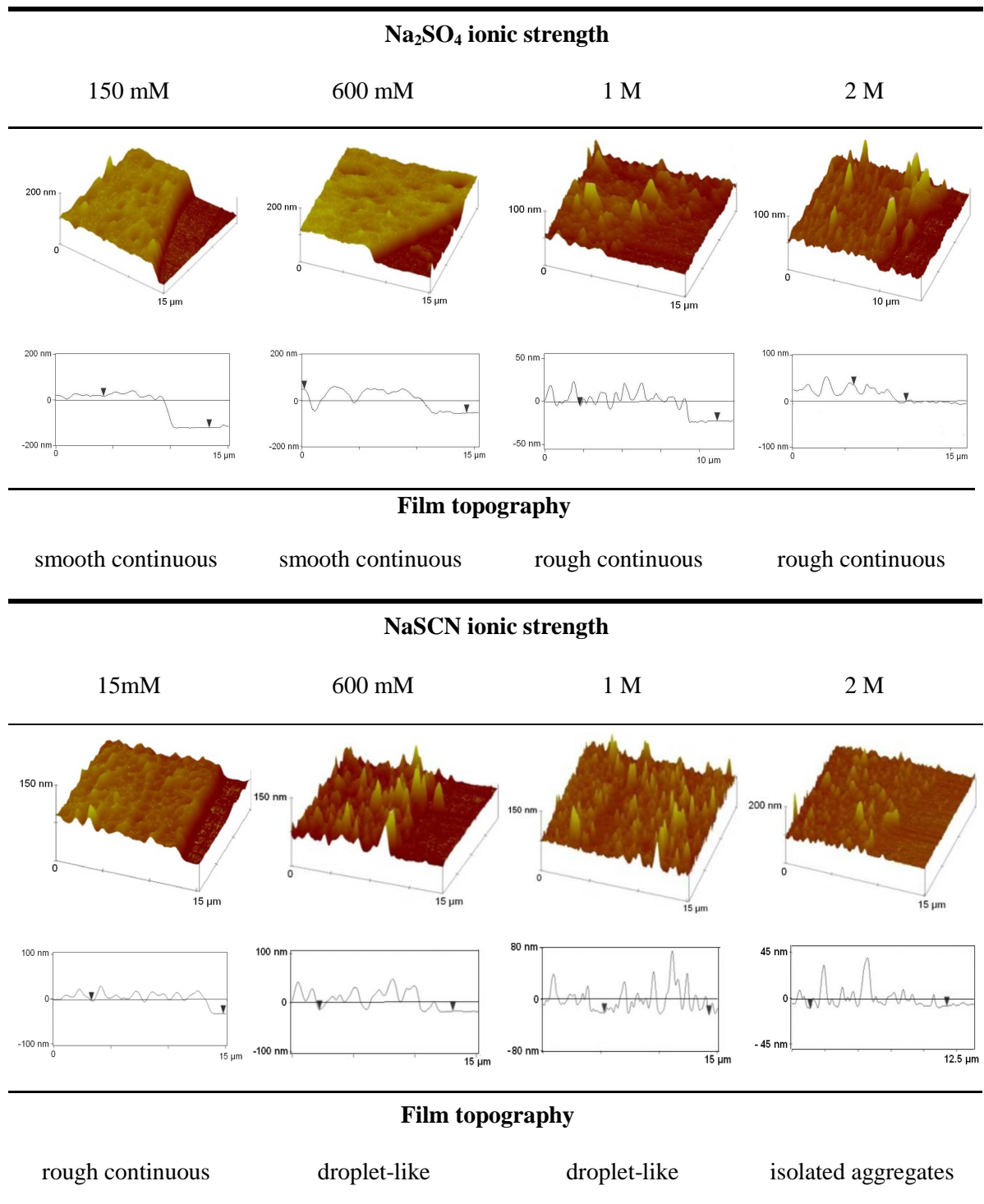


Figure 3.9: 3D AFM images and profilometric sections, obtained by AFM in contact mode in liquid environment, of a scratched PAH-CD-(PHPMA-Fc/PHPMA-CD)₇ film built in a 10 mM HEPES buffer solution at pH 7.4 in the presence of Na₂SO₄ and NaSCN at different ionic strengths. Polymer solutions were prepared at 0.1 mg.mL⁻¹.

Table 3.4: Evolution of the thickness and the roughness (RMS) of PAH-CD/(PHPMA-Fc/PHPMA-CD)₇ films built in 10 mM HEPES buffer solution at pH 7.4 in the presence of Na₂SO₄, NaF, NaSCN and NaClO₄ at different ionic strengths. Polymer solutions were prepared at 0.1 mg.mL⁻¹.

	Ionic strength	log K	d_{AFM}	RMS	RMS/thickness	Film topography
	(M)	(± 0.04)	(nm)	(nm)	(%)	
Na₂SO₄	0	3.23	116	9	8	smooth continuous
	150	3.31	132	9	7	smooth continuous
	300	-	120	8	7	
	600	3.37	90	10	11	
	800	-	66	8	12	rough continuous
	1000	3.49	30	8	27	
	2000	-	22	11	50	droplet-like
	Ionic strength	log K	d_{AFM}	RMS	RMS/thickness	Film topography
	(M)	(± 0.04)	(nm)	(nm)	(%)	
NaF	150	3.35	170	8	5	smooth continuous
	300	-	138	7	5	
	600	3.38	88	7	8	
	700	-	88	7	8	
	800	-	62	10	16	
	900	3.51	54	6	11	
	Ionic strength	log K	d_{AFM}	RMS	RMS/thickness	Film topography
	(M)	(± 0.04)	(nm)	(nm)	(%)	
NaSCN	15	3.25	31	8	26	rough continuous
	150	-	9	10	111	droplet-like
	600	3.04	14	23	164	
	1000	3.00	12	22	184	
	2000	2.98	0	17	-	isolated aggregates
	Ionic strength	log K	d_{AFM}	RMS	RMS/thickness	Film topography
	(M)	(± 0.04)	(nm)	(nm)	(%)	
NaClO₄	15	-	70	12	17	smooth continuous
	150	3.11	46	9	19	
	300	-	69	10	14	
	600	3.05	45	12	27	rough continuous
	800	-	32	12	38	
	1000	2.99	35	8	23	
	2000	3.01	10	10	100	
3000	2.7	6	7	117	droplet-like	

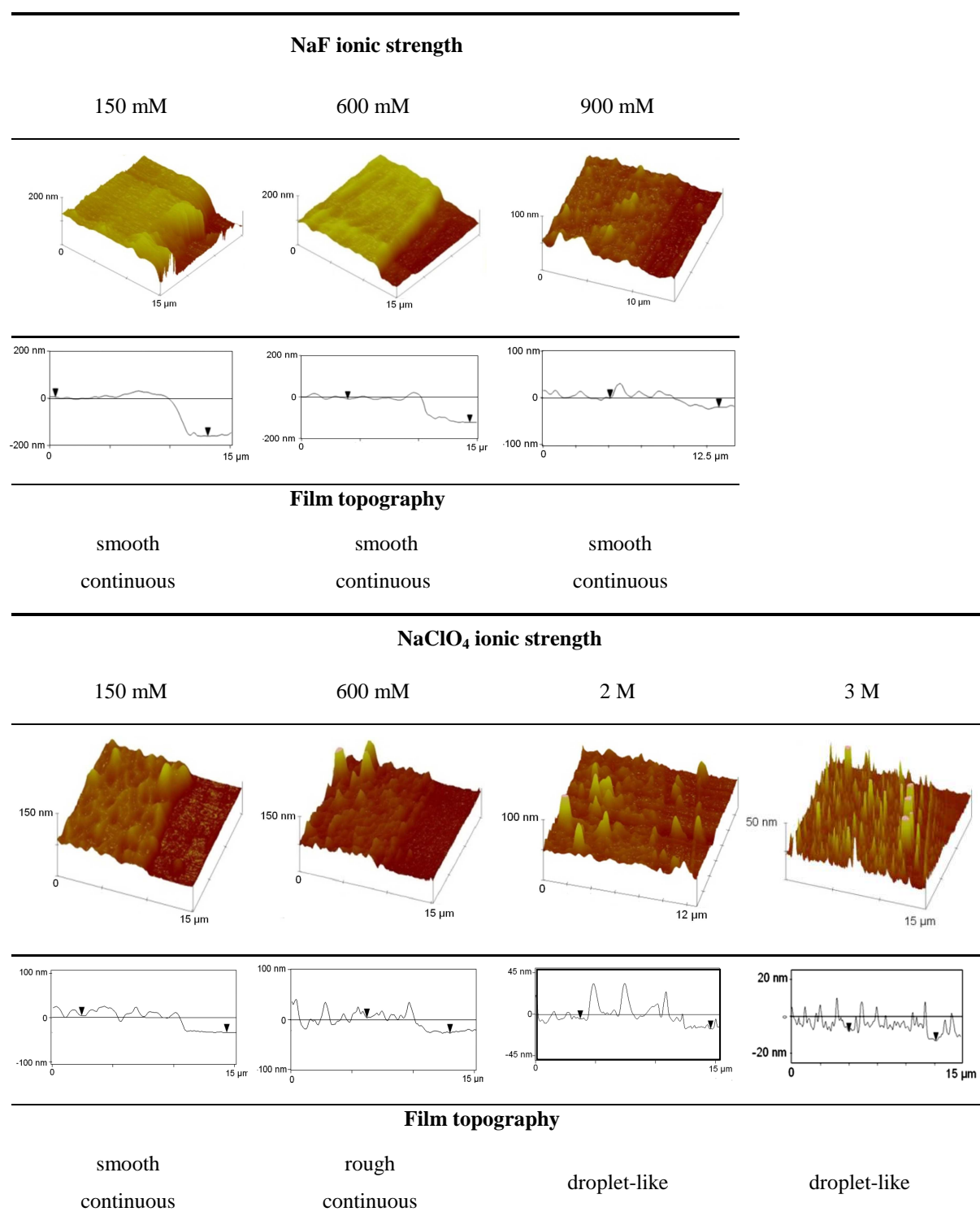


Figure 3.10: 3D AFM images and profilometric sections, obtained by AFM in contact mode in liquid environment, of scratched PAH-CD-(PHPMA-Fc/PHPMA-CD)₇ films built in 10 mM HEPES buffer solution at pH 7.4 in the presence of NaF and NaClO₄ at different ionic strengths. The polymer solutions were prepared at 0.1 mg.mL⁻¹.

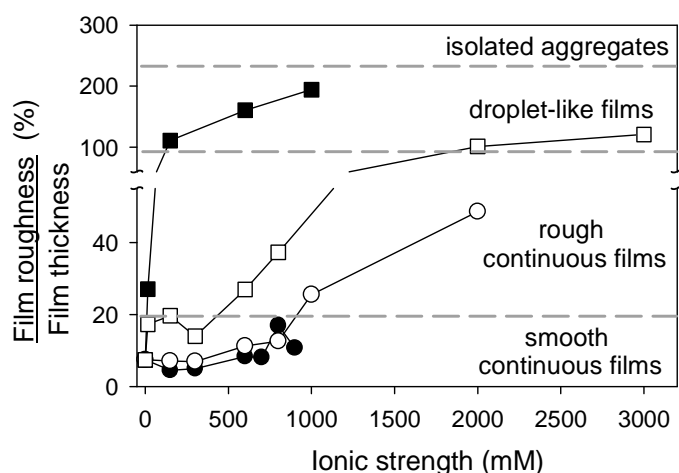


Figure 3.11: Evolution of the roughness to thickness ratio of a PAH-CD-(PHPMA-Fc/PHPMA- β -CD)₇ film as a function of (●) NaF, (○) Na₂SO₄, (■) NaSCN and (□) NaClO₄ ionic strength. The film was built in 10 mM HEPES at pH 7.4 with a polymer concentration of 0.1 mg.mL⁻¹.

The roughness to thickness ratio of PAH-CD-(PHPMA-Fc/PHPMA-CD)₇ films as a function of the ionic strength for the four studied salts is represented in Figure 3.11. By strengthening the host-guest interaction, the topography of the PHPMA-CD/PHPMA-Fc films changes from smooth and continuous to droplet-like. Whereas for the weakest host-guest interactions ($\log K = 2.7$ at 3 M NaSCN), no PHPMA-CD/PHPMA-Fc film buildup is obtained. This was also found for PHPMA-CD/PHPMA-Py buildup where $\log K = 2.69$ for β -CD/Py in water. This is represented schematically in Figure 3.12. These results seem to confirm that the strength of the interaction between the two polymers constituting the film strongly influences the film buildup. Intermediate interaction strength seems to be required to form continuous films whereas if too low, the interaction strength limits the film buildup.

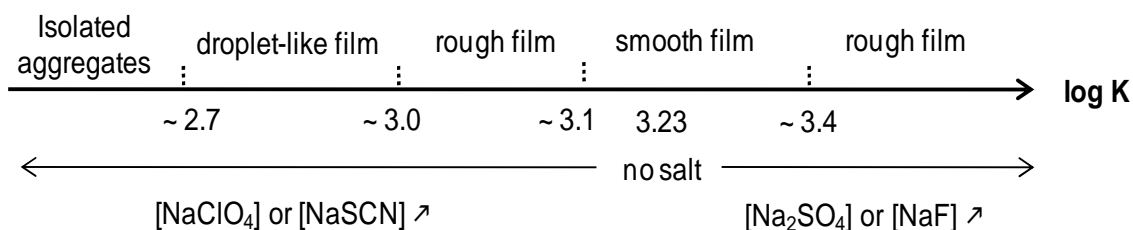


Figure 3.12: Schematic representation of the influence of the ionic strength on the topography of PHPMA-CD/PHPMA-Fc multilayers, via the tuning of the β -CD/Fc association constant.

3.5 Conclusion

We investigated the influence of the strength of non-covalent host-guest interactions between β -CD and Py, Fc, and Ad on the structure of PHPMA-CD/PHPMA-Py, PHPMA-CD/PHPMA-Fc and PHPMA-CD/PHPMA-Ad films formed in a step-by-step manner. In solution, the strength of the inclusion complex is increasing in the order $\text{Py}/\beta\text{-CD} < \text{Fc}/\beta\text{-CD} < \text{Ad}/\beta\text{-CD}$. Depending upon this strength, the buildup process is limited to the formation of isolated aggregates for PHPMA-CD/PHPMA-Py, leads to smooth continuous films for PHPMA-CD/PHPMA-Fc and to droplet-like films, which do not cover entirely the substrate, for PHPMA-CD/PHPMA-Ad.

To study in a systematic way the influence of the strength of the host-guest interactions on the topography of the films, PHPMA-CD/PHPMA-Fc films were built in the presence of different sodium salts at different ionic strengths. For weak host-guest interactions, only isolated aggregates are formed on the substrate. As the interaction strength of the host-guest interactions increases (increase of $\log K$) the formed films go through a droplet-like structure, before becoming continuous but rough for stronger interactions. When the interaction is further increased, the films become smooth before becoming rough again at still higher interaction strength.

Further studies are needed to verify if these conclusions apply to other step-by-step constructed polymer films. Moreover, the interactions between the polymers and the substrate should be taken into account to get a general picture of the initial steps of layer-by-layer polymer film constructions. Nevertheless, this study constitutes, to our knowledge, the first attempt to rationalize the comprehension of the initial steps of a polymer multilayer buildup as a function of the polymer interaction strength.

Chapter 3 references

1. Decher, G., Fuzzy Nanoassemblies: Toward Layered Polymeric Multicomposites, *Science*, **1997**, 277 (5330), 1232-1237.
2. Decher, G., et al., *Multilayer Thin Films - Sequential Assembly of Nanocomposite Materials*. 2003, Weinheim, Germany: Wiley-VCH.
3. Lvov, Y., et al., Assembly, structural characterization, and thermal behavior of layer-by-layer deposited ultrathin films of poly(vinyl sulfate) and poly(allylamine), *Langmuir*, **1993**, 9, 481.
4. Kim, D.K., et al., Morphology of multilayers assembled by electrostatic attraction of oppositely charged model polyelectrolytes, *Thin Solid Films*, **1999**, 350 (1-2), 153-160.
5. Caruso, F., et al., 1. Ultrathin multilayer polyelectrolyte films on gold: Construction and thickness determination, *Langmuir*, **1997**, 13 (13), 3422-3426.
6. Delcorte, A., et al., Adsorption of polyelectrolyte multilayers on polymer surfaces, *Langmuir*, **1997**, 13, 5125.
7. Hsieh, M.C., et al., Surface "priming" for layer-by-layer deposition: Polyelectrolyte multilayer formation on allylamine plasma-modified poly(tetrafluoroethylene), *Macromolecules*, **1997**, 30, 8453.
8. Decher, G., et al., Buildup of ultrathin multilayer films by a self-assembly process. Consecutively alternating adsorption of anionic and cationic polyelectrolytes on charges surface., *Thin Solid Films*, **1992**, 210/211, 831-835.
9. Yoo, D., et al., Controlling bilayer composition and surface wettability of sequentially adsorbed multilayers of weak polyelectrolytes, *Macromolecules*, **1998**, 31, 4309-4318.
10. Clark, S.L., et al., The role of secondary interactions in selective electrostatic multilayer deposition, *Langmuir*, **2000**, 16 (26), 10206-10214.
11. Schmitt, J., et al., Internal structure of layer-by-layer adsorbed polyelectrolyte films: A neutron and x-ray reflectivity study, *Macromolecules*, **1993**, 26, 7058-7063.
12. Kharlampieva, E., et al., Spin-Assisted Layer-by-Layer Assembly: Variation of Stratification as Studied with Neutron Reflectivity, *Langmuir*, **2009**, 25 (24), 14017-14024.
13. Felix, O., et al., Are sprayed LbL-films stratified? A first assessment of the nanostructure of spray-assembled multilayers by neutron reflectometry, *Comptes Rendus Chimie*, **2009**, 12 (1-2), 225-234.
14. Picart, C., et al., Buildup mechanism for poly(L-lysine)/hyaluronic acid films onto a solid surface, *Langmuir*, **2001**, 17 (23), 7414-7424.

15. Picart, C., et al., Molecular basis for the explanation of the exponential growth of polyelectrolyte multilayers, *Proc. Natl. Acad. Sci. USA*, **2002**, 99 (20), 12531-12535.
16. Cini, N., et al., Step-by-Step Assembly of Self-Patterning Polyelectrolyte Films Violating (Almost) All Rules of Layer-by-Layer Deposition, *Journal of the American Chemical Society*, **2010**, 132 (24), 8264-8265.
17. Guillaume-Gentil, O., et al., From nanodroplets to continuous films: how the morphology of polyelectrolyte multilayers depends on the dielectric permittivity and the surface charge of the supporting substrate, *Soft Matter*, **2011**, 7 (8), 3861-3871.
18. Cerda, J.J., et al., Modeling strategies for polyelectrolyte multilayers, *European Physical Journal-Special Topics*, **2009**, 177, 129-148.
19. Messina, R., Polyelectrolyte multilayering on a charged planar surface, *Macromolecules*, **2004**, 37 (2), 621-629.
20. Dobrynin, A.V., Theory and simulations of charged polymers: From solution properties to polymeric nanomaterials, *Current Opinion in Colloid & Interface Science*, **2008**, 13 (6), 376-388.
21. Stockton, W.B., et al., Molecular-Level Processing of Conjugated Polymers. 4. Layer-by-Layer Manipulation of Polyaniline via Hydrogen-Bonding Interactions, *Macromolecules*, **1997**, 30, 2717-2725.
22. Yang, S.Y., et al., Micropatterning of polymer thin films with pH-sensitive and cross-linkable hydrogen-bonded polyelectrolyte multilayers, *Journal of the American Chemical Society*, **2002**, 124 (10), 2100-2101.
23. Sukhishvili, S.A., et al., Layered, Erasable, Ultrathin Polymer Films, *Journal of the American Chemical Society*, **2000**, 122, 9550-9551.
24. Quinn, J.F., et al., Next generation, sequentially assembled ultrathin films: beyond electrostatics, *Chemical Society Reviews*, **2007**, 36 (5), 707-718.
25. Suzuki, T., et al., Construction of positively-charged layered assemblies assisted by cyclodextrin complexation, *Chem. Commun.*, **2002**, 164-165.
26. Van der Heyden, A., et al., Multilayer films based on host-guest interactions between biocompatible polymers, *Chem. Commun.*, **2006**, 3220-3222.
27. Wang, Z.P., et al., Stepwise assembly of the same polyelectrolytes using host-guest interaction to obtain microcapsules with multiresponsive properties, *Chemistry of Materials*, **2008**, 20 (13), 4194-4199.
28. Dubacheva, G.V., et al., Unlimited growth of host-guest multilayer films based on functionalized neutral polymers, *Soft Matter*, **2010**, 6 (16), 3747-3750.
29. Rekharsky, M.V., et al., Complexation thermodynamics of cyclodextrins, *Chemical Reviews*, **1998**, 98 (5), 1875-1917.

30. Eftink, M.R., et al., Cyclodextrin inclusion complexes - studies of the variation in the size of alicyclic guests *Journal of the American Chemical Society*, **1989**, 111 (17), 6765-6772.
31. Blyshak, L.A., et al., Evidence for non-inclusional association between alpha-cyclodextrin and polynuclear aromatic hydrocarbons, *Analytica Chimica Acta*, **1990**, 232, 239-243.
32. Yi, Z.P., et al., Investigation of buffer-cyclodextrin systems, *Physical Chemistry Chemical Physics*, **1999**, 1 (3), 441-444.
33. Rohrbach, R.P., et al., An Equilibrium and Kinetic Investigation of Salt-Cycloamylose Complexes, *J. Phys. Chem.*, **1977**, 81 (10), 944-948.
34. Chamberlain, R.V., et al., Electrostatically-induced inclusion of anions in cyclodextrin monolayers on electrodes, *Langmuir*, **2000**, 16 (3), 1388-1396.
35. Sasaki, M., et al., Kinetic-Study on Inclusion Compound Formation Reaction of Beta-Cyclodextrin Polymer with Scn^- Using the Electric-Field Pulse Technique, *Journal of Physical Chemistry*, **1983**, 87 (1), 5-6.
36. Kano, K., et al., Tetraarylporphyrins as probes for studying mechanism of inclusion-complex formation of cyclodextrins. Effect of microscopic environment on inclusion of ionic guests, *Chemistry Letters*, **1996** (11), 925-926.
37. Goyenechea, N., et al., Inclusion complexes of nabumetone with beta-cyclodextrins: thermodynamics and molecular modelling studies. Influence of sodium perchlorate, *Luminescence*, **2001**, 16 (2), 117-127.
38. Dey, J., et al., Effect of sodium perchlorate on the binding of 2-(4'-aminophenyl)- and 2-(4'-(N,N'-dimethylamino)phenyl)benzothiazole with beta-cyclodextrin in aqueous solution, *Journal of Physical Chemistry A*, **1998**, 102 (1), 301-305.
39. Harries, D., et al., Solutes probe hydration in specific association of cyclodextrin and adamantane, *Journal of the American Chemical Society*, **2005**, 127 (7), 2184-2190.
40. Gurnev, P.A., et al., The Dynamic Side of the Hofmeister Effect: A Single-Molecule Nanopore Study of Specific Complex Formation, *Chem.phys.chem*, **2009**, 10 (9-10), 1445-1449.

Chapter 4:

Antibacterial and antifungal self-defensive polysaccharides multilayer films

Chapter 4:

Antibacterial and antifungal self-defensive polysaccharides multilayer films

Summary

4.1 Introduction	137
4.2 Physical-chemical characterization of CHI/HA-CTL-C films	138
4.3 Antibacterial and antifungal assays of CHI/HA-CTL-C films	142
4.4 Mechanism of pathogen growth inhibition of CHI/HA-CTL-C films	144
4.5 Biocompatibility tests of CHI/HA-CTL-C films.....	146
4.6 Conclusion.....	148
Chapter 4 references	150

4.1 Introduction

Prevention of pathogen colonization of implantable medical devices constitutes a major medical and financial issue (see bibliographic overview part 1.4.1). Various approaches based on immobilization or release of bactericidal substances, using self-assembled monolayers or grafting of polymers have been explored and extensively reviewed [1, 2]. PEM films emerged as a simple and efficient approach to functionalize surfaces in a controlled way [3, 4]. The first antibacterial PEM films were designed by insertion of silver nanoparticles [5-10]. Later on, hydrophobic bactericide using dendritic block copolymer [11] and silver ion containing liposomes [12] were inserted in PEM films to obtain efficient bactericidal coatings. Chitosan based PEM films were demonstrated to be antibacterial against *Escherichia coli* and *Enterococcus faecalis* [6, 13, 14]. Antibiotics, like gentamicin, have been inserted in hydrolysable [15] or crosslinked PEM films [16] to be later released. Despite of an improvement of the antibacterial activity of the films, the use of antibiotics or silver particles have serious drawbacks because of their limited efficiency, their toxicity or their role in the emergence of multi-resisting pathogens [17, 18].

Natural antimicrobial peptides (AMPs) gain increased attention due to their broad spectrum of antimicrobial activity and their low cytotoxicity [2]. They predominantly cause disruption of the membrane integrity of pathogen agents and thus unlikely initiate the development of resistance [2]. Positively charged AMPs were already used as a part of the PEM architecture to obtain antibacterial effect by contact or by release [16, 19]. Active PEM films with embedded antifungal peptides were also reported [20, 21]. The recent resistance of *C. albicans* to antifungal therapies [22, 23] and of *S. aureus* to antibiotics points out the need of multifunctional coatings that prevent infections of both yeast and bacteria. Up to now, only few systems share both properties. They are mainly based on silver coating [24] or quaternary ammonium cationic molecules as surfactant [25], synthetic polymer [26] or silane [27].

To our knowledge, no coating based on AMPs possessing both properties has been reported so far. To achieve this goal, we proposed to use bovine cateslytin (CTL), a chromogranin A (CgA) derived peptide, an endogenous protein, secreted with its numerous natural derived peptides by nervous, endocrine and immune cells during infection [28] acting in the innate immunity system [29]. CTL acts in the micromolar range with a wide spectrum of antimicrobial activities against Gram-positive bacteria, yeasts and filamentous fungi, without cytotoxic effect on mammalian cells [30, 31]. Moreover, it is very stable against

bacterial proteases [32]. We used polysaccharide multilayer films based on CTL-C-functionalized hyaluronic acid as polyanion and chitosan as polycation that were deposited on a planar surface with the aim of designing a self-defensive coating against both bacteria and yeasts (Figure 4.1). A cystein residue (C) was added at the C-terminal end of the CTL sequence to allow its grafting to HA. HA and CHI are biodegradable by enzymatic hydrolysis with hyaluronidase [33] and chitosanase [34] respectively. The ability of *Staphylococcus* [35], *Candida* species [36] and *M. luteus* to degrade HA, by producing hyaluronidase, should allow the CTL-C to be released from PEM films only in the presence of the pathogens. This coating could be thus named as self-defensive since it is related to a local change of the environment of the coating due to the pathogens themselves.

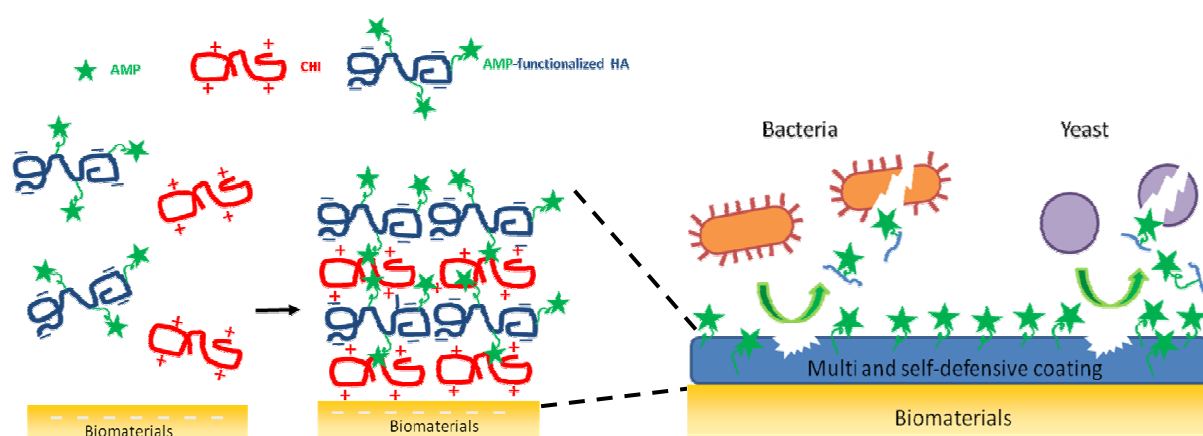


Figure 4.1: Schematic representation of CHI/HA multilayers functionalized by an antimicrobial peptide (AMP) and its activity towards bacteria and yeasts based on the degradation of the film.

4.2 Physical-chemical characterization of CHI/HA-CTL-C films

CTL-C peptide was covalently coupled to HA in two steps using successively the carbodiimide chemistry to graft maleimide functions on HA and the thiol-maleimide coupling reaction to graft CTL-C on the modified HA. Synthetic procedures of CTL-C peptide and its conjugation to HA are described in Annex B. After dialysis and freeze-drying, a coupling ratio of 5% was determined by $^1\text{H-NMR}$, corresponding to the grafting of approximately 5 CTL-C peptides for 100 HA dimer units. The antimicrobial and antifungal activities of CTL and modified CTL were tested in solution against two bacterial strains *M. luteus* and *S. aureus* (ATCC 25923) and a yeast *C. albicans*. Minimal inhibitory concentration (MIC) in peptide of

CTL, CTL-C and HA-CTL-C were determined using bacterial and fungal assays. CTL-C remains antimicrobial at micromolar concentration ($< 100 \mu\text{M}$) and displays an even better activity against *M. luteus* compared to the cystein free CTL peptide. In comparison with the non-grafted CTL-C peptide, MIC value of HA-CTL-C increases from 35 to 45 μM for *S. aureus* and from 20 to 25 μM for *C. albicans* (Table 4.1). In the case of *M. luteus*, the MIC of HA-CTL-C (5 μM) is five times higher than that of free CTL-C (1 μM). In spite of this decrease in efficiency, the CTL-C peptide covalently linked to HA polymer can still be considered as antimicrobial, acting in the micromolar range.

Table 4.1: Minimal inhibitory concentration (MIC_{100} in μM) of CTL, CTL-C and HA-CTL-C measured in solution leading to a complete inhibition of pathogens. In the case of HA-CTL-C, the MIC values given correspond to the concentration in CTL-C.

Pathogens	MIC_{100} (μM in peptide)		
	CTL	CTL-C	HA-CTL-C
<i>S. aureus</i>	30	35	45
<i>M. luteus</i>	5	1	5
<i>C. albicans</i>	20	20	25

The buildup of CHI/HA-CTL-C films was monitored by SPR. A linear increase of the mass adsorbed is observed at each deposited layer of polysaccharide indicating the buildup of the film (Figure 4.2).

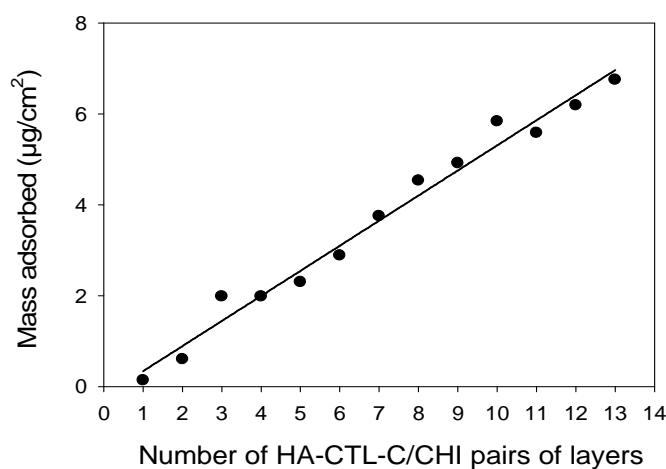


Figure 4.2: Evolution of the mass adsorbed, measured by SPR, for the buildup of PEI(HA-CTL-C/CHI) multilayer film as a function of the number of deposited pairs of layers. The straight line serves to guide the eye.

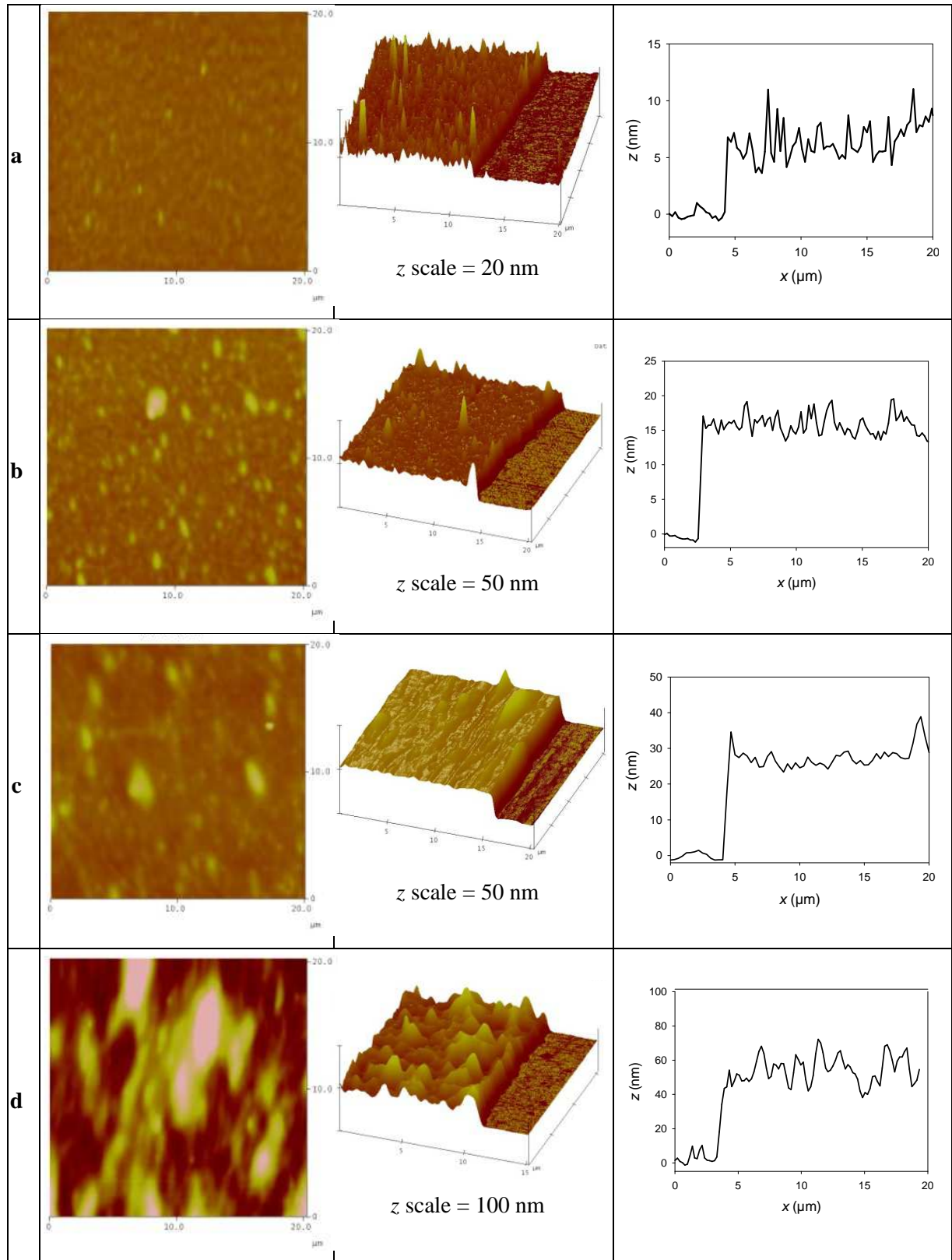


Figure 4.3: AFM images of non-scratched and 3D images and their profilometric sections of scratched $PEI(HA-CTL-C/CHI)_n$ films built at (a) 5, (b) 10, (c) 15 and (d) 30 bilayers obtained in height mode in dry state.

We investigated the topography and the roughness of CHI/HA-CTL-C films at different numbers of deposition steps by means of AFM in dry state (Figure 4.3). It was difficult to obtain good quality AFM images in the wet state due to the viscoelasticity of the films as we found for CHI/HA films in our previous work [37]. AFM imaging allows measuring film thickness after scratching. Table 4.2 summarizes the thicknesses and roughnesses measured by AFM. With 5 bilayers, the surface is already entirely covered with a 5 nm thick film with a roughness of 1.6 nm. As the buildup process goes on, the film thickness increases up to 52 nm at 30 bilayers. The film grows linearly up to 30 bilayers (Figure 4.4) and the film roughness increases up to 16.5 nm (for 30 pairs of layers).

Table 4.2. Thicknesses and roughnesses of $PEI(HA-CTL-C/CHI)_n$ films built at different number of deposited pair of layers, n . The errors on the thickness values measured by AFM were obtained from the measurement of three different areas.

n	d_{AFM} (nm)	RMS (nm)
5	5 ± 1	1.6 ± 0.1
10	17 ± 2	4.2 ± 0.8
15	28 ± 3	4.6 ± 0.9
30	52 ± 9	16.5 ± 2.8

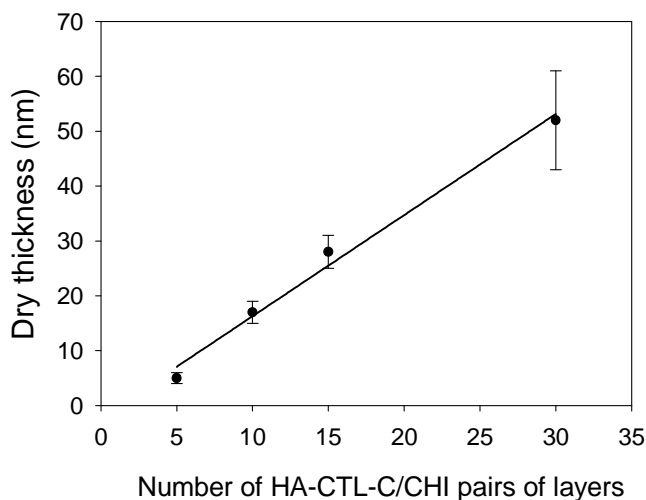


Figure 4.4: Evolution of the thickness of $PEI(HA-CTL-C/CHI)$ films, measured by AFM in dry state after scratching, at different number n of pairs of layers.

4.3 Antibacterial and antifungal assays of CHI/HA-CTL-C films

After characterization of CHI/HA-CTL-C multilayers buildup, the antibacterial and antifungal activities of the functionalized films were evaluated against two strains of bacteria (*M. luteus* and *S. aureus*) and one yeast strain (*C. albicans*). The influence of the number of embedded functionalized layers was studied by monitoring pathogen growth for different films with increasing number of CHI/HA-CTL-C bilayers. To this aim, PEI(HA/CHI)_{15-n}-(HA-CTL-C/CHI)_n films, with $n = 0, 5, 10$ and 15 , and PEI(HA-CTL-C/CHI)₃₀ films were built. Pathogens were incubated for 24 h in contact with CHI/HA-CTL-C films at 37°C for bacteria strains and at 30°C for *C. albicans*. For each pathogen, the microbial growth was measured at different times (1 h, 4 h, 6 h and 24 h) by determination of the optical density at 620 nm (OD₆₂₀) of the microbial suspension in contact with the film (Figure 4.5a-c).

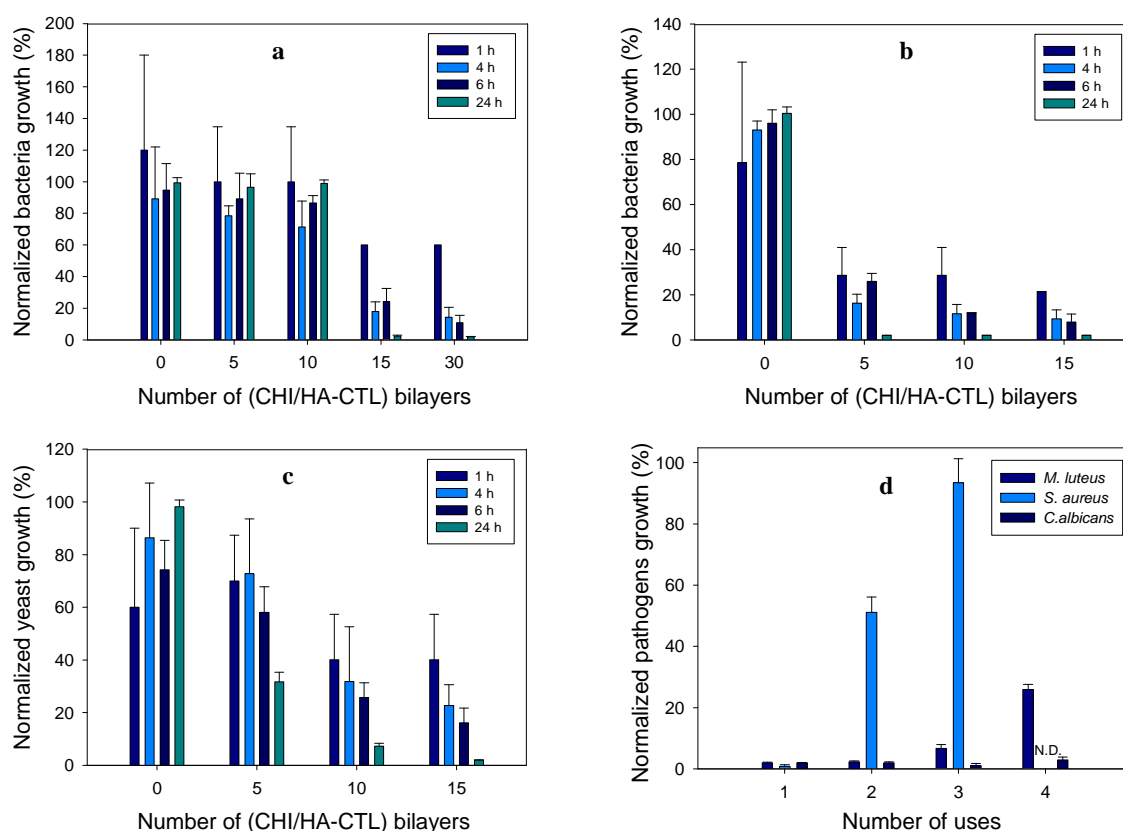


Figure 4.5: Normalized growth of (a) *S. aureus*, (b) *M. luteus* and (c) *C. albicans* incubated for 1 to 24 h in contact with PEI(HA/CHI)_{15-n}-(HA-CTL-C/CHI)_n with $n = 0$ to 15 and PEI(HA-CTL-C/CHI)₃₀ multilayer films. (d) Normalized growth of *S. aureus* incubated on PEI(HA-CTL-C/CHI)₃₀ and *M. luteus* and *C. albicans* incubated on PEI-(HA-CTL-C/CHI)₁₅ films, as a function of the number of uses. The film was brought in contact with a fresh pathogen suspension for 24 h. Every 24 h, the supernatant is removed and replaced by a fresh suspension and its OD₆₂₀ is measured. The normalization was performed with respect to OD₆₂₀ measured in the absence of film and antibiotics taken as 100% growth and in the presence of antibiotic taken as 0% growth. ND means not determined.

For each tested pathogen, we observed that by increasing the number of CHI/HA-CTL-C bilayers the normalized microbial growth decreases. An important decrease of microbial growth is obtained for at least 5 bilayers for *M. luteus* and *C. albicans* and 15 bilayers for *S. aureus*. After 6 h of incubation, at least 70% of inhibition is obtained with 15 bilayers for all tested pathogens. After 24 h of incubation, the growth of *M. luteus*, *C. albicans* and *S. aureus* are fully inhibited with 5, 15 and 30 CHI/HA-CTL-C bilayers, respectively. These results are in agreement with the MIC values of HA-CTL-C in solution (Table 4.1) that follow the same trend towards the different pathogens.

In order to check if the films can be reused several times as antimicrobial coatings, the growth of the three pathogens was monitored when incubated for 24 h in contact with reused PEI(HA-CTL-C/CHI)₁₅ films for *M. luteus* and *C. albicans* and PEI(HA-CTL-C/CHI)₃₀ film for *S. aureus*. To this aim, a fresh pathogen suspension was brought in contact with the functionalized film. After an incubation of 24 h, the supernatant was withdrawn and replaced by a fresh pathogen suspension. After each withdrawal, the OD₆₂₀ of the supernatant was measured to determine pathogen growth after 24h of incubation. When *M. luteus* and *C. albicans* suspensions in contact with PEI(HA-CTL-C/CHI)₁₅ film are renewed every 24 h, a complete inhibition was observed at least for two and three cycles of use respectively. A significant decrease in efficiency of PEI(HA-CTL-C/CHI)₁₅ film is detectable after the following renewal of pathogens suspension (Figure 4.5d). *S. aureus* growth is only inhibited by 40% for the second use of the PEI(HA-CTL-C/CHI)₃₀ film and becomes fully inefficient in the third cycle. In parallel, the supernatants withdrawn were incubated with fresh pathogen suspensions for 24 h and the OD₆₂₀ was also measured (Figure 4.6). No inhibition of growth was observed showing that there is no or a weak amount (quite less than the MIC) of CTL-C released in solution.

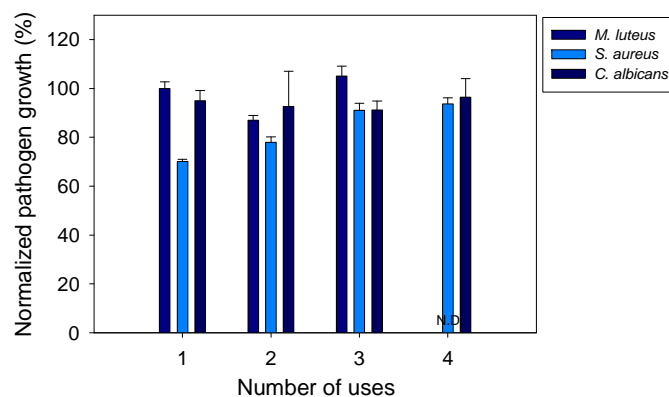


Figure 4.6: Normalized growth of *S. aureus*, *M. luteus* and *C. albicans*, incubated for 24 h in contact with the supernatant withdrawn from CHI/HA-CTL-C films used in Figure 4.5d.

4.4 Mechanism of pathogen growth inhibition of CHI/HA-CTL-C films

To clarify the mechanism of HA-CTL-C inhibition, we synthesized fluorescently labelled HA^{FITC}-CTL-C and HA^{FITC} to analyze the films after contact with the pathogens. *S. aureus* and *C. albicans* are known to secrete hyaluronidase, a class of enzymes able to hydrolyze HA [35, 36]. The cutting of one constitutive partner of the film should lead to its degradation as it was observed by Etienne et al. [38]. We were then interested in imaging PEI(HA^{FITC}/CHI)₁₅ films, by CLSM, before and after 24 h of contact with the pathogens. The three pathogens induce the degradation of CHI/HA films with, however, some differences in the resulting film morphologies (Figure 4.7).

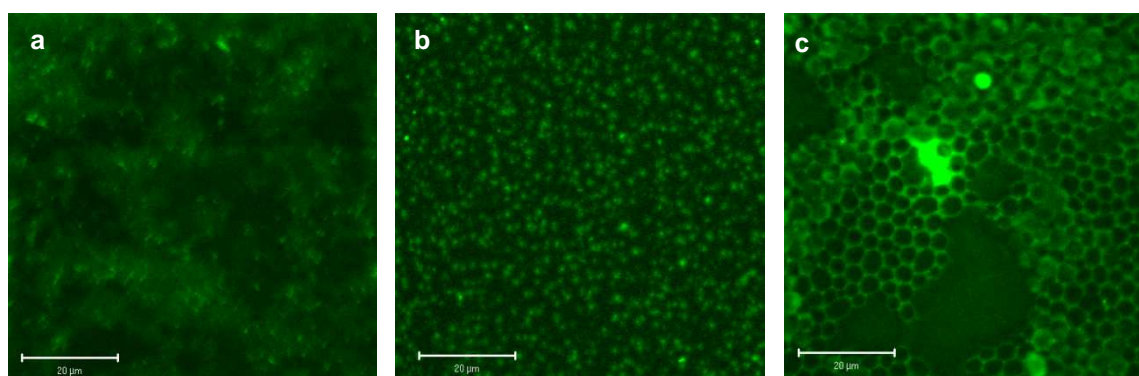


Figure 4.7: CLSM images of PEI(HA^{FITC}/CHI)₁₅ after 24 h of incubation with (a) *S. aureus*, (b) *M. luteus* and (c) *C. albicans*. All the films underwent a PFA treatment. The scale bars represent 20 μm.

After 24h of incubation with *S. aureus*, CHI/HA^{FITC} films were almost totally degraded (Figure 4.7a). The film appears inhomogeneous with fluorescent dots after incubation with *M. luteus* (Figure 4.7b). *C. albicans* induces the formation of honeycombs in the film due to the degradation of HA (Figure 4.7c). Degradation of HA should release CTL-C in the supernatant and promote the contact between CTL-C peptides and the pathogens. To check this hypothesis, we built hyaluronidase resistant films functionalized by CTL-C. CTL-C grafted on poly(allylamine hydrochloride) was thus synthesized and used to build poly(acrylic acid)/CTL-C functionalized poly(allylamine hydrochloride) (PAA/PAH-CTL-C) film. After 24h of incubation, (PAA/PAH-CTL-C)₁₅ films show no inhibition against *C. albicans*. This emphasizes the fact that the antimicrobial activity of the CHI/HA-CTL-C film is due to its degradation by the pathogens. This property renders the film specifically active in the presence of hyaluronidase secreted by the pathogens. Pathogens thus initiate their own death

when brought in contact with the CHI/HA-CTL-C film. Even though the film is degraded with time in the presence of pathogens, it can be reused at least two and three times without losing its activity against *M. luteus* and *C. albicans*.

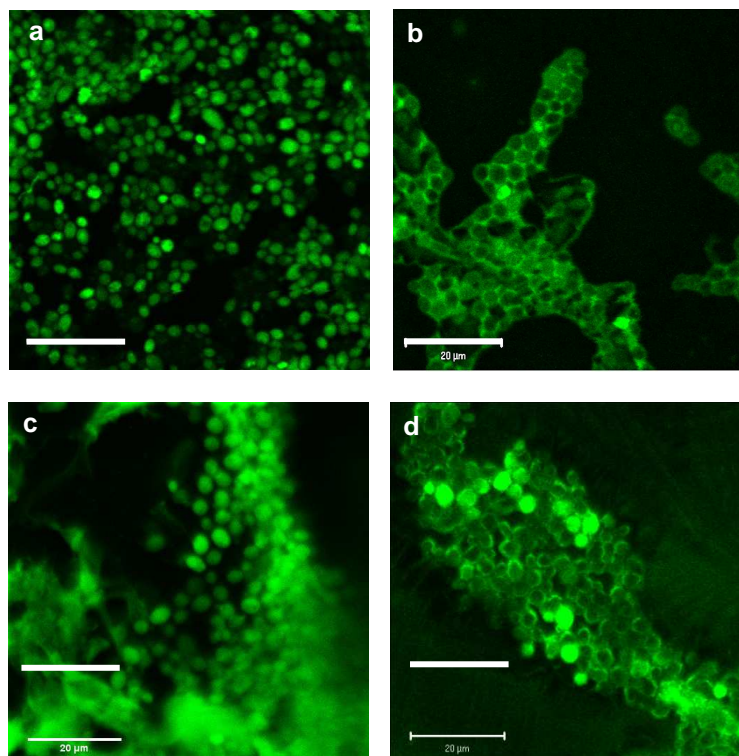


Figure 4.8: CLSM images of *C. albicans*, after 45 min of incubation, (a) in the presence of HA^{FITC}-CTL-C in solution (50 μ M in peptide), (b) in the presence of HA^{FITC} in solution, (c) in contact with PEI(HA^{FITC}-CTL-C/CHI)₁₅ and (d) in contact with PEI(HA^{FITC}/CHI)₁₅ multilayer films. The scale bars represent 20 μ m.

Using fluorescently labelled CTL-C, a previous study showed that the peptides penetrate into cell membranes and accumulate inside yeasts [30, 31]. The interactions of HA^{FITC}-CTL-C and HA^{FITC} with *C. albicans* was thus studied when solubilized in solution or embedded in multilayer films. After 45 min of incubation at 30°C with HA^{FITC} or HA^{FITC}-CTL-C in solution, *C. albicans* were observed by CLSM. The fluorescent HA^{FITC}-CTL-C was detectable in cytoplasm without inducing cell lysis (Figure 4.8a). On the contrary, HA^{FITC} is clearly observed all around the yeast cells, stacking probably on the membranes and leading to a honeycomb structure (Figure 4.8b). This suggests that CTL-C can cross the cell membrane, even when it is coupled to HA, leading to an accumulation of HA inside the cytoplasm. To image them by CLSM, the films were treated by paraformaldehyde (PFA) to fix the pathogen in contact. This treatment was first applied on the films to evaluate its effect. PFA treatment induces no change in the case of CHI/HA^{FITC} films in contrary to CHI/HA^{FITC}-

CTL-C films (Figure 4.9) where heterogeneities appear. *C. albicans* were incubated for 45 min at 30°C in contact with PEI(HA^{FITC}-CTL-C/CHI)₁₅ film and then observed by CLSM. Among the heterogeneities due to PFA treatment, a strong green fluorescence is observed mainly inside the yeast (Figure 4.8c). In the case of CHI/HA^{FITC} films, a little fluorescence is localized inside the yeasts and only few of them are strongly fluorescent (Figure 4.8d). In spite of its insertion into the PEM films, CTL-C allows the penetration of HA^{FITC}-CTL-C inside the yeasts explaining the activity of the films.

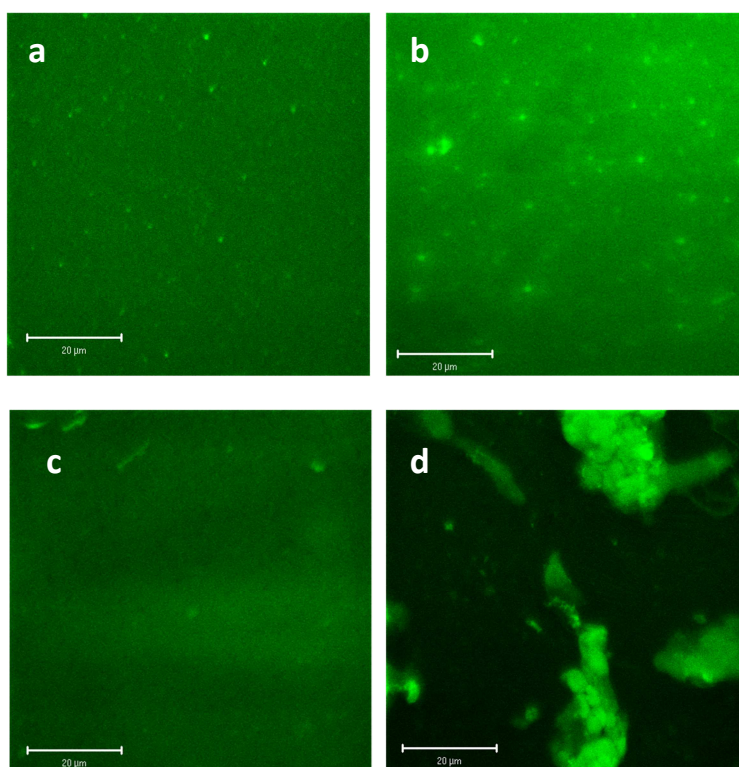


Figure 4.9: CLSM images of PEI(HA^{FITC}/CHI)₁₅ (a) before and (b) after paraformaldehyde (PFA) treatment and of PEI(HA^{FITC}-CTL-C/CHI)₁₅ (c) before and (d) after PFA treatment. PFA treatment was performed to allow the observation of polysaccharide multilayer films after contact with pathogens. The films are put into contact for 30 min with 4% paraformaldehyde in phosphate buffer saline (PBS) at pH 7.3 and, after several rinsing with PBS, were covered with Moviol 4-88 (Aldrich, Steinheim, Germany). The scale bars represent 20 μm.

4.5 Biocompatibility tests of CHI/HA-CTL-C films

Finally, it is important to ensure that the film is not cytotoxic to healthy wound healing cells. Fibroblasts are one of the first anchorage-dependent cells to come at an implant surface during the wound healing process. The viability of human gingival fibroblasts (HGFs) cultivated on PEI(HA-CTL-C/CHI)₁₅ films, compared to PEI(HA/CHI)₁₅ films and glass

substrate, has been evaluated through their mitochondrial activity, monitored by Alamar blue™ assays.

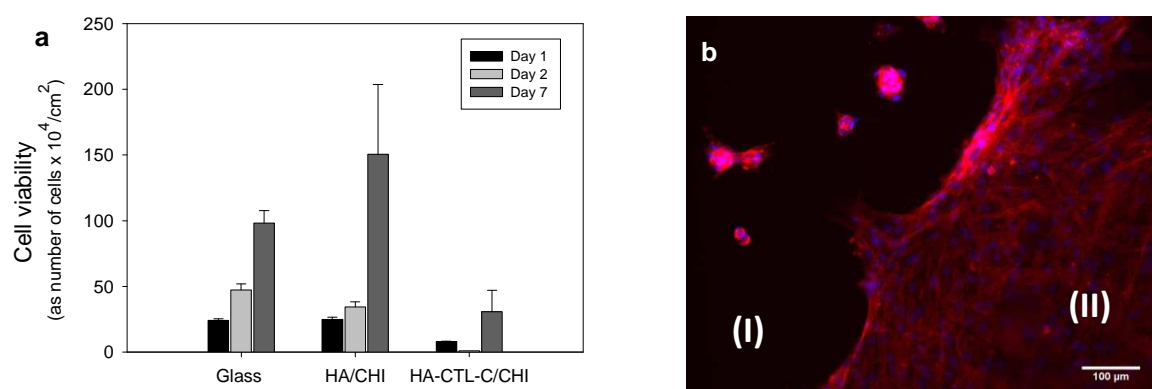


Figure 4.10: (a) Viability of HGFs, evaluated by metabolic activity of cells, cultured on PEI(HA/CHI)₁₅, named HA/CHI and PEI(HA-CTL-C/CHI)₁₅, named HA-CTL-C/CHI, films built on glass substrates. Cell viability was determined by Alamar Blue™ assays after 1, 2 and 7 days of culture. The values represent the mean and the standard deviation of three films. (b) Cytoskeleton visualization by actin filament immunofluorescent staining with phalloidin® (red labeling) and DAPI nuclei counterstaining (blue labeling) of HGFs after 24 h of culture on half coated glass substrate by PEI(HA-CTL-C/CHI)₁₅: the areas represent (I) the HA-CTL-C/CHI film and (II) the bare glass substrate, respectively.

After one day, the metabolic cell activity measured on CHI/HA-CTL-C films is already lower compared to CHI/HA films and non-coated glass substrate (Figure 4.10a). The good biocompatibility of CHI/HA films towards HGFs, mediated *via* CD44 receptor, was already reported in our previous work [37]. After 7 days of culture, the number of viable HGFs on CHI/HA-CTL-C films represents 25% of viable HGFs on CHI/HA films. The functionalization of HA by CTL-C peptide induces a lower adhesion of HGFs which seems to slow down the proliferation of cells. Knowing that HA-CTL-C in solution at 100 μM did not show any cytotoxicity, such behavior would suggest that the multilayers are not cytotoxic. To discriminate between cytotoxic or low initial adhesion properties of CHI/HA-CTL-C, we performed two experiments. First, after 24 h of contact, suspended cells harvested from CHI/HA-CTL-C film supernatant were passed to fresh culture plates. After 24 h of culture, many cells readily attached and spread as fresh cells. Second, we analyzed the biocompatibility of films by a complementary assay based on cell spreading *via* cytoskeleton arrangement when the cells are seeded on a glass substrate half coated by (HA-CTL-C/CHI)₁₅. After 24 h, HGFs adhere on the glass substrate (Figure 4.10b, zone II), but to a lesser degree on (HA-CTL-C/CHI)₁₅ film (Figure 4.10b, zone I). After 24 h of culture, a confluent layer with a typical fibroblastic cell shape and with polymerized F-actin fibers is

observed on the glass substrate (Figure 4.11a). On the CHI/HA-CTL-C film, cells appear less elongated and have a peripheral actin distribution (Figure 4.11b). This indicates that (HA-CTL-C/CHI)₁₅ films are not cytotoxic but seem rather anti-adherent towards HGFs. It is known that persistent excessive functions of fibroblasts have been linked to detrimental fibrous tissue formation which may cause implant failure. The present results of decreased fibroblast adhesion on functionalized substrate with CHI/HA-CTL-C films shows promise for implant applications.

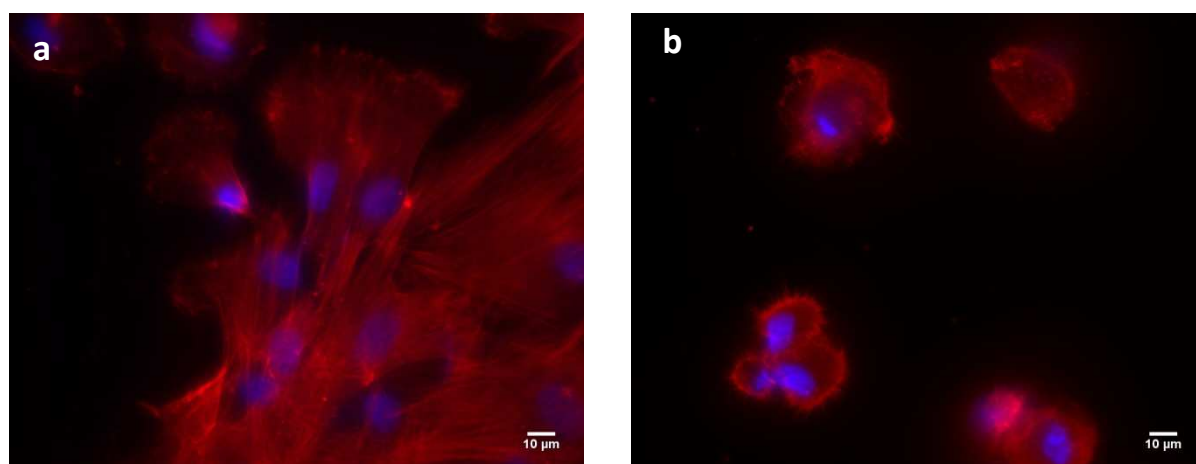


Figure 4.11: Immunolabeling of HGFs after 24 h of culture on (a) a glass substrate and (b) on PEI(HA-CTL-C/CHI)₁₅ film. The cytoskeleton was visualized by actin filament immunocytochemistry staining with phalloidin® (red labeling) and the nuclei with DAPI counterstaining (blue labeling) of HGFs. The scale bars represent 10 µm.

4.6 Conclusion

In conclusion, we designed a new surface coating based on polysaccharide multilayer films containing a functionalized HA with 5% of CTL-C, a peptide possessing both antibacterial and antifungal properties. Antimicrobial properties of CTL-C were preserved when grafted on HA either in solution or when embedded into PEM films. After 24 h of incubation, CHI/HA-CTL-C films fully inhibit the development of *S. aureus* and *C. albicans*, which are common and virulent pathogens agents encountered in care-associated diseases. The presence of CTL-C peptides on HA allows the penetration of the modified polysaccharide inside *C. albicans* after 45 min of contact. The secretion of hyaluronidase by all tested pathogens seems to be responsible for HA-CTL-C release from the film and for its activity. We introduced thus for the first time the concept of self-defensive coating since the release of

the antimicrobial peptide is triggered by enzymatic degradation of the film due to the pathogens themselves. The film can keep its activity during 3 cycles of use against fresh incubated *C. albicans* suspension. Furthermore, the limited fibroblasts adhesion, without cytotoxicity, on CHI/HA-CTL-C films highlights a medically relevant application to prevent infections on catheters or tracheal tubes where fibrous tissue encapsulation is undesirable.

Chapter 4 references

1. Banerjee, I., et al., Antifouling Coatings: Recent Developments in the Design of Surfaces That Prevent Fouling by Proteins, Bacteria, and Marine Organisms, *Advanced Materials*, **2011**, 23 (6), 690-718.
2. Glinel, K., et al., Antibacterial surfaces developed from bio-inspired approaches, *Acta biomaterialia*, **2012**, 8 (5), 1670-84.
3. Decher, G., Fuzzy Nanoassemblies: Toward Layered Polymeric Multicomposites, *Science*, **1997**, 277 (5330), 1232-1237.
4. Gribova, V., et al., Polyelectrolyte Multilayer Assemblies on Materials Surfaces: From Cell Adhesion to Tissue Engineering, *Chemistry of Materials*, **2012**, 24 (5), 854-869.
5. Dai, J.H., et al., Catalytic nanoparticles formed by reduction of metal ions in multilayered polyelectrolyte films, *Nano Letters*, **2002**, 2 (5), 497-501.
6. Fu, J.H., et al., Construction of antibacterial multilayer films containing nanosilver via layer-by-layer assembly of heparin and chitosan-silver ions complex, *Journal of Biomedical Materials Research Part A*, **2006**, 79A (3), 665-674.
7. Shi, Z., et al., In vitro antibacterial and cytotoxicity assay of multilayered polyelectrolyte-functionalized stainless steel, *J Biomed Mater Res A*, **2006**, 76 (4), 826-34.
8. Lee, D., et al., Antibacterial properties of Ag nanoparticle loaded multilayers and formation of magnetically directed antibacterial microparticles, *Langmuir*, **2005**, 21 (21), 9651-9659.
9. Li, Z., et al., Two-level antibacterial coating with both release-killing and contact-killing capabilities, *Langmuir*, **2006**, 22 (24), 9820-9823.
10. Lee, D., et al., Formation of nanoparticle-loaded microcapsules based on hydrogen-bonded multilayers, *Chemistry of Materials*, **2005**, 17 (5), 1099-1105.
11. Nguyen, P.M., et al., Extended release antibacterial layer-by-layer films incorporating linear-dendritic block copolymer micelles, *Chemistry of Materials*, **2007**, 19 (23), 5524-5530.
12. Malcher, M., et al., Embedded silver ions-containing liposomes in polyelectrolyte multilayers: Cargos films for antibacterial agents, *Langmuir*, **2008**, 24 (18), 10209-10215.
13. Fu, J.H., et al., Construction of anti-adhesive and antibacterial multilayer films via layer-by-layer assembly of heparin and chitosan, *Biomaterials*, **2005**, 26 (33), 6684-6692.

14. Bratskaya, S., et al., Adhesion and viability of two enterococcal strains on covalently grafted chitosan and chitosan/kappa-carrageenan multilayers, *Biomacromolecules*, **2007**, 8 (9), 2960-2968.
15. Chuang, H.F., et al., Polyelectrolyte multilayers for tunable release of antibiotics, *Biomacromolecules*, **2008**, 9 (6), 1660-1668.
16. Pavlukhina, S., et al., Polymer Multilayers with pH-Triggered Release of Antibacterial Agents, *Biomacromolecules*, **2010**, 11 (12), 3448-3456.
17. Verran, J., et al., Factors affecting microbial adhesion to stainless steel and other materials used in medical devices, *International Journal of Artificial Organs*, **2005**, 28 (11), 1138-1145.
18. Bruellhoff, K., et al., Surface coating strategies to prevent biofilm formation on implant surfaces, *International Journal of Artificial Organs*, **2010**, 33 (9), 646-653.
19. Shukla, A., et al., Controlling the release of peptide antimicrobial agents from surfaces, *Biomaterials*, **2010**, 31 (8), 2348-2357.
20. Karlsson, A.J., et al., Polyelectrolyte Multilayers Fabricated from Antifungal beta-Peptides: Design of Surfaces that Exhibit Antifungal Activity Against *Candida albicans*, *Biomacromolecules*, **2010**, 11 (9), 2321-2328.
21. Etienne, O., et al., Antifungal coating by biofunctionalized polyelectrolyte multilayered films, *Biomaterials*, **2005**, 26 (33), 6704-12.
22. Ramage, G., et al., *Candida* biofilms on implanted biomaterials: a clinically significant problem, *Fems Yeast Research*, **2006**, 6 (7), 979-986.
23. Lupetti, A., et al., Molecular basis of resistance to azole antifungals, *Trends in Molecular Medicine*, **2002**, 8 (2), 76-81.
24. Prucek, R., et al., The targeted antibacterial and antifungal properties of magnetic nanocomposite of iron oxide and silver nanoparticles, *Biomaterials*, **2011**, 32 (21), 4704-4713.
25. Botequim, D., et al., Nanoparticles and Surfaces Presenting Antifungal, Antibacterial and Antiviral Properties, *Langmuir*, **2012**, 28 (20), 7646-7656.
26. Hu, F.X., et al., Antibacterial and antifungal efficacy of surface functionalized polymeric beads in repeated applications, *Biotechnology and Bioengineering*, **2005**, 89 (4), 474-484.
27. Oosterhof, J.J.H., et al., Effects of quaternary ammonium silane coatings on mixed fungal and bacterial biofilms on tracheoesophageal shunt prostheses, *Applied and Environmental Microbiology*, **2006**, 72 (5), 3673-3677.
28. Helle, K.B., et al., The endocrine role for chromogranin A: A prohormone for peptides with regulatory properties, *Cellular and Molecular Life Sciences*, **2007**, 64 (22), 2863-2886.

29. Zhang, D., et al., Prognostic value of chromogranin a at admission in critically ill patients: A cohort study in a medical intensive care unit, *Clinical Chemistry*, **2008**, 54 (9), 1497-1503.
30. Briolat, J., et al., New antimicrobial activity for the catecholamine release-inhibitory peptide from chromogranin A, *Cellular and Molecular Life Sciences*, **2005**, 62 (3), 377-385.
31. Shooshtarizadeh, P., et al., The antimicrobial peptides derived from chromogranin/secretogranin family, new actors of innate immunity, *Regulatory Peptides*, **2010**, 165 (1), 102-110.
32. Aslam, R., et al., Chromogranin A-derived peptides are involved in innate immunity, *Current medicinal Chemistry*, **2012**, 19, 4115-4123.
33. Menzel, E.J., et al., Hyaluronidase and its substrate hyaluronan: biochemistry, biological activities and therapeutic uses, *Cancer Letters*, **1998**, 131 (1), 3-11.
34. Serizawa, T., et al., Enzymatic hydrolysis of a layer-by-layer assembly prepared from chitosan and dextran sulfate, *Macromolecules*, **2002**, 35 (23), 8656-8658.
35. Larkin, E.A., et al., Staphylococcus aureus: The Toxic Presence of a Pathogen Extraordinaire, *Current Medicinal Chemistry*, **2009**, 16 (30), 4003-4019.
36. Shimizu, M.T., et al., Studies on hyaluronidase, chondroitin sulphatase, proteinase and phospholipase secreted by Candida species, *Mycoses*, **1996**, 39 (5-6), 161-167.
37. Cado, G., et al., Polysaccharide Films Built by Simultaneous or Alternate Spray: A Rapid Way to Engineer Biomaterial Surfaces, *Langmuir*, **2012**, 28 (22), 8470-8478.
38. Etienne, O., et al., Degradability of polysaccharides multilayer films in the oral environment: an in vitro and in vivo study, *Biomacromolecules*, **2005**, 6 (2), 726-33.

Chapter 5:
CTL-C based dimers and dendrimer:
syntheses and biological tests in solution

Chapter 5:

CTL-C based dimers and dendrimer: syntheses and biological tests in solution

Summary

5.1 Introduction	155
5.2 Syntheses of CTL-C based dimers and dendrimer	155
5.2.1 Choice of the linkers	156
5.2.2 Syntheses of CTL-C dimers and dendrimer monitored by HPLC.....	157
5.3 Determination of the minimal inhibitory concentration.....	161
5.3.1 CTL-C dimers and dendrimer G1	162
5.3.2 “D”-CTL-C	163
5.4 Evaluation of the toxicity	164
5.5 Evaluation of the inflammatory response	165
5.6 Conclusion.....	167
Chapter 5 references	168

5.1 Introduction

In the previous chapter, we developed a self-defensive antibacterial and antifungal coating based on a polysaccharide multilayer film with embedded antimicrobial peptides (AMPs). After 24 h of incubation, the growth of *M. luteus*, *C. albicans* and *S. aureus* was fully inhibited with respectively 5, 15 and 30 HA-CTL-C/CHI pairs of layers. Since layer-by-layer deposition can be time consuming, it seems interesting to decrease the number of pairs of layers while keeping the antimicrobial activity. For reaching this goal, more AMPs should be embedded per bilayer, i.e. HA should be functionalized with a higher number of CTL-C. The first idea that comes in mind is to increase the number of maleimide groups grafted on the HA and thus also the number of CTL-C. However, when the number of maleimide groups grafted on the HA is increased, the polymer obtained is very gel-like and not water soluble anymore rendering further functionalization by CTL-C impossible. Another approach would be to maintain the number of maleimide groups grafted on the HA at 5% and to increase the number of CTL-C grafted per maleimide unit. That is the reason why a closer interest in CTL-C based dimers and dendrimers was taken. Besides, it was already reported in the literature that multivalent presentation of antimicrobial peptides can increase their efficiency [1-4]. It helps indeed AMPs to act together to form membrane pores. It was also underlined that the length of the linker between two AMPs forming the dimer or the dendrimer core can be critical since it gives more or less flexibility to the peptides [5]. It is also reported in the literature that D-diastereomeric AMPs (D-AMPs) are less sensitive to proteolytic enzymes compared to the L- diastereomeric AMPs, which leads sometimes to an increase in antimicrobial properties [6, 7].

In this work, we investigated original compounds such as CTL-C based dimers with different linker's lengths, a CTL-C based dendrimer and a CTL-C in D-configuration ("D"-CTL-C). They are intended to be inserted into antimicrobial coatings but their antimicrobial properties, their toxicity and for some, their inflammatory properties were first studied in solution.

5.2 Syntheses of CTL-C based dimers and dendrimer

In order to study the influence of the linker's length on the antimicrobial activity, four different dimers were designed. Their syntheses were based on the reaction of a linker ended

on both sides by two maleimide groups and the thiol group of the CTL-C (Figure 5.1b) through the thiolene click reaction (Figure 5.1a) [8]. The synthetic pathway of the dendrimer is similar to the dimer's one at the exception that the linker had three maleimide groups instead of two (Figure 5.1c).

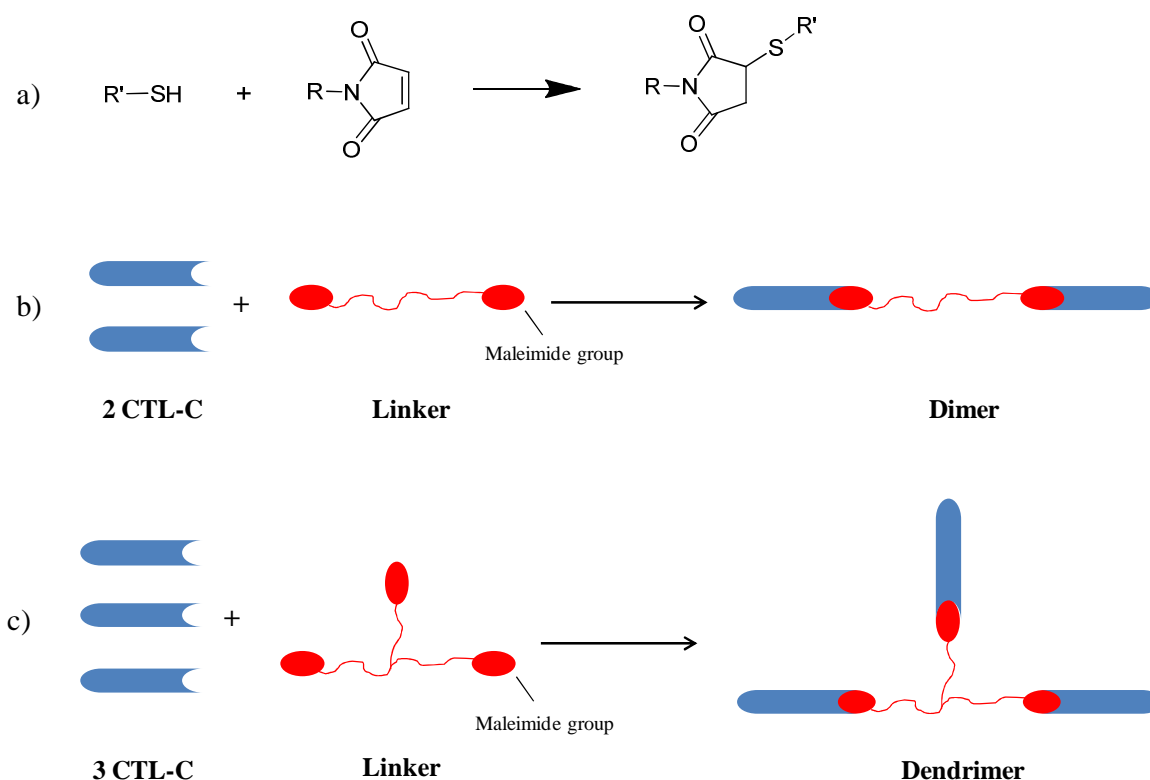


Figure 5.1: (a) Thiol-maleimide click reaction. (b) Synthetic pathway of a CTL-C based dimer: two CTL-C peptides react with a linker ended by two maleimide groups through a thiol-maleimide click reaction. (c) Synthetic pathway of a CTL-C based dendrimer: three CTL-C peptides react with a linker ended by three maleimide groups through a thiol-maleimide click reaction.

5.2.1 Choice of the linkers

Four different linkers, noted linker D1, linker D4, linker D6 and linker G1 were synthesized. One of the linker was commercially available: linker D15. The names of the linkers were attributed depending on the length between the two nitrogen atoms of their maleimide groups. The shorter linker possessed 9 covalent bonds between the two nitrogen atoms and was named D1. The linker D4 was named so because it is four times longer than D1, the linker D6 was 6 times longer than D1 and so on. This nomenclature is not exact but facilitates the notation of the dimers and also allows being able to directly compare the

lengths of the dimers. Linker G1 was used to synthesize a CTL-C based dendrimer. All linkers are reported Table 5.1.

Table 5.1: Names and chemical structure of the linkers used for the synthesis of CTL-C based dimers and dendrimer.

Name	Chemical structure
Linker D1	
Linker D4	
Linker D6	
Linker D15	
Linker G1	

The dimers were named according to the linker that has been used for their synthesis. For example, the dimer DX was obtained from the reaction of two CTL-C peptides with the linker DX.

5.2.2 Syntheses of CTL-C dimers and dendrimer monitored by HPLC

All CTL-C dimers (D1, D4, D6 and D15) and the dendrimer G1 have been synthesized by mixing one molar equivalent of the linker with two molar equivalents of the CTL-C for the

synthesis of the dimers or three molar equivalents of the CTL-C for the synthesis of the dendrimer. The reaction was performed at 60°C in water for the linkers G1, D6 and D15 or in a 7:3 water:acetonitrile solution for the linkers D1 and D4, since they are not water soluble. It was beforehand checked that CTL-C is not degraded and kept its full antimicrobial activity after a 24 h incubation in water at 60°C. The reactions were all followed by reverse-phase HPLC (C18 phase), where a solvent gradient was going from a polar solvent to a rather apolar solvent with time (see method 2.2.5 in Chapter 2) and the absorbance was measured at 214 nm. Only the dimer D1 and the dendrimer's synthesis will be presented in details here but all other syntheses of dimers were realized the same way.

Synthesis of the dimer D1

At $t = 0$ h, CTL-C was incubated with the linker D1 in a 7:3 water:acetonitrile solution. 2 μ L of the mixture was immediately injected in the HPLC. The reaction was then brought to 60°C. Two large peaks and a very small one are present in the chromatogram at $t = 0$ h (Figure 5.2): the peak, whose retention time is 22.87 min, corresponds to the linker D1 and the one, whose retention time is 24.04 min, corresponds to the CTL-C. There is also a small peak at 24.95 min that probably corresponds to the linker D1 that has been functionalized with one CTL-C and that was called "mono-functionalized". After 1 h, a new peak appears at 24.79 min that corresponds to the formation of the dimer D1. The peak of the linker and the peak of the CTL-C decrease whereas the peak of the "mono-functionalized" increases showing that the reaction occurs. After 23 h, the quantity of dimer has largely increased (33% conversion). The linker has been completely consumed and CTL-C is still present. The peak of the "mono-functionalized" has decreased meaning that all the linkers have reacted on one of their side and that only dimers are formed at this point. The kinetic of the reaction was highly slowing down after 2 days (Figure 5.3). After 5 days, the conversion of "mono-functionalized" into dimer was about 64%, so 0.2 molar equivalent of CTL-C was added to increase the conversion rate into dimers. An addition of CTL-C was again repeated after 6 days. After one more day, with 78%, the conversion was not complete yet. The reaction was however stopped. Preparative HPLC was used to purify the mixture of dimers and "mono-functionalized" in order to only retrieve the dimer, which was then lyophilized. The dimer D1's mass was controlled by MALDI-TOF mass spectrometry (Dithranol matrix). With a theoretical m/z of 4233.09 Da and a m/z obtained by MALDI-TOF of 4232.72 Da, we confirmed that dimer D1 was obtained.

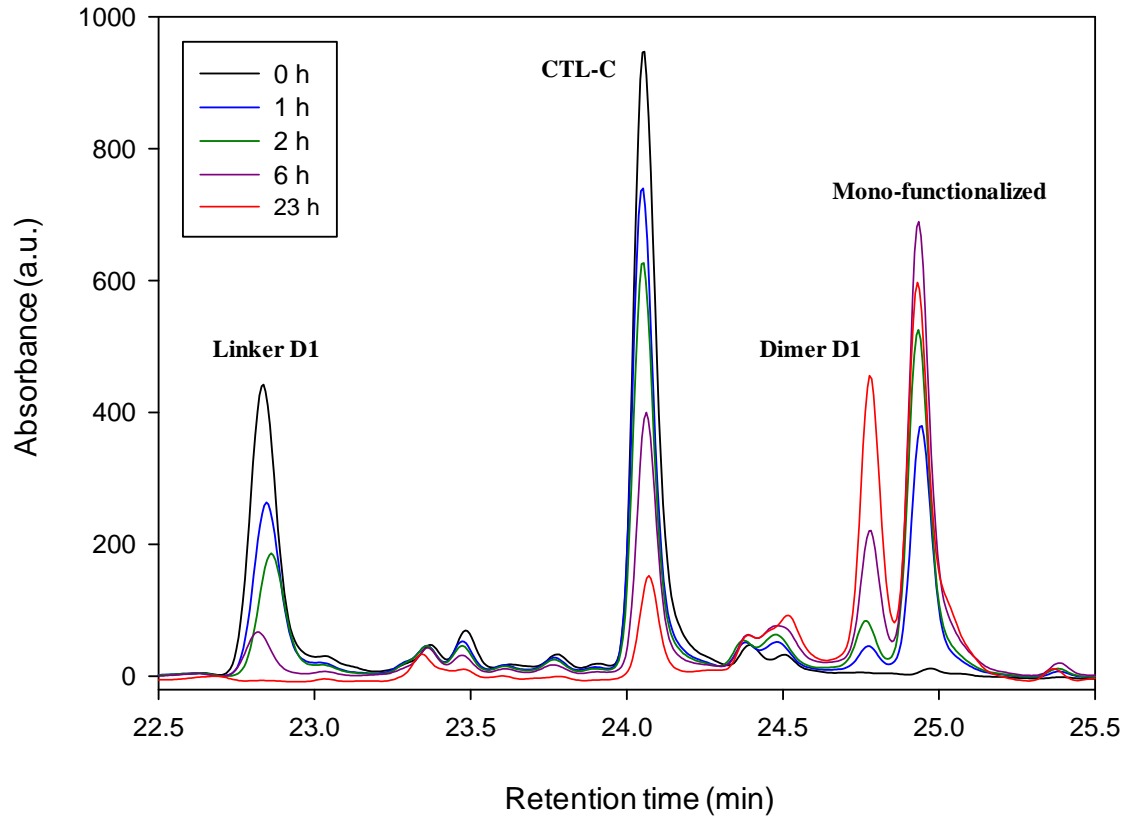


Figure 5.2: Chromatogram of a reversed-phase HPLC following the conversion of the dimer D1 over time.

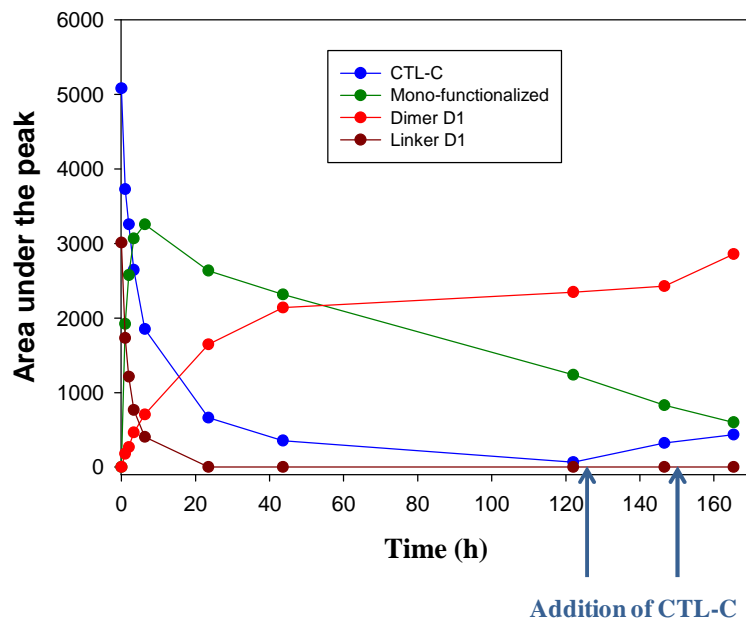


Figure 5.3: Kinetic of the synthesis of dimer D1 by evaluation of the area under the peak taken from the HPLC chromatogram.

Synthesis of the dendrimer G1

CTL-C was incubated with the linker G1 in water at 60°C. 2 μ L of the mixture was immediately injected in the HPLC. At $t = 0$ h, three large peaks and a very small one are present in the HPLC chromatogram (Figure 5.4). The peak, whose retention time is 26.28 min, corresponds to the linker G1 and the ones, whose retention times are 24.04 and 25.64 min, correspond to the CTL-C and the “mono-functionalized”, respectively. The small peak with a retention time at 25.16 min corresponds to the linker G1 that has been functionalized with two CTL-C and was called “bi-functionalized”. After 1 h, a new peak appears at 24.95 min that corresponds to the formation of the dendrimer. The linker is completely consumed showing that the functionalization of the linker by one CTL-C is very fast. The peaks of “mono-functionalized” and “bi-functionalized” continued to increase showing that the reaction occurs. At $t = 5$ h, the peak of “mono-functionalized” is very small and the peak of “bi-functionalized” starts to decrease showing that most linkers have been functionalized at least twice. After 23 h, the quantity of dendrimer has largely increased; a conversion rate of 58% was found. The “mono-functionalized” and the CTL-C have been completely consumed.

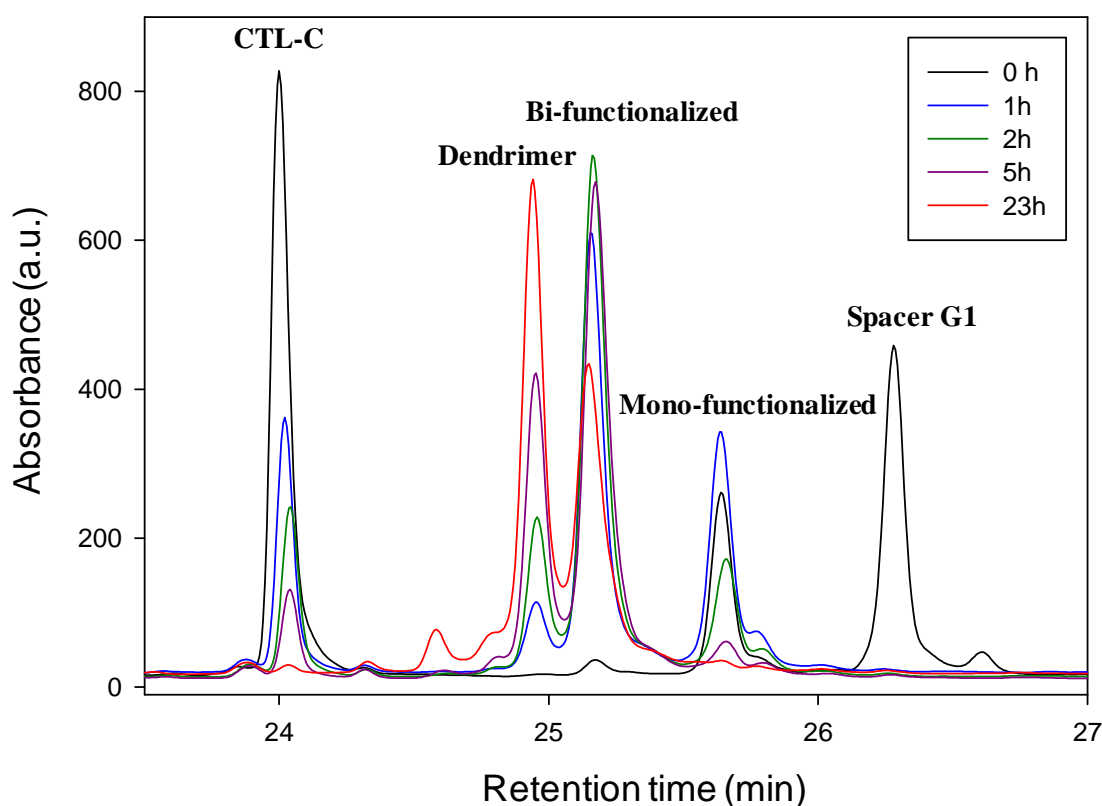


Figure 5.4: Chromatogram of a reversed-phase HPLC following the conversion of the dendrimer over time.

Some CTL-C has been added after 23 h of reaction to increase the kinetic of the reaction (Figure 5.5). After 3 days, with a conversion rate of 87% and no more evolution of the reaction, the synthesis was stopped. In order to get rid of the excess peptide, the solution was dialyzed for 4 days using a membrane (ZellusTrans, Roth) with a cut-off of 3500. The mixture containing “bi-functionalized” and dendrimer was then lyophilized. A new HPLC injection was performed and by measuring the area under the peaks, we estimated that what will be called dendrimer in the following work is made of 90% dendrimer and of 10% “bi-functionalized” dendrimer.

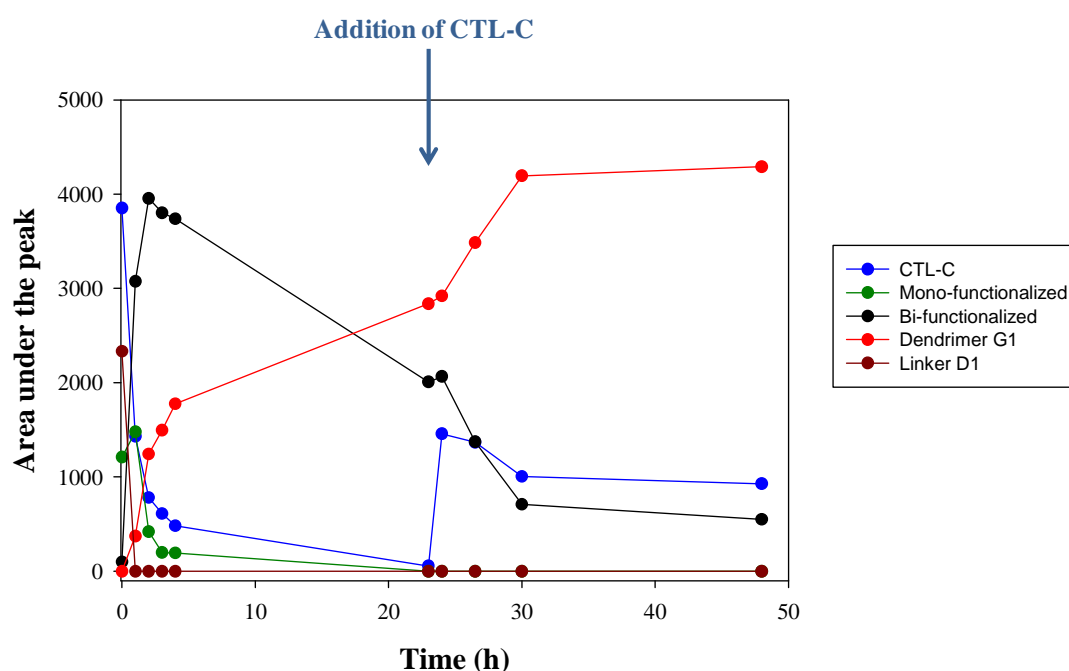


Figure 5.5: Kinetic of the synthesis of dendrimer G1 by evaluation of the area under the peak taken from the HPLC chromatogram.

D1, D4, D6, D15 and G1 were all synthesized with a conversion rate comprised between 72 and 97%, the highest conversion rate being obtained for D4 after only 20 h of reaction and without any further addition of CTL-C.

5.3 Determination of the minimal inhibitory concentration

Four pathogen strains have been used to test the antimicrobial properties of the new CTL-C derived peptides: *M. luteus*, *S. aureus*, methicillin-resistant *staphylococcus aureus* (MRSA) and *C. albicans*. Among the four selected strains, *M. luteus* is the less virulent

bacterium. *S. aureus* is known to be virulent and is often involved in device-related systemic infections. MRSA is a more resistant form of *S. aureus*, that has developed a resistance to some antibiotics including penicillins, making it harder to treat with standard types antibiotics and thus more dangerous. *C. albicans* is a virulent human yeast that causes candidiasis in human and can also enhance *S. aureus* resistance to antibiotics by symbiotic interactions.

5.3.1 CTL-C dimers and dendrimer G1

The minimal inhibitory concentrations (MICs) of the CTL-C based dimers and of the dendrimer G1 have been determined for the four pathogens listed above and are reported in Table 5.2. They are expressed in μM of CTL-C in order to be directly compared with the CTL-C values.

Table 5.2: Minimal inhibitory concentration (MIC) of the different CTL-C dimers and of dendrimer G1 on four pathogen strains. The MIC is expressed in μM of CTL-C. MRSA stands for methicillin-resistant *Staphylococcus aureus* and ND for not determined.

	MIC ₁₀₀ (μM in CTL-C)			
	<i>M. luteus</i>	<i>S. aureus</i>	MRSA	<i>C. albicans</i>
CTL-C	3	30	50	20
Dimer D1	2	30	30	25
Dimer D4	5	> 100	ND	ND
Dimer D6	< 10	> 100	> 100	20
Dimer D15	3	> 100	ND	ND
Dendrimer G1	5	50	ND	ND

The results gathered in Table 5.2 show that the length of the linker is an important factor only in the case of *S. aureus* and MRSA. All tested peptides have similar MIC values against *M. luteus* and *C. albicans* compared to the CTL-C ones, which are respectively 3 μM and 20 μM , the small differences being due only to the experiments themselves. Regarding *S. aureus*, only the dimer D1 and the dendrimer G1 display an activity similar to CTL-C, even if the dendrimer G1 exhibits a slightly higher, but significant, MIC value. What does not appear in Table 5.4 is that the dimer D4 exhibits 40% of bacterial growth inhibition at 100 μM , whereas the dimers D6 and D15 are completely inactive until at least 100 μM . This leads to think that above a certain length, the dimers lose their activity against *S. aureus* but this

phenomenon happens gradually with the length of the linker. The dendrimer G1 possesses also short linker chains but slightly longer than the dimer D1 ones; which explains that the dendrimer G1 keeps an activity against *S. aureus* but with a higher MIC value than the dimer D1. It seems thus that the PEG chain forming the linker of the dimers reduces the accessibility of the peptides to *S. aureus*, which forms clusters in solution, and therefore their antibacterial activities. The dimer D1 and the dimer D4 were also tested on MRSA. Similar results to the one obtained for *S. aureus* were found. However, dimer D1 displayed a higher antibacterial activity than CTL-C, leading us to hypothesize that a multivalent presentation of CTL-C was favored in this case.

To conclude, the length of the linker was proven to be critical on the activity against *S. aureus* and MRSA, but not against *M. luteus* and *C. albicans*. When an activity was conserved, it was always in the range of the CTL-C one. No increased efficiency due to a potential multivalent presentation of the CTL-C to the pathogens was observed, with the exception of the dimer D1 against MRSA strains.

5.3.2 “D”-CTL-C

The minimal inhibitory concentration of the “D”-CTL-C has been determined for *S. aureus*, MRSA and *C. albicans* (Table 5.3). *M. luteus* has been excluded due to its low MIC value and thus the inability to discriminate the best candidate to replace CTL-C. They are expressed in μM of CTL-C in order to be directly compared with the CTL-C values.

Table 5.3: Minimal inhibitory concentration (MIC) of CTL-C and “D”-CTL-C on three pathogen strains. The MIC is expressed in μM of CTL-C. MRSA stands for methicillin-resistant *Staphylococcus aureus*.

	MIC ₁₀₀ (μM in CTL-C)		
	<i>S. aureus</i>	MRSA	<i>C. albicans</i>
CTL-C	35	50	20
“D”-CTL-C	20	20	10

The results gathered in Table 5.3 show that the MIC values of “D”-CTL-C were found to be systematically lower than the MIC values of CTL-C. The MIC value was one third lower for *S. aureus*, half lower for *C. albicans* and 60% lower for MRSA. “D”-CTL-C, probably due to a higher stability against microbial proteases, exhibits better antimicrobial

activities than CTL-C whatever the pathogen, CTL-C being naturally a L-CTL-C. This is in good agreement with the literature. For example, Carmona et al. compared the antimicrobial activity of an AMP called Pandinin 2 (Pin2) and its D-diastereomer, and showed a gain of activity of 50% for the D-diastereomer when tested against *E.coli* and *S. agalactiae* [6]. The same value was obtained for *C. albicans* in our case. However, compared to Pin2, the activity of D-Pin2 was not improved against *S. aureus*. In our case, we obtained the less difference of activities between the diastereomers for *S. aureus*.

5.4 Evaluation of the toxicity

In order to further continue the study of all these peptides, their toxicity was assessed using an *in vitro* hemolysis assay [9]. As further described in the materials and methods part 2.3.4, the toxicity of the peptides in solution was assessed by incubating them with red blood cells for 40 min at 37°C and evaluating the number of disrupted red blood cells by the release of hemoglobin to the extracellular environment. Once again, the concentrations given for the dimers and the dendrimer are expressed in μM of CTL-C. By considering that a value over 10% of lysis means that a peptide is toxic, this test showed that the dendrimer G1 with 25% of red blood cell lysis is already toxic at 50 μM . The dimer D1 begins to be slightly toxic at 100 μM and the dimer D6 at 200 μM , so at much higher value than their MIC. With respectively 1% and 6% of erythrocyte lysis, CTL-C and “D”-CTL-C are not toxic until at least 200 μM . (Figure 5.6).

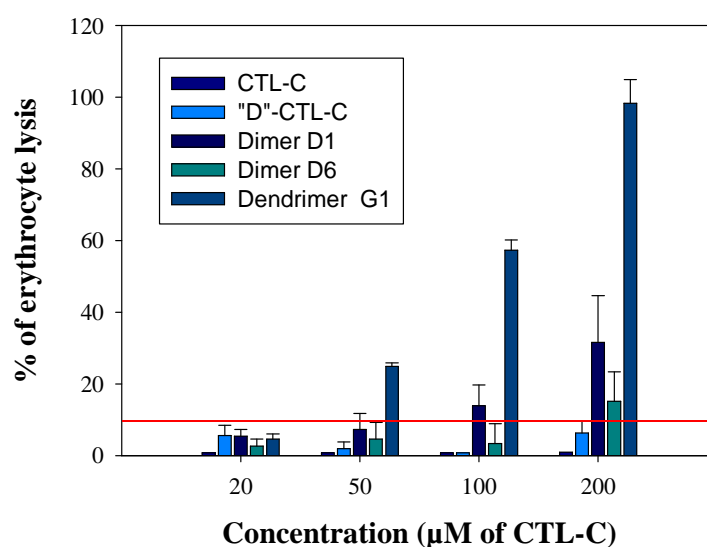


Figure 5.6: Percentage of erythrocytes lysis depending on the concentration of peptides in CTL-C μM . A peptide that possesses a percentage of erythrocytes lysis over 10% is considered as toxic.

5.5 Evaluation of the inflammatory response

Besides microbial infection, inflammation is a common coexisting issue that affects the functionality and the longevity of medical implants inserted in a living tissue. Implant-associated inflammation is caused by injury to vascularized connective tissue and the foreign body reaction. This results in fibrotic encapsulation that compromises implant performance [10]. Combining antimicrobial and anti-inflammatory properties into a biomaterial intended to be in contact with a living tissue seems thus to be of great interest.

Based on this idea, we decided to check the inflammatory response of the CTL-C and the dimer D1 since they both display good antimicrobial properties and are not toxic for erythrocytes at their MIC values. To this aim, we performed a luciferase assay in order to quantify the activity of NF- κ B, a transcription factor responsible for the expression of numerous pro-inflammatory cytokines [11], on monocytic cell line. The luciferase assay is described in details in the materials and methods part 2.3.5. Briefly, the peptides (at 20 μ M in CTL-C) were incubated with monocytes (THP-1) that have been previously transfected with a plasmid expressing the luciferase gene (reporter gene) under the control of the NF- κ B promoter. Therefore, when the NF- κ B promoter is activated, the gene encoding the luciferase is expressed and the enzyme is produced. In the presence of its substrate, the luciferase enzyme emits light that can be quantified using a luminometer (Figure 5.7).

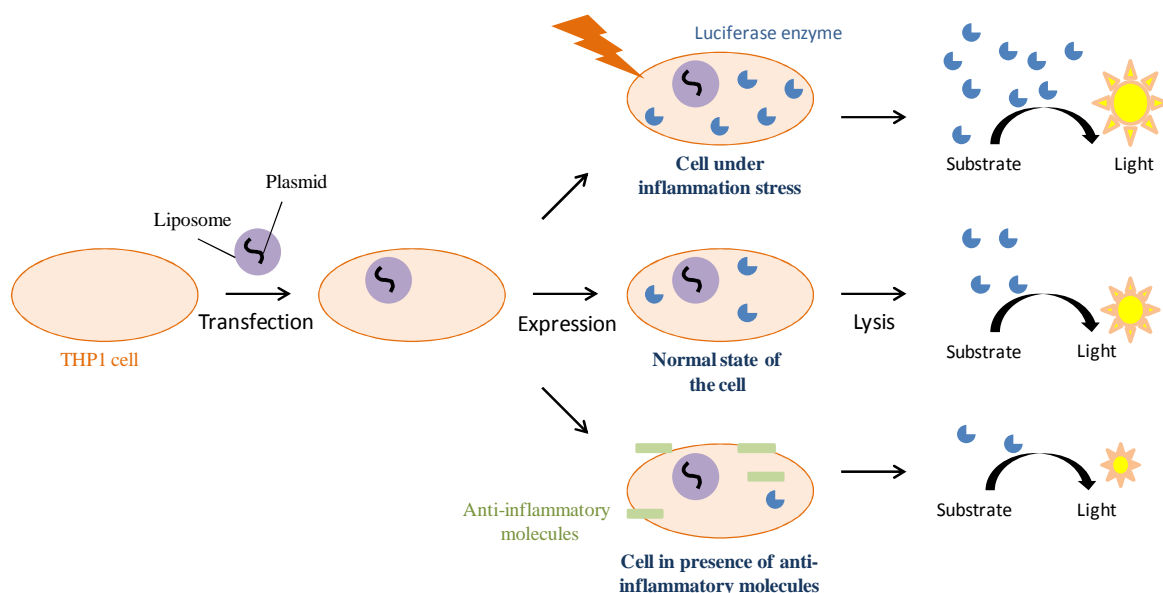


Figure 5.7: Schematic representation of the inflammatory test principle. THP1 cells were transfected with liposomes encapsulating plasmids expressing the luciferase gene under the control of the NF- κ B promoter. Under a pro-inflammatory state, NF- κ B will be activated thus triggering the luciferase expression. In contrast, in the absence of pro-inflammatory stimuli, the luciferase will not be expressed. Anti-inflammatory stimuli can also block the NF- κ B pathway and reduce the basal level of luciferase expression.

The quantity of NF- κ B was evaluated via the luciferase activity. The luciferase activity was normalized at 100% at $t = 0$ h with untreated THP1 cells. This determines the basal activity. After 6 h of incubation between the peptides and the monocytes, the luciferase activity has decreased to 74% for CTL-C and to 24% for dimer D1 (Figure 5.8). This means that the activity of NF- κ B has also decreased, suggesting that the peptides could induce an anti-inflammatory response already after 6 h of incubation. Besides, the anti-inflammatory response of the dimer D1 seems better than the CTL-C one. After 24 h, the luciferase activity is 10% for CTL-C and 8% for dimer D1.

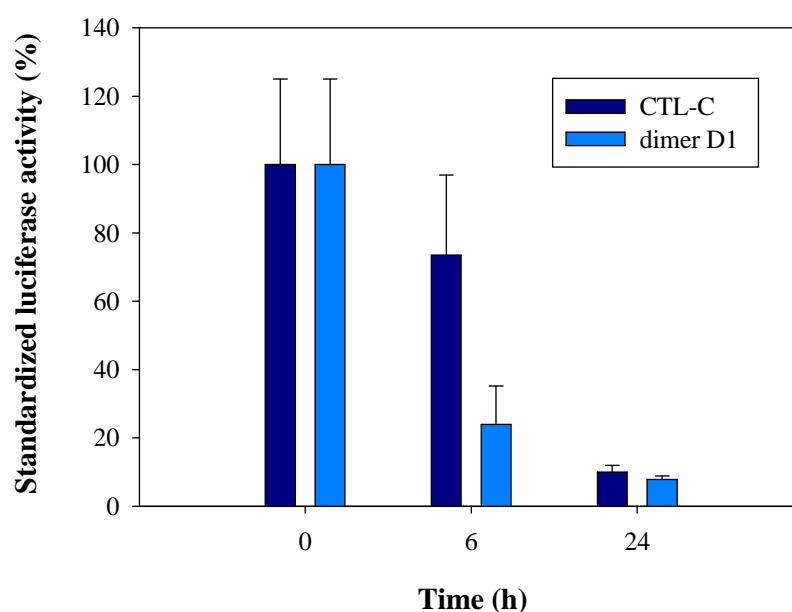


Figure 5.8: Normalized luciferase activity entailed by CTL-C and dimer D1 when incubated with THP-1 cells at $t = 0, 6$ and 24 h. The 100% of luciferase activity at $t = 0$ h corresponds to the fact that there is always a basal level of NF- κ B activity in cells. A decrease in the basal luciferase activity is a mark of an anti-inflammatory response.

This assay shows that CTL-C and dimer D1 both display anti-inflammatory properties on monocytes. The dimer D1 seems to act faster since it induces a decrease in the activity of NF- κ B only after 6 h of incubation with THP-1 cells, whereas the ability of CTL-C to decrease the activity of NF- κ B is lower. After 24 h, the two peptides give a similar result. This experiment has been conducted only once leading to preliminarily results that need to be confirmed.

5.6 Conclusion

In this chapter, the synthesis of four original CTL-C based dimers and one dendrimer was performed. Along with CTL-C and “D”-CTL-C, their antimicrobial properties were assessed. It was shown that “D”-CTL-C exhibits an activity 30 to 60 % higher than CTL-C, depending on the pathogen tested. Besides, whereas the dimers and the dendrimer kept a similar activity than CTL-C when tested against *M. luteus* or *C. albicans*, the importance of the linker’s length of the dimers was demonstrated when tested against *S. aureus* or a MRSA strain. Dimer D1 kept indeed a similar activity compared to CTL-C but dimers with longer linker chain lost their activity until at least 100 μM . The toxicity of all the molecules was then evaluated. At 50 μM , above the MIC values of all the peptides, only the dendrimer G1 was reported to be toxic. Finally, a preliminary test was conducted on CTL-C and dimer D1 that demonstrated their ability to reduce the activity of NF- κB on a monocytic cell line proving thus their anti-inflammatory properties. To complete this study, the inflammatory effects of “D”-CTL-C should be assessed. It would also be interesting to test the inflammatory effects of CTL-C and dimer D1 on cells under inflammatory condition. Finally, a future step would be to graft the dimer D1 or the “D”-CTL-C on hyaluronic acid in order to build a PEM film and observe if its antimicrobial properties are improved compared to a (CHI/HA-CTL-C) film and if the coating also exhibits anti-inflammatory properties.

Chapter 5 references

1. Chamorro, C., et al., Enhancing membrane disruption by targeting and multivalent presentation of antimicrobial peptides, *Biochimica Et Biophysica Acta-Biomembranes*, **2012**, 1818 (9), 2171-2174.
2. Tam, J.P., et al., Antimicrobial dendrimeric peptides, *European Journal of Biochemistry*, **2002**, 269 (3), 923-932.
3. Mintzer, M.A., et al., Exploiting Dendrimer Multivalency To Combat Emerging and Re-Emerging Infectious Diseases, *Molecular Pharmaceutics*, **2012**, 9 (3), 342-354.
4. Giehm, L., et al., Dendrimers destabilize proteins in a generation-dependent manner involving electrostatic interactions, *Biopolymers*, **2008**, 89 (6), 522-529.
5. Stach, M., et al., Membrane disrupting antimicrobial peptide dendrimers with multiple amino termini, *Medchemcomm*, **2012**, 3 (1), 86-89.
6. Carmona, G., et al., Improved Protease Stability of the Antimicrobial Peptide Pin2 Substituted with D-Amino Acids, *Protein Journal*, **2013**, 32 (6), 456-466.
7. Grieco, P., et al., The effect of D-amino acid substitution on the selectivity of temporin L towards target cells: Identification of a potent anti-Candida peptide, *Biochimica Et Biophysica Acta-Biomembranes*, **2013**, 1828 (2), 652-660.
8. Elduque, X., et al., Straightforward Synthesis of Cyclic and Bicyclic Peptides, *Organic Letters*, **2013**, 15 (8), 2038-2041.
9. Shin, S.Y., et al., Structure-antibacterial, antitumor and hemolytic activity relationships of cecropin A-magainin 2 and cecropin A-melittin hybrid peptides, *Journal of Peptide Research*, **1999**, 53 (1), 82-90.
10. Anderson, J.M., Biological responses to materials, *Annual Review of Materials Research*, **2001**, 31, 81-110.
11. Natoli, G., et al., The genomic landscapes of inflammation, *Genes & Development*, **2011**, 25 (2), 101-106.

Chapter 6:

Toward the design of a robust antimicrobial coating for medical catheter

Chapter 6:

Toward the design of a robust antimicrobial coating for medical catheter

Summary

6.1 Introduction	171
6.2 Chemical crosslinking of PEM films and mechanical characterization.....	172
6.3 PU surface modification and covalent grafting of a PEM film	177
6.3.1 Development of flat PU surfaces.....	178
6.3.2 Functionalization of PU surfaces.....	181
6.3.3 Buildup up of CHI-SH/HA-P-CTL-C films on PU surfaces.....	183
6.4 Buildup of antimicrobial step-by-step crosslinked PEM films on PU surfaces.....	184
6.5 Conclusion.....	185
Chapter 6 references	187

6.1 Introduction

In chapter 4, we have developed a self-defensive antibacterial and antifungal coating based on a CHI/HA polysaccharide multilayer film with embedded antimicrobial peptides. We decided here to improve this coating and make it usable for a concrete application. We chose to functionalize polyurethane-based catheters commonly used in the hospitals and well known to be a possible source of bacterial infection. In addition to antimicrobial properties, **mechanical rigidity** of the PEM film as well as its **strong attachment onto the polyurethane (PU)** are also features required to avoid any degradation of the coating when the catheter is introduced in the body.

Two approaches can be used to improve the mechanical properties of CHI/HA PEM films [1]. The first approach consists in crosslinking the PEM film after buildup by using carbodiimide chemistry. Carbodiimide reagents activate the carboxylic acid groups of HA, allowing the nucleophilic addition of amine groups from CHI, leading to amide bonds [2]. The second one is based on the step-by-step crosslinking of each layer using chemically modified CHI and HA by suitable reactive functions. The second strategy was chosen because it is time saving and does not require the use of toxic carbodiimide reagents.

Once the mechanical properties of the coating through the chemical crosslinking of the PEM film were proved, PU surfaces were then functionalized by polydopamine (PDA) to allow a covalent grafting of the PEM films (Figure 6.1). Finally, the antimicrobial properties of the functionalized PU were tested against *M. luteus*, *S. aureus* and *C. albicans*.

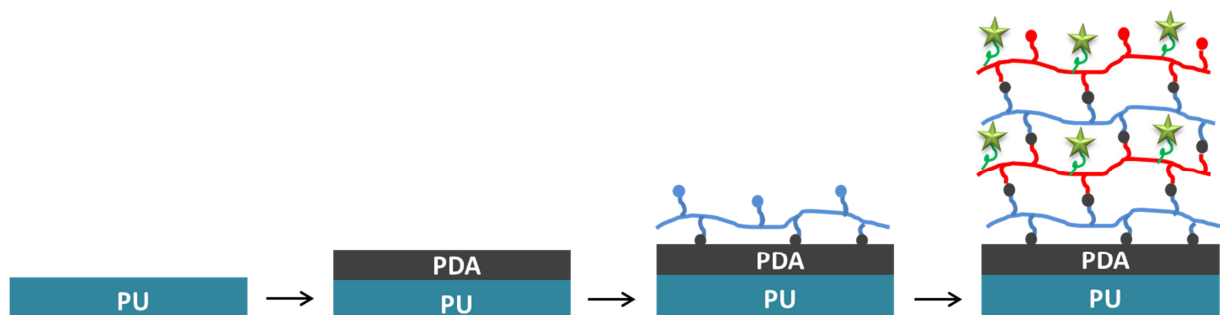


Figure 6.1: Schematic representation of the functionalization of polyurethane (PU) by polydopamine (PDA) followed by the covalent grafting of the step-by-step crosslinked PEM film.

6.2 Chemical crosslinking of PEM films and mechanical characterization

Chitosan and hyaluronic acid were chemically modified by thiol groups (CHI-SH) and pyridyl disulfide groups (HA-P), respectively. A modification degree of ~5% was determined by ^1H NMR for each polysaccharide. A second modification onto HA-P with the peptide CTL-C provided the polymer HA-P-CTL-C (~2% of grafting). Preparation of all polymers is described in Annexe B. Thiol groups and pyridyl disulfide react readily and rapidly together at room temperature in an irreversible way through a thiol disulfide exchange reaction as shown in Figure 6.2.

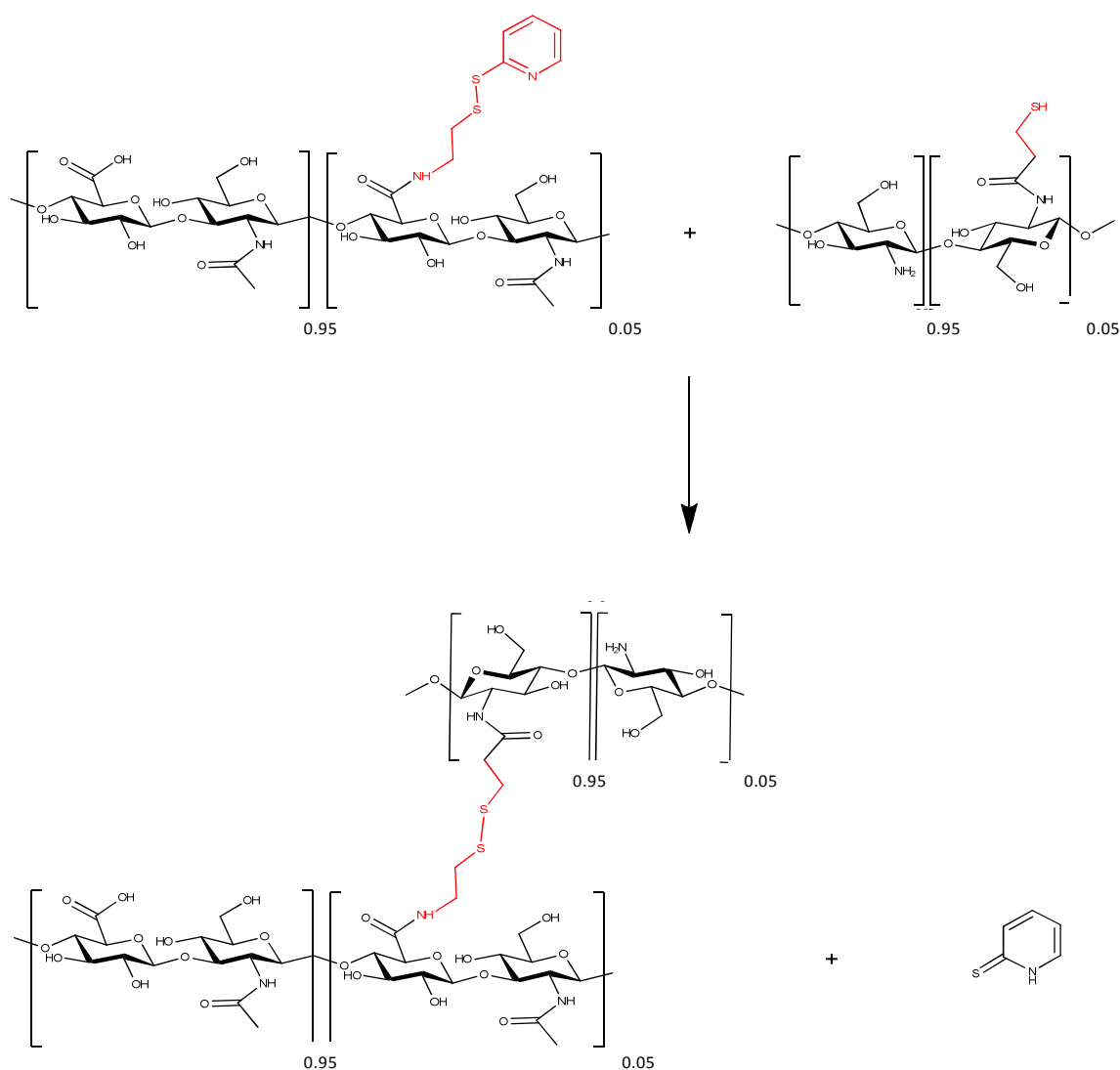


Figure 6.2: Chemical coupling between CHI-SH and HA-P that occurs spontaneously in the PEM film: thiol group from CHI-SH exchanges with the thiopyridyl moiety on HA-P leading to a new disulfide bond, and formation of thiopyridone. This last compound is able to exchange with the new disulfide bond: this chemical crosslinking is irreversible.

The buildup of PEI(HA-P/CHI-SH) and PEI(HA-P-CTL-C/CHI-SH) films was monitored by QCM-D as well as the buildup of a PEI(HA/CHI) film (Figure 6.3). Despite chemical modifications introduced along CHI and HA backbones, electrostatic adsorption occurs and leads to PEM buildup. On the contrary to the exponential buildup observed in case of CHI/HA multilayers, a linear increase of the frequency shift was observed for both CHI-SH/HA-P and CHI-SH/HA-P-CTL-C. A level off of the frequency shift was obtained after 8 deposited pairs of layers.

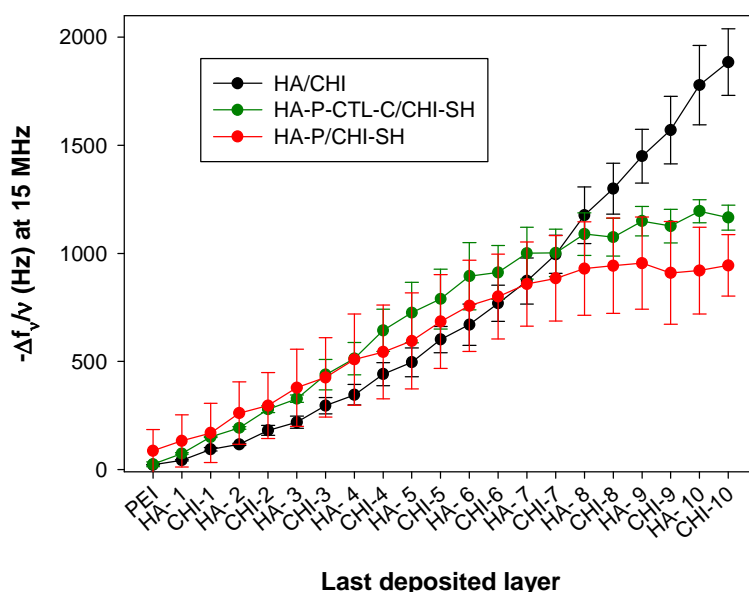


Figure 6.3: Evolution of the normalized frequency shift $-\Delta f_v/\nu$ measured at 15 MHz ($\nu = 3$) by QCM-D as a function of the last deposited layer for PEI(HA/CHI), PEI(HA-P-CTL-C/CHI) and PEI(HA-P/CHI-SH) films. Polymer solutions were prepared at 0.2 mg/mL in 150 mM NaCl buffer at pH 5.5. The data represents the mean and the standard deviation of minimum two independent experiments.

The step-by-step crosslinking could be confirmed through the UV measurement of the thiopyridone release. Unfortunately, QCM buildup does not produce enough amount of this compound to be detectable. Thus, we performed indirect experiments to confirm the chemical reticulation. QCM and AFM were used for this investigation.

CHI-SH/HA-P was put in contact with a highly concentrated NaBr solution (5 M NaBr at pH 5.5) during 5 min “to screen” the electrostatic interactions between the positively charged amine groups of CHI-SH and the negatively charged carboxylic groups of HA-P. In the case of non-crosslinked PEM, i.e. CHI/HA, a rapid dissolution was obtained leading to about 30% of decrease of the frequency shift (Figure 6.4). This dissolution was further emphasized when the film was put in contact with the buildup buffer (150 mM NaCl at pH

5.5). About 70% of the CHI/HA film was dissolved. In the case of a CHI-SH/HA-P film, the frequency shift was increased resulting from a swelling of the film. When the film was put in contact with the buildup buffer, the frequency shift decreased back to its original value. No loss of mass was recorded. These observations are in agreement with an efficient crosslinking of the CHI-SH/HA-P film.

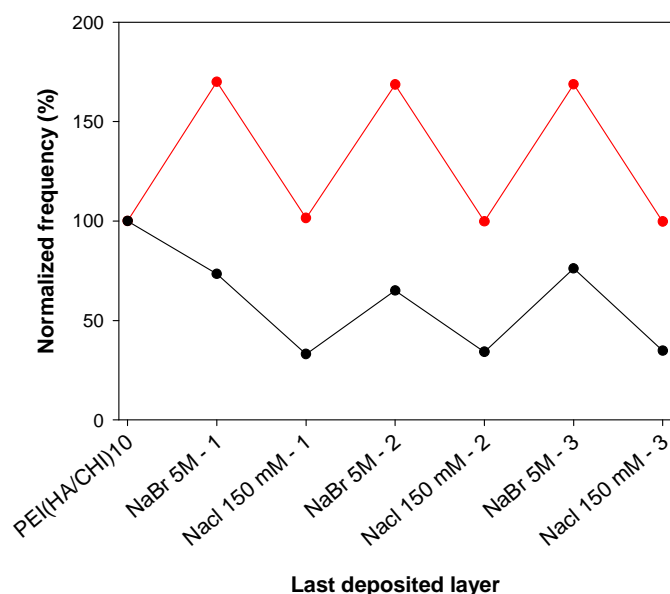


Figure 6.4: Evolution of the normalized frequency shift $-\Delta f/\nu$ measured at 15 MHz ($\nu = 3$) by QCM-D. PEI(HA/CHI)₁₀ (black curve) and PEI(HA-P/CHI-SH)₁₀ (red curve) films were built in 150 mM NaCl at pH 5.5. Only the last polyelectrolyte deposition is presented in the graphic. Three injections of a 5 M NaBr solution in alternation with the buffer solution (150 mM NaCl) were performed.

PEI(HA/CHI)₁₀, PEI(HA-P/CHI-SH)₁₀ and PEI(HA-P-CTL-C/CHI-SH)₁₀ films were imaged by AFM in dry state before and after contact with a 5 M NaBr solution (Figure 6.5). All films cover the whole substrate. PEI(HA/CHI)₁₀ film has a thickness of 56 ± 4 nm after buildup that decreases to 9 nm after contact with a 5 M NaBr solution. PEI(HA-P/CHI-SH)₁₀ and PEI(HA-P-CTL-C/CHI-SH)₁₀ have both a thickness of about 40 nm after buildup and kept a similar thickness even after contact with a 5 M NaBr solution. RMS roughness values are comprised between 23 and 47 nm; rough films were obtained in all cases. The absence of thickness variation of CHI-SH/HA-P and CHI-SH/HA-P-CTL-C films when brought in contact with a 5 M NaCl solution is another argument in favor of the chemical reticulation.

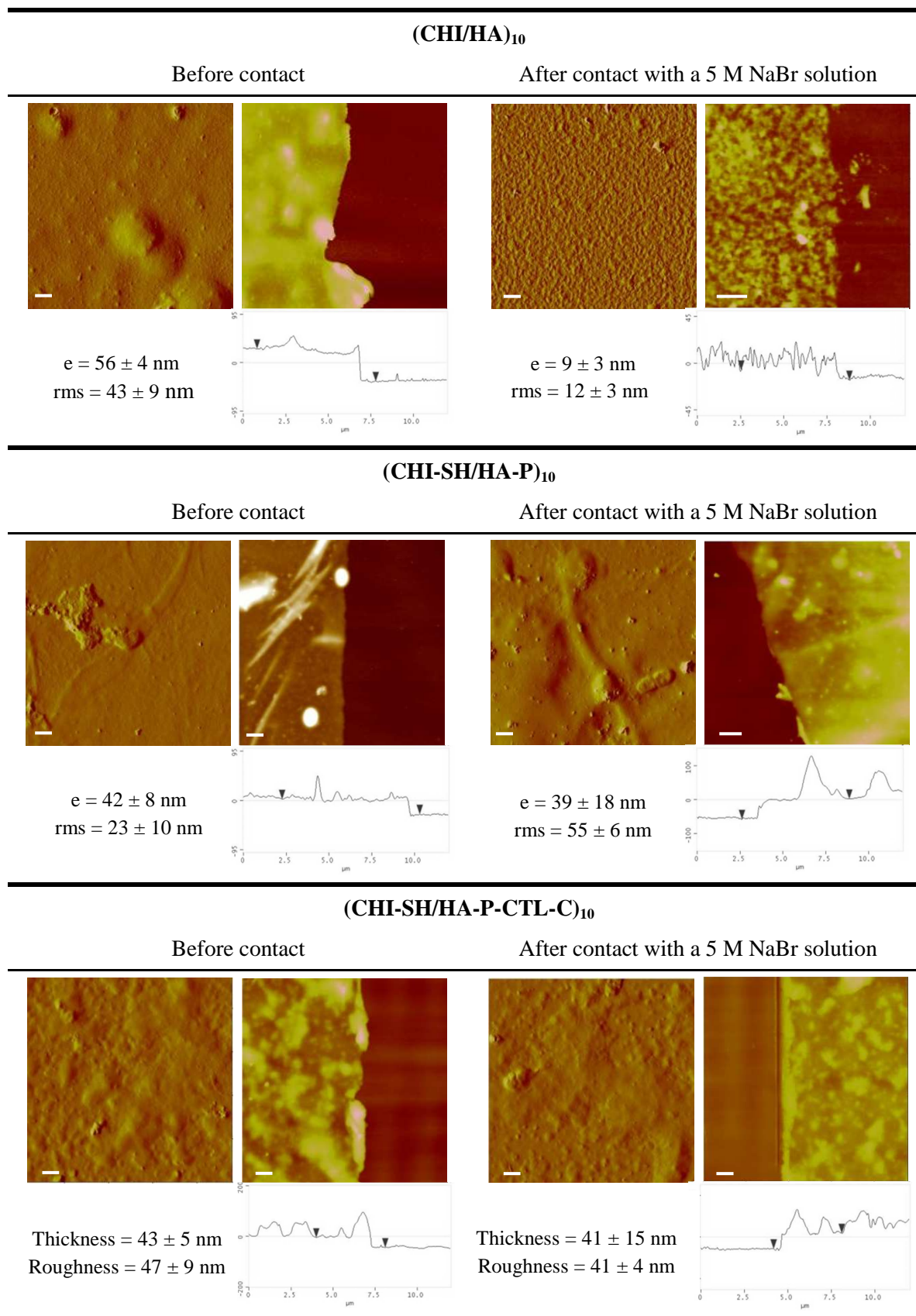


Figure 6.5: Topographies and profilometric sections ($15 \times 15 \mu\text{m}^2$) of scratched PEI(HA/CHI)₁₀, PEI(HA-P/CHI-SH)₁₀ and PEI(HA-P-CTL-CL/CHI-SH)₁₀ films obtained by AFM in contact mode and in dry state. The thickness were evaluated on scratched films on at least three profilometric sections and the roughness on AFM images ($15 \times 15 \mu\text{m}^2$) of non-scratched films.

Chemical crosslinking of PEM films creates reticulation points into the film, leading to an increase of their Young's modulus [3]. Two PEM films, CHI-SH/HA-P and CHI/HA, both composed of 20 bilayers in order to obtain film thicknesses above 500 nm, were analyzed by AFM force using a colloidal probe. These measurements have been performed by Dr. Gregory Francius (LCPME, Nancy). Typical AFM force-distance curves obtained for PEI(HA/CHI)₂₀ (Figure 6.6a) and PEI(HA-P/CHI-SH)₂₀ (Figure 6.6b) are shown in Figure 6.6. For each force-distance curve, an elastic modulus can be calculated according to Sneddon model (see 2.2.3). 1024 force-distance curves have been determined per PEM film. A distribution of elastic moduli could thus be obtained (Figure 6.6c and Figure 6.6d).

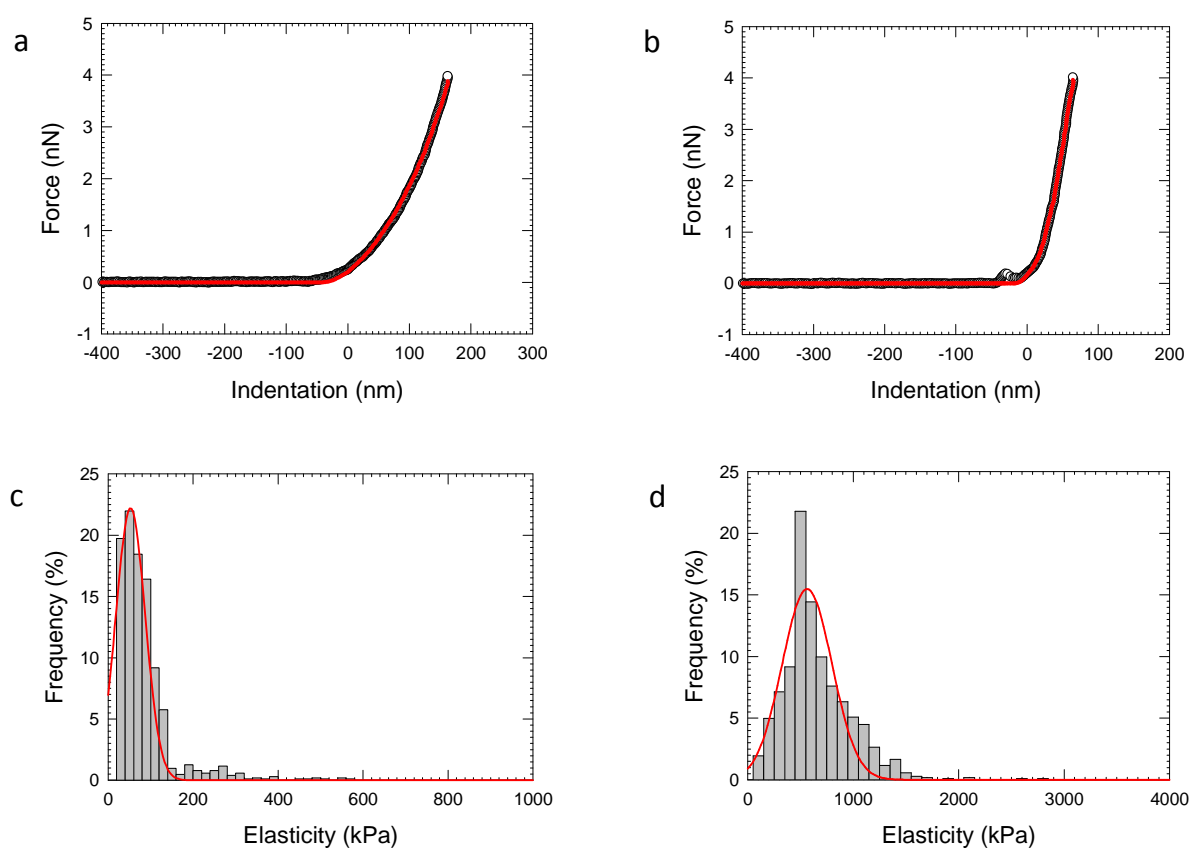


Figure 6.6: Typical AFM force-distance curves obtained for (a) PEI(HA/CHI)₂₀ and (b) PEI(HA-P/CHI-SH)₂₀. (c) and (d) are the data extracted from 1024 AFM force-distance curves like (a) and (b), respectively, using Sneddon model.

From the elastic moduli distribution, an average Young's modulus could be determined for PEI(HA/CHI)₂₀ and PEI(HA-P/CHI-SH)₂₀. The values are reported in Table 6.1.

Table 6.1: Young's moduli of PEI/(HA/CHI)₂₀ and PEI/(HA-P/CHI-SH)₂₀ PEM films determined by AFM force-distance curves.

PEM film	Young's Modulus (kPa)
(CHI/HA) ₂₀	51 ± 17
(CHI-SH/HA-P) ₂₀	576 ± 136

The Young's modulus of a PEI(HA/CHI)₂₀ film was found around 51 kPa, whereas a value of 576 kPa was obtained in the case of a PEI/(HA-P/CHI-SH)₂₀ film. The crosslinked multilayer, PEI(HA-P/CHI-SH)₂₀, exhibits thus a tenfold of magnitude higher than the non-crosslinked PEI(HA/CHI)₂₀ film.

Films dissolution experiments performed with NaBr 5M solution and monitored by both QCM and AFM provided strong arguments in favor of an efficient crosslinking of the PEI(HA-P/CHI-SH)₁₀ film. This reticulation was confirmed by the comparison of the Young's modulus between PEI(HA/CHI)₂₀ and PEI(HA-P/CHI-SH)₂₀ films: the reticulated film is tenfold more rigid than the non-reticulated film.

Modulation of the film rigidity could be realized through an increase of the modification degree of HA-P and CHI-SH. We considered that the possibility to tune the mechanical properties of our system is on and thus in the second part of this project, we focused our investigation on the modification of PU surface for the covalent grafting of our PEM film.

6.3 PU surface modification and covalent grafting of a PEM film

Surface characterization instruments, such as QCM or ellipsometer, are techniques developed to analyze flat surfaces. Medical catheters have a tubular form and thus we prepared first a thin film of PU as model substrate. Modification of PU surfaces via polydopamine coating was then investigated. Finally, the covalent grafting of CTL-C peptides or PEM films modified by CTL-C was studied by QCM and XPS.

6.3.1 Development of flat PU surfaces

We aimed to functionalize catheters provided by Prof. Francis Schneider (Head of the medical intensive care unit of Strasbourg's hospital), named "Hémocath_(PUR) 60" from Vygon company. To develop PU flat model surfaces to run in our project, commercial PU Selectophore® in pellets purchased from Sigma-Aldrich was used. First of all, we checked by ¹H NMR analysis that the polymer composition of the polyurethane-based catheter is similar to the one from Sigma-Aldrich. A medical catheter was cut in several pieces and heated at 100°C in dimethylformamide (DMF) during 11 h. The catheter was dissolved leading to a colorless and homogenous solution, except the presence of some white particles (3-5% in weight). These particles, that may be charges used to provide elasticity to the material, were filtered and the DMF was removed under reduced pressure. The obtained colorless solid residue (92-95% in weight) was dissolved in deuterated chloroform (CDCl₃) and analyzed by ¹H NMR (Figure 6.7). This spectrum is entirely similar to the one corresponding to the commercially available reference of the PU from Sigma-Aldrich. Thus, we used the commercially available source of PU to prepare thin flat substrates.

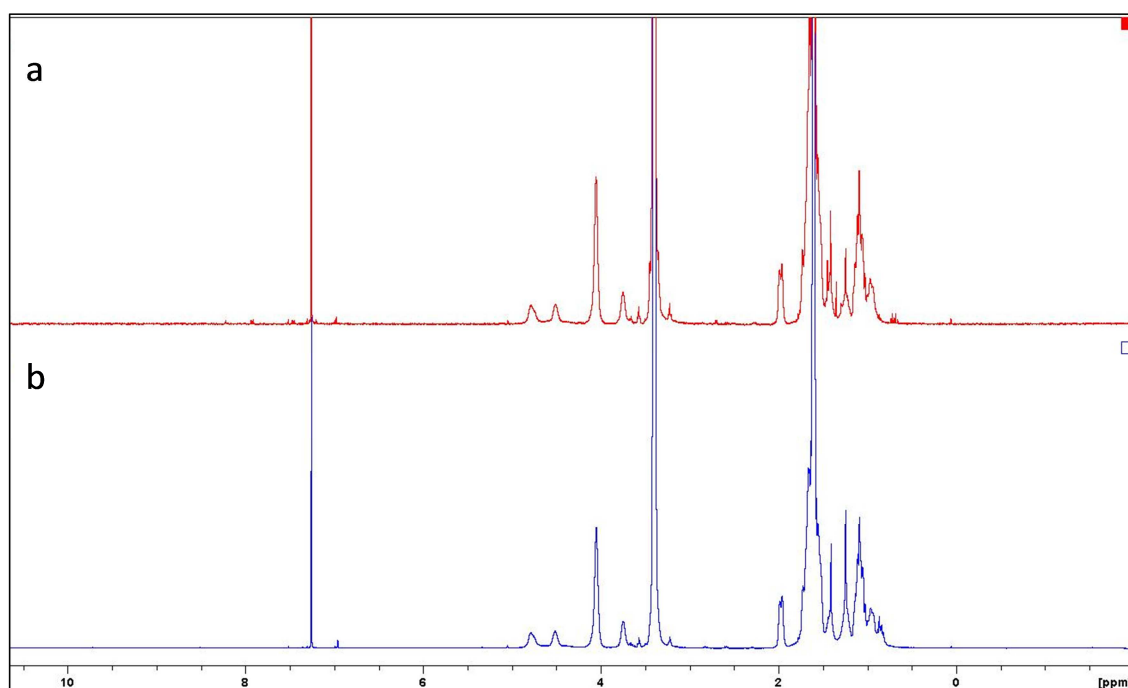


Figure 6.7: ¹H NMR (400 MHz) spectrum performed in CDCl₃ of (a) the polymer extracted from a medical Vygon's catheter and (b) the commercial polyurethane (Selectophore®, Sigma-Aldrich).

An easy way reported in the literature to fabricate flat PU surfaces on a substrate is by spin-coating [4, 5]. Different parameters, such as the polyurethane concentration and the spin-

coater rotational speed were tuned to coat silicon wafers (14 mm × 14 mm). A minimal volume of 65 μL of PU solution prepared in THF was deposited at the center of the silicon wafer at rest. The substrate was then rotated at high speed in order to spread the PU solution by centrifugal force. Ellipsometry was used to determine the thickness of the obtained PU layer. The detailed procedure and the influence of the PU concentration as well as the rotational speed on the coating buildup are given below.

Variation of the PU concentration

We first studied the influence of the concentration of PU with solutions of 2% wt, 1% wt, 0.5% wt and 0.1% wt in THF. The time of the rotation was fixed at 150 s, the rotational speed at 5000 rpm and the acceleration at 2500 rpm. 2% wt PU solutions led to inhomogeneous PU films probably due to the high viscosity of the solution. For all lower PU concentrations, the obtained PU coatings were homogeneous according to optical microscope visualization and ellipsometry. The thickness of the PU coating was linear as a function of the PU concentration (Figure 6.8). It varies from 10 to 100 nm for concentrations ranging from 0.1% to 1% wt of PU.

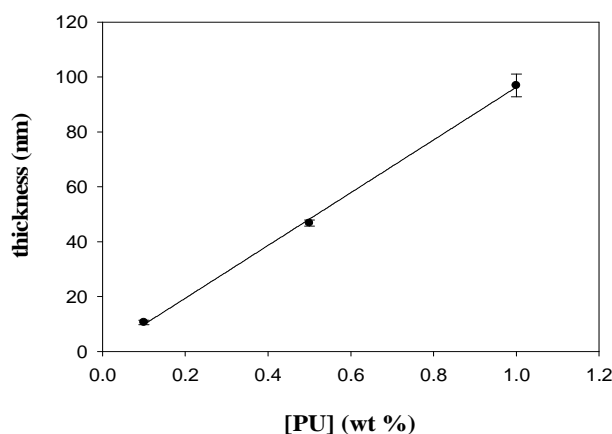


Figure 6.8: Thickness of PU coating depending on the PU concentration in THF. The time of rotation was fixed at 150 s, the rotational speed at 5000 rpm and the acceleration was equal to half the rotational speed. The data represents the mean and the standard deviation of minimum three independent experiments.

Variation of the rotational speed

Fixing the PU concentration at 1% wt and the rotational time at 150 s, the influence of the rotational speed was also studied. It was varied between 2000 and 12000 rpm, which is the maximal speed of our spin-coater (Figure 6.9). The acceleration was always fixed equal to half the rotational speed. At 2000 rpm, the thickness of the PU layer is around 135 nm and

decreases until reaching a plateau at a thickness of 80 nm above 10000 rpm. It was chosen to use a rotational speed of 10000 rpm for the rest of our study.

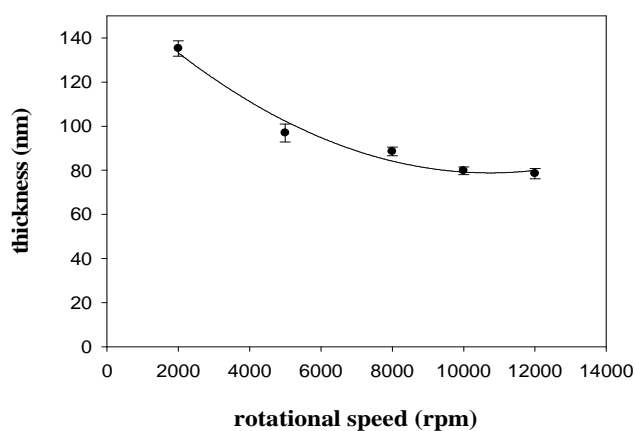


Figure 6.9: Thickness of a polyurethane layer depending on the rotational speed. The time was fixed at 150 s, the PU concentration at 1% wt and the acceleration was equal at half the rotational speed. The data represents the mean and the standard deviation of minimum three independent experiments.

The influence of the rotation time was also studied. Fixing PU concentration at 1% wt and the rotational speed at 10000 rpm, the rotation time was varied between 30 s and 200 s. PU layers between 78 and 82 nm were obtained showing no influence of the rotation time. The solvent evaporation seems in this case to be very fast.

Taking into account these results, optimized spin-coating conditions were chosen. They are summarized in Table 6.2 and will always be the conditions used afterwards in this chapter.

Table 6.2: Summary of the optimized spin-coating conditions to obtain a PU layer of about 80 nm.

Optimized spin-coating conditions	
Rotational speed	10000 rpm
Acceleration	5000 rpm
PU concentration in THF	1% wt
Time of rotation	150 s
Volume deposited	65 μ L

AFM images of the spin-coated PU layer on the silicon wafer substrate using the conditions of Table 6.2 were performed in contact mode and in dry state (Figure 6.10). The topography image in Figure 6.10 seems to show that PU surface is rough but the rms is only

of 2.9 ± 0.6 nm. This is likely due to the fast evaporation of the solvent. Determined from 5 different profilometric sections, the thickness of the PU coating is of 80 ± 4 nm, which is in perfect agreement with the value obtained by ellipsometry (79 ± 2 nm).

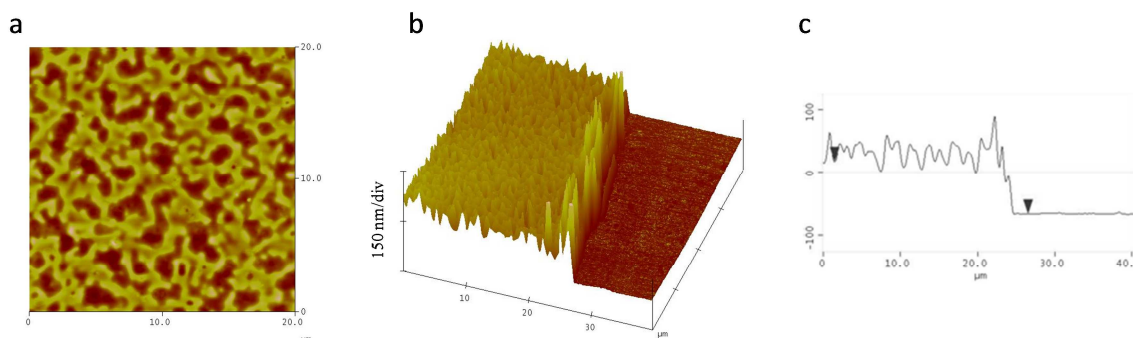


Figure 6.10: (a) Topography, (b) 3D and (c) profilometric sections of a PU layer deposited on a silicon wafer using the conditions of Table 6.2 obtained by AFM in contact mode and in dry state.

In order to check the potential influence of the substrate beneath the PU, a glass slide and a gold QCM crystal, both of 14 mm in diameter, were also coated using the same conditions. Thicknesses of 77 ± 8 nm and 76 ± 9 nm were found by AFM for the gold QCM crystal surface and the glass substrate, respectively. This shows that the beneath substrate has no influence on the PU layer thickness formation by spin-coating.

6.3.2 Functionalization of PU surfaces

In order to obtain a covalent attachment on PU surfaces of the step-by-step crosslinked PEM films described in the beginning of this chapter, polydopamine (PDA) was used to (1) functionalize PU surfaces by dip-coating and to (2) anchor the PEM film (Figure 6.11). This choice was motivated by the fact that dopamine is reported in the literature to form a thin and strong surface-adherent film through a polymerization process onto a wide range of inorganic and organic materials [6]. Furthermore, PDA represents also a layer that can be covalently modified by the introduction of chemical groups [7, 8] such as amino or thiol derivatives.

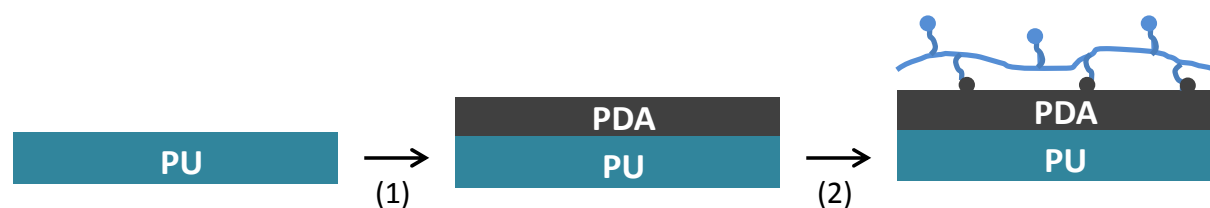


Figure 6.11: Schematic representation of the functionalization of polyurethane (PU) (1) by polydopamine (PDA) followed (2) by the covalent grafting of the first polyelectrolyte from the step-by-step crosslinked PEM film.

(1) Functionalization of PU by polydopamine

The surface functionalization by polydopamine (Figure 6.11 step(1)) has been inspired by the procedure described by Lee et al. [6]. Both flat PU surfaces (14 mm diameter) and PU-based catheter pieces have been functionalized. Dopamine (3-hydroxytyramine hydrochloride, Alfa Aesar) was dissolved in a 10 mM TRIS solution at pH 8.5 to obtain a 2 mg.mL^{-1} solution. Flat PU substrates or PU-based catheter pieces, deposited in a 24-well cell plate, were put under stirring with 1 mL of dopamine solution at room temperature for 18 hours. The PU substrates took a slightly black color suggesting the polymerization of the dopamine. They were then extensively rinsed with Milli-Q water and sonicated for 10 min. The substrates are noted PDA-PU surfaces and PDA-PU-catheter surfaces in the rest of the study.

(2) Functionalization of the polydopamine layer

CHI-SH polymer chains can react with catechol groups from the polydopamine layer. Nucleophilic groups, such as thiol or amine present on CHI-SH, can indeed be added on oxidized catechol groups through Michael reaction. This covalent coupling reaction should lead to the anchoring of a crosslinked CHI-SH/HA-P PEM film (Figure 6.11 step(2)). To validate this hypothesis, CTL-C was first used as model molecule to be grafted on the polydopamine layer since it possesses thiol moieties as well (cysteine in C-terminal position). First of all, the polydopamine layer has to be oxidized in order to exhibit quinone reactive functions on the surface. For that, 1 mL of a 1 mg.mL^{-1} NaIO_4 aqueous solution was put in contact with the PDA-PU-coated substrates for 30 min. After this oxidation step, 1 mL of a 1 mg.mL^{-1} CTL-C solution in 10 mM TRIS at pH 8.5 was put in contact with PDA-PU-coated substrates for 14 hours. The substrates were then extensively rinsed with Milli-Q water and sonicated for 10 min. They are noted CTL-C-PDA-PU surfaces and CTL-C-PDA-PU-catheter surfaces in the rest of the study.

XPS analyses were performed to confirm both the PU functionalization by polydopamine and the further reaction with the thiol moieties from the CTL-C. Table 6.3 reports the carbon, oxygen, nitrogen and sulfur compositions (in percentage) of a flat PU surface, a PDA-PU surface, a CTL-C-PDA-PU surface, a catheter surface, a PDA-catheter surface and a CTL-C-PDA-catheter surface.

Our own home made PU surface was initially composed of 74.51% C_{1s} , 2.04% N_{1s} and 19.17% O_{1s} . For a PDA-PU surface, the percentage of N_{1s} increased from 2.04% to 6.01%.

Dopamine possessing an amine moiety, it suggests the formation of a PDA layer on the PU surface. For a CTL-C-PDA-PU surface, the percentage of C_{1s} slightly decreased whereas the percentage of N_{1s} and S_{2p} increased from 6.01% to 12.76% and from 0.08% to 0.8 %, respectively. The increase in S_{2p}, related to the thiol functions of CTL-C, indicates the successful immobilization of the peptide.

Similar results were obtained on PU-based catheter pieces. We demonstrated thus that the functionalization of a PU surface is possible by using dopamine and forming a PDA layer that can then further react to form covalent bond with thiol containing molecules.

Table 6.3: Composition of a flat PU surface, a dopamine functionalized flat PU surface, a CTL-C functionalized flat PU surface, a piece of catheter, a dopamine functionalized piece of catheter and a CTL-C functionalized piece of catheter obtained by XPS analysis.

	C _{1s} %	N _{1s} %	O _{1s} %	S _{2p} %
Flat PU surface	74.51	2.04	19.17	0.08
PDA-PU surface	74.59	6.01	19.32	0.08
CTL-C-PDA-PU surface	68.21	12.76	18.23	0.8
Catheter surface	76.18	2.88	16.24	1.81
PDA-catheter surface	73.8	5.18	19.89	0
CTL-C-PDA-catheter surface	68.19	10.66	19.72	0.56

6.3.3 Buildup up of CHI-SH/HA-P-CTL-C films on PU surfaces

Since the buildup of PEM films is known to be dependent on the beneath substrates, we checked if the buildup of a CHI-SH/HA-P-CTL-C film is possible on a PDA-PU surface. In order to monitor the PEM buildup by QCM, a gold QCM crystal was functionalized by polydopamine *ex-situ*. After NaIO₄ activation, the crystal was then placed in the QCM cell and the buildup of CHI-SH/HA-P-CTL-C was monitored by QCM-D (Figure 6.12).

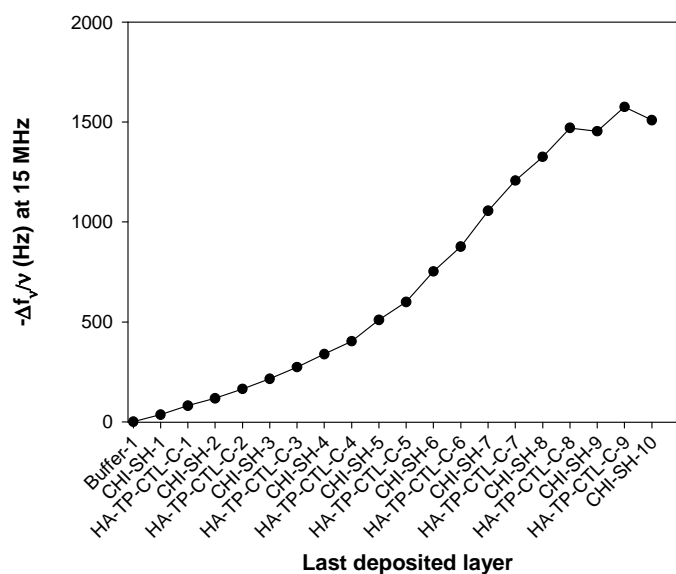


Figure 6.12: Evolution of the normalized frequency shift $-\Delta f/v$ measured at 15 MHz ($\nu = 3$) by QCM-D as a function of the last deposited layer for the buildup of a (CHI-SH/HA-P-CTL-C)_{9,5} film on the top of a gold QCM crystal that has been covered with a PU layer, functionalized by a polydopamine layer and activated with NaIO₄ ex-situ. Polymer solutions were prepared at 0.2 mg.mL⁻¹ in 150 mM NaCl buffer at pH 5.5.

A frequency shift about 1500 Hz was reached after 10 pairs of layer which is similar to the deposition of CHI/HA on PEI coated QCM crystal. The buildup of CHI-SH/HA-P-CTL-C is thus effective on PDA-PU coated substrates.

6.4 Buildup of antimicrobial step-by-step crosslinked PEM films on PU surfaces

The last step of our study was to evaluate the antimicrobial properties of CHI-SH/HA-P-CTL-C films built on PDA functionalized PU coated flat substrate. The normalized growth inhibition was determined for (CHI-SH/HA-P-CTL-C)₁₅ films after 4 h, 6 h and 24 h of incubation with *M. luteus*, *S. aureus*, and *C. albicans* (Figure 6.13). The growth inhibition was superior to 90% after 6 h and 24 h in the case of *M. luteus*. For *C. albicans*, the growth inhibition was about 100% after 6 h but decreased to 33% after 24 h. For *S. aureus*, the growth inhibition was of 79% after 4 h and decreased to 27% after 6 h. This means that step-by-step crosslinked (CHI-SH/HA-P-CTL-C)₁₅ films exhibit antimicrobial properties only against *M. luteus* since the inhibition is almost total after 24h of contact. Against *C. albicans* and *S. aureus*, the coating exhibits antimicrobial properties only for the first hours, and then it

slowly loses them, faster against *S. aureus* than against *C. albicans*. This probably means that all the antimicrobial peptides have been consumed. These results are coherent with the results obtained in Chapter 4 for the PEI(HA-CTL-C/CHI)₁₅ film, where the growth of *M. luteus*, *C. albicans* and *S. aureus* were fully inhibited with respectively 5, 15 and 30 HA-CTL-C/CHI pairs of layers after 24 h of incubation. Knowing that HA-P-CTL-C possesses only 1.5% of CTL-C grafting ratio in comparison with HA-CTL-C having 5%, 15 pairs of layers of CHI-SH/HA-P-CTL-C have less immobilized CTL-C than 15 pairs of layers of CHI/HA-CTL-C.

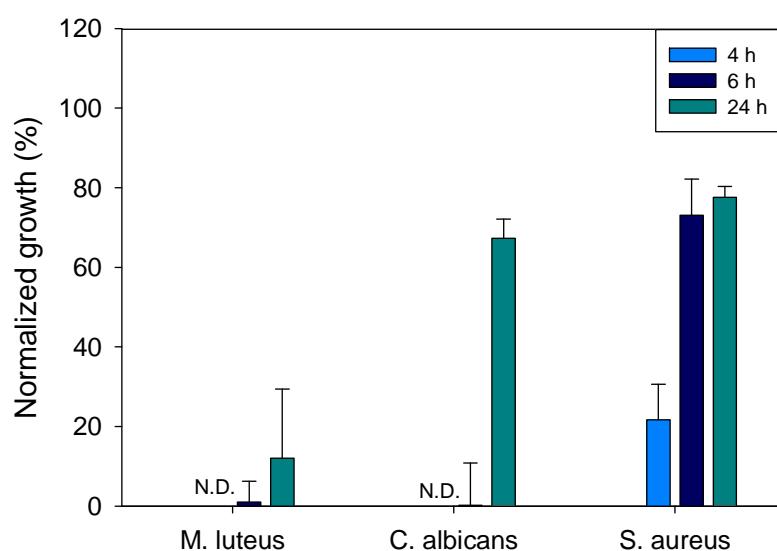


Figure 6.13: Normalized growth for (HA-P-CTL-C/CHI-SH)₁₅ films after 4 h, 6 h and 24 h of incubation with *S. aureus*, *M. luteus* and *C. albicans*. ND means not determined.

6.5 Conclusion

We studied in this chapter an easy way to crosslink chitosan and hyaluronic acid in a step-by-step manner. By functionalization of CHI and HA with reactive moieties, step-by-step crosslinked PEM films could be obtained showing a better stability in high salt concentration and having a higher Young's modulus compared to non-crosslinked CHI/HA films. Using a simple method to coat flat substrates with a PU layer similar to catheters composition, we asserted that polydopamine could be used to functionalize PU and further react with thiol groups. This allowed the covalent anchoring of step-by-step crosslinked CHI-SH/HA-P-CTL-C films that still exhibit antimicrobial properties against *M. luteus* after 24 h of incubation. The coating is also active against *S. aureus* for 4 h and against *C. albicans* for at least 6 h.

The work reported in this chapter constitutes a preliminary study for the functionalization of catheters by robust antimicrobial PEM films. For further investigations, the percentage of CTL-C grafted on the HA-P should be increased to obtain better antimicrobial properties against *S. aureus* in particular. Besides, it would be interesting to evaluate the inflammatory properties of the coating since we know that the peptide CTL-C exhibits anti-inflammatory properties.

Chapter 6 references

1. Rydzek, G., et al., Strategies for covalently reticulated polymer multilayers, *Soft Matter*, **2012**, 8 (38), 9738-9755.
2. Picart, C., et al., Controlled degradability of polysaccharide multilayer films in vitro and in vivo, *Advanced Functional Materials*, **2005**, 15 (11), 1771-1780.
3. Schneider, A., et al., Polyelectrolyte multilayers with a tunable Young's modulus: Influence of film stiffness on cell adhesion, *Langmuir*, **2006**, 22 (3), 1193-1200.
4. Cozzens, D., et al., Surface Characterization and Protein Interactions of Segmented Polyisobutylene-Based Thermoplastic Polyurethanes, **2011**, 14160-14168.
5. Mustapha Chouiki, J.D., Gisèle boiteux, Valérie Massardier, Synthèse et caractérisation d'un composite poly(p-phénylènevinylène)/polyuréthane, *Matériaux*, **2002**.
6. Lee, H., et al., Mussel-inspired surface chemistry for multifunctional coatings, *Science*, **2007**, 318 (5849), 426-430.
7. Wu, J.J., et al., Mussel-Inspired Chemistry for Robust and Surface-Modifiable Multilayer Films, *Langmuir*, **2011**, 27 (22), 13684-13691.
8. Cao, Y.Z., et al., Mussel-Inspired Chemistry and Michael Addition Reaction for Efficient Oil/Water Separation, *Acs Applied Materials & Interfaces*, **2013**, 5 (10), 4438-4442.

Conclusion and outlooks

The layer-by-layer assembly is the coating technique at the center of this thesis. In a first part, since only few studies described the use of host-guest interactions to build multilayer films and none of them focused on the topography of the formed films, a physical chemical study of neutral polymer multilayer films based only on host-guest interactions was conducted. In the second part, the layer-by-layer assembly of polysaccharides combined with the use of antimicrobial peptides was demonstrated to be a powerful tool to develop robust self-defensive antimicrobial coatings.

In the first part of the thesis (chapter 3), we investigated the influence of the host-guest interactions strength on the topography of neutral polymer multilayer films. Poly(*N*-hydroxypropylmethacrylamide) (PHPMA) was chosen as neutral polymer backbone and was grafted with β -cyclodextrin (β -CD) and different hydrophobic guest molecules: pyrene (Py), ferrocene (Fc) and adamantane (Ad). The strength of the inclusion complex in solution is increasing in the following order: $\text{Py}/\beta\text{-CD} < \text{Fc}/\beta\text{-CD} < \text{Ad}/\beta\text{-CD}$. The strength of the host-guest interaction was thus first modulated by changing the hydrophobic guest involved in the multilayer buildup. We showed that the strength of the interaction between the two polymers constituting the film strongly influenced the film buildup. The buildup was indeed very limited for PHPMA-CD/PHPMA-Py, whereas it led to smooth continuous films for PHPMA-CD/PHPMA-Fc and to droplet-like films, which do not cover entirely the substrate, for PHPMA-CD/PHPMA-Ad. The strength of the Fc/ β -CD interaction, evaluated beforehand by ITC measurement in solution, was then tuned by the type and the concentration of the salt. PHPMA-CD/PHPMA-Fc films were built in the presence of different sodium salts at different ionic strengths. For weak host-guest interactions, only isolated aggregates are formed on the substrate. As the interaction strength of the host-guest increases, the formed films go through a droplet-like structure, before becoming continuous but rough for stronger interactions. When the interaction is further increased, the films become smooth before to be rough again at still higher interaction strength. So, intermediate interaction strength seems to be required to form continuous films, whereas, if too low, the interaction strength limits the film buildup. With this study, we attempted to rationalize the comprehension of the initial steps of a polymer multilayer buildup as a function of the polymer interaction strength.

In the second part of the thesis, we developed PEM films for the functionalization of implants in order to inhibit the adhesion and the proliferation of pathogens. In the biomaterial field, numerous PEM films were intended for this purpose but none of them until now exhibited both antibacterial and antifungal properties.

We designed in chapter 4 a new surface coating based on polysaccharide multilayer films containing CTL-C functionalized HA at 5% in grafting ratio. CTL is a natural antimicrobial peptide possessing both antibacterial and antifungal properties. After 24 hours of incubation, CHI/HA-CTL-C films fully inhibited the development of *C. albicans* and *S. aureus*, which are common and virulent pathogens agents encountered in care-associated diseases, with 15 and 30 pairs of layers, respectively. The release of the antimicrobial peptides was triggered by the enzymatic degradation of the film due to the pathogens themselves introducing the concept of self-defensive coating. The antimicrobial peptides, even grafted on HA, were then observed to penetrate inside *C. albicans* after 45 min of contact. We demonstrated the ability of the PEM film to keep its activity during 3 cycles of use against fresh incubated *C. albicans* suspension. Moreover, we showed limited fibroblasts adhesion, without cytotoxicity, on CHI/HA-CTL-C films, which highlights a medically relevant application to prevent infections on catheters where fibrous tissue encapsulation is undesirable.

In chapter 5, we synthesized different CTL-C based dimers with various lengths and one dendrimer in order to improve the bioactivity of the original peptide. The D-diastereomeric CTL-C, noted “D”-CTL-C, was also studied. By determining the MIC, we showed that “D”-CTL-C exhibits an activity 30 to 60% higher than CTL-C depending on the pathogen. Concerning the dimers and the dendrimer, a similar activity compared to CTL-C was observed against *M. luteus* and *C. albicans*. Against *S. aureus* and the MRSA (methicillin-resistant *S. aureus*) strains, only the dimer D1, the shorter one, kept a similar activity compared to CTL-C. Indeed, longer dimers have no activity until at least 100 μM . The toxicity of the different dimers, the dendrimer and the “D”-CTL-C was assessed by hemolysis assays. At 50 μM , so above the MIC, only the dendrimer G1 was reported to be toxic. Finally, a preliminary test was conducted on CTL-C and dimer D1 that demonstrated their anti-inflammatory properties. To complete this study, since it is the most promising peptide, the inflammatory effects of “D”-CTL-C should be assessed. Testing the inflammatory effects of CTL-C, “D”-CTL-C and dimer D1 on cells under inflammatory condition would allow confirming the anti-inflammatory properties of these peptides.

In chapter six, we showed the possibility to develop a robust self-defensive antibacterial and antifungal PEM film. By functionalization of CHI and HA with reactive moieties, step-by-step cross-linked PEM films were obtained showing a better stability in high salt concentration and having a higher Young's modulus compared to non-cross-linked CHI/HA films. Using a simple method, we showed that dopamine could be used to functionalize PU, a polymer used for catheters, with a polydopamine layer that can further react with thiol or amine groups, allowing the covalent attachment of step-by-step cross-linked CHI-SH/HA-P-CTL-C films that still exhibit antimicrobial properties against *M luteus* after 24 h. The coating is also active against *S. aureus* for 4 h and against *C. albicans* for at least 6 h.

An outlook of this work would be to increase the percentage of CTL-C grafted on the crosslinkable polysaccharides in order to obtain better antimicrobial properties, against *S. aureus* and MRSA in particular. Besides, it would be interesting to evaluate the inflammatory properties of the coating since we showed that the peptide CTL-C exhibits anti-inflammatory properties. This developed coating would have antimicrobial and anti-inflammatory properties using only one type of bioactive molecules (CTL-C). Using polysaccharides would allow the degradation of the film and then the release of the peptide. However, this degradation due to hyaluronidase is not specific to pathogens. Indeed, hyaluronidase is also produced by mammalian cells. To develop specific degradable PEMs, one of the ideas would be to graft CTL-C on synthetic polyelectrolytes through the use of a peptidic linker that would be specifically cleaved by the pathogen.

Annexes

Annexe A:

Syntheses of PAH-CD, PHPMA-CD and PHPMA-G (G = Ad, Fc and Py)

Summary

A1. Synthesis of PAH-Cd,	195
A2. Synthesis of a polymer precursor: PHPMA-N₃	195
A3. Synthesis of PHPMA-CD	198
A4. Synthesis of PHPMA-Ad	198
A5. Synthesis of PHPMA-Fc	199
A6. Synthesis of PHPMA-Py	200
Annexe A references	201

^1H NMR and ^{13}C NMR spectra were recorded respectively on Bruker Advance DPX300 (300 MHz) and DPX400 (400 MHz) spectrometers. The NMR chemical shifts are reported in ppm relative to tetramethylsilane or tert-butanol (1.24 ppm).

Infrared spectra were obtained on a Thermo Electron Corporation Nicolet 380 FT-IR equipped with ATR. Merck RP-18 F254S plates were used for analytical thin layer chromatography. Silica gel 60 (particle: 40 – 60 μm) was employed for flash chromatography.

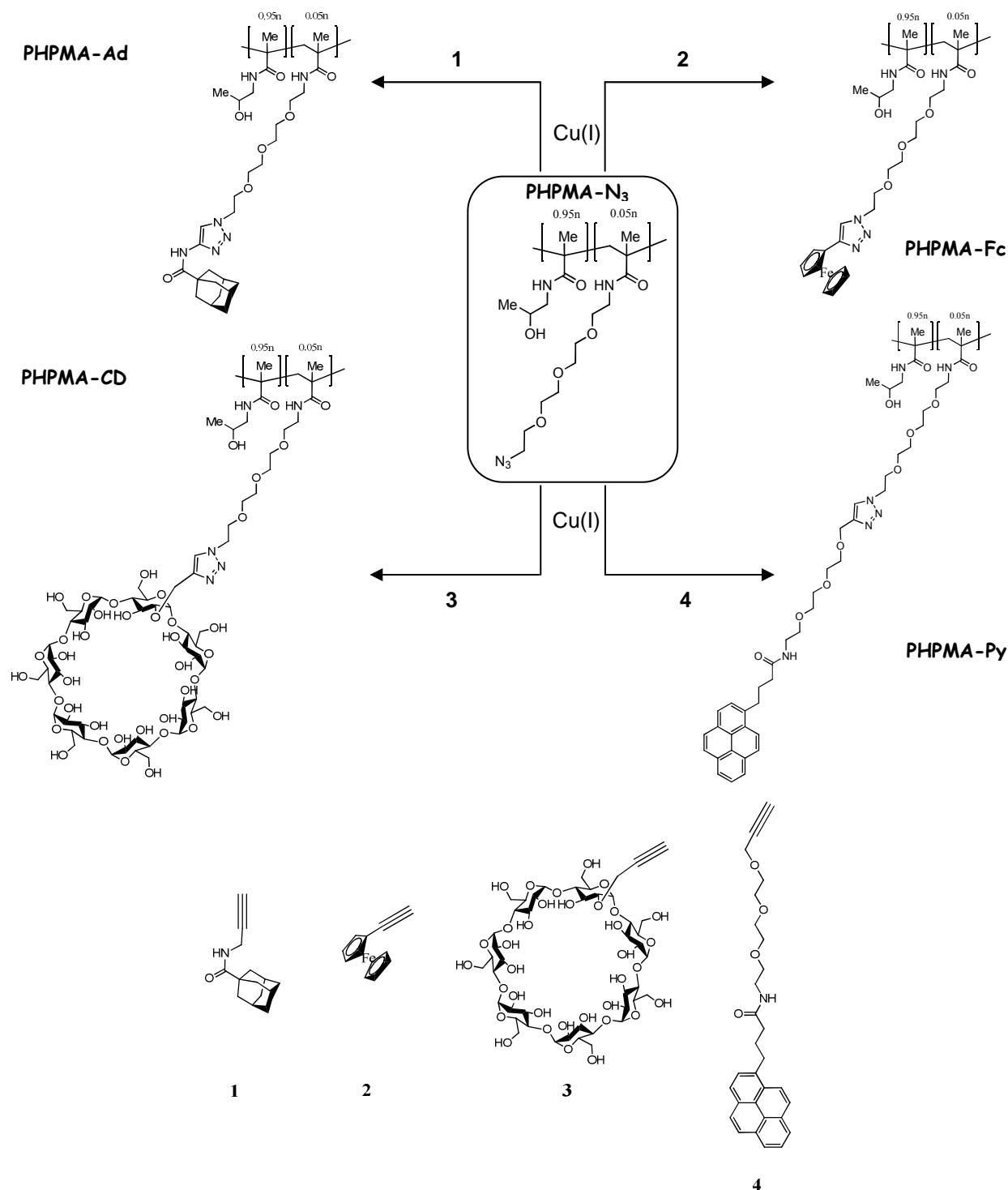
Molecular weight of all PHPMA was determined by SEC by using dynamic light scattering and refractive index: the dn/dc was determined as 0.170.

A1. Synthesis of PAH-Cd,

Poly(allylamine hydrochloride) bearing 8% β -cyclodextrin moieties, named PAH-CD, was prepared by Dr. Loïc Jierry (as well as all the other syntheses in this annexe) according to reported procedure [1].

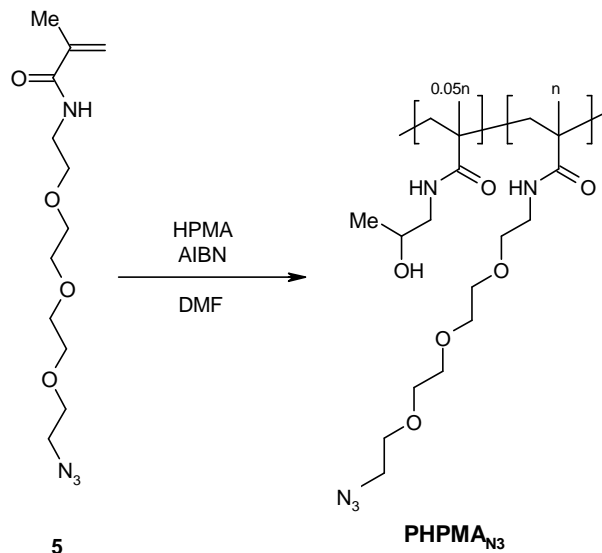
A2. Synthesis of a polymer precursor: PHPMA-N₃

The preparation of PHPMA-G (G = Ad, Fc and Py) and PHPMA-CD has been done through a convergent synthetic pathway leading to the desired polymers having all the same degree of modification (5%) and roughly the same lengths of molecular chains. Indeed, a common polymer precursor, named PHPMA-N₃ (5% of azide groups), was prepared by Dr. Loïc Jierry according to a modified synthetic procedure previously reported [2]. PHPMA-N₃ was modified by using the CuAAC click reaction in presence of the suitable alkyne derivatives **1**, **2**, **3** or **4** (Scheme S1).



Scheme S1: General synthetic pathway of both PHPMA-G (G = Ad, Fc and Py) and PHPMA-CD from PHPMA-N₃ and alkyne derivatives **1**, **2**, **3** or **4**.

PHPMA-N₃ has been prepared by radical copolymerization of hydroxypropylmethacrylamide (HPMA) and monomer **5** (Scheme S2). The synthesis of **5** was done according to reference [2].



*Scheme S2: Preparation of PHPMA-N₃ by radical copolymerization from HPMA and monomer **5**.*

A solution containing a combination of HPMA (300 mg, 2.1 mmol, purchased from Polysciences), monomer **5** (0.21 mmol) and a catalytic amount of AIBN (1.6 mg, 9.74 μ mol, purchased from Aldrich and recrystallised twice in MeOH) in DMF (2.5 mL) is degassed 20 minutes with argon and stirred for 48 hours at 60 °C. The reaction mixture is diluted with 2 mL of methanol and added dropwise to 50 mL of ethyl acetate. This precipitation step was performed twice. Then, the white solid is collected by filtration, washed with ethyl acetate and dried in vacuum. Comparison of ¹H NMR integration signals at 3.60-3.35 ppm (all CH₂ of ethylene oxide spacer) and at 2.88 ppm (NH-CH₂-CH(OH)(CH₃)) of PHPMA) gives a degree of modification of 5% \pm 1-2%.

PHPMA_{N₃} (yield = 75%)

¹H NMR (DMSO-*d*₆, 400 MHz) : 7.20 (br s, NH), 4.71 (br s, OH), 3.70 (br s, CHOH), 3.58 (br s, O-CH₂-CH₂-O), 3.49 (br s, CH₂-NH), 3.42 (br s, CH₂-CH₂-N₃), 2.88 (br s, NH-CH₂-CH(OH)(CH₃)), 1.90-1.59 (br s, C(CH₃)-CH₂-C(CH₃)), 1.00 (br s, CH₃), 0.80 (br s, CH₃) ; IR (neat) : 3313, 2980, 2925, 2110, 1640, 1590; SEC : Mn= 34040 g/mol, Mw = 92640 g/mol, PDI = 2.72.

A3. Synthesis of PHPMA-CD

PHPMA-N₃ (50 mg, 5% of N₃ groups), β-CD monoalkyne **3** (25 mg, 0.02 mmol), were prepared according to reference [3]. CuSO₄·5H₂O (2 mg, 0.008 mmol) and sodium ascorbate (3 mg, 0.015 mmol) were dissolved in Milli-Q water (3 mL). The mixture was stirred overnight at 35°C. Then, the reaction mixture was slowly added dropwise to 30 mL of acetone/Milli-Q water (19/1). The precipitate was filtered and dissolved in 2 mL of Milli-Q water. This precipitation step was repeated twice. After filtration, a greenish-white solid was isolated and dried under high vacuum 48 hours. Then, this solid was dissolved in 5 mL of Milli-Q water and dialyzed 12h against 0.5 M NaCl (1L) and Milli-Q water (1L) during 3 days (Spectra/Por, cut off at 4000-6000). Milli-Q water was changed every 24h. Freeze-dried of the dialyzed compound provide PHPMA-CD has a white solid. Comparison of ¹H NMR integration signals at 8.20 (br s, 1H, from triazole group) and at 2.98 (br s, 2H from PHPMA backbone) gives 5% of modification degree.

PHPMA-CD (yield=38%)

¹H NMR (D₂O, 400 MHz): 8.20 (s, 1H, triazole), 7.19 (br s, 1H, NH PHPMA), 5.71 (br m, H CD), 4.81 (br d, CD), 4.53 (br s, CD), 4.46 (br s, CD), 3.82 (br s, H CD), 3.66 (br s, H from EO spacer), 3.60 (br s, PHPMA), 2.98 (br s, PHPMA), 1.99-1.50 (br s, PHPMA), 1.02 (br s, PHPMA), 0.81 (br s, PHPMA); SEC: Mn= 45160 g/mol, Mw = 83420 g/mol, PDI = 1.85.

A4. Synthesis of PHPMA-Ad

To prepare PHPMA-Ad, the precursor polymer PHPMA-N₃ was brought in contact with copper(I) trifluoromethanesulfonate benzene complex (CuOTf) and alkyne derivative **1**. Compound **1** was synthesized according to reference [4]. PHPMA-N₃ (50 mg, 5% of N₃ groups), compound **1** (8.5 mg, 0.04 mmol) and copper(I) trifluoromethanesulfonate benzene complex (1 mg, 0.002 mmoles, purchased from Aldrich) were dissolved in methanol (2.5 mL) in a Schlenk tube. The mixture was degassed 20 minutes with argon and stirred overnight at 40°C under argon. Then, the reaction mixture was slowly added dropwise to 30 mL of ethyl acetate under stirring. A yellow-green precipitate is formed and filtered (size porosity 4). Then, the resulting precipitate was dissolved in methanol (2 mL). This precipitation step was repeated twice. The yellowish solid obtained was dissolved in 3 mL of Milli-Q water.

Lyophilisation of this aqueous solution provided PHPMA-Ad as white solid. By using IR spectroscopy, no bands from free azide groups (2110 cm^{-1}) of PHPAM- N_3 were detected. Thus, we considered the PHPMA-Ad substituted by 5% of adamantane moieties.

PHPMA-Ad (yield=69 %)

$^1\text{H NMR}$ (D_2O , 400 MHz): 7.97 (br s, 1H triazole), 3.97 (br s), 3.67 (br s), 3.28 (br s), 3.25 (br s), 3.13 (br s), 2.25 (br s), 2.10-1.70 (very large peak), 2.09 (br s), 1.91 (br s), 1.82 (br s), 1.24 (br s), 1.05 (br s); **SEC**: $M_n = 37530$, $M_w = 97740\text{ g/mol}$, $\text{PDI} = 2.82$.

A5. Synthesis of PHPMA-Fc

PHPMA- N_3 (50mg, 5% of N_3 groups), ethynylferrocene **2** (10 mg, 0.05 mmol purchased from Aldrich) and copper trifluoromethanesulfonate benzene complex (1mg, 0.002 mmoles purchased from Aldrich) were dissolved in methanol (2.5 mL) in a Schlenk tube. The mixture was degassed 20 minutes with argon and stirred overnight at 40°C under argon. Then, the reaction mixture was slowly added dropwise to 30 mL of ethyl acetate. The red precipitate was filtered and dissolved again in methanol (2 mL). This precipitation step was repeated twice. The red solid obtained was dissolved in 3 mL of Milli-Q water and pass through a very short amount of celite (filtration). Lyophilisation of the aqueous solution provided PHPMA-Fc as red solid. By using IR spectroscopy, no bands corresponding to $\text{C}\equiv\text{C}$ bond (2117 cm^{-1}) from ethynylferrocene **2** and no bands from free azide groups (2110 cm^{-1}) were detected. Furthermore, by $^1\text{H NMR}$ spectroscopy, it is possible to distinguish signals belonging to the free ethynylferrocene compound **2** than those from PHPMA-Fc: in our case, no traces of the starting ethynylferrocene **2** were observed. Thus, we considered the PHPMA-Fc substituted by 5% of ferrocene moieties.

PHPMA-Fc (yield=30%)

$^1\text{H NMR}$ ($\text{DMSO-}d_6$, 400 MHz): 8.07 (br s, H triazole) 7.40 (br s, NH), 4.80 (br s, OH), 4.54 (br s, $2\times\text{CH}$ substituted cyclopentadiene), 4.32 (br s, $2\times\text{CH}$ substituted cyclopentadiene), 4.05 (br s, $5\times\text{CH}$ cyclopentadiene), 3.70 (br s, CHOH), 3.60-3.40 (br m, $\text{O-CH}_2\text{-CH}_2$ from the EO linker overlapped with H_2O in $\text{DMSO-}d_6$), 3.10 (br s, $\text{NH-CH}_2\text{-CH(OH)(CH}_3\text{)}$), 2.10-1.60 (br s, $\text{C(CH}_3\text{)-CH}_2\text{-C(CH}_3\text{)}$), 1.20 (br s, CH_3), 0.90 (br s, CH_3); **SEC**: $M_n = 37130\text{ g/mol}$, $M_w = 90590\text{ g/mol}$, $\text{PDI} = 2.44$.

A6. Synthesis of PHPMA-Py

To prepare PHPMA-Py, the precursor polymer PHPMA-N₃ was brought in contact with CuOTf and alkyne-pyrene derivative **2**. Compound **2** is prepared by coupling reaction between 1-pyrenebutyric acid and compound **5** (**5** has been prepared according to reference [5]).

1-pyrenebutyric acid (1.0 equiv., 288 mg, 1.00 mmoles) is dissolved in 3 mL CH₂Cl₂ at 0°C. First 1-hydroxybenzotriazole (HOBt.2H₂O) (0.4 equiv., 68 mg, 0.4 mmoles) and *N*-(3-dimethylaminopropyl)-*N*-ethylcarbodiimide hydrochloride (EDCI) (1.5 equiv., 287.5 mg, 1.5 mmoles) are added as a solid directly to the reaction mixture under stirring. Compound **5** (1 equiv., 223.5 mg, 1 mmoles) is added following by the addition of pyridine (1 mL). The mixture is stirred overnight and the temperature is increased slowly from 0°C to 25°C. At 0°C, 5 mL HCl 10% is added drop by drop into the reaction mixture and the organic layer is washed with 2 × 3 mL distilled water, treated with 5 mL of saturated NaHCO₃, washed with 2 × 3 mL distilled water and finally dried with MgSO₄. After removal of organic solvent under reduced pressure, the residue is purified by chromatography using the following conditions as eluent: from ethyl acetate/CH₂Cl₂ 6/4 to 4/6 (R_f = 0.2). The compound **2** is isolated as an orange oil with 51% yield (230 mg, 0.55 mmoles).

¹H NMR (CDCl₃, 400 MHz) : 8.31 (d, 1H, ³J=20.5 Hz), 8.16 (d, 1H, ³J=12.5 Hz), 8.15 (d, 1H, ³J=12.5 Hz), 8.11 (d, 1H, J=1 Hz), 8.08 (broad s, 1H), 8.02 (broad s, 1H), 7.95 (d, 1H, ³J=7.5 Hz), 7.85 (d, 1H, ³J=7.5 Hz), 7.87 (d, 1H, ³J=8.0 Hz), 6.08 (broad s, 1H), 4.12 (d, 2H, ⁴J=2.1 Hz), 3.58 (s, 8H), 3.55 (broad d, 2H, ³J=6.0 Hz), 3.48 (m, 2H), 3.40 (t, 2H, ³J=7.0 Hz), 2.39 (t, 1H, ⁴J=2.1 Hz), 2.31 (m, 3H), 2.22 (m, 3H); ¹³C NMR (CDCl₃, 100 MHz) : 172.71, 136.01, 131.42, 130.92, 129.91, 128.78, 127.50, 127.36, 127.35, 126.68, 125.85, 125.08, 124.99, 124.89, 124.80, 124.76, 123.46, 79.55, 74.68, 70.45, 70.26, 70.13, 69.85, 69.04, 58.35, 39.21, 35.98, 32.80, 27.45.

PHPMA-N₃ (50 mg, 5% of N₃ groups), compound **2** (26 mg, 0.056 mmol) and copper trifluoromethanesulfonate benzene complex (2 mg, 0.004mmoles, purchased from Aldrich) were dissolved in methanol (2.5 mL) in a Schlenk tube. The mixture was degassed 20 minutes with argon and stirred 35°C under argon during 24 hours. Then, the reaction mixture was slowly added dropwise to 30 mL of ethyl acetate. The red precipitate was filtered and dissolved again in methanol (2 mL). This precipitation step was repeated twice. The greenish

solid obtained was suspended in 10 mL of Milli-Q water, dialyzed with 1 M NaCl during 24 h and five days again MilliQ water (Spectra/Por cut off 4000-6000). Lyophilisation of the dialyzed solution provided PHPMA-Py as a white solid. By using IR spectroscopy, no bands from free azide groups from starting PHPMA-N₃ (2110 cm⁻¹) were detected. Thus, we considered the PHPMA-Py substituted by 5% of pyrene moieties.

PHPMA-Py (yield=45%)

¹H NMR (DMSO-*d*₆, 400 MHz): 8.50-8.00 (br m, H aromatic from pyrene ring), 7.95 (br s, H triazole), 7.17 (br s, NH PHPMA), 4.69 (br s), 4.10 (br s), 3.71 (br s), 3.55 (br s), 3.45 (br s), 2.98 (br s), 2.00-1.50 (very br s), 1.01 (br s), 0.85 (br s); **SEC**: Mn= 36460 g/mol, Mw = 69300 g/mol, PDI = 1.91.

Annexe A references

1. Dubacheva, G.V., et al., Unlimited growth of host-guest multilayer films based on functionalized neutral polymers, *Soft Matter*, **2010**, 6 (16), 3747-3747.
2. Jierry, L., et al., Influence of Cu(I)-Alkyne pi-Complex Charge on the Step-by-Step Film Buildup through Sharpless Click Reaction, *Macromolecules*, **2010**, 43 (8), 3994-3997.
3. Casas-Solvas, J.M., et al., Ferrocene-beta-Cyclodextrin Conjugates: Synthesis, Supramolecular Behavior, and Use as Electrochemical Sensors, *Chemistry-a European Journal*, **2009**, 15 (33), 8146-8162.
4. Hashmi, A.S.K., et al., Gold catalysis: Mild conditions for the synthesis of oxazoles from N-propargylcarboxamides and mechanistic aspects, *Organic Letters*, **2004**, 6 (23), 4391-4394.
5. Norberg, O., et al., Photo-Click Immobilization of Carbohydrates on Polymeric Surfaces-A Quick Method to Functionalize Surfaces for Biomolecular Recognition Studies, *Bioconjugate Chemistry*, **2009**, 20 (12), 2364-2370.

Annexe B:

Syntheses of modified HA and CHI

Summary

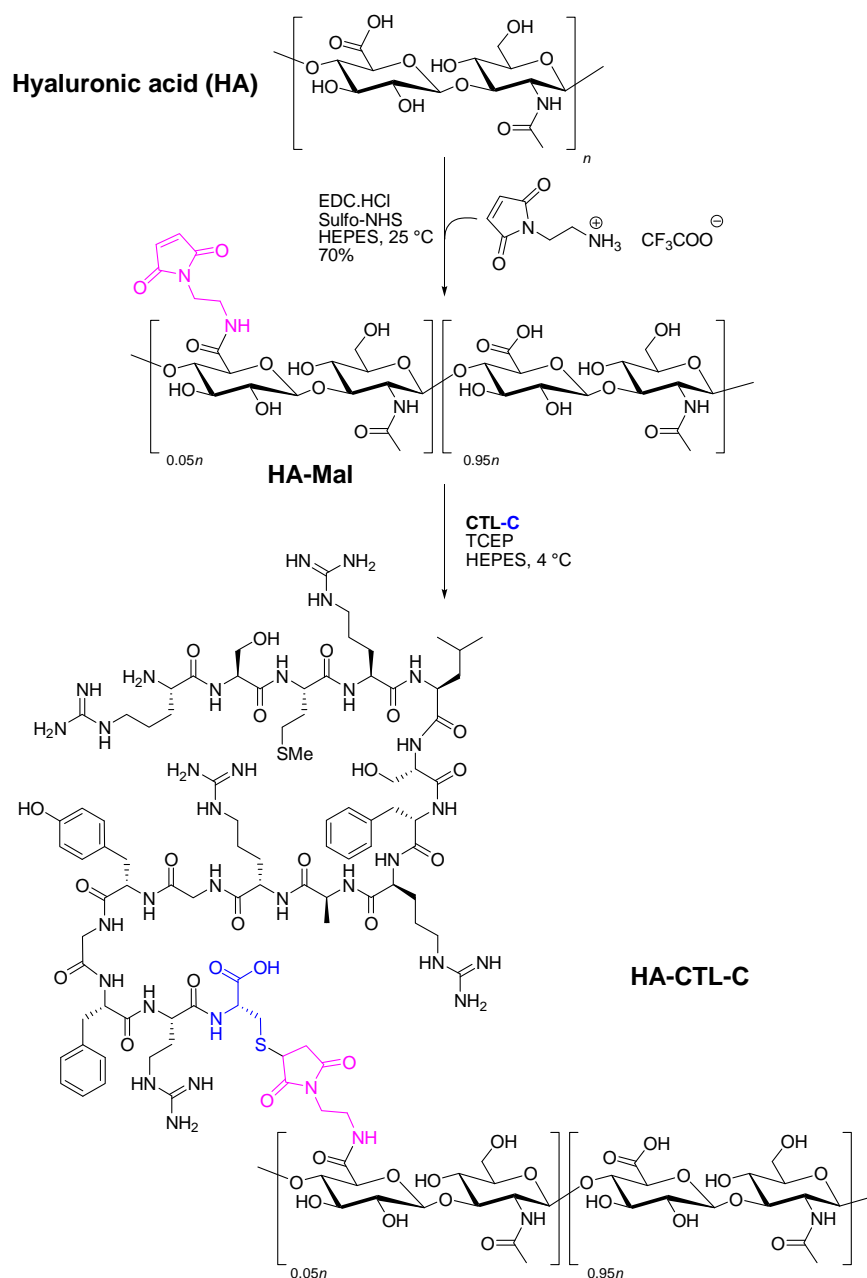
B1. Synthesis of HA-CTL-C	204
B2. Synthesis of HA^{FITC}	206
B3. Synthesis of HA^{FITC}-CTL-C.....	206
B4. Synthesis of CHI-SH.....	206
B5. Synthesis of HA-P	207
B6. Synthesis of HA-P-CTL-C	207
B7. Synthesis of PAH-CTL-C.....	207
Annexe B references.....	209

B1. Synthesis of HA-CTL-C

Hyaluronic acid (HA) 420 000 Da, was functionalized with maleimide group according to previously reported method [1]. HA (100.9 mg) was dissolved in 15 mL of 0.01M HEPES buffer (pH 6). EDC (35.2 mg) and sulfo-NHS (10.2 mg) were added to this solution and the resulting mixture was stirred 2 h at room temperature. Afterwards, N-(2-aminoethyl) maleimide trifluoroacetate salt (6.7 mg) was added to the reaction mixture and let stirred for 20 h. The mixture was dialyzed (cut-off 12 000-14 000 Da) first against 0.5 M NaCl for one day and MilliQ water for 6 days. Water was changed every day. HA-Mal (86 mg) was obtained as a white solid after freeze-drying. The degree of substitution (DS) of HA-Mal, defined as the number of maleimide groups per 100 disaccharide unit of HA, was determined by ^1H NMR (D_2O , 400 MHz). All spectra were realized in D_2O containing 5% of *t*BuOH: the singlet of the *t*-butyl group of *t*BuOH was calibrated at δ 1.24 ppm and thus used as internal reference. The singlet at δ 7.1 ppm was assigned to the two symmetric protons on the double bond of the maleimide group. By comparing the integration of this signal with the singlet at δ 2.0 ppm, assigned to the methyl protons of the acetamide group, the DS was determined equivalent to 5%.

^1H NMR (D_2O , 400MHz, δ ppm): δ 6.9 (s, maleimide), 4.5 (br d, HA), 3.5 (m), 2.0 (s, acetyl group of HA).

The coupling reaction between HA-Mal 5% (80 mg) and CTL-C (10.1 mg) was performed at 4°C for 20 h in 16mL of 0.01M HEPES buffer (pH 6) and 50 μM of TCEP. Then, the mixture was dialyzed (cut-off 50 000Da) against 0.5 M NaCl for one day and MilliQ water for 6 days. Water was changed every day. Peptide-conjugated HA, named HA-CTL-C, was freeze-dried to provide a white solid with 80-85% of overall yield (\approx 79 mg). The DS, defined as the number of CTL-C peptide per 100 disaccharide units of HA, was determined by ^1H NMR (D_2O , 400 MHz). All aromatic signals between δ 7.0 and 7.5 ppm corresponding to the protons of the aminoacids Phe and Tyr were compared to the singlet at δ 2.0 ppm (assigned as the methyl group of the acetamide). A DS of 5% is determined.



^1H NMR (D_2O , 400MHz, δ ppm): 7.35 (br s, Ar aminoacid of CTL-C), 7.25 (br s, Ar aminoacid of CTL-C), 7.10 (br s, Ar aminoacid of CTL-C), 6.85 (br s, Ar aminoacid of CTL-C), 4.50 (br s, HA), 4.40 (br s, CTL-C), 3.10 (br s, CTL-C), 2.50 (br s, CTL-C), 2.00 (s, methyl from acetyl group of HA), 1.75 (br s, CTL-C), 0.95 (br s, CTL-C).

B2. Synthesis of HA^{FITC}

Fluorescein Isothiocyanate (FITC) has been covalently attached to HA according to the following procedure: a solution of FITC (41 μmol dissolved in 2 mL of DMSO) and a solution of HA (0.31 μmol dissolved in 18 mL of deionized water) were mixed. The resulting solution was then adjusted at pH 9 by using a 0.01M NaOH solution. The reaction mixture was stirred for 12 h at room temperature. Then, 40 mL of deionized water was added and this final mixture was dialyzed (cut-off: 12 000 – 14 000 Da) against deionized water until no absorbance was detected in the water ($\lambda = 494 \text{ nm}$). The obtained compound is a yellowish solid and corresponds to functionalized HA by 1% of fluorescein. The $^1\text{H NMR}$ (D_2O) spectra of HA^{FITC} is identical to the non-modified HA. Because of the very low loading of fluorescein on HA, the $^1\text{H NMR}$ (D_2O) spectra of HA^{FITC} is identical to the non-modified HA.

B3. Synthesis of HA^{FITC}-CTL-C

HA^{FITC}-CTL-C polymer has been prepared from HA-Mal. This polymer was labeled with 1% FITC as described above to provide HA^{FITC}-Mal. Then, CTL-C peptide reacted with free maleimide group to lead to HA^{FITC}-CTL-C as a yellow solid. The procedure used to get HA^{FITC}-CTL-C was identical to the one described above to prepare HA-CTL-C. $^1\text{H NMR}$ (D_2O) spectra of HA^{FITC}-CTL-C was identical to the spectra of HA-CTL-C.

B4. Synthesis of CHI-SH

Chitosan was chemically modified by thiol groups (CHI-SH) at 5% in grafting ratio by Benoit Frisch's team. To a solution of chitosan (250 mg, 1.55 mmol) in HCl 1M (2 mL) were added deionized water (25 mL), N-ethyl-N'-(3-dimethylaminopropyl)carbodiimide hydrochloride (239 mg, 1.25 mmol), mercaptopropionic acid (12 mg, 0.108 mmol) and N-hydroxysulfosuccinimide sodium salt (78 mg, 0.36 mmol). After three days of stirring at room temperature, the reaction medium was dialyzed, first against deionized water (with HCl 5mM) during 12 h, then twice against deionized water containing 5 mM HCl and 1% wt NaCl during 12 h and finally against 1mM HCl for 12 h. Water was freeze-dried to provide 216 mg of CHI-SH. $^1\text{H NMR}$ (300 MHz, D_2O): 3.78-3.33 (m, 5H), 3.04-2.92 (m, 2H), 1.87 (s, 0.2H). The proportion of thiol groups along HA was determined by comparison of the $^1\text{H NMR}$

integrations of the broad peak at 3.04-2.92 ppm (CH_2 in C6 position of the sugar unit of chitosan) and the integration of the peak at 1.87 ppm ($\text{CH}_2\text{-CH}_2$) from the pyridine disulfide group.

B5. Synthesis of HA-P

HA was modified by pyridine disulfide groups (HA-P) at 5% in grafting ratio by Benoit Frisch's team. To a solution of HA (150 mg, 0.359 mmol) in deionized water (10 mL), were added N-ethyl-N'-(3-dimethylaminopropyl)carbodiimide hydrochloride (68 mg, 0.359 mmol), N-hydroxysulfosuccinimide sodium salt (78 mg, 0.359 mmol), diisopropylethylamine (4 μL , 0.002 mmol) and 2-(2-pyridyldithio)ethylamine (5.56 mg, 0.025 mmol). After 24 h of stirring at room temperature, the reaction medium was dialyzed, first against deionized water containing 1% wt NaCl during 12 h and then twice against pure milli Q water during 12 h. Water was freeze-dried providing 150 mg of HA-P. ^1H NMR (300 MHz, D_2O): 8.36 (m, 0.05H), 7.79 (m, 0.10H), 7.25 (m, 0.05H), 4.47-3.24 (m, 12H), 2.84-2.78 (m, 0.2H), 1.92 (s, 3H). The proportion of pyridine disulfide groups along HA was determined by comparison of the ^1H NMR integrations of the peak at 1.92 ppm (acetyl group from HA) and the integration of the broad peak at 2.84-2.78 ppm ($\text{CH}_2\text{-CH}_2$) from the pyridine disulfide group.

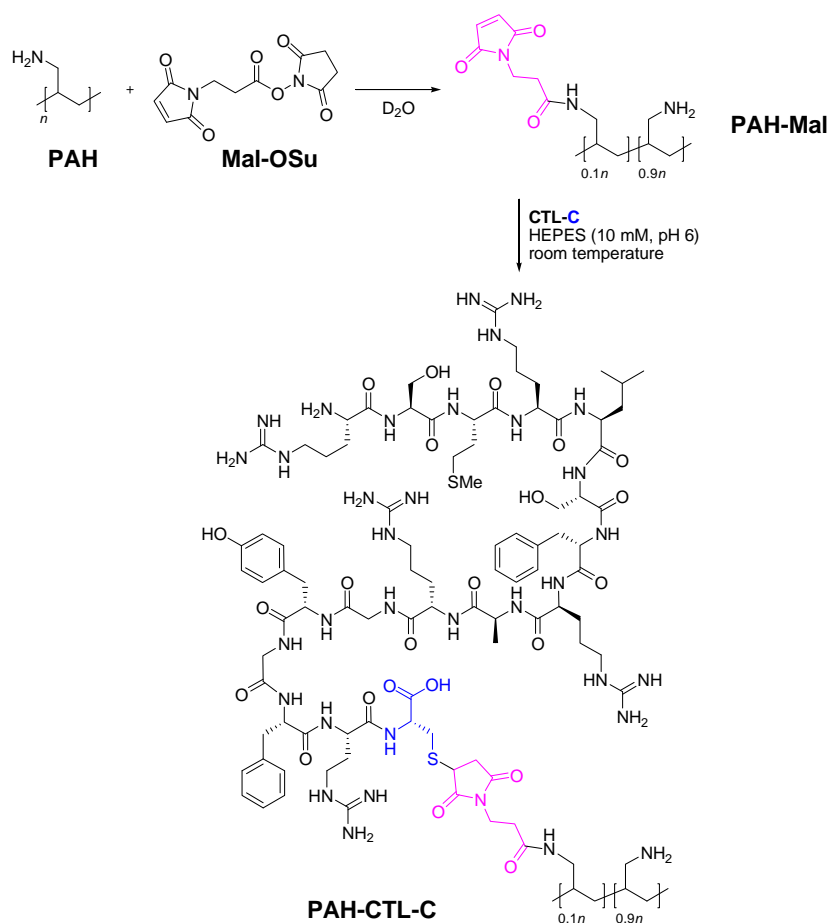
B6. Synthesis of HA-P-CTL-C

The coupling reaction between HA-P 5% (27.9 mg) and CTL-C (2.0 mg) was performed the same way that the coupling reaction between HA-Mal 5% and CTL-C, i.e. at 4°C for 20 h in a 0.01M HEPES buffer (pH 6) and 50 μM of TCEP. Then, the mixture was dialyzed (cut-off 50 000Da) against 0.5 M NaCl for one day and MilliQ water for 6 days. Water was changed every day.

B7. Synthesis of PAH-CTL-C

To a solution of PAH (22.16 mg) in D_2O (0.6 mL) was added Mal-OSu (15 mg). The resulting mixture was stirred mechanically at room temperature until RMN monitoring indicated total consumption of the reagent (48 h). Evaporation of solvent provided the desired PAH-Mal (27 mg) as a white solid which was used without further purification. The DS of

PAH-Mal was determined by ^1H NMR (400MHz, D_2O) and defined as the number of maleimide groups per 100 allylamine units of PAH. NMR Spectrum was realized in D_2O and calibrated at δ 4.79 ppm (residual water). The singlet at δ 6.9 ppm was assigned to the two symmetric protons on the double bond of the maleimide group. By comparing the integration of this signal with the singlet at δ 3.1 ppm, assigned to the $\text{CH}_2\text{-NH}$ protons of the allylamine group, the DS was determined equivalent to 10%.



^1H NMR (D_2O , 400MHz, δ ppm): δ 6.9 (s, maleimide), 3.8 (t, Mal- $\text{CH}_2\text{-CH}_2\text{-CO}$), 3.1 (br s, CH_2 of PAH), 2.7 (t, Mal- $\text{CH}_2\text{-CH}_2\text{-CO}$), 2.1 (br s, CH of PAH), 1.6 (br s, CH_2 of PAH).

The coupling reaction between PAH-Mal 10% (1.5 mg) and CTL-C (15.6 mg) was performed overnight at room temperature in 0.6 mL of 10 mM HEPES buffer solution in D_2O (pH 6). Then, the mixture was dialyzed (cut-off: 12 000 – 14 000 Da) against MilliQ water for 6 days (water was changed every day). Peptide-conjugated PAH, named PAH-CTL-C, was

freeze dried to provide a white solid (17 mg). This quantitative yield and the ^1H NMR described below allowed us to define a 10% DS (number of CTL-C peptide per 100 allylamine units of PAH).

^1H NMR (D_2O , 400MHz, δ ppm): 7.35 (br s, Ar aminoacid of CTL-C), 7.25 (br s, Ar aminoacid of CTL-C), 7.13 (br s, Ar aminoacid of CTL-C), 6.86 (br s, Ar aminoacid of CTL-C), 3.67-4.68 (m, CTL-C), 3.10 (br m, PAH and CTL-C), 2.50-2.68 (br m, CTL-C), 1.34-2.18 (br m, PAH and CTL-C), 0.96 (br s, CTL-C).

Annexe B references

1. Wall, S.T., et al., Multivalency of Sonic hedgehog conjugated to linear polymer chains modulates protein potency, *Bioconjugate Chemistry*, **2008**, 19 (4), 806-812.

Résumé de thèse en français

1 Introduction

La surface d'un biomatériau est le lieu privilégié des interactions avec son environnement (matrice extracellulaire, cellules, etc...). Le principal défi consiste à maîtriser ces interactions par la fonctionnalisation de surface. La méthode de fonctionnalisation de surface la plus étudiée et la plus simple à mettre en œuvre est le dépôt couche par couche (layer-by-layer en anglais, LbL). Introduite par Gero Decher au début des années 1990 [1], cette technique permet d'obtenir des films multicouches par interactions électrostatiques et grâce à l'excès de charges qui apparaît à la surface par adsorption alternée de polyanions, polymères chargés négativement, et de polycations, polymères chargés positivement (Figure 1). L'épaisseur des films peut être facilement contrôlée en faisant varier plusieurs paramètres tels que le nombre de couches, la masse molaire, la concentration et la nature des polyélectrolytes, le pH et la force ionique. D'autres types d'interactions telles que les liaisons hydrogènes [2], les complexes métal-ion [3] ou bien encore les interactions hôte-invité [4-7] permettent aussi la construction de films multicouches. L'intérêt des films multicouches dans le domaine des biomatériaux réside principalement dans la possibilité de pouvoir leur conférer une fonctionnalité biologique spécifique par insertion de protéines, de peptides ou de médicaments.

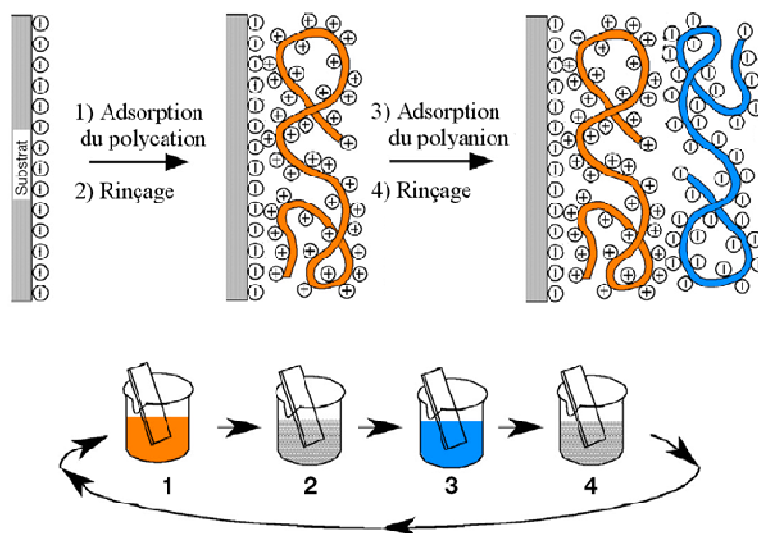


Figure 1 : Schéma simplifié de la construction de multicouches de polyélectrolytes par adsorptions successives de polycations et de polyanions suivies par un rinçage.

Mon travail de thèse comporte deux volets. Le premier volet aborde l'étude physico-chimique de films multicouches de polymères neutres basés sur des interactions de type hôte-invité, en particulier sur l'influence de la force du complexe d'inclusion sur la topographie de ces films. En collaboration avec Marie-Hélène Metz-Boutigue de l'UMR 1121 INSERM (Strasbourg), le deuxième volet traite du développement de nouveaux revêtements antimicrobiens auto-défensifs contre les infections microbiennes du *Staphylococcus aureus* (*S. aureus*) et du *Candida albicans* (*C. albicans*). La fonctionnalisation d'oligomères, de dendrimères et de polysaccharides par un peptide antimicrobien, la cateslytine, a été réalisée afin d'étudier son activité antimicrobienne ainsi que sa réponse inflammatoire en solution puis sous forme de revêtements.

2 Construction de multicouches de polymères neutres basée sur des interactions de type hôte-invité

2.1 Contexte

Comme décrit dans l'introduction, la cohésion des films multicouches repose initialement sur des interactions électrostatiques mais elle peut également être assurée par d'autres types d'interactions telles que l'interaction hôte-invité. Le terme « hôte-invité » est utilisé pour désigner un complexe d'inclusion dans lequel une molécule invitée est piégée à l'intérieur de la cavité interne d'une molécule plus large : la molécule hôte. Les forces mises en jeu sont des forces intermoléculaires. Dans le domaine biomédical et pharmaceutique, les cyclodextrines sont les molécules hôtes les plus utilisées et notamment la β -cyclodextrine (β -CD). Cette dernière peut former des complexes d'inclusion avec des molécules hydrophobes (Figure 2) dont l'adamantane (AD), le ferrocène (Fc) ou encore le pyrène (Py).

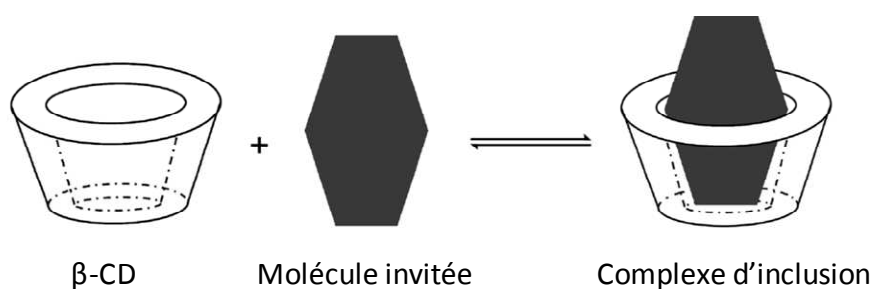


Figure 2 : Représentation schématique de la formation d'un complexe d'inclusion (1:1) entre la β -cyclodextrine (β -CD) et une molécule invitée.

Dans la littérature, la construction de différents films multicouches basés sur des interactions hôte-invité a été décrite. Dans ces études, deux polycations, l'un modifié par la β -cyclodextrine et l'autre par un groupement invité, ont été déposés successivement. Cependant, à cause des répulsions électrostatiques entre les chaînes identiquement chargées, le nombre de dépôts atteints était limité à 2 ou 3 bicouches [5, 6]. En 2010, notre groupe a utilisé un polymère neutre, le poly(N-hydroxypropylmethacrylamide) (PHPMA), modifié par des groupements β -cyclodextrine (β -CD) et ferrocène (Fc) afin de construire un film multicouche de 15 bicouches [7].

A ce jour, aucune caractérisation structurale n'a été réalisée sur ce type de films multicouches dont la cohésion est maintenue par interactions hôte-invité. Nous nous sommes donc intéressés à la construction de films multicouches de polymères neutres basée sur des interactions de type hôte-invité et en particulier à l'influence de la force du complexe d'inclusion sur la topographie de ces films multicouches.

2.2 Modulation de la force du complexe d'inclusion grâce à l'invité

Dans un premier temps, nous nous sommes intéressés à l'influence de l'invité sur la force du complexe d'inclusion. Le pyrène (Py), le ferrocène (Fc) et l'adamantane (Ad) ont été choisis comme molécules invitées sachant qu'en solution, l'interaction hôte-invité du complexe d'inclusion augmente dans cet ordre : $\text{Py}/\beta\text{-CD} < \text{Fc}/\beta\text{-CD} < \text{Ad}/\beta\text{-CD}$. La synthèse de polymères neutres portant le groupement β -CD (PHPMA-CD) ou les trois molécules invitées (PHPMA-Fc, PHPMA-Py et PHPMA-AD) a été réalisée avec un taux de greffage de 5% sur un même PHPMA (Figure 3). Un polycation possédant des groupements β -CD (PAH-CD) a également été synthétisé pour servir de couche d'accroche et promouvoir la construction du film multicouche.

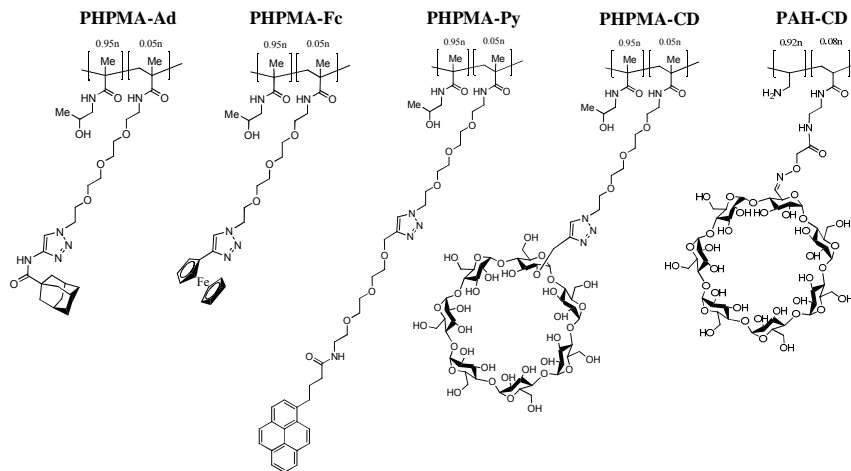


Figure 3: Structures chimiques des polymères neutres fonctionnalisés : PHPMA-Ad, PHPMA-Fc, PHPMA-Py, PHPMA-CD et PAH-CD.

Les films multicouches ont été construits selon la technique de dépôt couche par couche, c'est-à-dire en déposant alternativement une couche de PHPMA-CD et une couche de PHPMA portant un groupement Fc, Py ou AD. Leur construction a été suivie par microbalance à cristal de quartz (QCM) et leur topographie a été déterminée par microscopie à force atomique (AFM).

Dans le cas du système PHPMA-CD/PHPMA-Py, la construction du film est limitée et seulement quelques agrégats sont obtenus. Dans le cas des films PHPMA-CD/PHPMA-Fc et PHPMA-CD/PHPMA-Ad, le film multicouche croît de manière linéaire. Des films lisses, avec une rugosité inférieure à 20 % de l'épaisseur, sont obtenus dans le cas du PHPMA-CD/PHPMA-Fc alors que des films rugueux de type « gouttelettes » (rugosité supérieure à l'épaisseur) sont obtenus dans le cas du PHPMA-CD/PHPMA-Ad (Figure 4).

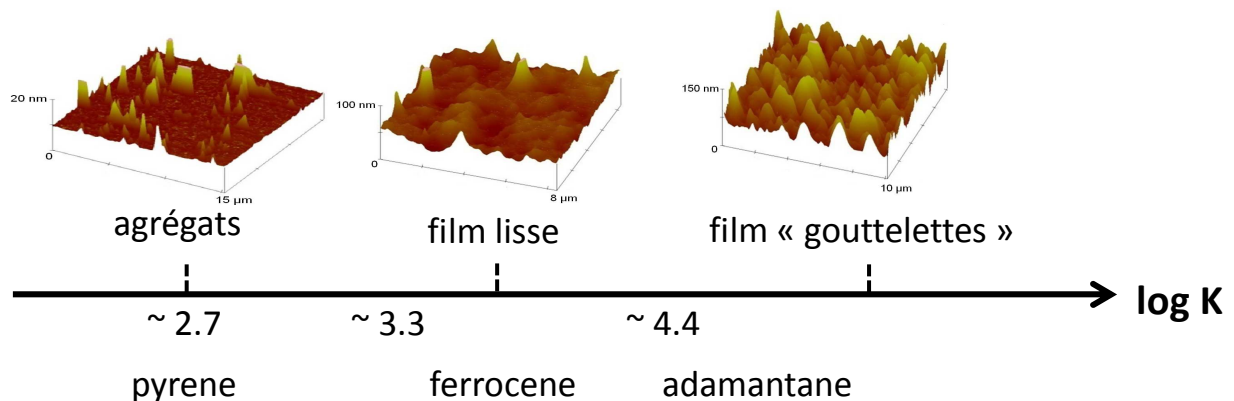


Figure 4 : Représentation schématique de l'influence de l'invité G sur la topographie des films multicouches PHPMA-CD/PHPMA-G.

2.3 Modulation de la force du complexe d'inclusion Fc/ β -CD

Dans un deuxième temps, nous avons étudié l'influence de la force du complexe d'inclusion sur la topographie de films multicouches (PHPMA-Fc/PHPMA-CD) en jouant sur la présence de sels de sodium et leur force ionique. En effet, il est rapporté dans la littérature que les sels ainsi que leur force ionique ont une influence sur l'affinité entre AD et β -CD. Cependant, rien n'est décrit sur le couple Fc/ β -CD. Nous avons donc d'abord étudié par titration calorimétrique isotherme (ITC) l'influence sur l'affinité du couple Fc/ β -CD de différents sels de sodium (NaF, Na₂SO₄, NaSCN et NaClO₄) et à différentes forces ioniques (0 à 1 M) (Figure 5). Nous avons obtenu deux comportements différents (Figure 5). Dans le cas d'ions chaotropes tels que SCN⁻ et ClO₄⁻, la constante d'affinité entre le ferrocène et la β -cyclodextrine diminue avec la force ionique tandis que dans le cas d'ions cosmotropes tels que F⁻ et SO₄²⁻, elle augmente avec la force ionique. Ces résultats indiquent qu'il est possible de moduler l'affinité du couple Fc/ β -CD par la présence de sels de sodium et par leur force ionique.

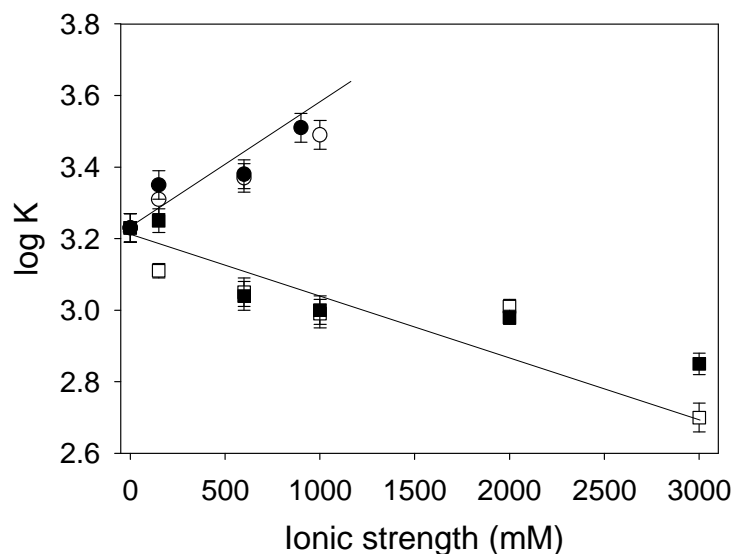


Figure 5: Constantes d'affinité ($\log K$) de $Fc(MeOH)_2/\beta$ -CD, mesurées par ITC, en fonction de la force ionique du sel (●) NaF, (○) Na₂SO₄, (■) NaSCN et (□) NaClO₄.

Afin d'étudier de manière systématique l'influence de la force d'interaction hôte-invité sur la topographie des films, des films multicouches PHPMA-CD/PHPMA-Fc ont été construits en présence de différents sels de sodium (Na₂SO₄, NaF, NaClO₄ et NaSCN) et à différentes forces ioniques (0 à 3 M). Pour de faibles interactions entre Fc et β -CD, lors de la

construction de films PHPMA-CD/PHPMA-Fc, seuls quelques agrégats se déposent sur le substrat. Quand l'interaction augmente, la rugosité du film diminue et conduit à la formation de films lisses alors que des films rugueux sont observés pour les fortes interactions entre Fc et β -CD (Figure 6 et Figure 7).

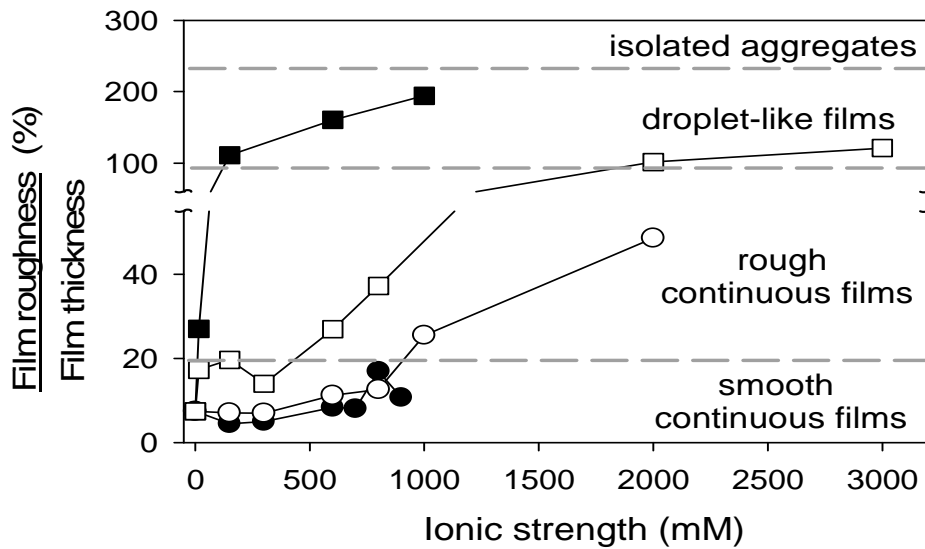


Figure 6 : Evaluation du rapport de la rugosité sur l'épaisseur d'un film PAH-CD(PHPMA-Fc/PHPMA-CD)₇ en fonction de la force ionique de (●) NaF, (○) Na₂SO₄, (■) NaSCN et (□) NaClO₄. Le film a été construit en présence de 10 mM HEPES à pH 7,4 et à une concentration en polymères de 0,1 mg.mL⁻¹.

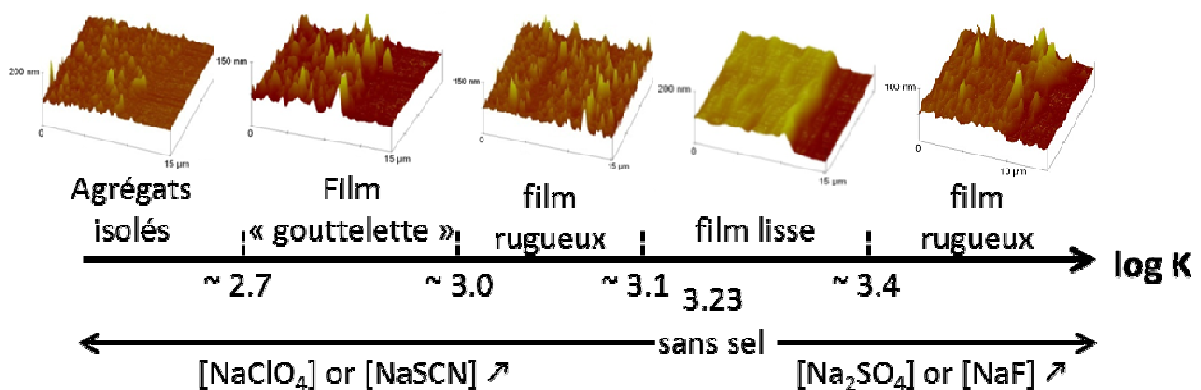


Figure 7 : Morphologies 3D, obtenues par AFM en mode contact en milieu liquide, de films PAH-CD-(PHPMA-Fc/PHPMA-CD)₇ construits pour différentes valeurs de constante d'affinité Fc/ β -CD.

3 Développement de nouveaux revêtements antimicrobiens

3.1 Contexte

De nos jours, la mise en place de dispositifs médicaux dans le corps humain tels que les cathéters concerne des actes hospitaliers de base répétés quotidiennement. Ces dispositifs sont souvent la voie d'accès pour les infections bactériennes pouvant entraîner des septicémies voire le décès du patient. La prévention de la colonisation bactérienne d'implants et des dispositifs médicaux constitue donc un enjeu médical et financier majeur. *S. aureus* est l'un des pathogènes les plus virulents développés dans le cas de maladies nosocomiales. *C. albicans* est une levure qui est également couramment rencontrée. De plus associée à *S. aureus*, *C. albicans* peut accroître les effets néfastes de l'infection.

3.2 Revêtement antibactérien et antifongique auto-défensif

Différents revêtements antibactériens ont été développés pour limiter les infections au niveau des dispositifs médicaux [8]. Cependant, peu de revêtements incluent à la fois des propriétés antibactériennes et antifongiques. Ainsi, nous avons développé un revêtement antibactérien et antifongique auto-défensif composé de films multicouches de polysaccharides libérant des peptides antimicrobiens uniquement en présence d'agents pathogènes (Figure 8).

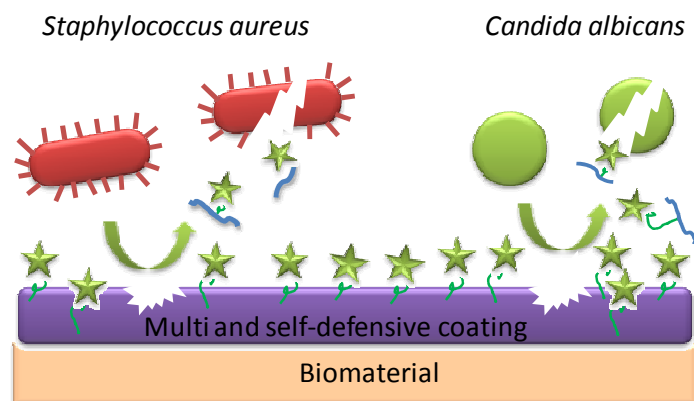


Figure 8 : Représentation schématique d'un revêtement antimicrobien auto-défensif.

Dérivée de la chromogranine A, la cateslytine (CTL) est un peptide à la fois antibactérien et antifongique ayant des propriétés anti-inflammatoires. Ainsi son utilisation se

révèle prometteuse dans le traitement des maladies nosocomiales. Nous avons choisi d'utiliser le chitosan (CHI) en tant que polycation et l'acide hyaluronique (HA) en tant que polyanion pour la construction du film multicouche. Il s'agit en effet de deux polysaccharides qui sont largement utilisés dans le domaine biomédical car biocompatibles et ils possèdent également l'avantage d'être dégradables par des enzymes secrétées par *S. aureus* et *C. albicans*. La CTL a été greffée sur le HA (HA-CTL) avant d'être immobilisée à la surface d'un matériau par un dépôt couche par couche. Au bout de 24 h, la croissance de *S. aureus* et *C. albicans* est inhibée à 100% au contact d'un film (CHI/HA-CTL)_n de respectivement 30 et 15 bicouches. Des observations en microscopie confocale ont permis de mettre en évidence la dégradation des films et la pénétration du peptide libéré dans les pathogènes. Ces films au contact de cellules humaines ne présentent aucune toxicité mais montrent des propriétés d'anti-adhérence ce qui en fait un revêtement de choix pour la fonctionnalisation d'implants médicaux temporaires tels que les cathéters.

Dans le but d'utiliser ce revêtement auto-défensif à la surface de cathéters, il est nécessaire de procéder à quelques améliorations. Deux améliorations principales ont été étudiées dans le cadre de cette thèse.

La première amélioration visée a été l'augmentation des propriétés antimicrobiennes du peptide initialement utilisé. En effet, le dépôt couche par couche est un procédé coûteux en terme de temps; par exemple pour élaborer le film multicouche possédant les 30 bicouches nécessaires pour inhiber totalement la croissance de *S. aureus* en 24 h, il faut un temps minimum 10 heures. Pour diminuer le temps d'élaboration d'un film, il est donc nécessaire de diminuer le nombre de bicouches, c'est-à-dire d'augmenter les propriétés antimicrobiennes de chaque bicouche et donc finalement du peptide initialement utilisé (Figure 9).



Figure 9 : Représentation schématique de l'ancien revêtement incluant la cateslytine comme peptide antimicrobien (à gauche) et du nouveau revêtement incluant le nouveau peptide à définir possédant de meilleures propriétés antimicrobiennes que la cateslytine et permettant ainsi d'élaborer un film multicouche avec un nombre de bicouches inférieur pour une même efficacité (à droite).

La deuxième amélioration visée est l'augmentation de la rigidité mécanique du revêtement. En effet, la cohésion du revêtement est basée jusque-là sur des interactions électrostatiques et comme il est nécessaire d'augmenter sa tenue mécanique pour l'utiliser sur un cathéter, nous avons cherché à attacher le revêtement de façon covalente sur le cathéter et également à réticuler les polymères constituant la multicouche entre eux (Figure 10).

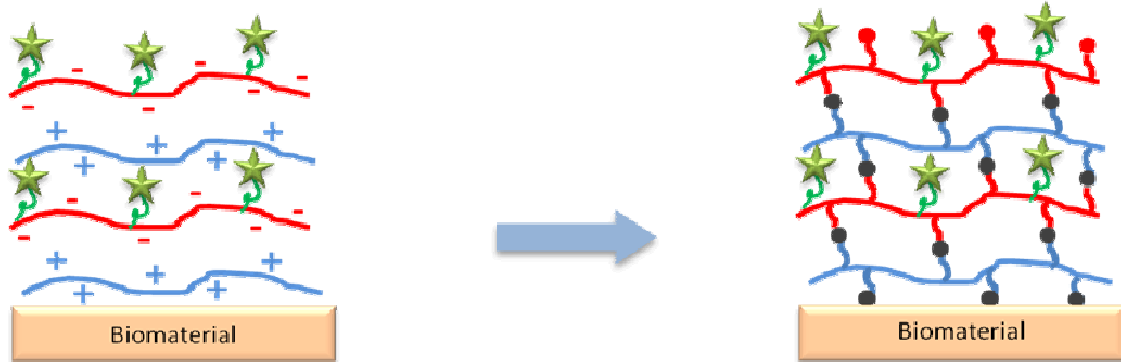


Figure 10 : Représentation schématique de l'ancien revêtement dont la cohésion est assurée par des interactions électrostatiques (à gauche) et du nouveau revêtement attaché de façon covalente sur le cathéter et dont la cohésion est assurée par des liaisons covalentes (à droite).

3.3 Amélioration des propriétés antimicrobiennes de la CTL-C : dimères et dendrimère de CTL-C

Afin d'augmenter les propriétés initiales de la CTL-C, deux stratégies ont été développées. La première idée a été d'utiliser un peptide similaire à la CTL-C mais en remplaçant les acides aminés naturellement L par des acides aminés en conformation D (Figure 11).

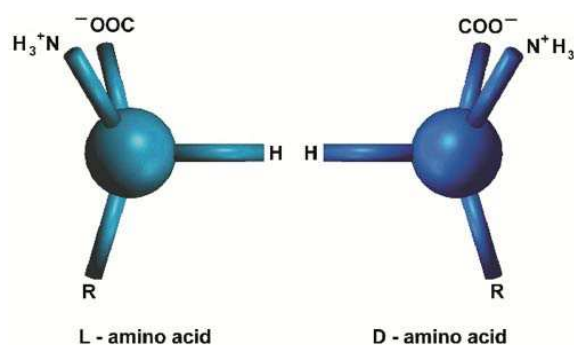


Figure 11 : Représentation schématique d'un acide aminé en conformation L (à gauche) et d'un acide aminé en conformation D (à droite).

Il est en effet reporté dans la littérature que les liaisons peptidiques entre des acides aminés D sont moins sensibles aux protéases des bactéries et donc que les peptides antimicrobiens en conformation D peuvent posséder de meilleures propriétés antimicrobiennes que leur peptide similaire en conformation classique.

La deuxième stratégie étudiée a été de synthétiser des dimères de CTL de différentes longueurs d'espaceur et un dendrimère possédant trois unités CTL (Figure 12). En effet, une présentation multivalente de peptides a été reportée dans la littérature comme pouvant augmenter l'efficacité des propriétés antimicrobiennes de certains peptides.

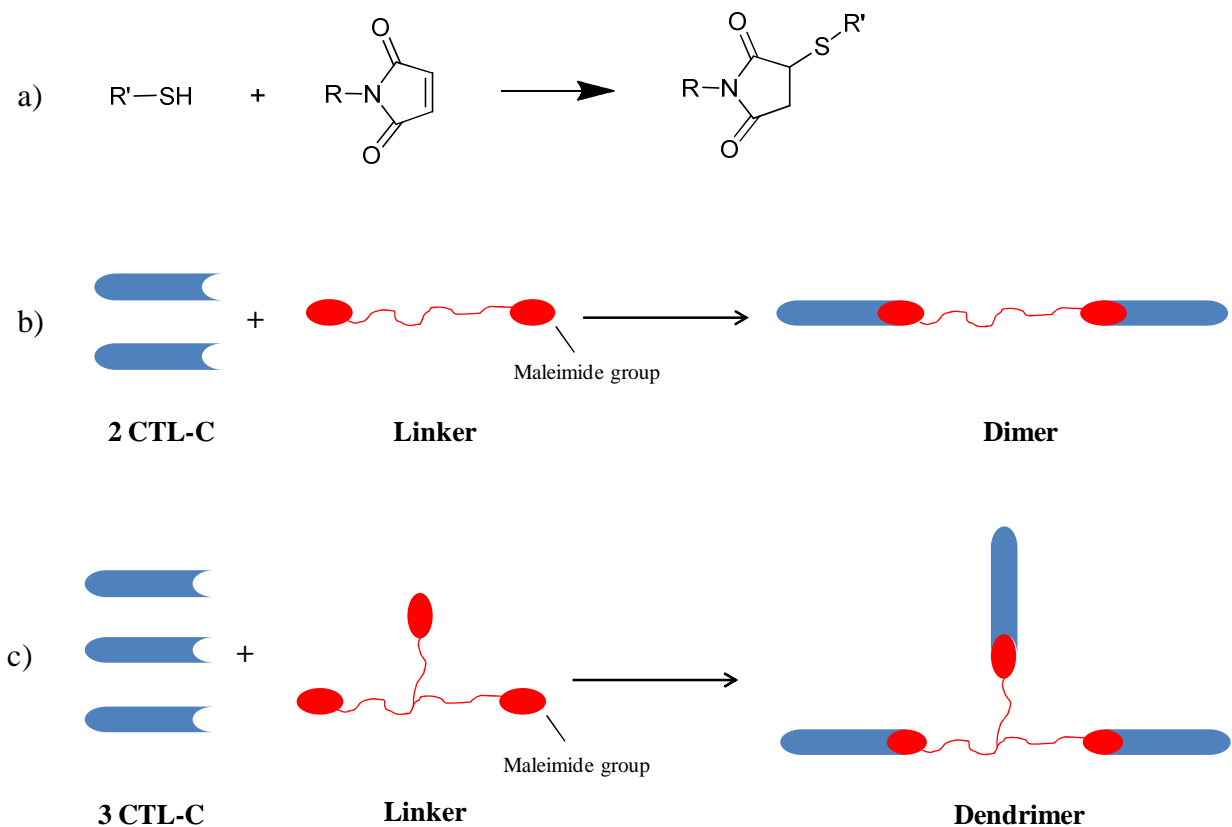


Figure 12 : (a) Réaction click thiol-maléimide. (b) Voie de synthèse d'un dimère à base de CTL-C : deux peptides CTL-C réagissent avec un espaceur terminé par deux groupements maléimide grâce à une réaction click thiol-maléimide. (c) Voie de synthèse d'un dendrimère à base de CTL-C : trois peptides CTL-C réagissent avec un espaceur terminé par trois groupements maléimide grâce à une réaction click thiol-maléimide.

Le peptide en conformation D, noté « D »-CTL-C, a été synthétisé par Protéogenix, compagnie spécialisée dans la synthèse de peptides. En revanche, la synthèse des dimères et du dendrimère de CTL-C a été effectuée au laboratoire et suivie par chromatographie en phase liquide à haute performance (HPLC). Leur masse a été contrôlée par Maldi-Tof.

Des tests antimicrobiens ont été réalisés sur 4 souches pathogènes : *S. aureus*, *C. albicans*, *Micrococcus luteus* et une souche de *S. aureus* résistance aux antibiotiques, Methicillin-résistant *S. aureus* (MRSA). Nous avons démontré que le peptide « D »-CTL-C possède des propriétés antimicrobiennes de 30 à 66% supérieures à celles du CTL-C selon la souche testée. Concernant les multimères, nous avons montré que tous les dérivés gardent une activité antibactérienne quasi équivalente à celle de la CTL non modifiée contre *Micrococcus luteus* et *C. albicans*. Par contre dans le cas de *S. aureus*, la longueur de l'espaceur des dimères semble avoir une influence fondamentale sur l'activité antibactérienne. Pour un espaceur long (46 unités éthylène glycol), l'activité antimicrobienne est totalement perdue alors que pour un espaceur court (3 unités éthylène glycol) l'activité antimicrobienne est équivalente voire supérieure, contre MRSA par exemple, à celle de la CTL-C.

Des tests inflammatoires préliminaires ont été également réalisés sur les meilleurs candidats pour remplacer CTL-C, à savoir « D »-CTL-C et le dimère possédant l'espaceur le plus court. Les résultats ont montré de meilleures propriétés anti-inflammatoires pour ses deux nouveaux peptides que la CTL non modifiée. Après 6 heures d'incubation en contact avec des cellules THP-1, les deux nouveaux peptides sont de 3 à 4 fois plus anti-inflammatoires que la CTL non modifiée.

3.4 Augmentation de la rigidité mécanique du revêtement

Afin d'augmenter les propriétés mécaniques du revêtement, nous avons travaillé sur deux points essentiels : l'attachement covalent du revêtement au cathéter et la réticulation covalente du film multicouche. Pour cela, nous avons d'abord élaboré par spin-coating des surfaces d'épaisseur contrôlée en polyuréthane (PU) pour imiter la composition d'un cathéter. Ensuite, ses surfaces ont été fonctionnalisées par une couche de polydopamine (PDA). En effet, la dopamine est connue dans la littérature pour s'auto-polymériser et former une couche fine de PDA à la surface de tout type de matériaux. L'avantage de cette couche de PDA est

que, une fois oxydée, elle peut réagir ensuite avec des groupements nucléophiles. Elle peut donc réagir avec les amines du chitosan et ainsi attacher le film multicouche de façon covalente à la surface. Nous avons ensuite utilisé un procédé de réticulation étape par étape des polysaccharides (Figure 13).

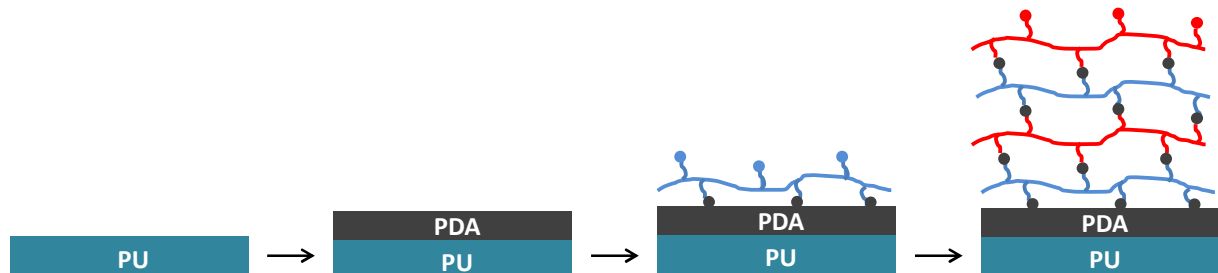


Figure 13 : Stratégie mise en place pour déposer par liaison covalente un film multicouche réticulé étape par étape sur une surface polyuréthane (PU) imitant la composition d'un cathéter. Une couche de polydopamine (PDA) est d'abord déposée sur le PU et réagit ensuite avec les amines du chitosan.

La vérification de toutes les étapes de fonctionnalisation a été réalisée par spectrométrie photoélectronique X (XPS).

La réticulation étape par étape des polysaccharides est basée sur la réaction chimique entre les groupements pyridyl disulfide (TP) et thiol (SH). Le CHI a été modifié chimiquement par des groupements thiol (CHI-SH) et le HA par des groupements pyridyl disulfide (HA-P). Après construction du film HA-P/CHI-SH, la robustesse du film a été testée en le mettant au contact d'une solution à 5 M NaBr. Le film CHI/HA non réticulé se dissout au contact de cette solution par écrantage des interactions électrostatiques entre les polysaccharides. Dans le cas du film HA-P/CHI-SH, un gonflement réversible est obtenu. Des essais qualitatifs ont également été réalisés. Grâce à des expériences force-distance en AFM, les modules d'Young ont pu être déterminés. Avec un module d'Young d'environ 550 kPa pour un film (HA-P/CHI-SH)₂₀, contre 50 kPa pour un film (HA/CHI)₂₀, nous avons démontré que la réticulation du film multicouche avait bien eu lieu.

Après avoir montré la possibilité de réticuler le film multicouche étape par étape, nous avons vérifié ses propriétés antimicrobiennes. Pour cela, CTL-C a été greffé à 1,5% sur HA-P (HA-P-CTL-C). Etant donné un greffage moins important sur le HA, les propriétés antimicrobiennes de ce revêtement se sont révélées inférieures à celles obtenues dans le cas

du premier revêtement auto-défensif que nous avons développé. Cependant, le film multicouche réticulé présente une inhibition totale de *M. luteus* après 24 h, de *C. albicans* pour au moins 6 h et de *S. aureus* pour au moins 4 h.

Références du résumé en français

1. Decher, G., Fuzzy Nanoassemblies: Toward Layered Polymeric Multicomposites, *Science*, **1997**, 277 (5330), 1232-1237.
2. Zhang, Y., et al., Novel alternating polymer adsorption surface activation self-assembled film based on hydrogen bond, *Thin Solid Films*, **2003**, 437, 280-284.
3. Krass, H., et al., Layer-by-Layer Self-assembly of a Polyelectrolyte Bearing Metal Ion Coordination and Electrostatic Functionality, *Chemistry of Materials*, **2003**, 15 (1), 196-203.
4. Suzuki, I., et al., Construction of positively-charged layered assemblies assisted by cyclodextrin complexation, *Chemical communications* **2002** (2), 164-5.
5. Van der Heyden, A., et al., Multilayer films based on host-guest interactions between biocompatible polymers, *Chemical communications* **2006** (30), 3220-2.
6. Wang, Z.P., et al., Stepwise assembly of the same polyelectrolytes using host-guest interaction to obtain microcapsules with multiresponsive properties, *Chemistry of Materials*, **2008**, 20 (13), 4194-4199.
7. Dubacheva, G.V., et al., Unlimited growth of host-guest multilayer films based on functionalized neutral polymers, *Soft Matter*, **2010**, 6 (16), 3747-3747.
8. Glinel, K., et al., Antibacterial surfaces developed from bio-inspired approaches, *Acta biomaterialia*, **2012**, 8 (5), 1670-84.

Summary: The surface of a material is the privileged location, where the interactions between the material and its environment take place. In the field of biomaterials, the challenge is to control these interactions. A very versatile coating technique is the layer-by-layer deposition, which consists in the alternated deposition of polyanions and polycations. The cohesion of polyelectrolyte multilayer films is primarily ensured by electrostatic interactions but was extended to other driving forces such as host-guest interactions. Our work was constituted of two main parts.

In the first part, the buildup of neutral polymer multilayer films based on host-guest interactions was studied and in particular the influence of β -cyclodextrin/ferrocene interaction strength on the topography of these films. The host-guest interaction strength was first modulated by involving different guests (adamantane, ferrocene and pyrene) in the buildup. Then, β -cyclodextrin/ferrocene interaction strength was tuned by the presence of different types and concentrations of salts during the multilayer buildup. Intermediate interaction strength seems to be required to form continuous films, whereas, if too low, the interaction strength limits the film buildup.

In the second part, motivated by the fact that the prevention of pathogen colonization of implantable medical devices constitutes a major medical and financial issue, polyelectrolyte multilayers were used as tools to develop new antimicrobial coatings. Polysaccharide multilayer films containing cateslytin, an antimicrobial peptide, fully inhibited in 24h the development of *Candida albicans* and *Staphylococcus aureus*, which are common and virulent pathogens agents encountered in care-associated diseases. The release of the antimicrobial peptides was triggered by the enzymatic degradation of the film due to the pathogens themselves introducing the concept of self-defensive coating. The non-cytotoxicity of the film, towards human cells, highlights a medically relevant application to prevent infections on catheters. Different cateslytin based dimers with various lengths and one dendrimer were synthesized in order to improve the bioactivity of the original peptide, *i.e.* antimicrobial and anti-inflammatory properties. In order to obtain mechanically robust antimicrobial films, polyurethane (polymer that composes catheters) was functionalized with a polydopamine layer that can further react with thiol or amine groups, allowing the covalent attachment of step-by-step cross-linked antimicrobial polysaccharide films.

Keywords: Layer-by-layer, antimicrobial coating, polyelectrolyte multilayer films, host-guest interaction

Résumé : La surface d'un matériau est le lieu privilégié des interactions entre le matériau et son environnement. La technique couche-par-couche, qui consiste en un dépôt alterné de polyanions et de polycations, ouvre de nouvelles perspectives dans le domaine des biomatériaux pour le contrôle de ces interactions. La cohésion des films multicouches de polyélectrolytes est principalement assurée par des interactions électrostatiques mais a été étendue à d'autres forces motrices telles que les interactions hôte-invité. Nos travaux s'articulent autour de deux axes principaux.

D'une part, nous nous sommes intéressés aux films multicouches de polymères neutres basés sur des interactions hôte-invité et en particulier à l'influence de la force du complexe d'inclusion β -cyclodextrine/ferrocène sur la topographie de ces films. La force de l'interaction hôte-invité a d'abord été modulée en associant différents invités (l'adamantane, le ferrocène et le pyrène) avec la β -cyclodextrine. La force du complexe β -cyclodextrine/ferrocène a été ensuite modulée par la présence de différents sels de sodium à différentes forces ioniques au cours de la construction du film. Une force d'interaction intermédiaire du complexe semble être nécessaire pour former des films continus, tandis que, si elle est trop faible, la force d'interaction limite la construction du film.

D'autre part, motivé par le fait que la prévention des infections microbiennes des dispositifs médicaux implantables constitue un problème médical et financier majeur, nous avons développé de nouveaux revêtements antimicrobiens grâce à la technique couche-par-couche. Des films multicouches à base de polysaccharides contenant la cateslytine, un peptide antimicrobien, permettent l'inhibition en 24h du développement de *Candida albicans* et *Staphylococcus aureus*, qui sont des agents pathogènes communs et virulents rencontrés dans les maladies nosocomiales. La libération des peptides antimicrobiens est déclenchée par la dégradation enzymatique du film en présence des agents pathogènes. Le revêtement est ainsi qualifié d'auto-défensif. La non-cytotoxicité du film vis-à-vis des cellules humaines permet une application cliniquement pertinente pour prévenir les infections sur les cathéters. Des dimères à base de cateslytine de différentes longueurs et un dendrimer ont été synthétisés afin d'améliorer l'activité biologique du peptide d'origine, *i.e.* ses propriétés antimicrobiennes et anti-inflammatoires. Afin d'élaborer des films antimicrobiens mécaniquement robustes, le polyuréthane (polymère entrant dans la composition des cathéters) a été fonctionnalisé par une couche de polydopamine qui peut ensuite réagir avec des groupements thiol ou amine, permettant la fixation covalente des films de polysaccharides antimicrobiens réticulés étape par étape.

Mots clés: Couche-par-couche, revêtement antimicrobien, multicouches de polyélectrolytes, interaction hôte/invité
